

LOUGHBOROUGH
UNIVERSITY OF TECHNOLOGY
LIBRARY

AUTHOR/FILING TITLE

SADULLIS, S

ACCESSION/COPY NO.

185777/02

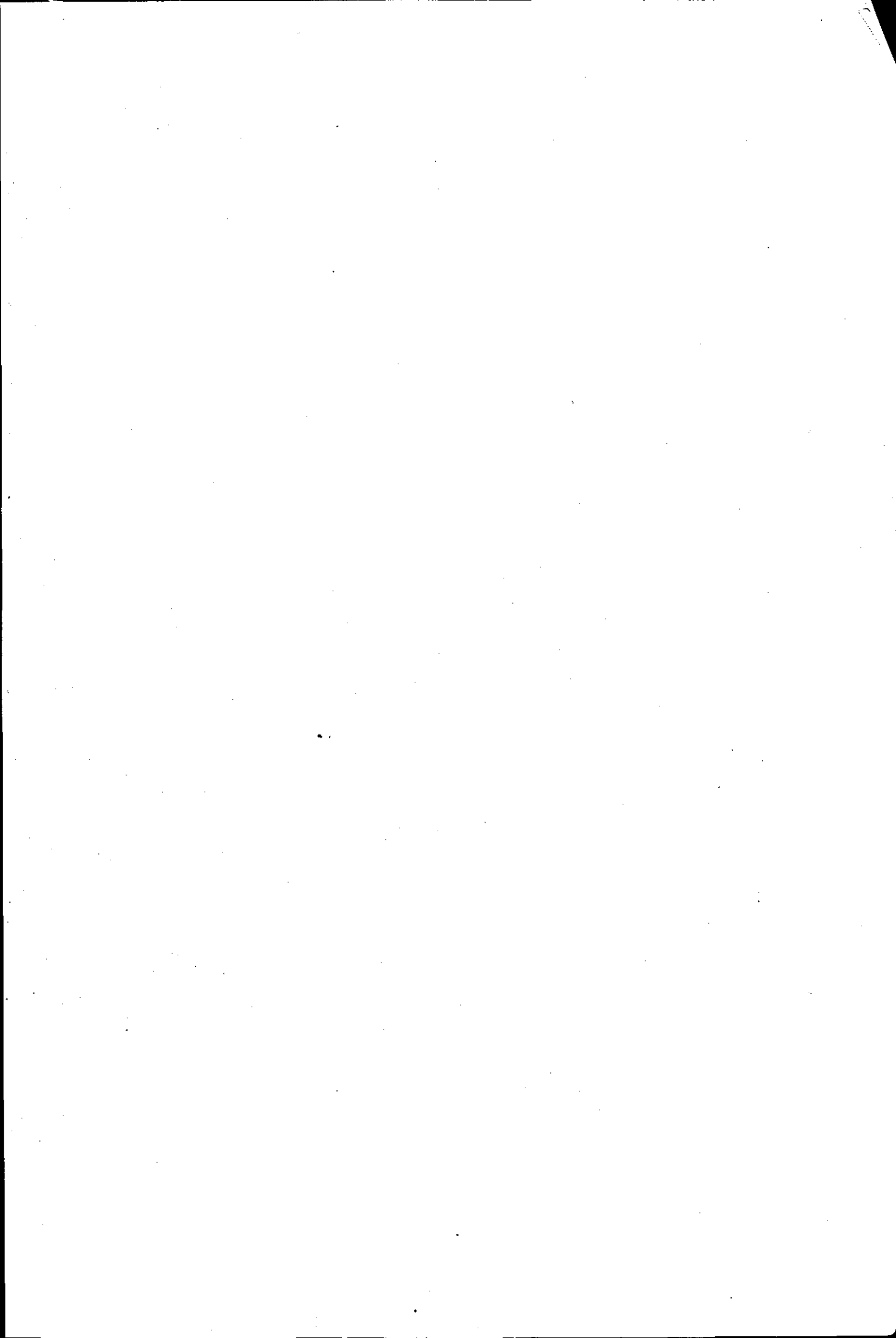
VOL. NO.

CLASS MARK

1 JUL 1987	LOAN COPY	
01. JUL 81	- 2 JUL 1988	
2 JUL 1989	- 1 JUL 1994	
7 JUL 1992	30 JUN 1995	
08. MAR 95		
08. JUN 95		

018 5777 02





AN OPTIMAL RIDE CONTROL SYSTEM

FOR AN EXECUTIVE JET AIRCRAFT

BY

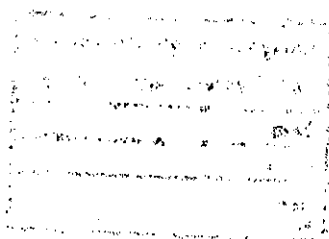
SOLON L.A. SAOULLIS, B.Sc.

A Master of Science Thesis submitted
in partial fulfilment of the requirements
for the award of Master of Science
of the Loughborough University of Technology

SUPERVISOR: Dr. D. McLean
Department of Transport Technology

Loughborough University of Technology Library	
Date	July 80
Class	
Acc. No.	185777/02

To My Parents



ACKNOWLEDGEMENTS

I would like to express my deep gratitude to my parents for their continuous encouragement and support throughout my education.

Also I would like to thank my supervisor, Dr. McLean, who helped me and inspired my work at Loughborough University.

SYNOPSIS

Aircraft specifically designed for short take-off and landing (STOL) operations are particularly sensitive to atmospheric turbulence and produce relatively high levels of vertical and lateral accelerations. These acceleration levels cause discomfort, which is unacceptable in modern transport aircraft. Such aircraft ought to have their dynamics improved by the action of a ride quality control system (R.C.S.) which should effectively reduce these accelerations thereby improving comfort.

Little attention has been given to date to the problem of designing R.C.S. for executive jets. But with the developing use of such aircraft which are increasingly of the STOL type the demand for an effective R.C.S. has intensified. A few earlier studies used conventional theory to derive the required control laws but so far the use of modern control theory to derive laws based on a multivariable description of the aircraft responses has not been widely tried.

Multivariable control theories can be applied to STOL aircraft by making use of the active control technology (A.C.T.) concept. This research has employed both A.C.T. and modern control theory to derive a suitable optimal control system which uses several aerodynamic control surfaces in such a way that the required reduction of the acceleration levels can be achieved. The optimal control law used to provide ride quality control involved the use of elevator, rudder and ailerons, in

conjunction with spoilers, and horizontal and vertical canards. The subject aircraft chosen for this work was a specially-modified NASA Jetstar. The uncoupled equations of motion of the aircraft, together with disturbances due to atmospheric turbulence, were simulated on a digital computer. Frequency response methods were also used to provide information for comparison with results from conventional control.

The experimental investigations involved consideration of the combination of surface activity, the effects of non-linearities in the surface actuators and the dynamic response to both manoeuvre commands and stochastic disturbances. The best results, expressed in terms of reduction of the levels of the normal and lateral acceleration, were obtained when all available controls were activated simultaneously and reductions of the order of 40% were achieved. The effect of the optimal control law on the aircraft handling qualities was also investigated and compared with idealised models.

CONTENTS

	<u>PAGE</u>
SYNOPSIS	i
<u>Chapter 1:</u> INTRODUCTION	
1.1 Problem Description	1
1.2 Historical Background	3
1.3 The Scope of the Work	11
<u>Chapter 2:</u> RIDE CONTROL FOR A STOL AIRCRAFT	
2.1 Introduction	16
2.2 Comfort Criteria	19
2.3 Ride Quality Criteria	23
2.3.1 Ride Discomfort Index	23
2.3.2 Ride Comfort Rating	25
2.4 Brief Investigation on the Motion Factors Influencing Ride Comfort	28
2.5 Means of Controlling Ride Comfort	29
2.6 Longitudinal Ride Control	32
2.6.1 Direct Lift Control Analysis	32
2.6.2 Longitudinal Control Surface Configuration	38
2.6.2.1 Spoilers Characteristics	38
2.6.2.2 Horizontal Canards Definition	43
2.7 Lateral Ride Control	45
2.7.1 Analysis of Lateral Acceleration Constituents	45
2.7.2 Vertical Canard Definition	52
2.8 Equations of Motion	54

<u>Chapter 3: MODELLING OF ATMOSPHERIC TURBULENCE</u>		
3.1	Introduction	57
3.2	Analytical Representation of Turbulence	60
3.3	Power Spectral Analysis	64
3.3.1	Power Spectral Density Function Definition	64
3.3.2	Computer Simulation of Atmospheric Turbulence	67
3.3.2.1	Signal Transmission in Linear Systems	68
3.3.2.2	Digital Simulation of the Dryden Model	70
3.4	Some Concluding Notes	80
3.4.1	Relative Significance of u_g, p_g, r_g and q_g	80
3.4.2	Results from the Simulation of Atmospheric Turbulence	82
 <u>Chapter 4: OPTIMAL RIDE CONTROL SYSTEMS FOR AIRCRAFT</u>		
4.1	Introduction	86
4.2	Representation of Acceleration in Terms of State and Control Variables	87
4.3	Linear Quadratic Problem (L.Q.P.) Formulation	91
4.4	The Output Regulator Problem	98
4.5	Description of the Digital Programs 'WAYMX' and 'OUTREG'	101
4.5.1	Determination of Appropriate Q and G Matrices	101
4.5.1.1	Choice of the Maximum Values for the State and Control Vectors for Longitudinal Motion	103
4.5.1.2	Choice of the Maximum Values for the State and Control Vectors for Lateral Motion	105

	<u>PAGE</u>
4.5.2 Determination of the Optimal Feedback Matrix (K^0) for the Output Regulator	107
4.6 Handling Qualities Requirements for an Executive Jet Aircraft	108
4.7 Closed-loop Response	112
4.8 A Model Matching Method for Handling Qualities Improvement	114
4.8.1 Implicit Model Following	114
4.8.2 Selection of the Model Matrix (L)	116
4.8.2.1 Selection of a Model for Longitudinal Motion	117
4.8.2.2 Selection of a Model for Lateral Motion	118
<u>Chapter 5:</u> MATHEMATICAL MODELS OF THE ACTUATING ELEMENTS	
5.1 Introduction	121
5.2 Mathematical Models of the Actuating Elements Employed	124
5.3 Power Limitation of the Actuating Elements	129
<u>Chapter 6:</u> ANALYSIS OF THE DYNAMIC RESPONSE OF THE MODIFIED JETSTAR AIRCRAFT	
6.1 Introduction	133
6.2 Analysis of the Dynamic Response of the Modified Jetstar Aircraft Subjected to Command Inputs	135
6.2.1 Dynamics of the Uncontrolled Aircraft	135
6.2.1.1 Longitudinal Motion Analysis	136
6.2.1.2 Lateral Motion Analysis	144
6.2.2 Dynamics of the Optimally Controlled Aircraft	153
6.2.2.1 Longitudinal Motion Analysis	156
6.2.2.2 Lateral Motion Analysis	172

	<u>PAGE</u>
6.3 Analysis of the Dynamic Response of the Modified Jetstar in Turbulent Flight	186
6.3.1 Longitudinal Motion Analysis	187
6.3.2 Lateral Motion Analysis	206
<u>Chapter 7:</u> DESIGN METHOD FOR A RIDE QUALITY CONTROL SYSTEM (R.C.S.)	
7.1 Introduction	218
7.2 Ride Quality Benefits from the Use of Optimal R.C.S. on the Modified Jetstar (CCV)	219
7.3 Discussion and Future Recommendations for a R.C.S. Design Method	225
7.3.1 Aerodynamic Efficiency of the Selected Control Surfaces for the R.C.S.	226
7.3.2 Effectiveness of the Optimal Feedback Control Laws	231
7.3.2.1 Choice of the Weighting Matrices Q and G	231
7.3.2.2 Choice of the Model Matrix	234
7.4 The Role of Digital Simulation in the Design of an Optimal R.C.S.	237
<u>Chapter 8:</u> CONCLUSIONS	239
REFERENCES	243
<u>APPENDICES:</u>	
Appendix A: Derivation of the \hat{Q} and \hat{G} Matrices for the Output Regulator	253
Appendix B: Airplane Classification	255
Appendix C: Frequency Responses of the Actuator Dynamics Employed	257
Appendix D: General Characteristics of the Basic Jetstar Aircraft	259

CHAPTER 1

INTRODUCTION

1.1 PROBLEM DESCRIPTION

When an aircraft encounters atmospheric turbulence the randomly induced loads on its wings and body, due to the gusts, tend to disturb its motion which is characterised by unwanted vertical and lateral acceleration.

The ride discomfort for the crew and passengers of an aircraft depend on the duration and frequency of occurrence of particular levels of normal and lateral accelerations. Factors such as wing-loading, altitude, speed of operation, structural modes et al determine the ride quality sensitivity of an aircraft. To provide acceptable ride characteristics an aircraft may need to be equipped with an automatic flight control system (a.f.c.s.) by means of which it may be possible to achieve the necessary attenuation of those undesirable features of ride quality which are introduced by encountering atmospheric turbulence. Such a.f.c.s. are referred to as ride control systems (R.C.S.) and such a system is usually designed to provide an aircraft with the capability of suppressing undesirable accelerations induced in flight.

The need for investigation of effective R.C.S. has intensified in recent years with the advent of the Short Take Off and Landing (STOL) aircraft and the economic pressure for its wider development in short haul air transportation. The low wing-loading associated with STOL aircraft (maximum 8000 N/ m^2) makes it particularly sensitive to atmospheric turbulence. Since the STOL class aircraft is usually designed to operate at low altitudes where atmospheric turbulence is more likely to exist the need to provide acceptable ride comfort by incorporating R.C.S. on this type of aircraft is evidently necessary. Consequently the investigation of the design of such a system is particularly timely.

The design of optimal R.C.S. and its performance was investigated in this research using as an example aircraft the Jetstar which is an executive jet characterised by its low wing-loading (2100 N / m^2 for this study). Because turbulence is more likely to occur at low altitudes, as it was indicated above, the flight conditions selected for the subject aircraft was, approach, which implies low speed low altitude.

The optimal design was studied by means of digital simulation.

1.2 HISTORICAL BACKGROUND

Ride quality has been of concern to aeronautical designers since the inception of manned flight, particularly in respect of controlling the motion of the vehicle in gusty conditions. As experience of flight accumulated it was learned that the structure of the aircraft must be designed such that the airframe would withstand the most severe atmospheric conditions envisaged. However, the constraints which the gust loads imposed on aircraft design came in time to have an undesirable influence on the resulting motion of the aircraft. Consequently designers deliberately considered special methods of achieving some alleviation of the loads sustained by the airframe due to encountering atmospheric turbulence (for example Hunsaker and Wilson [1915]). Whenever these means of alleviation involved feedback control it was evident that the accelerations experienced by the aircraft were reduced and consequently some measure of improvement of the ride quality of the aircraft was being obtained simultaneously. Thus a ride quality system will provide some improvement in the aircraft's capability to withstand gust loads as well as improving the ride motion of the aircraft in response to commands or to its passage through a patch of atmospheric turbulence.

The first recorded investigation of G.L.A. systems was that presented by Sprater in the USA in 1914 (Sprater [1914]) which was entitled "Stabilizing device to counteract the disturbance and prevent it from having an injurious effect on the stability of the machine". However, it was not until 1937, when the work of Von Karman and Taylor provided a suitable mathematical description of atmospheric turbulence (Von Karman [1937] and Taylor [1937]) that interest in the problems of G.L.A. and R.C. was renewed.

In general two approaches have been used to design G.L.A. or R.C. systems: the open- and the closed-loop design philosophies.

Early open-loop designs were based on aeromechanical control to alleviate the gust loads. Waterman [1930] built an aircraft with wings attached to the fuselage by skewed hinges. The wings were balanced by pneumatic struts for steady lift forces. Unsteady lift loads caused the wings to deflect, thus reducing the angle of attack. This system, however, could not provide adequate lateral control since deflection of the ailerons in turn caused the wings to deflect. In 1938 Hirsch conducted model tests of a flap-type alleviation system (Hirsch [1938]) which employed the horizontal stabilizer as an angle of attack sensor. He was the first to recognize the need to concentrate on long wavelength absorption and was not concerned with the sensor lag of this configuration. Hirsch developed this approach after World War II when he installed his system on a twin-engined aircraft.

In the early 50's the open-loop design philosophy was investigated by many researchers in this field. Most of these designs were based on an angle of attack vane mounted on a nose boom. By means of this vane the relative direction of the gust and the pressure changes were measured. The output signals from the vane were filtered before being transmitted to the control surfaces. It was hoped that by optimizing the parameters of the open-loop control law desirable ride control and gust load alleviation could be achieved. However, it was not sufficiently appreciated at the time that a gust field has significant components normal to the plane of symmetry of the aircraft nor that some secondary aerodynamic effects (such as downwash, time delay in the development of lift,

aeroelastic deflections of wings, etc.) are also significant.

In 1949 the Bristol Brabazon was equipped with a G.L.A. system. This system was never tested in flight, because of other problems in the flight test programme as the aircraft project was cancelled before the appropriate phase of the flight test programme was reached. The Brabazon used symmetrical deflection of the ailerons in response to gust signals which were detected by a vane mounted on the aircraft nose.

In 1951 details of a study of R.C.S. were published (Phillips and Kraft [1951]). In this project direct lift flaps were driven through a fixed gearing to the elevator from signals transmitted from an angle of attack vane. Downwash effects at the tail due to flaps were corrected with a small inboard portion of the flaps driven in direction opposite to the main flaps. This control system was tested aboard a C-45 aircraft and a reduction of approximately 45% of normal acceleration was achieved without degrading the handling qualities of the aircraft.


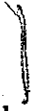

In 1953 the Royal Aircraft Establishment carried out some flight tests using a R.C.S. in a Avro Lancaster bomber. The vertical component of atmospheric turbulence was sensed by a 'wind incidence motor' mounted on a boom ahead the nose of the aircraft. The derived electrical analogue signal was used to command symmetric aileron deflection so as to reduce anticipated lift increment. The results from this investigation were unsatisfactory, however, it was found that the handling qualities were seriously impaired because of a marked reduction of stability that arose from the very large adverse pitching moment created by the symmetrical aileron deflection (Zbrojek [1953]).


In 1957 there was reported work involving the implementation of Wiener's optimum filter theory for the minimization of the open-loop aircraft response to atmospheric turbulence (Tobak [1957]). Tobak assumed that a sensor signal proportional purely to fluctuations in angle of attack was available. His analysis validated some of the results obtained earlier by means of classical analysis by Phillips and Kraft.

At the beginning of the 1970's Coupry [1971] proposed a system for open-loop G.L.A. based on a similar analysis to that of Tobak. This G.L.A. system was investigated in simulation and also in flight tests of the Mirage IIIB fighter. It was shown that by using vanes, gyroscopes and accelerometers and employing Wiener's optimal control theory substantial reduction of acceleration could be achieved, a result confirmed in the simulation tests but not confirmed from the flight tests.

In recent years NASA has supported studies concerned with the implementation of an aeromechanical system for R.C. and G.L.A. on a Cessna 172, a light aircraft. In 1974 and 1975 the results obtained from the investigation of such a system were presented (Roesch and Harlan [1974], Stewart [1975]). The aeromechanical system studied employed small auxiliary wings to sense changes in angle of attack and to drive the flaps to compensate the resulting incremental lift. This system provided a reduction of normal acceleration of about 50%.

The open-loop design philosophy for the early R.C.S. and G.L.A.s came about mainly due to the inadequate knowledge of the complete dynamics and stability characteristics of aircraft, particularly the unsteady aerodynamic effects and the effects due to structural flexibility, and

also from the lack of availability of sufficiently fast servomechanisms which were required for the successful implementation of the design. The open-loop design does not affect the stability of the aircraft. On the contrary the closed-loop design can adversely affect the stability and the handling qualities of an aircraft if the feedback gains are not chosen properly. However, because fast servomechanisms were unavailable it was necessary to sense the gust in advance to give more time for action at the expense of precision. As servoactuator performance improved it was realized that it was feasible to counteract the gust forces at the moment as they were actually occurring and that the sensing could then be achieved by means of strapped down accelerometers and gyros.   

The closed-loop design philosophy unlike open-loop schemes does not require any explicit knowledge of the atmospheric turbulence field. It is based on the continuous correction of the output variables of the aircraft by means of feedback to control surfaces being employed which means that careful analysis of the effect of the feedback law on the handling qualities of the aircraft considered must be undertaken. It is the simplification of the sensor requirements associated with closed-loop system which makes this approach more attractive from a practical viewpoint. 

In 1955 a proposal for a R.C.S. based upon the closed-loop design philosophy was made in which the linear and angular acceleration of the aircraft were sensed and used to drive auxiliary control surfaces (such as direct lift flaps) and elevators to produce the control forces and moments needed to minimize the aircraft accelerations (Atwood et al [1955]).

In 1965 the USAF and its contractors commenced an extensive

development programme on the B-52 aircraft known as the load alleviation and mode suppression (LAMS) programme. The first results were reported in 1969 (Burris and Bender [1969]). Also in 1969 the results obtained from a computer study of the design of an optimal direct lift control for the B-52 was presented (Lorenzetti et al [1969]). In this study optimal control was employed to derive the feedback gains which were used to drive the control surfaces consisting of the elevator, spoilers and symmetric deployed ailerons. The feedback states considered were the normal acceleration, pitch angle and pitch rate. With this configuration a reduction of normal acceleration at the c.g. of the aircraft of 50% was achieved. Later the work involved with the design of a R.C.S. for the Control configured vehicle (CCV) B-52 was reported (Stockdale and Poyneer [1973]). The objective of this study was to reduce the normal and lateral accelerations acting at the pilot station of the aircraft by 30%. To achieve this design objective auxiliary horizontal and vertical canards were incorporated in the design. By using pitch rate feedback to elevator and normal acceleration feedback to the horizontal canards a 30% reduction of normal acceleration was achieved. Similarly a 40% reduction of lateral acceleration was achieved by means of feeding back yaw angle and lateral acceleration to the rudder and vertical canard respectively.

In 1972 a research involving a R.C.S. for longitudinal and lateral ride control for a STOL aircraft was published (Holloway et al [1972]) The longitudinal R.C.S. consisted of elevator and trailing edge flaps driven by pitch rate and normal acceleration feedbacks. A reduction of 70% of normal acceleration was achieved in this way. Also the lateral R.C.S. reduced the lateral acceleration by 60% by using the rudder driven by

feedback signals from yaw angle and lateral acceleration. A similar longitudinal R.C.S. configuration to that proposed by Holloway et al achieved a 50% reduction of normal acceleration (Oehman [1973]).

In the same year a feasibility study for a R.C.S. for a STOL aircraft investigated the De Havilland Twin Otter equipped with elevator, symmetrical deflected ailerons and spoilers, and rudder for longitudinal and lateral ride control respectively (Gordon and Dodson [1972]). Pitch rate and normal acceleration, and yaw rate and lateral acceleration were used as feedback signals in the longitudinal and lateral ride control schemes. Although a 50% reduction of normal acceleration was achieved the lateral ride control system was found to create major difficulties due to conflicting requirements on the rudder. Several other studies (Lallman [1974], Erkenlens and Schuring [1975] et al) have been conducted in recent years on R.C.S. for STOL aircraft. Most of these studies used the same principles and were successful.

A R.C.S. for a NASA Jetstar aircraft has also been studied by Lapins (Lapins [1975]). His was the first study based on the closed-loop design philosophy which was tested in flight. His work involved three R.C.S., two for longitudinal and one for the lateral case all of multiloop feedback type. Two sets of unique control surfaces, direct-lift flaps and side-force generators, were used in addition to elevator and rudder for the mechanization. The simulation results achieved 50% reduction of normal acceleration and a reduction of 80% for lateral acceleration. The flight tests confirmed the results for longitudinal motion whereas the results for lateral motion indicated that only a 30% reduction of lateral acceleration could be achieved. However, it was concluded that, although the R.C.S.

resulted in significant reductions of accelerations, it failed to provide the aircraft with adequate handling qualities to meet the criteria in terms of pilot opinion. It was therefore deduced that a stability augmentation system (SAS) would also have to be incorporated to provide adequate handling qualities.

A recent study conducted by McLean [1978] employed modern control theories such as optimal control and model matching to design a G.L.A.s for a large flexible aircraft. In this study the CCV/A.C.T. approach was followed to tailor the G.L.A.s for the aircraft. The longitudinal control system used horizontal canards together with the conventional elevator whereas the lateral control system used a vertical canard in conjunction with ailerons and rudder. Substantial reductions for both longitudinal and lateral accelerations were achieved together with effective attenuation of the considered structural modes.

1.3 SCOPE OF THE WORK

The purpose of this research was to design an optimal ride control system (R.C.S.) for an executive jet aircraft by using the active control technology (A.C.T.) concept.

The advent of A.C.T. has caused changes in the design process for modern aerospace vehicles and it promises important improvements in future control capabilities.

In a recent publication (Ostgaard and Sworzel [1977]) the experience and knowledge summarized from the LAMS programme and the development of the CCV YF16 were assessed in the following manner:-

'Advanced flight control technology is a very significant driver in the design optimisation of both future military and civil aircraft. Acceptance of highly reliable fly-by-wire control systems and rapid advances in electronics technology are opening new avenues for exploration by the aircraft designers. Inclusion of the flight control system specialist with specialists in structure aerodynamics and propulsion during preliminary design effects a synergetic benefit. The design philosophy has become known as the Control Configured Vehicle approach to design, or the application of active control technology'.

With the advances of control science and technology it is now possible to treat multivariable control systems. But only since the recent advances in electronics have these control theories been capable of implementation on an aircraft.

The implementation of the A.C.T. concept makes it desirable to employ modern control theories for the design of a closed-loop R.C.S.

The approach which was used for the design of such an optimal R.C.S. for a rigid body aircraft was based on the evaluation of optimal feedback control laws derived from the theories of linear optimal control and model-matching. Figure 1.1 illustrates the block diagram of the closed-loop R.C.S. which was the subject of this research. The optimal control required that the feedback law depended on the availability of every state variable. The gains of the linear feedback law were constant. Full state feedback was fed by means of the optimal feedback matrix to the control vector of the aircraft.

Three feedback control laws were investigated. Two of these were derived from optimal control and the third from model matching theory. The two optimal feedback control laws were employed for the minimization of the accelerations associated with the aircraft's longitudinal and lateral motions. The model matching control was used to ensure that acceptable handling qualities resulted from the closed loop control and also to reduce the acceleration levels induced on the aircraft.

The control surfaces involved were the conventional control surfaces (such as elevator, rudder and ailerons) and an auxiliary direct lift control (D.L.C.) and a side force control (D.S.F.C.) surface (horizontal canards and spoilers for longitudinal motion were used; for lateral motion a vertical canard was used). The dynamics and the nonlinearities associated with the actuators were considered for each control surface. Atmospheric turbulence was simulated by means of the use of the

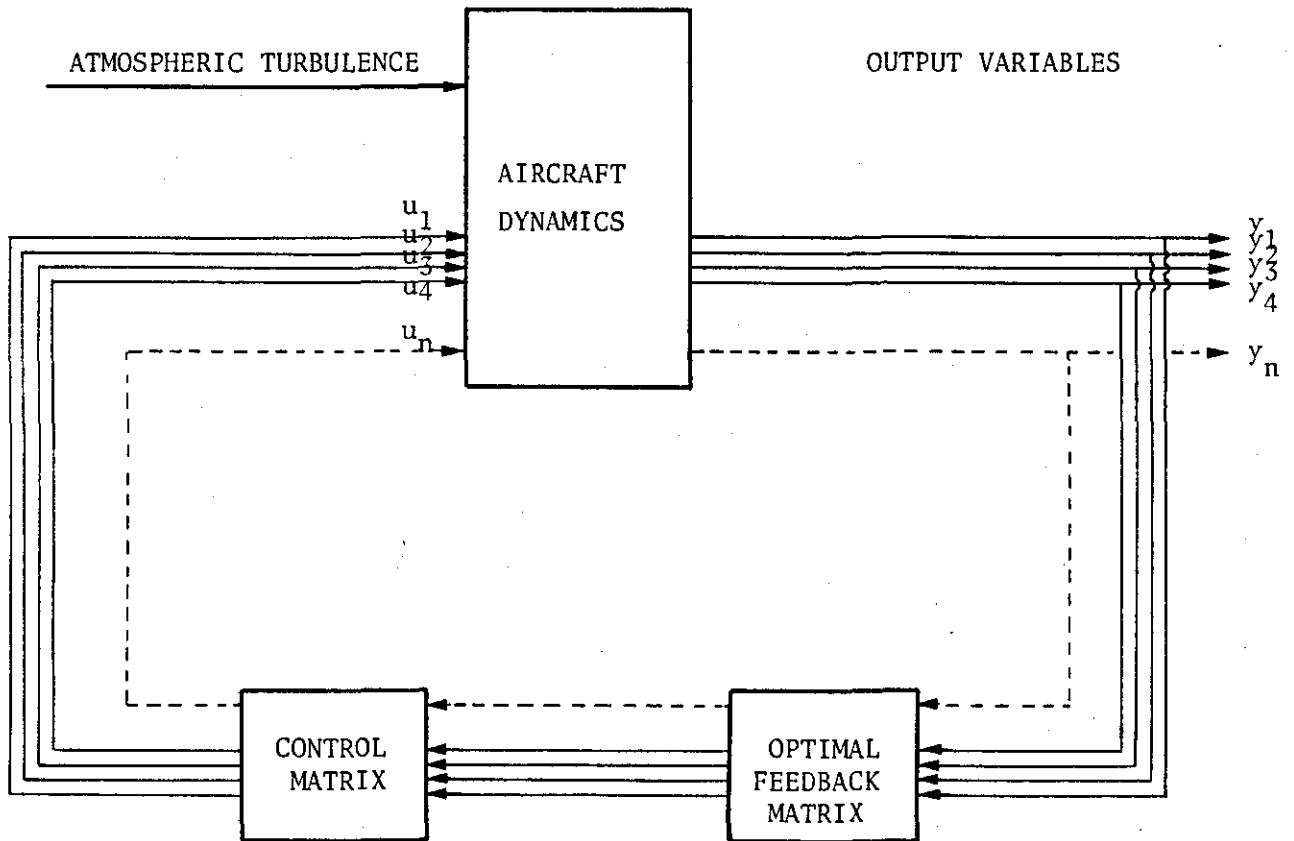


FIGURE 1.1: Block Diagram of the Closed-Loop Design Philosophy for an Optimal R.C.S.

Dryden filter. The simulation of the dynamic responses of the aircraft was achieved by means of a digital simulation language, SLAM (Simulation Language for Analog Modelling) which is automatically translated into FORTRAN IV.

In Chapter 2 an analysis of the factors affecting ride comfort is developed. Then in the same chapter it is described how D.L.C. and D.S.F.C. can be implemented to control the accelerations induced on the aircraft. A description in terms of the force and moment coefficients of the auxiliary control surfaces employed (spoilers, horizontal and vertical canards) are also given in this chapter.

Chapter 3 is concerned with the modelling of atmospheric turbulence. A mathematical representation of turbulence is given first and it is shown how the power spectral density analysis can be employed to formulate atmospheric turbulence for digital simulation. The Dryden model was chosen to represent atmospheric turbulence. At the end of this chapter the simulation results are summarized and considered.

In Chapter 4 the theory which was used to derive the feedback control laws for the R.C.S. is presented. A brief presentation of the linear quadratic problem (L.Q.P.) and the theory of the output regulator are used to introduce the optimal control concepts employed in this research. The effects on the dynamic characteristics of an aircraft of closing the loop by feedback control are considered separately. Model matching theory is described and it is shown how it can be used to derive control laws which will provide acceptable handling qualities for an aircraft.

The actuator dynamics and its mathematical modelling are presented in Chapter 5 where an account of the physical limitations associated with the actuators is given together with their definition.

In Chapter 6 the results obtained from this research are presented and an analysis of the uncontrolled aircraft dynamics is also given together with the results of several digital simulation studies. The dynamic performance of the controlled aircraft employing the various feedback control laws obtained from optimal control and model matching theories was studied for both command and turbulence inputs and these results are also presented.

In Chapter 7 can be found a discussion of the results obtained from the research. This discussion is accompanied by a suggested method for the design of the optimal R.C.S. which could be obtained with the methods adopted in this study.

Chapter 8 presents the conclusions and recommendations for further work based upon the results obtained from the research work reported in this thesis.

CHAPTER 2

RIDE CONTROL FOR A STOL AIRCRAFT

2.1 INTRODUCTION

As a result of increasing public demand for short haul air transportation the Short Take Off and Landing (STOL) aircraft has been found to be the best solution in terms of economy, noise reduction and traffice relief (NASA SP-320 [1972]).

The advent of the STOL aircraft has basically resulted from the need to design an aircraft with short take-off and landing capabilities. For such aircraft the take-off (or landing) distance can be decreased resulting in a reduction of the time of occupation of the runway. The shortness of the take-off length depends upon how fast a lift force greater than the aircraft weight can be generated. It can be shown (Stinton [1966]) that

$$U = k \sqrt{\left(\frac{W}{S}\right) \frac{1}{\rho} / \left(\frac{T}{W} - \frac{1}{(L/D)}\right)} \quad (2.1)$$

where

U: is the speed of the aircraft in still air, and may be, for example, the take-off speed (U_{to})

k: is a constant of proportionality

W: is the weight of the aircraft

S: is the wing area

ρ : is the air density

T: is the net propulsive force

L: is the lift force

and D: is the drag force.

From (2.1) it can be seen that provided everything else is constant the take-off speed can be decreased if the wing loading, (W/S) is decreased. If the take-off speed is decreased then the runway length may be reduced. Similar treatment of (2.1) gives the same conclusions for the landing phase.

Although reducing the wing loading on an aircraft is beneficial in terms of take-off (or landing) performance, it introduces other operational deficiencies such as sensitivity to gust loads. It can be shown (Taylor [1966]) that

$$\sigma_{a_z} = \xi \{ \rho U (\partial C_L / \partial \alpha) g / 2 (W/S) \} \sigma_{w_g} \quad (2.2)$$

where:

σ_{a_z} : is the root mean square (r.m.s.) value of the aircraft's acceleration at the c.g. position

ξ : is the gust response factor

$(\partial C_L / \partial \alpha)$: is the variation of lift coefficient with angle of incidence

σ_{w_g} : is the r.m.s. value of the normal to flight path component of atmospheric turbulence

(2.2) correlates the r.m.s. aircraft acceleration at the c.g. position to the r.m.s. value of the atmospheric turbulence. It can be seen that by reducing the wing loading of an aircraft it becomes more sensitive to gust loading by increasing the r.m.s. levels of acceleration. In order to suppress these acceleration levels and to overcome the high level of workload required from the pilot in turbulent conditions a ride quality control system (R.C.S.) is normally required for a STOL transport aircraft.

Ride quality control is taken to refer to an automatic control system whose purpose is to reduce the accelerations to which passengers and crew are subject to acceptable levels. The ride quality improvement on the performance of an aircraft due to its automatic control system will be judged only if appropriate ride quality criteria are considered as the basis for comparison.

Well defined criteria for ride comfort do not exist, although a great deal of research is taking place nowadays in order to extend the present knowledge and understanding of this very complex matter. However, plenty of ride comfort models have been proposed so far by several researchers in this field. Two likely measures of the ride quality are the ride discomfort index (R.D.I.) and ride comfort rating.

2.2 COMFORT CRITERIA

From data obtained from surveys of the attitudes, habits and journey preferences of air travellers with STOL aircraft the relative importance, in terms of comfort, of various parameters was established (Jacobson and Kuhlthau [1973]) and is represented in the following figure.

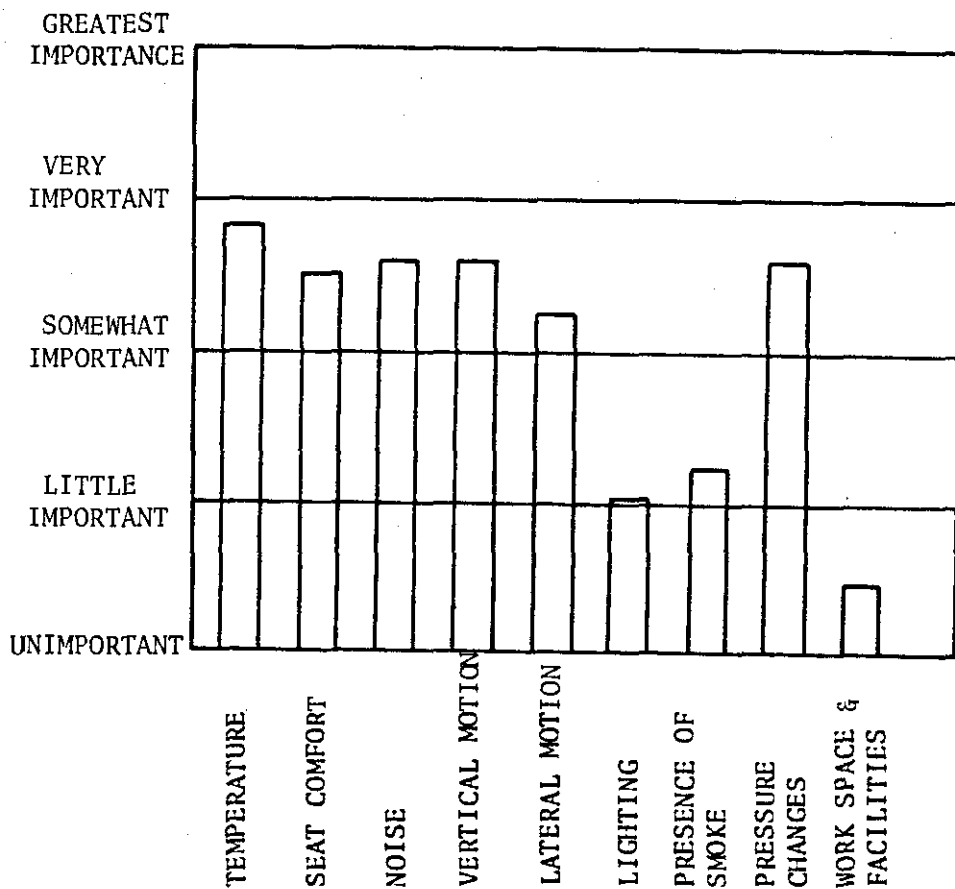


FIGURE 2.1: Relative importance of the various factors determining aircraft comfort

In determining the overall comfort it is evident from Figure 2.1 that the factors due to the aircraft's motion are important. Of course the above data do not always represent the actual situation. For example, if heavy turbulence is encountered then the effects of aircraft motion would become more dominant as may be seen from the above figure. For the

purposes of this research it was desirable to determine which were the constituents of the aircraft motion which most affect comfort. From several studies carried out elsewhere it may be deduced that two major factors of the aircraft motion affect comfort. These are:

- (a) The periodicity (or frequency) of a particular mode of motion
- (b) The intensity of the motion occurring

The frequency ranges associated with organic interference with humans can be summarized as follows (Erkenlens and Schuring [1975]).

Frequency band 0.1-1.0 Hz

This frequency band is associated with motion sickness and occurs during flight manoeuvres and also during flight in high velocity gusts.

Frequency band 1.0-30 Hz

Motion in this frequency band induces important resonance phenomena in the human body and these arise from turbulence excitation of the structural modes.

Above 30 Hz the effects are readily attenuated and become less important in relation to human body reaction. These frequencies may arise for example from the engines.

For a STOL aircraft with rigid body modes the frequency band in which it exhibits sensitivity is between 0.1 and 10 Hz. Therefore, an unaugmented STOL aircraft is expected to provide undesirable effects in terms of comfort.

The International Organization of Standardization (I.S.O.) has proposed exposure limits for normal and lateral body vibration for a range

of frequencies from 1 Hz up to 60 Hz. The standard applies to human exposure to whole-body vibration. The limits are intended to apply to any periodic or random motion. A number of these limits are illustrated in graphical form in Figure 2.2 and Figure 2.3. The lowest level of the reduced comfort boundaries is that below which no discomfort should be experienced. From the graphs it is evident that the limits vary with exposure time.

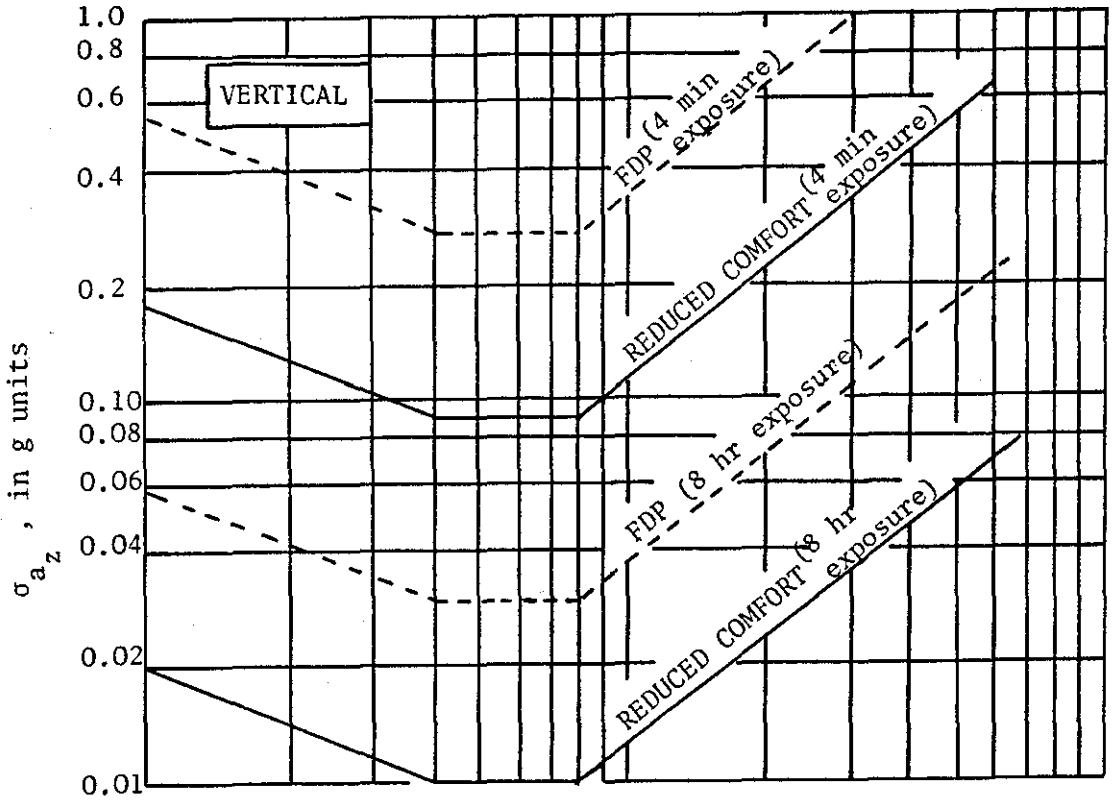


FIGURE 2.2: I.S.O. Proposed Comfort Limits for Vertical Body Vibration

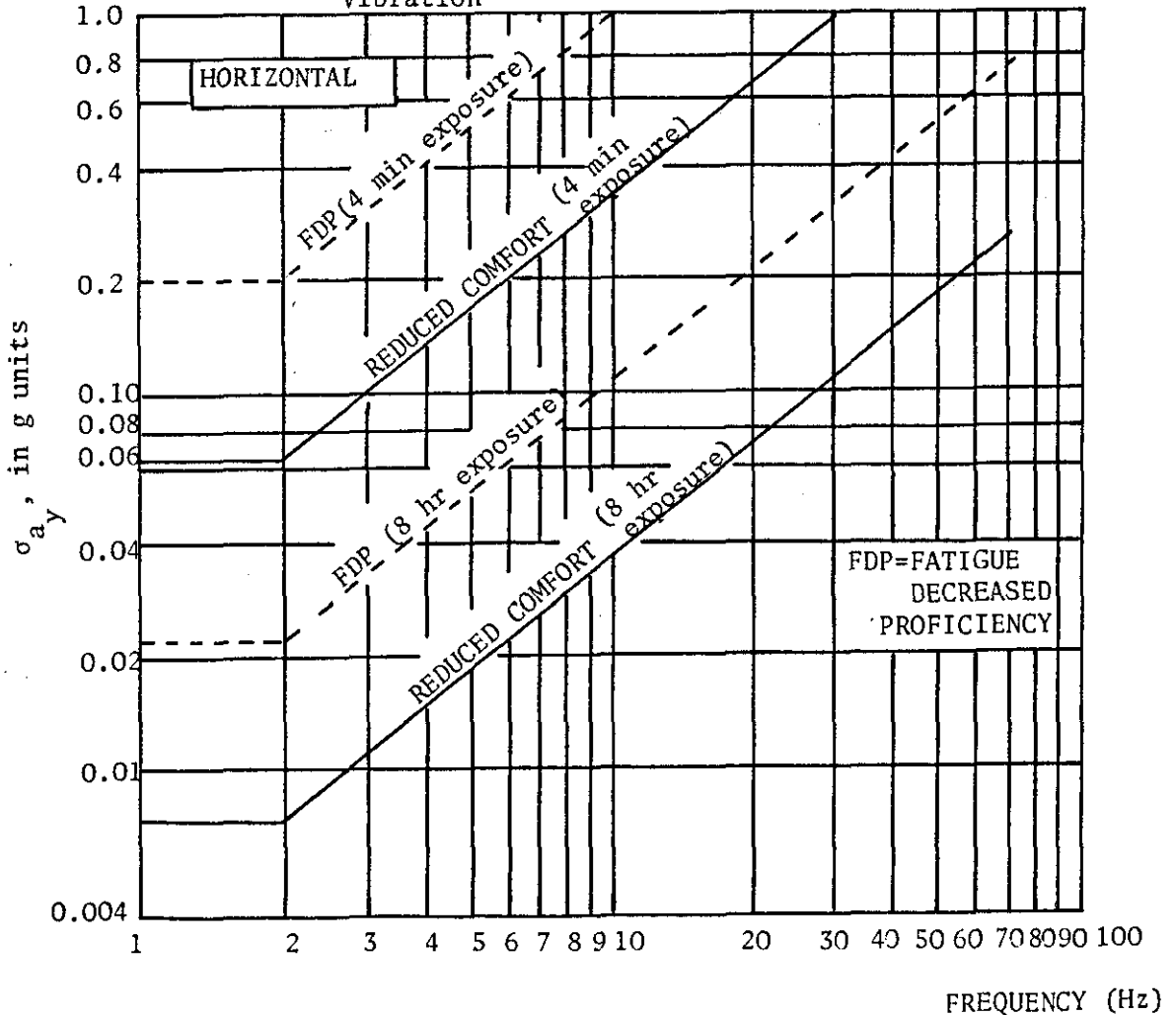


FIGURE 2.3: I.S.O. Proposed Comfort Limits for Lateral Body Vibration

2.3 RIDE QUALITY CRITERIA

There are, to date, two proposed measures of ride quality: the ride discomfort index (R.D.I.) which can be derived from the equations of motion of the aircraft, and ride comfort rating which is basically obtained from experimental data.

2.3.1 Ride Discomfort Index (R.D.I.)

A R.D.I. has been proposed in the USAF military specification document MIL-F-9490D. The index is proportional to the ratio of the wing-lift slope to wing loading, viz,

$$I_{RD} = \frac{kC_{L\alpha}}{W/S} = \frac{kSC_{L\alpha}}{W} \quad (2.3)$$

where k is a constant of proportionality and $C_{L\alpha}$ is the wing slope curve. For the longitudinal rigid-body motion, the dimensional stability derivative Z_w is given by

$$Z_w = - \frac{\rho S U_0}{2m} (C_{L\alpha} + C_D) \quad (2.4)$$

In flight through turbulence it may be assumed that $C_{L\alpha} \gg C_D$, thus

$$Z_w = - \frac{\rho S U_0}{2m} C_{L\alpha} = - \frac{\rho U_0}{2k} g I_{RD} \quad (2.5)$$

Using the short period approximation for the rigid body dynamics the heave motion is represented by:

$$\dot{w} = Z_w w + U_0 q + \sum_{j=1}^p Z_{\delta_j} \delta_j \quad (2.6)$$

where $j=1,2,\dots,p$ and p is the total number of the motivators.

The normal acceleration at the c.g. rigid body aircraft is given by:

$$a_{z_{c.g.}} = \dot{w} - U_0 q$$

Hence:

$$\begin{aligned} a_{z_{c.g.}} &= z_w w + \sum_{j=1}^p z_{\delta_j} \delta_j \\ &= -\frac{\rho U_0}{2k} g I_{RD} w + \sum_{j=1}^p z_{\delta_j} \delta_j \end{aligned} \quad (2.7)$$

Thus for a given control surface activity, if $a_{z_{c.g.}}$ is minimized I_{RD} will also be minimized for that flight condition. However, I_{RD} also influences the stability, and hence the flying qualities of the aircraft.

The static margin of an aircraft is defined as

$$\frac{C_{M_\alpha}}{C_{L_\alpha}} = -\frac{x_{ac}}{c} \quad (2.8)$$

then from (2.3)

$$I_{RD} = \frac{kS}{W} \frac{C_{M_\alpha}}{-(x_{ac}/c)} \quad (2.9)$$

Hence, it can easily be shown that

$$I_{RD} = \frac{2kI_y}{\rho U_0 W} \frac{M_w}{x_{ac}} \quad (2.10)$$

From (2.5) it can be seen that

$$I_{RD} = -\frac{2k}{\rho U_0 g} z_w \quad (2.11)$$

Therefore to minimize I_{RD} by using an automatic flight control system implies that the control system must augment the static margin, and must reduce either z_w or M_w . If C_{M_α} is small for an aircraft then I_{RD} is low and the aircraft will be expected to have favourable gust response in terms of ride quality. If z_w or M_w will be reduced then the short period dynamics will be affected and an augmentation control system might be required to provide acceptable handling qualities for the aircraft. one!

2.3.2 Ride Comfort Rating

Ride comfort rating has been assessed by conducting extensive surveys of opinions of airline passengers in U.S.A. and also from ground and airborne simulations in the same country. It is generally recognized that the comfort of aircraft passengers is affected by numerous physical and physiological factors (Figure 2.1). There have been attempts to derive comfort models that include the effects of manoeuvres, environment and seating space comfort. (Jacobson et al [1978]). Although factors such as environment etc. cannot be disregarded in the design of any transport aircraft it was beyond the scope of this research to consider comfort models other than those based on aircraft motions.

Ride comfort rating is based on a rating scale describing the ride comfort from very uncomfortable to very comfortable. Wolf, Rezek and Gee [1975] defined ride comfort on a basis of a five-point rating scale. Their model was based on passengers opinions of ride comfort obtained from experiments using the NASA Jetstar airborne simulator. For cases where the normal accelerations were greater than 1.6 times the transverse accelerations as for the Jetstar aircraft the ratings arrived at were as follows:

$$C = 2.0 + 7.6 \sigma_{a_y} + 11.9 \sigma_{a_z} \quad (2.12)$$

where σ_{a_y} and σ_{a_z} are expressed in units of g. Table 2.1 shows how ride quality is judged for different values of C by the five-point rating scale.

Rating, C	Ride Description
1	Very comfortable
2	Comfortable
3	Acceptable
4	Uncomfortable
5	Very uncomfortable

TABLE 2.1

An alternative seven-point comfort rating scale using seven points was proposed by Schoonorer [1975]. The following model was derived using linear regression analysis applied to the survey data:

$$C = 1.65 + 8.32 \sigma_{a_x} + 15.1 \sigma_{a_y} + 21.5 \sigma_{a_z} + 0.183 \sigma_p - 1.2 \sigma_q - .238 \sigma_r \quad (2.13)$$

Both Wolf and Schoonorer found that passengers were about twice as sensitive to lateral as to vertical acceleration.

Jacobson and Kuhthau [1973] however, developed a comfort model to study the effects of various combinations of the motion variables over extended ranges of frequencies, amplitude and rates of change. Their comfort criterion was based on a five-point rating scale. They defined comfort, C, as being related to the r.m.s. accelerations and the cross correlation. Thus,

$$C = C_0 + \sum_{j=1}^6 \alpha_j \sigma_{a_j}^{v_j} + \sum_{j=1}^6 \sum_{i=j+1}^6 \beta_{ij} \sigma_{a_{ij}}^{\mu_{ij}} \quad (2.14)$$

where

$$\sigma_{a_j} = \left[\frac{1}{T} \int_0^T a_j^2(t) dt \right]^{1/2} \quad (2.15)$$

are the r.m.s. accelerations in the vertical, transverse, longitudinal, pitch, roll and yaw directions and

$$\sigma_{a_{ij}} = \left[\frac{1}{T} \int_0^T a_i(t) a_j(t) dt \right]^{1/2}, \quad i \neq j \quad (2.16)$$

are the cross correlations of each variable with all others. The α_i 's and β_{ij} 's are weighting factors and the ν_i 's and μ_{ij} 's are scaling exponents. A physical interpretation of the model is to consider α 's and β 's as sensitivities of the human subject to the different directions of acceleration. The scaling exponents are representative of the non-linearity of the human sensor. From data obtained from a large number of flights (2.14) reduced to:

$$C = 1.8 + 11.5 \sigma_{a_z} + 5.0 \sigma_{a_y} + 1.0 \sigma_{a_x} + 0.25 \sigma_{\dot{q}} + 0.4 \sigma_{\dot{p}} + 1.9 \sigma_{\dot{r}} \quad (2.17)$$

Jacobson, Kuhlthau and Richards [1975] now using a seven-point comfort scale, proposed a further model:

$$C = 2.1 + 17.1 a_y + 17.2 a_z \quad (2.18)$$

Several other such comfort models have been proposed by other authors but those discussed here are more commonly used in U.S.A. and in most other aviation circles.

2.4 BRIEF INVESTIGATION ON THE MOTION FACTORS INFLUENCING RIDE COMFORT

From equations (2.12), (2.13), (2.14), (2.17) and (2.18) it is apparent that comfort due to motion of an aircraft depends principally upon the levels of normal and lateral acceleration. It can also be inferred from (2.13) and (2.17) that comfort depends on σ_q or σ_q^2 , σ_p or σ_p^2 , σ_r or σ_r^2 , but the weighting of these factors in the equations indicates that the relative importance of the linear accelerations is greater. It has also been seen that if the comfort rating, C, is reduced then comfort increases according to the rating scale. In other words, comfort increases when normal and lateral accelerations are reduced. From (2.7) it can be seen that if a policy of minimizing the normal acceleration is adopted then the R.D.I. is minimized resulting in better ride. The same result could be expected for a R.D.I. for lateral motion. Such an index has not yet been proposed but the general principle of minimizing acceleration to improve ride quality has been adopted for lateral motion in this research. The need for minimization of the acceleration levels becomes greater in the presence of atmospheric turbulence where as may be seen from (2.2) the intensity of the acceleration is directly proportional to the intensity of turbulence. From the above discussion and also from Section 2.1 where general STOL aircraft characteristics were presented, it is obvious that for such aircraft a ride quality control system may be included with advantage to provide comfort to the pilot and passengers by reducing the lateral and normal accelerations which are produced by the controlled aircraft.

2.5 ACTIVE CONTROL AS MEANS OF IMPROVING RIDE QUALITY

With the advances of science and technology higher targets for the performance, life, etc. of an aircraft developed the concept of multi-variable aircraft control systems. In order to fulfil these requirements a considerable amount of research has been carried out in recent years in the fields of modern mathematics. The products of this research resulted in new methods of approach and analysis for multivariable control systems. The use of multi-input, multi-output control theories in automatic flight control systems has made it feasible to apply the concept of Active Control Technology (A.C.T.) in the design of a modern aircraft.

Active control technology could be defined (McLean [1978]) as the use of an automatic flight control system to drive simultaneously many control surfaces and auxiliary direct generators of force or moment to dynamically improve both the flight characteristics and the structural behaviour of the aircraft.

Therefore, the purpose of A.C.T. is to provide, in conjunction with advanced electronic technology and control theory, the potential to improve the performance and the operational flexibility of an aircraft.

It is generally agreed that the most significant improvement in aircraft performance and structural behaviour can be achieved by using any or all of six major A.C.T. functions:

1. Relaxed Static Stability (R.S.S.)
2. Manoeuvre Load Control (M.L.C.)
3. Fatigue Control (F.R.)
4. Ride Control (R.C.)
5. Flutter Mode Control (F.M.C.)
6. Gust Load Alleviation (G.L.A.)

The benefits which may result from applying these A.C.T. functions are dependent on several aircraft parameters. The only function which is considered beneficial, independent of the speed range of the aircraft, is Ride Control. The effectiveness of a ride control system designed for an aircraft depends on two major factors:

1. Selection of appropriate aerodynamic control surface configuration
2. Design of control system

In the past most of the ride control systems designed for STOL aircraft have used conventional control theory and employed direct lift control (D.L.C.) for normal acceleration control. D.L.C. is defined as the use of an independent, fast response high lift control surface(s) which in conjunction with conventional controls such as elevator may achieve direct control on the lift forces acting on the aircraft.

For longitudinal ride control the most appropriate lift control point is direct lift control located on the wing, since gust induced change in wing lift is the main contributor for poor longitudinal ride. As a result most of the ride control systems employing D.L.C. use spoilers or flaps on the upper surface or the trailing wing of the aircraft respectively. Most of the longitudinal ride control systems that have been developed in recent years for STOL aircraft have employed D.L.C. action in conjunction with the elevator. (Holloway et al [1972], Oehman [1973], Gordon and Dotson [1973], Lallman [1974], Jacobson and Lapins [1977], etc.). Some other studies consider only flap elements for longitudinal ride control (Stewart [1975], Ekerlens and Schuring [1975] etc.). In nearly all these studies, which employ conventional control theory to obtain the control

law and its feedback elements, normal acceleration and pitch rate have been used as the feedback signals.

For lateral ride control the most appropriate control surface is the rudder since the fin is the greatest source of laterally induced accelerations. Most of the studies for lateral ride control for STOL aircraft use rudder with feedback of yaw angle (or yaw rate) and lateral acceleration. An important point raised by Gordon and Dotson [1973] from their studies on a lateral ride control system for a DH-6 Twin Otter was the following:

"A lateral force surface located near the c.g. would be required to achieve the design goal".

This statement implies the need for a direct sideforce generator to provide direct sideforce control (D.S.F.C.). Jacobson and Lapins [1977] have employed a sideforce generator (on a Jetstar aircraft). It was located near the c.g. of the aircraft and the lateral ride control system involved its use together with the rudder. In this research the aerodynamic control surface schemes were chosen to consist of elevator, spoilers and horizontal canards for longitudinal ride control and rudder, aileron and vertical canards for lateral ride control. The use of all the mentioned auxiliary force and moment generators implies a control configured vehicle (C.C.V.) which, by making use of active control technology will attempt to improve ride quality. Assuming the availability of an onboard computers modern control theory may be used to derive the control scheme to drive the control surface configuration. Before dealing with the feedback control laws required from the C.C.V. aircraft some insight into the control action of the considered control surfaces will be given in the following Sections 2.6 and 2.7.

2.6 LONGITUDINAL RIDE CONTROL

In the preceding Section 2.5 some aerodynamic control surface configurations which have been used in the past for longitudinal ride quality control on STOL aircraft were presented.

In this research three control surfaces for longitudinal ride control were examined. These were the elevator, spoilers and horizontal canards. All the control surface configurations resulting from any possible combination of these controls were examined. In order to show the relative importance of each of these control surfaces in terms of its D.L.C. effectiveness on normal acceleration the following analysis is employed. (Pinsker [1968]).

2.6.1 Direct Lift Control Analysis

Assume an aircraft to be equipped with a control system which applies a control lift $L(\delta)$ at an effective moment arm x_δ with respect to the centre of gravity (c.g.). The incidence generated lift $L(\alpha)$ acts at the aerodynamic centre which is located at a distance x_n from the c.g. This distance defines the c.g. margin, k_n , by

$$k_n = - \frac{x_n}{\bar{c}} = - \frac{C_{M_\alpha}}{C_{L_\alpha}} \quad (2.19)$$

where \bar{c} is the mean chord and C_{M_α} and C_{L_α} are the non-dimensional coefficients of pitching moment and lift due to angle of incidence respectively. Using the above notation and the lift slopes

$$C_{L_\alpha} = \frac{\partial C_L}{\partial \alpha}, \quad C_{L_\delta} = \frac{\partial C_L}{\partial \delta} \quad (2.20)$$

The equations for steady longitudinal motion can be written as:

$$C_{L_\alpha} \frac{x_\alpha}{\bar{c}} \alpha + m_q \frac{c}{U} q + C_{L_\delta} \frac{x_\delta}{\bar{c}} \delta = 0 \quad (2.21)$$

$$\frac{\rho}{2} U^2 S \{C_{L_\alpha} \alpha + C_{L_\delta} \delta\} = m g n \quad (2.22)$$

where

$$m_q = \frac{\partial C_M}{\partial \left(\frac{q\bar{c}}{U}\right)} \quad (2.23)$$

and is known as the pitch damping derivative. Also,

n : is the load factor.

In this analysis only increments with respect to level flight are considered and so C_{L_q} can be ignored.

With the following kinematic relationship,

$$q = \frac{n}{U} g \quad (2.24)$$

(2.21) and (2.22) can be solved for

$$\frac{dn}{d\delta} = C_{L_\delta} \frac{\rho U^2}{2W/S} \frac{\frac{x_\alpha}{\bar{c}} - \frac{x_\delta}{\bar{c}}}{\frac{x_\alpha}{\bar{c}} + \frac{m}{\mu}} \quad (2.25)$$

where

$$\mu = \frac{2m}{\rho S \bar{c}} \quad (2.26)$$

and is known as the relative density.

The distance $(x_\delta - x_\alpha)$ is the distance of the aerodynamic centre (a.c.) of the control lift from the a.c. of the aircraft. This control lift moment arm has the characteristic of being independent of the c.g. position and after division by the mean chord, \bar{c} , takes the non-dimensionalized form,

$$k_\delta = \frac{x_\alpha - x_\delta}{\bar{c}} \quad (2.27)$$

This margin is defined in the same way as the conventional margins of longitudinal stability theory being positive if the control lift acts aft the a.c. of the aircraft. Figure 2.4 illustrates a relative position of the margins k_n, k_δ and H_m which is the manoeuvre margin and is defined as,

$$H_m = - \frac{x}{c} \frac{q}{\alpha} = - \frac{m}{\mu} q \quad (2.28)$$

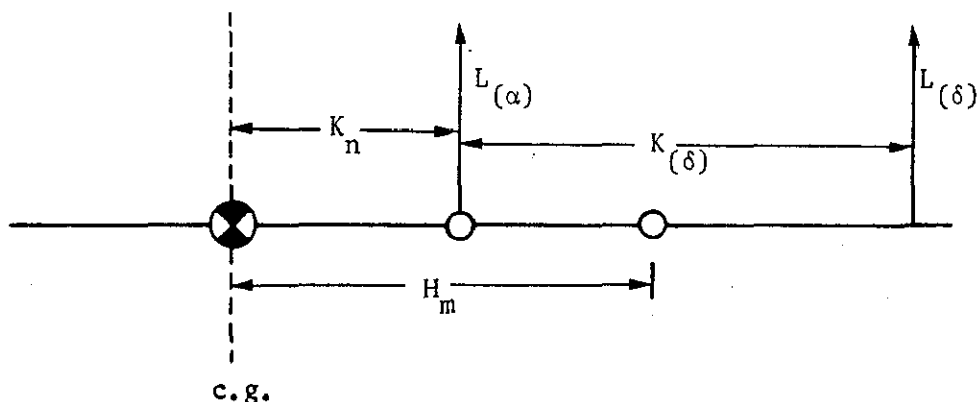


FIGURE 2.4: Definition of longitudinal static stability and control margins

(2.25) can be rewritten as

$$\frac{n}{\delta} = - C_{L_\delta} \frac{\rho U^2}{2W/S} \frac{k_\delta}{H_m} \quad (2.29)$$

The above equation is generally applicable whether the aircraft is controlled by a conventional elevator or horizontal canards or spoilers.

The initial response in normal acceleration to a step application of control is given by

$$\frac{n_0}{\delta} = C_{L_\delta} \frac{\rho U^2}{2W/S} \quad (2.30)$$

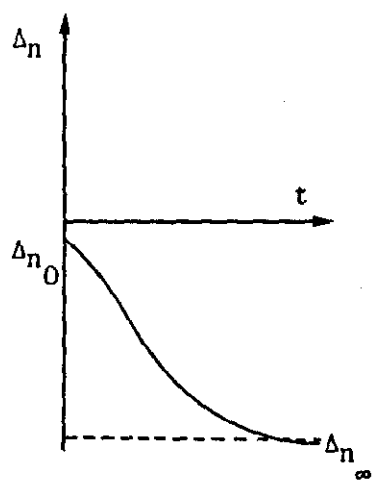
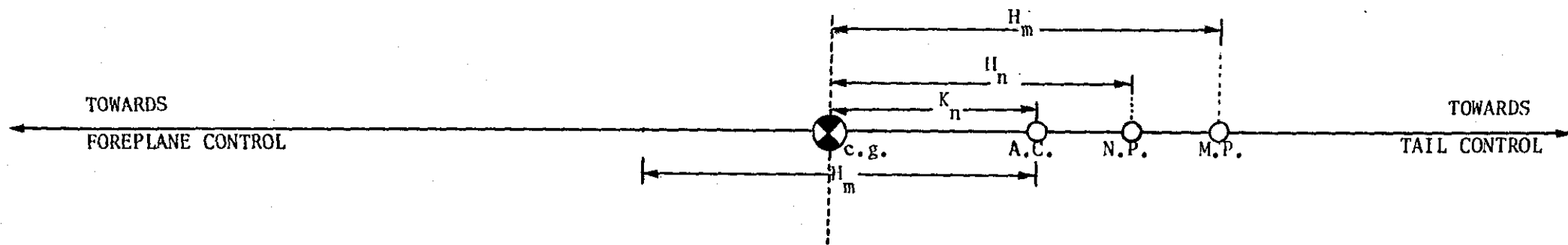
dividing (2.29) by (2.30):

$$\frac{n}{n_0} = - \frac{k_\delta}{H_m} \quad (2.31)$$

From (2.31) it can be seen that the ratio (k_δ/H_m) defines an amplification of the steady final normal acceleration to the initial value. Holding the short period dynamics of an aircraft, with damping factor as a constant, and varying the control moment arm, k_δ , to cover the whole spectrum from conventional elevator to spoilers and horizontal canards control the normal acceleration responses of the aircraft are given in Figure 2.5.

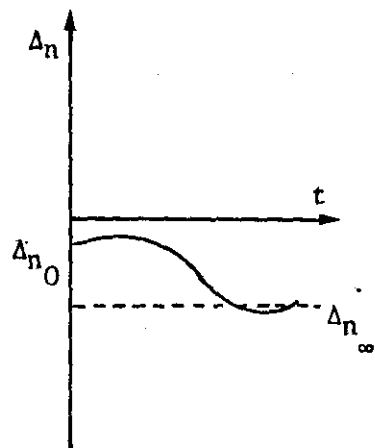
Considering some typical cases illustrated in Figure 2.5 for different positions of the controller the following conclusions may be obtained:

- (i) For $k_{\delta} \gg H_m$. This is the case of the rear elevator or moving tailplane. The steady final response is much longer and in the opposite sense to, the initial response. If the elevator moment arm is sufficiently large the initial adverse response will be hardly noticeable and for all practical purposes the control can be treated as a pure pitching-moment generator.
- (ii) $k_{\delta} = 0$. The control lift acts at the aerodynamic centre of the aircraft. The steady manoeuvring response is zero, which means that apart from imparting an initial lift impulse to the aircraft, the control is unable to control normal acceleration.
- (iii) $k_{\delta} = -H_m$. This is the condition for 'pure' direct lift control. The initial n commanded by the control is identical to the steady response. It can be said that the pilot has practically instantaneous control over lift. All the lift commanded by the pilots control is generated by the control mechanism without utilizing the potential of the aircraft to produce lift via incidence, even as long term response. Aerodynamically this is not attractive in flight conditions where performance and hence economy is determined by maximum available lift.
- (iv) $(-k_{\delta}) > H_m$. If the control lift acts further forward than $-H_m$, the initial direct control lift will be further amplified by the incidence response of the aircraft. Although this is not the ideal form of direct lift control, it will still have the advantage of a large

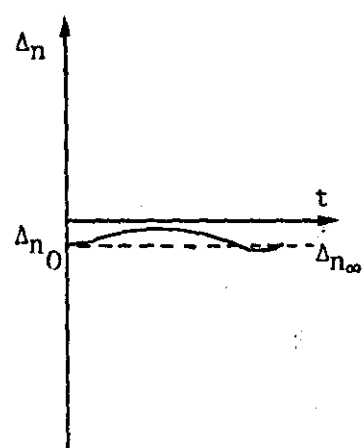


$$K_\delta \ll (-H_m)$$

Foreplane Control

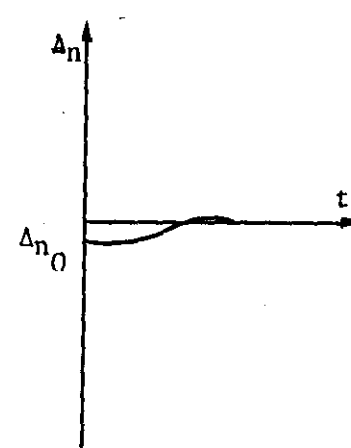


$$K_\delta < (-H_m)$$



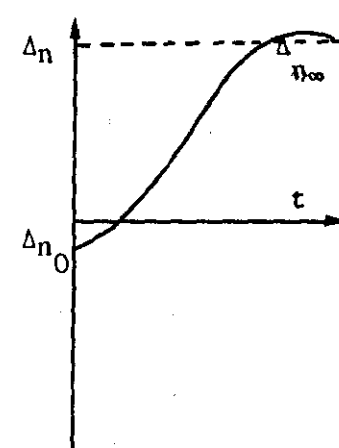
$$K_\delta = -H_m$$

Pure Direct Lift Control



$$K_\delta = 0$$

Direct Lift Control Acting at the Aerodynamic Centre



$$K_\delta \gg H_m$$

Conventional Tail Control

FIGURE 2.5: Change of Aircraft Control Characteristics with Location of Centre of Control Lift

immediate response to control and better lift utilization for sustained manoeuvres. This is in fact the most attractive regime for a practical direct lift control system.

- (v) $(-k_{\delta}) \gg H_m$. This case represents control lift acting a long way ahead of the aerodynamic centre of the aircraft, achieved typically with horizontal canards. The direct lift contribution to the aircraft response is now relatively small, but favourable. The response shows the same general characteristics as that of a conventionally controlled aircraft. The major portion of the lift commanded by the control is derived from change in incidence and the development of this lift is governed by the pitch response characteristic of the aircraft.

In the foregoing analysis the relative direct lift control characteristics of the elevator, spoilers and horizontal canards were obtained. However, it is important to emphasize that the above results were derived for a large aircraft with sluggish pitch responses, etc. For an executive jet aircraft the situation is not the same. Although the general assessment for the spoiler location will be identical the assessment for the elevator and canards will be different. This arises mainly from the smaller moment arms which a small aircraft possesses compared to those of a large aircraft. Nevertheless the analysis showed the general response characteristics that might be expected from a STOL aircraft and some useful information on the properties of the considered controls was obtained. This information, apart from giving general guidelines for the use of the longitudinal controls and their contribution to D.L.C., is not enough to predetermine their contribution in a dynamic analysis. Hence, in order to

obtain the necessary information on the dynamic responses of the aircraft to these controls, digital simulation should be called upon.

At this stage it is necessary to consider the control surface characteristics chosen for this study in order to represent the spoiler and horizontal canards force and moment coefficients.

2.6.2 Longitudinal Control Surface Configuration

As has been already stated, the aerodynamic control scheme considered for longitudinal ride control consisted of the elevator, spoilers and horizontal canards. The NASA Jetstar is already equipped with an elevator. However this study is not concerned with any design alterations of the original aircraft configuration other than adding auxilliary control surfaces for ride control. Hence, the elevator was considered to be the same with that used so far by the aircraft. However the addition of spoilers and horizontal canards required their specific definition in terms of their location and force and moment coefficients.

2.6.2.1 Spoiler characteristics

Extensive research in recent years has considered the spoilers as a particularly important control surface. Spoilers can be used as effective D,L,C. surfaces for flight path control as well as for reducing normal accelerations imposed on the aircraft. Results to date indicate that very adequate performance can be obtained from certain types of spoiler systems. In addition, the simplicity and light weight of such systems make them particularly attractive for use on light aircraft. From a study of spoilers effectiveness applied to the GA(W)-1 wing (Neuhart and Oetting [1977]) some useful information may be obtained. Figure 2.6 gives

a diagrammatic representation of the type of wing section which was considered in the above study.

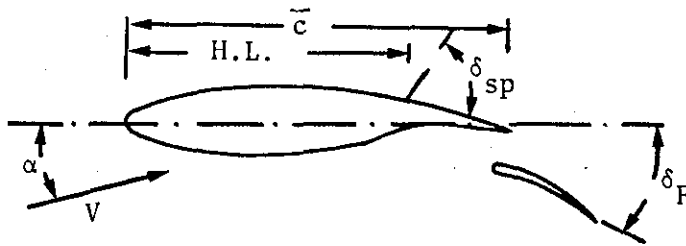


FIGURE 2.6: GA(W)-1 wing geometry

The following graphs were employed in order to show the aerodynamic effectiveness of spoiler. Figures 2.7, 2.8 and 2.9 show the aerodynamic effectiveness of a 15% chord spoiler located at 85% hinge line on the GA(W)-1 wing for angle of incidence $\alpha=0^\circ$.

The lift, drag and moment coefficients for all aerodynamic control surface are given (McRuer, Askenas, and Graham [1973]) by:

$$Z_{\delta} \triangleq \frac{1}{m} \frac{\partial Z}{\partial \delta} = - \frac{\rho U^2 S}{2m} C_{L_{\delta}} \quad (2.32)$$

$$X_{\delta} \triangleq \frac{1}{m} \frac{\partial X}{\partial \delta} = - \frac{\rho U^2 S}{2m} C_{D_{\delta}} \quad (2.33)$$

$$M_{\delta} \triangleq \frac{1}{I_y} \frac{\partial M}{\partial \delta} = \frac{\rho U^2 S \bar{c}}{2I_y} C_{M_{\delta}} \quad (2.34)$$

where $C_{L_{\delta}}$, $C_{D_{\delta}}$ and $C_{M_{\delta}}$ are by definition:

$$C_{L_{\delta}} = \frac{\partial C_L}{\partial \delta} \quad (2.35)$$

$$C_{D_{\delta}} = \frac{\partial C_D}{\partial \delta} \quad (2.36)$$

$$C_{M_{\delta}} = \frac{\partial C_M}{\partial \delta} \quad (2.37)$$

Hence, once ρ, U, S, m, \bar{c} and I_y are known for the specific aircraft the coefficients Z_{δ} , X_{δ} and M_{δ} can be determined if $C_{L_{\delta}}$, $C_{D_{\delta}}$ and $C_{M_{\delta}}$ are known. From Figures 2.7, 2.8 and 2.9 approximate values for $C_{L_{\delta}}$, $C_{D_{\delta}}$ and $C_{M_{\delta}}$ can be given from the slopes of the graphs. Assuming an approximate linear operation of the spoiler from 0° to 30° the above slopes may be found.

Hence, from Figure 2.7

$$C_{L_{\delta SP}} = \frac{\Delta C_L}{\Delta \delta_{SP}} = - \frac{0.54}{0.52} = - 1.03/\text{rad}. \quad (2.38)$$

also, from Figure 2.8

$$C_{D_{\delta SP}} = \frac{\Delta C_D}{\Delta \delta_{SP}} = \frac{.06}{.5} = .12/\text{rad}. \quad (2.39)$$

and from Figure 2.9

$$C_{M_{\delta SP}} = \frac{\Delta C_M}{\Delta \delta_{SP}} = \frac{.065}{.5} = .13/\text{rad}. \quad (2.40)$$

is this
OK or not?

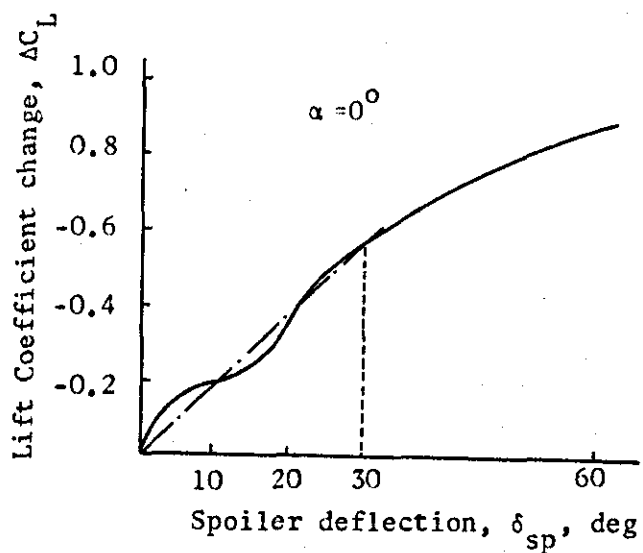


FIGURE 2.7

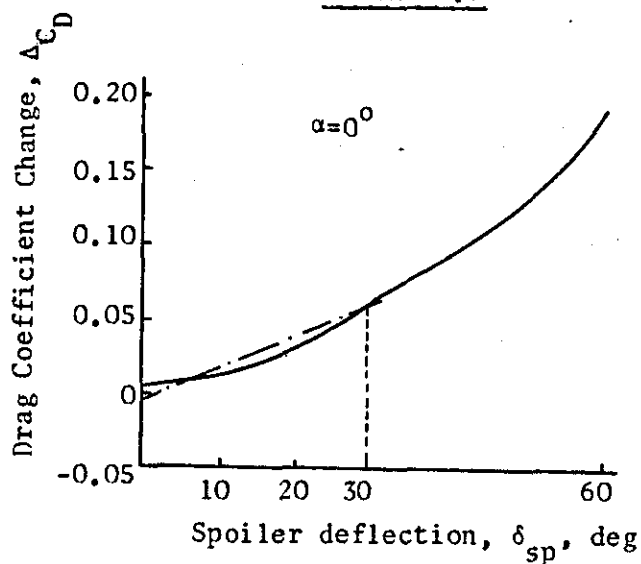


FIGURE 2.8

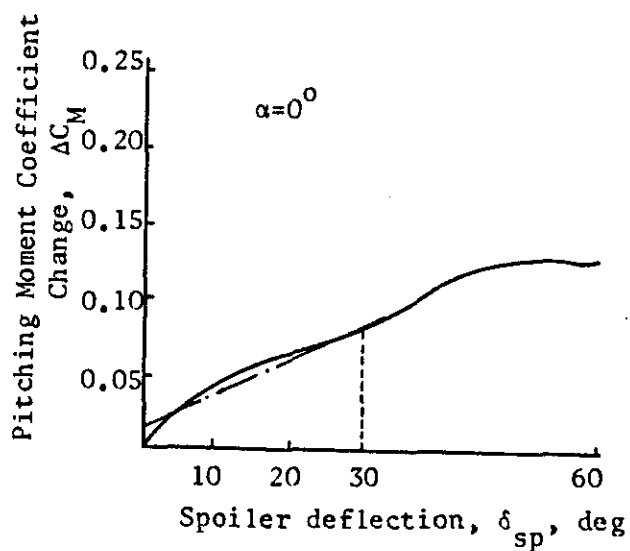


FIGURE 2.9

For Jetstar aircraft flying at sea level conditions the following spoiler coefficients may be obtained from (2.32), (2.33) and (2.34)

$$Z_{\delta_{SP}} = -0.0825S \quad (2.41)$$

$$X_{\delta_{SP}} = 0.0104S \quad (2.42)$$

$$M_{\delta_{SP}} = 0.0006S \quad (2.43)$$

For spoilers effective area of 10ft^2 the above equations result in the following spoiler derivatives:

$$Z_{\delta_{SP}} = -0.825 \quad (2.42) \quad \text{dim.}$$

$$X_{\delta_{SP}} = 0.104 \quad (2.43)$$

$$M_{\delta_{SP}} = 0.006 \quad (2.44)$$

In the absence of specific information from the manufacturers it was assumed that the force and moment derivatives chosen for the simulation of NASA Jetstar would be equivalent to the one-third of the corresponding derivatives for the elevator. The derivatives are given by:

$$Z_{\delta_{SP}} = -5.73 \quad (2.45)$$

$$X_{\delta_{SP}} = .656 \quad (2.46)$$

$$M_{\delta_{SP}} = -.753 \quad (2.47)$$

From comparison of (2.42), (2.43), (2.44) with (2.45), (2.46) and (2.47) it may be deduced that the spoilers chosen for the modified Jetstar appear to be more effective from those studied for the GA(W)-1 wing. However, no direct comparisons can be made since the Jetstar aircraft has a different type of wing. (NACA 63A112 at root and NACA 63A309 at tip).

2.6.2.2 Horizontal canards definition

Horizontal canards have been used in the past for military high performance aircrafts (YF-16, F-4, etc.) as well as supersonic transports (Tupolev 144, etc.). They have been primarily used for D.L.C. offering several options for flight path control (independent fuselage aiming, variable pitch control and vertical translation control). It should be noted, however, that the direct lift capability of horizontal canards does not arise from their effectiveness as lift producers. The canards can generate a considerable nose-up pitching moment (Figure 2.5) which may be trimmed by a trailing edge down horizontal tail deflection. This positive tail deflection for trim contributes a relatively large amount of incremental lift which, when added to the untrimmed canard increment, leads to a significant level of D.L.C. A symmetrical deflection of horizontal canards can be used for D.L.C., pitch control and longitudinal stability augmentation while an antisymmetrical deflection can be used for D.S.F.C. In this research only symmetrical deflection of the horizontal canards was considered and hence they were only used for longitudinal control.

Geometric Dimensions

The effectiveness of the horizontal canards as longitudinal controls depends upon the area and moment arm ratio with the conventional controller which in this case is the elevator. In this study the canards were located at a forward station, FS150, in line with the wing, while the centre of gravity location is at FS478. Hence the moment arm of the canards will be

$$x_{CH} = 478 - 150 = 328 \text{ in} \quad (2.48)$$

The moment arm of the elevator is

$$x_E = -391 \text{ in} \quad (2.49)$$

Also the effective area of the canards was chosen to be one quarter of that of the elevator thus

$$S_{CH} = .25 S_E \quad (2.50)$$

Derivatives

The effective moment generated by the canards is reduced by 0.25 (due to surface areas) and also by ratio of moment arms (328)/(391) with respect to that of the elevator. Therefore

$$X_{\delta_{CH}} = -X_{\delta_E} \left(\frac{1}{4}\right) \left(\frac{328}{391}\right) \quad (2.51)$$

$$Z_{\delta_{CH}} = -Z_{\delta_E} \left(\frac{1}{4}\right) \left(\frac{328}{391}\right) \quad (2.52)$$

$$M_{\delta_{CH}} = -M_{\delta_E} \left(\frac{1}{4}\right) \left(\frac{328}{391}\right) \quad (2.53)$$

The negative sign is arising from the negative moment arm of the elevator.

2.7 LATERAL RIDE CONTROL

In this research three control surface configurations were used for lateral ride control. The aerodynamic control surface configuration for the aircraft was composed of the rudder, ailerons and vertical canard. These controls were examined in terms of their effectiveness in all possible combinations.

2.7.1 Analysis of Lateral Acceleration Constituents

In order to demonstrate, if possible, the relative effectiveness of these controls on the lateral acceleration of the aircraft the following approximate equation of lateral acceleration of the conventional Jetstar (with rudder and ailerons) is employed.

$$a_{y_x} = Y_v v + xN_r r + xN_\beta \beta + (Y_{\delta_R} + xN_{\delta_R}) \delta_R + (xN_{\delta_A}) \delta_A \quad (2.54)$$

where a_{y_x} represents the lateral accelerations as measured at a distance x from the c.g. From (2.54) it can be seen that lateral acceleration is related to many factors. In order to make an estimate of the relative importance of the factors composing the above equation it is necessary to determine the importance and contribution of the coefficients $Y_v, N_r, N_\beta, Y_{\delta_R}, N_{\delta_R}$ and N_{δ_A} . The coefficients Y_v, N_r and N_β are the basic components of the damping and natural frequency of the dutch roll mode while $Y_{\delta_R}, N_{\delta_R}$, and N_{δ_A} determine the effectiveness of the rudder, and aileron.

Role of Y_v

This derivative is given by definition by

$$Y_v = \frac{\partial Y}{\partial v} = \frac{\rho U^2 S}{2} \frac{\partial C_y}{\partial v} = \frac{\rho U S}{2m} C_{y_\beta} \quad (2.55)$$

where

$$C_{y_\beta} = \frac{\partial C_y}{\partial \beta} \quad (2.56)$$

The major portion of C_{y_β} comes from the vertical tail. It is usually negative in sign and contributes substantially to the total damping.

Role of N_β

$$N_\beta = \frac{\rho U^2 S b}{2I_z} C_{n_\beta} \quad (2.57)$$

C_{n_β} is the "weather-cock" stability. The major portion of C_{n_β} comes from the vertical tail area and lever arm. It is very important for lateral dynamic characteristics and positive values of C_{n_β} signify static directional stability. High values of C_{n_β} aid the pilot in effecting coordinated turns and prevents excessive sideslip and yawing motions. In turbulence high values of C_{n_β} magnify disturbances from side gusts.

Role of N_r

$$N_r = \frac{\rho U S b^2}{4I_z} C_{n_r} \quad (2.58)$$

C_{n_r} is known as the 'yaw damping derivative'. The major contribution to this derivative comes from the vertical tail. C_{n_r} is desirable to be negative in sign and is proportional to the square of the tail level arm. It is the main contributor to the damping of the dutch roll mode and also is important to the spiral mode.

Role of Y_{δ_R}

$$Y_{\delta_R} = \frac{\rho U^2 S}{2m} C_{y_{\delta_R}} \quad (2.59)$$

$C_{y_{\delta_R}}$ effects are relatively unimportant in lateral stability and control, except when considering lateral acceleration feedback to an autopilot.

Role of N_{δ_R} and N_{δ_A}

These derivatives signify the effectiveness of the rudder and aileron as yawing moment generators.

From (2.54) it can be seen that for a specific manoeuvre reduction of a_{y_x} can be achieved if the absolute values of Y_v, N_r and N_β are reduced. To achieve the reduction of these derivatives the vertical tail size should be reduced ^{not necessarily (515m)} since all these derivatives are strongly influenced from this factor. Reducing the vertical tail size acceleration reduction will result but the dynamic characteristics of the aircraft are likely to be degraded. Minimization of N_β, Y_v and N_r will affect dutch roll, spiral mode characteristics and probably lateral static stability. Although for some studies (R.H. Lange et al [1975]) etc. minimization of the vertical tail size was of primary interest and stability augmentation systems were used to augment the lateral dynamic characteristics of the aircraft, here no attempt was made to change the original design of the aircraft other than to add auxiliary controls to improve ride. Therefore Y_v, N_β and N_r were regarded fixed in this research. However reduction of the lateral acceleration can be achieved by appropriate treatment of the coefficients of the control deflections. Inspection of the coefficients $(Y_{\delta_R} + xN_{\delta_R})$ and (xN_{δ_A}) of δ_R and δ_A respectively indicates that the rudder coefficient is most dominant by being larger. Even for small rudder deflections the rudder will dominate the lateral acceleration expression. The effectiveness of aileron is insignificant compared to that of the rudder. The need of a third control surface capable of controlling directional stability and effective enough to counterbalance little use of the rudder control is evident. The most appropriate control surface for this task is the vertical

canard. A small vertical canard located at a forward point of the fuselage would probably be able to share the work required from the rudder with less penalty on the lateral acceleration. The use of vertical canard would modify (2.54) as follows:

$$a_{y_x} = Y_v v + xN_r r + xN_\beta \beta + (Y_{\delta_R} + xN_{\delta_R}) \delta_R + (xN_{\delta_A}) \delta_A + (xN_{\delta_{CV}}) \delta_{CV} \quad (2.60)$$

From the preceding discussion it is apparent that no definite conclusions about possible favourable effectiveness of an auxiliary vertical canard can be drawn. It is therefore a matter of experimental investigation to assess the effectiveness of vertical canard and as such digital simulation is the most attractive means. Before embodying the vertical canard on the aircraft it is first necessary to define its dimensions so that its force and moment derivatives will be possible to be evaluated.

2.7.2 Vertical Canard Definition

Vertical canard has been employed on a very small number of aircraft and mainly on military (B-52, YF-16, F-4 and others). It can be used for D.S.F.C. offering several options for directional control (independent fuselage, azimuth control, variable yaw control and lateral translation control). The D.S.F.C. effectiveness arises from the rudder trimming of the yawing moment produced by the vertical canard. The vertical canard chosen for this research had a small surface area compared to the rudder and it was located underneath the fuselage and at the same forward station as horizontal canards.

Geometric dimensions

The vertical canard was located at a distance of 27.3ft forward of the centre of gravity. The area of the vertical canard was chosen to be

equivalent to .125 of that of the rudder. Hence,

$$S_{CV} = .125 S_R \quad (2.61)$$

Hence all the moments generated by the vertical canard will be 0.125 those generated by the rudder. However the moments generated depend upon the moment arms. The moment arm for the canard is +328.0" and for the rudder -391.0". Hence the moments generated by the same deflection of the canard will be further reduced (with respect to rudder values) by $-\frac{328}{391}$ i.e. for a given deflection the moments generated by the surfaces will act in opposite directions.

According to the above discussion the canard derivatives will be given as follows

$$Y_{\delta CV}^* = - Y_{\delta R}^* \left(\frac{1}{8}\right) \left(\frac{328}{391}\right) \quad (2.62)$$

$$L_{\delta CV}' = - L_{\delta R}' \left(\frac{1}{8}\right) \left(\frac{328}{391}\right) \quad (2.63)$$

$$N_{\delta CV}' = - N_{\delta R}' \left(\frac{1}{8}\right) \left(\frac{328}{391}\right) \quad (2.64)$$

2.8 EQUATIONS OF MOTION

The equations of motions of the Jetstar aircraft were formulated based on the assumptions that the longitudinal and lateral motions of the aircraft were uncoupled derived by using small perturbation theory, the aircraft was trimmed and that the aircraft behaved as a rigid body aircraft (i.e. no elastic modes of the aircraft were considered). The atmospheric turbulence components acting on the aircraft were also considered in the state space representation of the equations of motion.

The following state equation was employed to describe the longitudinal and lateral motions of the aircraft:

$$\dot{\underline{x}} = \underline{A}\underline{x} + \underline{B}\underline{u} + \underline{G}\underline{\eta} \quad (2.65)$$

where

\underline{x} is the n-dimensional state vector

\underline{u} is the m-dimensional control input vector

$\underline{\eta}$ is the s-dimensional gust input vector

A is an n×n state coefficient matrix

B is an n×m control input coefficient matrix

and G is an n×s gust input coefficient matrix.

2.8.1 Longitudinal Equations of Motion

The perturbed longitudinal equations of motion of the modified Jetstar for body axis system can be written in the form of (2.65) as follows:

$$\begin{bmatrix} \dot{u} \\ \dot{w} \\ \dot{q} \\ \dot{\theta} \end{bmatrix} = \begin{bmatrix} X_u & X_w & 0 & -g \\ Z_u & Z_w & u_0 & 0 \\ M_u & M_w & M_q & 0 \\ 0 & 0 & 1 & 0 \end{bmatrix} \begin{bmatrix} u \\ w \\ q \\ \theta \end{bmatrix} + \begin{bmatrix} X_{\delta E} & X_{\delta SP} & X_{\delta CH} \\ Z_{\delta E} & Z_{\delta SP} & Z_{\delta CH} \\ M_{\delta E} & M_{\delta SP} & M_{\delta CH} \\ 0 & 0 & 0 \end{bmatrix} \begin{bmatrix} \delta E \\ \delta SP \\ \delta CH \end{bmatrix} \\
 + \begin{bmatrix} -X_u & -X_w \\ -Z_u & -Z_w \\ -M_u & -M_w \\ 0 & 0 \end{bmatrix} \begin{bmatrix} u_g \\ w_g \end{bmatrix} \quad (2.66)^\dagger$$

The output normal acceleration at a distance x from the c.g. of the aircraft is given by

$$a_{z_x} = \ddot{w} - u_0 \dot{q} - x \cdot \ddot{q} \quad (2.67)$$

2.8.2 Lateral Equations of Motion

The lateral equations of motion of the modified Jetstar aircraft for body axis system can be written for primed stability derivatives in the form of (2.65) as follows:

$$\begin{bmatrix} \dot{\beta} \\ \dot{p} \\ \dot{r} \\ \dot{\phi} \\ \dot{\psi} \end{bmatrix} = \begin{bmatrix} Y_v & 0 & -1 & g/u_0 & 0 \\ L'_\beta & L'_p & L'_r & 0 & 0 \\ N'_\beta & N'_p & N'_r & 0 & 0 \\ 0 & 1 & 0 & 0 & 0 \\ 0 & 0 & 1 & 0 & 0 \end{bmatrix} \begin{bmatrix} \beta \\ p \\ r \\ \phi \\ \psi \end{bmatrix} +$$

[†]The term $-[M_w - (M_q/u_0)]\dot{w}_g$ was not shown in (2.66) since it is a small quantity. However, this quantity was included in the simulation of the Jetstar aircraft flight in turbulence.

$$+ \begin{bmatrix} Y'_{\delta_R} & Y'_{\delta_{CV}} & 0 \\ L'_{\delta_R} & L'_{\delta_{CV}} & L'_{\delta_A} \\ N'_{\delta_R} & N'_{\delta_{CV}} & N'_{\delta_A} \\ 0 & 0 & 0 \\ 0 & 0 & 0 \end{bmatrix} \begin{bmatrix} \delta_R \\ \delta_{CV} \\ \delta_A \end{bmatrix} + \begin{bmatrix} -Y'_v \\ -L'_\beta \\ -N'_\beta \\ 0 \\ 0 \end{bmatrix} \beta_g \quad (2.68)^\dagger$$

The output lateral acceleration at a fuselage station at x distance from the c.g. is given by the following equation:

$$a_{y_x} = \dot{v} - g\phi + u_0 r + x \cdot \dot{r} \quad (2.69)$$

[†]The terms $-L'_r \dot{\beta}_g$ and $-N'_r \dot{\beta}_g$ were not included in (2.68) for simplicity since it would be required to define the gust equations which are derived later in Chapter 3. Both these factors were considered in the simulation.

CHAPTER 3

MODELLING OF ATMOSPHERIC TURBULENCE

3.1 INTRODUCTION

The environment in which an aircraft operates is the source of all loads applied to it. When an aircraft flies through atmospheric turbulence it absorbs some of the energy in that turbulence field. Any turbulence field may be characterised by its velocity and that velocity can be decomposed into orthogonal components. It is the vertical and lateral components, i.e. those normal to the flight path, which produce loads on the aircraft. If the turbulence were known precisely the aircraft loads could be predicted from that knowledge, provided, of course, that the aerodynamic properties of the aircraft were also known. However, the atmosphere is in a state of continuous excitation, and, as a result, its motion is best described if it is approximated to a random process. Fortunately enough data have been obtained in recent years to permit an adequate understanding of the basic structure of atmospheric turbulence.

According to Von Karman (Von Karman [1937]), atmospheric turbulence may be considered to be a continuous, random, physical process which varies in three-dimensional space. In order to account for the statistical properties of the atmosphere the American authorities have adopted for the motion of the aircraft certain assumptions of linearity so that atmospheric turbulence may be defined by means of power spectral density (P.S.D.) functions. The power spectrum model is concerned both with the energy in relatively long patches of turbulence, and with its description with respect to wavelength. The aircraft response is then evaluated on the assumption of "Statistical equilibrium" between excitation and response. To introduce turbulence effects into any flight control study requires some simplification of the mathematical form representing

the turbulence. Before outlining the method of P.S.D. analysis it is important to indicate the assumptions made to ensure that the theory of representing turbulence in this way remains valid.

Assumptions

When atmospheric turbulence has to be accounted for it is generally considered acceptable to neglect the interaction with the main air flow, but even then only the simplest models are possible. The physical properties of the turbulence are identified over volumes chosen to be sufficiently small so that they are reasonably uniform.

The assumptions used in this study are:

- (a) Turbulence is homogeneous

The assumption of homogeneity implies that the statistical properties of turbulence are the same at each point in the field.

- (b) Turbulence is isotropic

Isotropy implies that the intensity of all three components of velocity, viz, u, w, v , are equal. This assumption implies that:

$$\sigma_{u_g} = \sigma_{v_g} = \sigma_{w_g} \quad (3.1)$$

where the σ_i are root mean square (r.m.s.) values. Isotropy also means that both the cross-correlation and cross-spectra between the three components vanish. Hence

$$\phi_{uv_g} = \phi_{uw_g} = \phi_{vw_g} = 0 \quad (3.2)$$

This property ensures that the statistical properties of turbulence are unaffected by any translation, reflexion or rotation of the axes used to define the three-dimensional space. By using this assumption

turbulence may be described relative to the body fixed axis system of the aircraft, which, in this study was the stability-axes set.

(c) Turbulent field is "frozen"

In traversing the velocity field of turbulence, any variations with time are statistically equivalent to any variations with distance. In other words the statistical characteristics of the disturbance input to an airplane flying through a turbulent field are not appreciably affected by the variation of that field with time; that is to say that turbulence may be treated as though it has a pattern "frozen" in space. This is often referred to as Taylor's hypothesis (Taylor [1937]).

Based on these assumptions a theory of the behaviour of the intensity and scale of turbulence may be described as a distribution of energy with an appropriate wavelength. Then two models commonly referred to in aviation literature as the Dryden model and Von Karman model, are first derived and then transformed into the frequency domain so that the P.S.D. analysis can be carried out. At the end of this chapter it is explained how the Dryden model can be used to generate atmospheric turbulence in a digital simulation.

3.2 ANALYTICAL REPRESENTATION OF TURBULENCE

Over the intervals of time and space which are of interest, the velocity field of the turbulence may be regarded as comprising a steady velocity mean value with a turbulent fluctuation superimposed.

When an aircraft penetrates turbulence the energy that it absorbs can be described in terms of the root mean square (r.m.s.) values of the velocities and the amplitude of these fluctuations. The feature that distinguishes one patch of atmospheric turbulence from another is the total turbulence intensity, σ , which may be defined as the kinetic energy of turbulence per unit mass of air. Thus:

$$\sigma^2 = \int_0^{\infty} \phi(k) dk \quad (3.3)$$

where $\phi(k)$ is the energy distribution of turbulence. The argument, k , is the inverse of the wavelength, λ , of the turbulence. The description of the kinetic energy of the turbulence in terms of wavelength, λ , is employed in order to represent the distribution of turbulence in terms of distance. The concept of inverse wavelength, k , is nothing more than a mathematical treatment of turbulence describing the frequency of appearance of a particular wavelength per unit length of travel. (It is similar to the frequency used in the frequency domain analysis). Note that (3.3) results in r.m.s. values of velocity which are twice the value of the kinetic energy per unit mass. (3.3) is therefore equivalent to the definition of the r.m.s. intensity of a random signal described in terms of its power and frequency, viz.

$$\sigma^2 = \int_0^{\infty} \phi(\omega) d\omega \quad (3.4)$$

The autocorrelation function of the turbulence velocity for two points x and $x+r$ along the x -axis is defined (Von Karman and Howarth [1938]) as:

$$R_{u_g}(r) = \overline{u(x)u(x+r)/u_g^2(x)} \quad (3.5)$$

where

$$\overline{u_g(x)u_g(x+r)} = \lim_{T \rightarrow \infty} \frac{1}{T} \int_0^T u_g(x)u_g(x+r)dr \quad (3.6)$$

$R_{u_g}(r)$ describes the degree in which the velocity $u_g(x)$ at point x is correlated to the velocity $u_g(x+r)$ at point $x+r$. From the conventional definition of autocorrelation function for a random stationary process and from its relationship to the P.S.D. function it can be deduced using (3.5) that

$$\phi_{u_g}(k) = 4\sigma_{u_g}^2 \int_0^{\infty} R_{u_g}(r) \cos(2\pi kr) dr \quad (3.7)$$

$$\phi_{w_g}(k) = 4\sigma_{w_g}^2 \int_0^{\infty} R_{w_g}(r) \cos(2\pi kr) dr \quad (3.8)$$

It has been shown (Von Karman and Howarth [1938]) that for incompressible flow

$$R_{w_g}(r) = R_{u_g}(r) + r/2 \frac{d}{dr} R_{u_g}(r) \quad (3.9)$$

When analytical functions are used to describe the energy density they will include a parameter which has the dimension of length and it will be proportional to the scale of the turbulence. The actual value of that scale may be chosen to be λ^\dagger , so that the quantity $k\phi(k)$ is a maximum, or it may be chosen for purely analytical convenience.

The turbulence scale length can be defined as

$$L = \int_0^{\infty} R_{u_g}(r) dr \quad (3.10)$$

or alternatively as

$$L = 2 \int_0^{\infty} R_{w_g}(r) dr \quad (3.11)$$

When the scale of turbulence is large compared with the aircraft

[†] $k = \lambda^{-1}$

surface being loaded the turbulence velocity may be assumed over the whole surface to be the same at any instant. The one-dimensional energy density for lateral turbulence $\phi_{lg}(k)$ is then applied. In the one-dimensional case the distance r will be in the direction of either $-x$ or $-y$ only.

It can be shown (Taylor [1965]) that the autocorrelation functions, $R_{ug}(r)$ and $R_{wg}(r)$, can be described as follows

$$R_{ug}(r) = [(r/a)^n / 2^{n-1} (n-1)!] k_n(r/a) \quad (3.12)$$

and

$$R_{wg}(r) = [(r/a)^n / 2^n (n-1)!] [2k_n(r/a) - (r/a)k_{n-1}(r/a)] \quad (3.13)$$

where

a and n are parameters governing the shape and scale of the above expressions;

k_n are Bessel functions with an imaginary argument

$(n-1)!$ are gamma functions when n is not a positive integer.

Substituting (3.12) and (3.13) in (3.10) and (3.11) and also using (3.9) the scale of turbulence is given by

$$L = [\sqrt{\pi}(n - \frac{1}{2})! / (n-1)!] a \quad (3.14)$$

The energy density functions for turbulence velocities both longitudinal and lateral, for the one-dimensional case are then obtained from (3.7) and (3.8). The solutions then reduce to:

$$\phi_{ug}(k) = 4\sigma_{ug}^2 L / (1 + 4\pi^2 a^2 k^2)^{n+1/2} \quad (3.15)$$

and

$$\phi_{wg}(k) = 2\sigma_{wg}^2 L [1 + 8\pi^2 a^2 k^2 (n+1)] / [1 + 4\pi^2 a^2 k^2]^{n+3/2} \quad (3.16)$$

where

$$a = [(n-1)! / \sqrt{\pi}(n - \frac{1}{2})!] L \quad (3.17)$$

(3.15) and (3.16) give the energy distributions in terms of the scale turbulence, L , and a shape parameter, n . By assigning values to n a

range of shapes may be obtained. If n is selected as $1/2$ the resulting formula is identical to the empirical model proposed by Dryden [1938]. When n is equal to $1/3$ then the model is identical to that proposed later by Von Karman, (Von Karman [1948]).

DRYDEN MODEL

When n is chosen as $1/2$ then from (3.17),

$$a = L \quad (3.18)$$

Hence,

$$\phi_{u_g}(k) = 4\sigma_{u_g}^2 L / [1 + (2\pi kL)^2] \quad (3.19)$$

and

$$\phi_{w_g}(k) = 2\sigma_{w_g}^2 L [1 + 3(2\pi kL)^2] / [1 + (2\pi kL)^2]^2 \quad (3.20)$$

Since it was assumed in Section 3.1 that the gust field was isotropic then it follows that:

$$\phi_{v_g}(k) \equiv \phi_{w_g}(k) \quad (3.21)$$

VON KARMAN MODEL

When n is selected as $1/3$, then, from (3.17),

$$a = [1.3399]L \quad (3.22)$$

Thus,

$$\phi_{u_g}(k) = 4\sigma_{u_g}^2 L / [1 + \{2\pi(1.339L)k\}^2]^{5/6} \quad (3.23)$$

and

$$\phi_{v_g}(k) = \phi_{w_g}(k) = 2\sigma_{w_g}^2 L [1 + 8/3\{2\pi(1.339L)k\}^2] / [1 + \{2\pi(1.339L)k\}^2]^{11/6} \quad (3.24)$$

3.3 POWER SPECTRAL ANALYSIS

The analytical method of using P.S.D. functions to determine the response of an aircraft to atmospheric turbulence has evolved through a continual effort to account more precisely for the unpredictable nature of gusts. P.S.D. analysis is often more effective in determining the true nature of aircraft response to turbulence than using a discrete gust model.

The form of mathematical model used to represent gusts in the digital simulation program, employed in this work, was derived from the P.S.D. method.

3.3.1 Power Spectral Density Function, $\phi(\omega)$

The power spectral density of any function, $x(t)$, is a real function which describes the distribution of the mean square value (m.s.v.) of $x(t)$ with frequency.

Any point on the graph of P.S.D. versus frequency represents the m.s.v. of $x(t)$ at some frequency within an infinitely narrow band centred about a particular frequency, ω . The P.S.D. function, $\phi(\omega)$, may be expressed as:

$$\phi(\omega) = \lim_{T \rightarrow \infty} \frac{|F(\omega)|^2}{T} \quad (3.25)$$

where $F(\omega)$ is the Fourier transform of the function $x(t)$ and it is defined as

$$F(\omega) = \int_{-T}^T x(t) e^{-j\omega t} dt \quad (3.26)$$

The m.s.v. of $x(t)$ can be obtained by integrating the P.S.D., $\phi(\omega)$, over all positive frequencies, viz.

$$\overline{x^2(t)} = \int_0^{\infty} \phi(\omega) d\omega \quad (3.27)$$

Thus, the square root of the area under the power spectrum curve is a measure of the root mean square (r.m.s.) value.

Typical power spectra of atmospheric turbulence are shown in Figure 3.1.

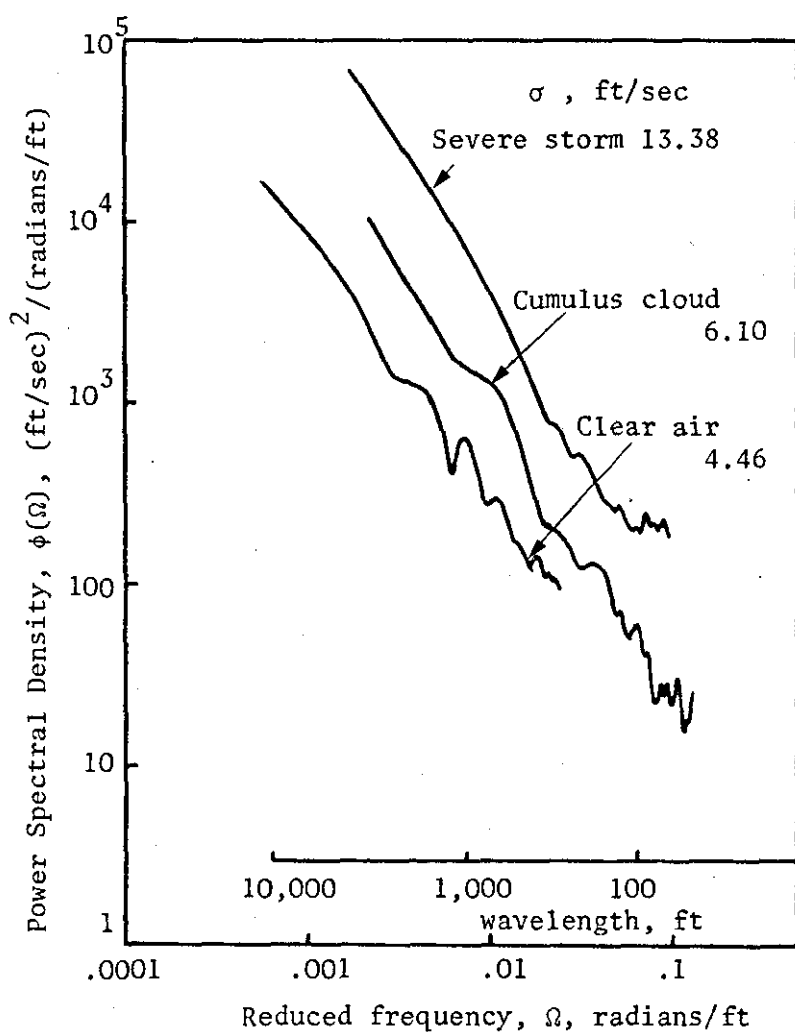


FIGURE 3.1: Typical Power Spectra of Vertical Gust Velocity

To remove the effects of variations in flight speed from one analysis to another, power spectra of the atmosphere are calculated on the basis of a spatial frequency, defined as:

$$\Omega = \frac{\omega}{u_0} \quad (3.28)$$

where u_0 is the relative speed of the airflow. The relation between the original and the transformed power spectra is given by

$$\phi(\omega) = \frac{1}{u_0} \phi(\Omega) \quad (3.29)$$

Spatial frequency (or wavenumber), Ω , can also be represented in terms of inverse wavelength, k , in the following way

$$\Omega = 2\pi k \quad (3.30)$$

which results in the linear transformation

$$\phi(k) = 2\pi \phi(\Omega) \quad (3.31)$$

Combining (3.28) with (3.30) and also (3.29) with (3.31) yields the relationships

$$k = \frac{\omega}{2\pi u_0} \quad (3.32)$$

and

$$\phi(k) = 2\pi u_0 \phi(\omega) \quad (3.33)$$

Using (3.32) and (3.33) the Dryden and Von Karman models can be represented by power density functions. (3.32) and (3.33) transform (3.19,20) and (3.23,24) into the following:

Dryden Model

$$\phi_{u_g}(\omega) = \sigma_{u_g}^2 \left(\frac{L_u}{\pi u_0} \right) \left(\frac{1}{1 + \left(\frac{L_u \omega}{u_0} \right)^2} \right) \quad (3.34)$$

$$\phi_{w_g}(\omega) = \sigma_{w_g}^2 \left(\frac{L_w}{\pi u_0} \right) \left(\frac{1 + 3(L_w \omega / u_0)^2}{[1 + (L_w \omega / u_0)^2]^2} \right) \quad (3.35)$$

Since it was assumed (section 3.1) that the gust field was isotropic then

$$\phi_{v_g}(\omega) = \sigma_{v_g}^2 \left(\frac{L_v}{\pi u_0} \right) \left(\frac{1+3(L_v \omega/u_0)^2}{[1+(L_v \omega/u_0)^2]^2} \right) \quad (3.36)$$

Von Karman Model

$$\phi_{u_g}(\omega) = \frac{2\sigma_w^2 L_v}{\pi u_0} \frac{1}{[1+\{1.339L_u \omega/u_0\}^2]^{5/6}} \quad (3.37)$$

$$\phi_{w_g}(\omega) = \frac{\sigma_w^2 L_w}{\pi u_0} \frac{[1+8/3(1.339L_w \frac{\omega}{u_0})^2]}{[1+\{1.339L_w \frac{\omega}{u_0}\}^2]^{11/6}} \quad (3.38)$$

similar expression to (3.38) can be used to represent $\phi_v(\omega)$ as in Dryden Model.

Since α and β are sometimes used in aircraft analysis rather than w and v the following conversions can be used

$$\phi_{\alpha_g}(\omega) = \frac{1}{u_0} \phi_{w_g}(\omega) \quad (3.39)$$

and

$$\phi_{\beta_g}(\omega) = \frac{1}{u_0} \phi_{v_g}(\omega) \quad (3.40)$$

3.3.2 Computer Simulation of Atmospheric Turbulence

This section presents an account of how atmospheric turbulence can be directly implemented in the digital simulation and how the effects upon the behaviour of the simulated model representing the aircraft can be incorporated.

3.3.2.1 Signal Transmission in Linear Systems

Figure 3.2 illustrates a general linear system which is completely described by its weighting function $h(t)$ relating the input $x(t)$ to the output $y(t)$

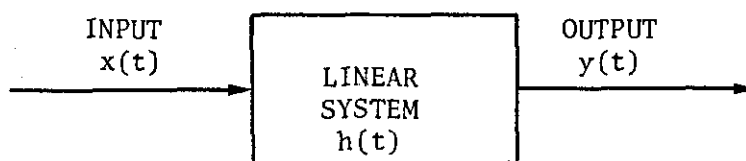


FIGURE 3.2: Block diagram of linear system

If $x(t)$ is a stochastic signal, the output $y(t)$ will be also a stochastic signal.

From the definition of convolution integral

$$y(t) = \int_{-\infty}^{\infty} dt_1 h(t_1) x(t-t_1) \quad (3.41)$$

and

$$y(t+\tau) = \int_{-\infty}^{\infty} dt_2 h(t_2) x(t+\tau-t_2) \quad (3.42)$$

By definition of the autocorrelation function, viz.

$$\phi_{xx}(\tau) = \lim_{T \rightarrow \infty} \frac{1}{2T} \int_{-T}^T dt y(t) y(t+\tau) \quad (3.43)$$

It can be shown (Newton, Gould, Kaiser [1957]) by using (3.41), (3.42)

and (3.43) that

$$\phi_{yy}(\tau) = \int_{-\infty}^{\infty} dt_1 h(t_1) \int_{-\infty}^{\infty} dt_2 h(t_2) \phi_{xx}(\tau+t_1-t_2) \quad (3.44)$$

Multiplying (3.44) both sides by $e^{-s\tau}$ and integrating over the infinite

range in τ yields the following Fourier transform

$$\int_{-\infty}^{\infty} d\tau e^{-s\tau} \phi_{yy}(\tau) = \int_{-\infty}^{\infty} d\tau e^{-s\tau} \int_{-\infty}^{\infty} dt_1 h(t_1) \int_{-\infty}^{\infty} dt_2 h(t_2) \phi_{xx}(\tau+t_1-t_2) \quad (3.45)$$

Now $e^{-s\tau}$ can be written as

$$e^{-s\tau} = e^{-s(\tau+t_1-t_2)} \cdot e^{st_1} \cdot e^{-st_2} \quad (3.46)$$

Therefore (3.45) becomes

$$\int_{-\infty}^{\infty} d\tau e^{-s\tau} \phi_{yy}(\tau) = \int_{-\infty}^{\infty} dt_1 e^{st_1} h(t_1) \int_{-\infty}^{\infty} dt_2 e^{-st_2} h(t_2) \int_{-\infty}^{\infty} d\tau e^{-s(\tau+t_1-t_2)} \phi_{xx}(\tau+t_1-t_2) \quad (3.47)$$

Employing the definitions of power spectral densities for the input and output signals in terms of the autocorrelation functions then

$$\phi_{xx}(s) \triangleq \frac{1}{2\pi} \int_{-\infty}^{\infty} d\tau e^{-s\tau} \phi_{xx}(\tau) \quad (3.48)$$

and

$$\phi_{yy}(s) \triangleq \frac{1}{2\pi} \int_{-\infty}^{\infty} d\tau e^{-s\tau} \phi_{yy}(\tau) \quad (3.49)$$

In other words the power spectral density of a signal is the Fourier transform of the autocorrelation function of the signal. Therefore, in view of (3.48) and (3.49), (3.47) becomes

$$\phi_{yy}(s) = H(-s)H(s)\phi_{xx}(s) \quad (3.50)$$

where $H(-s)$ and $H(s)$ are the Fourier transforms of the weighting functions $h(t_1)$ and $h(t_2)$. For real frequencies (3.50) becomes

$$\phi_{yy}(j\omega) = H(-j\omega)H(j\omega)\phi_{xx}(s) \quad (3.51)$$

For any realisable system the real part of the system function is an even function of frequency and the imaginary is an odd function of frequency. Thus $H(-j\omega)$ is the conjugate of $H(j\omega)$ and their product

is the square of the magnitude of $H(j\omega)$. Thus (3.51) can be written as

$$\phi_{yy}(j\omega) = |H(j\omega)|^2 \phi_{xx}(j\omega) \quad (3.52)$$

When the input to the linear filter is white noise then the P.S.D. function $\phi_{xx}(j\omega)=1$ and (3.52) becomes

$$\phi_{yy}(j\omega) = |H(j\omega)|^2 \quad (3.53)$$

3.3.2.2 Digital Simulation of the Dryden Model

As has already been shown, when the input to a filter is white noise, then the output power spectral density is related to the transfer function of the filter according to (3.53). Alternatively it could be said that if the power spectrum of the output function is known then the transfer function needed to produce the required output characteristics is also known provided only that the input spectrum is known. Since the power spectrum for white noise is unity then, when it is used as input, the required transfer function can be easily derived.

It has already been shown that for homogeneous, isotropic turbulence which satisfies Taylor's hypothesis, the power spectral density is known and it can be expressed mathematically. The frequency distributions of the gust spectra are described usually by the Dryden form of P.S.D., which approaches asymptotically to a constant value according to the -2 power of frequency, for high spatial frequencies (Ω). The Dryden form is relatively easy to simulate on a computer while that form proposed by Von Karman is very difficult to simulate due to its non-integer exponents.

Therefore employing the Dryden model to generate a simulated atmospheric turbulence, and combining equations (3.53) and (3.35), the following relationship is obtained

$$|H_{w_g}(s)|^2 = |kG_{w_g}(s)|^2 = (\sigma_{w_g}^2) \left(\frac{L_w}{\pi u_0} \right) \left(\frac{1+3(L_w \omega/u_0)^2}{[1+(L_w \omega/u_0)^2]^2} \right) \quad (3.54)$$

where k can be regarded as a scaling factor of the white noise and is defined as

$$k = \sigma_{w_g} \sqrt{\frac{L_w}{\pi u_0}} \quad (3.55)$$

To derive the transfer function of the model the following equation is used

$$|G(s)|^2 = G(s) G(-s) \quad (3.56)$$

from which $G_{w_g}(s)$ takes the following form

$$G_{w_g}(s) = \frac{1+(\sqrt{3} L_w/u_0)s}{\{1+(L_w/u_0)s\}^2} \quad (3.57)$$

Since digital simulation works in the time domain, it is necessary to re-express (3.57). By introducing the p -operator ($p = \frac{d}{dt}$), (3.57) can be rewritten as

$$G_{w_g}(p) = \frac{1+(\sqrt{3} L_w/u_0)p}{\{1+(L_w/u_0)p\}^2} \quad (3.58) \quad \begin{array}{l} \text{how to} \\ \text{simulate} \end{array}$$

The following block diagram shows the ideal situation for the digital simulation of atmospheric turbulence represented by a Dryden model.

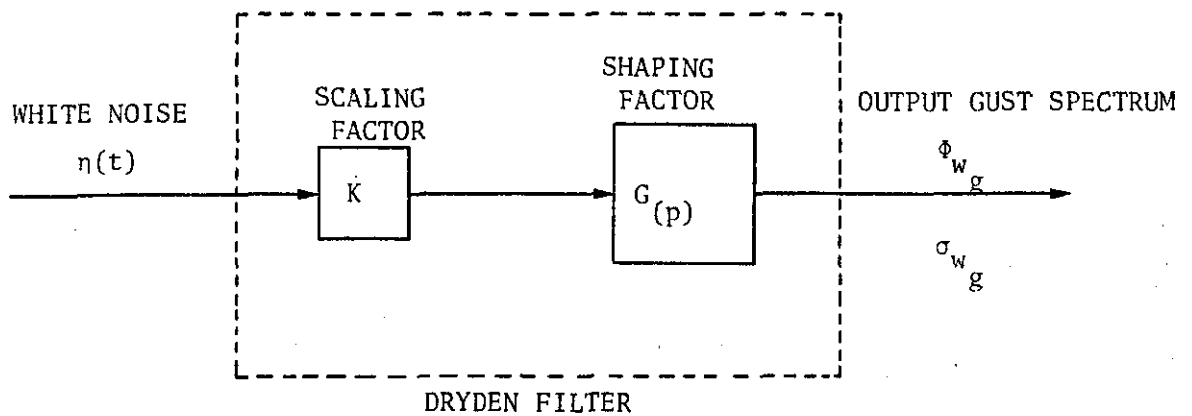


FIGURE 3.3: Ideal situation for turbulence simulation

Since white noise is a signal with a spectral content constant over an infinite frequency range it is impossible to produce in practice because it would require infinite power. However, it is possible to generate an approximation to white noise. Most noise generators produce a signal that is "approximately" white and Gaussian, that is, they have a flat frequency spectrum characteristic similar to white noise but only over a finite range of frequency. The pseudo-random number generator is a noise generator used in digital computer simulations. It consists of a program which produces numbers by using as a parameter a stream variable. Each time the sampling function is called the current value of the stream variable is operated on by a random number procedure to produce the next value in the sequence and a new value of the stream variable. For each separate stream variable an independent sequence of random numbers is produced.

The noise generator is called pseudo-random because the sequence of numbers produced is not truly random for it will repeat if run long enough. In most digital random number generators the program generates

the same sequence of random numbers each time unless a different sequence of the stream variable parameter is used. This was found to be very helpful during the simulation because in this way the results could be compared.

In this work a normal distribution noise generator was used in order to represent the noise input distribution.

The following block diagram shows how the Dryden model was used in the computer simulation.

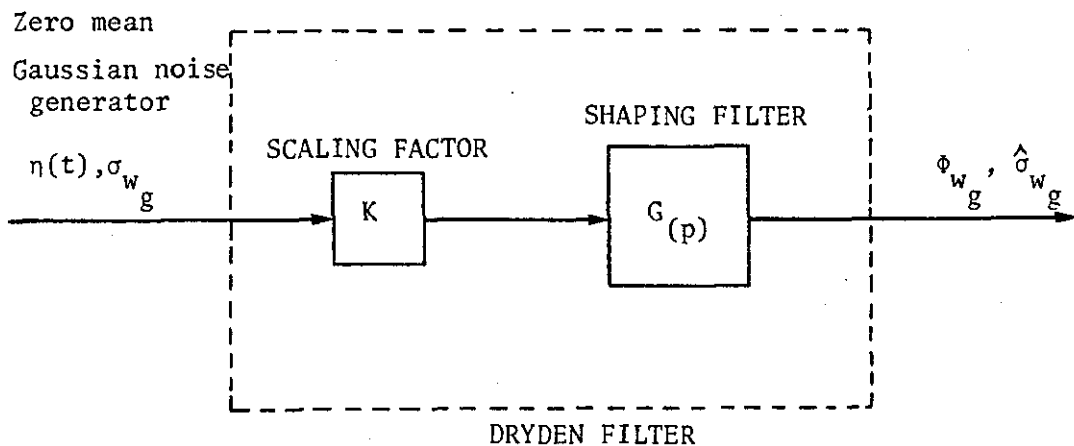


FIGURE 3.4: Actual simulation situation

According to the above presentation it can be seen that if the standard deviation of the Gaussian noise input is equal to the predicted r.m.s. value of the output variable then because of its multiplication with k which contains the expected r.m.s. value of the output signal (σ_{wg}) the final output r.m.s. value will vary according to a relationship of the form

$$\hat{\sigma}_{wg} \propto \sigma_{wg}^2 \quad (3.59)$$

This effect has been shown when the r.m.s. values of the output variables for different standard deviations of the input noise were plotted. The result was a parabolic relationship (Figure 3.5,3.6).

So far the model of atmospheric turbulence does not degrade the assumptions of homogeneity, isotropy and of the 'frozen' velocity field once all these were embodied in the power spectral density representation. A question arises about the fourth assumption made which assumes that the process describing the gusts is Gaussian. However, an important property of Gaussian variables is that "a linear combination of Gaussian random variables is also a Gaussian random variable". Thus the fourth assumption is valid.

Because the equations of motion describing the dynamic behaviour of the aircraft are most conveniently represented for simulation purposes in the state variable form, it becomes appropriate to express the dynamics of the Dryden filter in the same form.

State Representation of Dryden Model

According to (3.54), (3.55) and (3.57) the transfer function of the filter representing the normal to the flight path gust velocity $H_{wg}(s)$ can be defined as

$$H_{wg}(s) = k_1 \frac{(s+b)}{(s+a)^2} \quad (3.60)$$

where

$$\left. \begin{aligned} k_1 &= \sigma_{wg} \sqrt{\frac{3u_0}{\pi L_w}} \\ a &= u_0/L_w \\ b &= u_0/\sqrt{3} L_w \end{aligned} \right\} \quad (3.61)$$

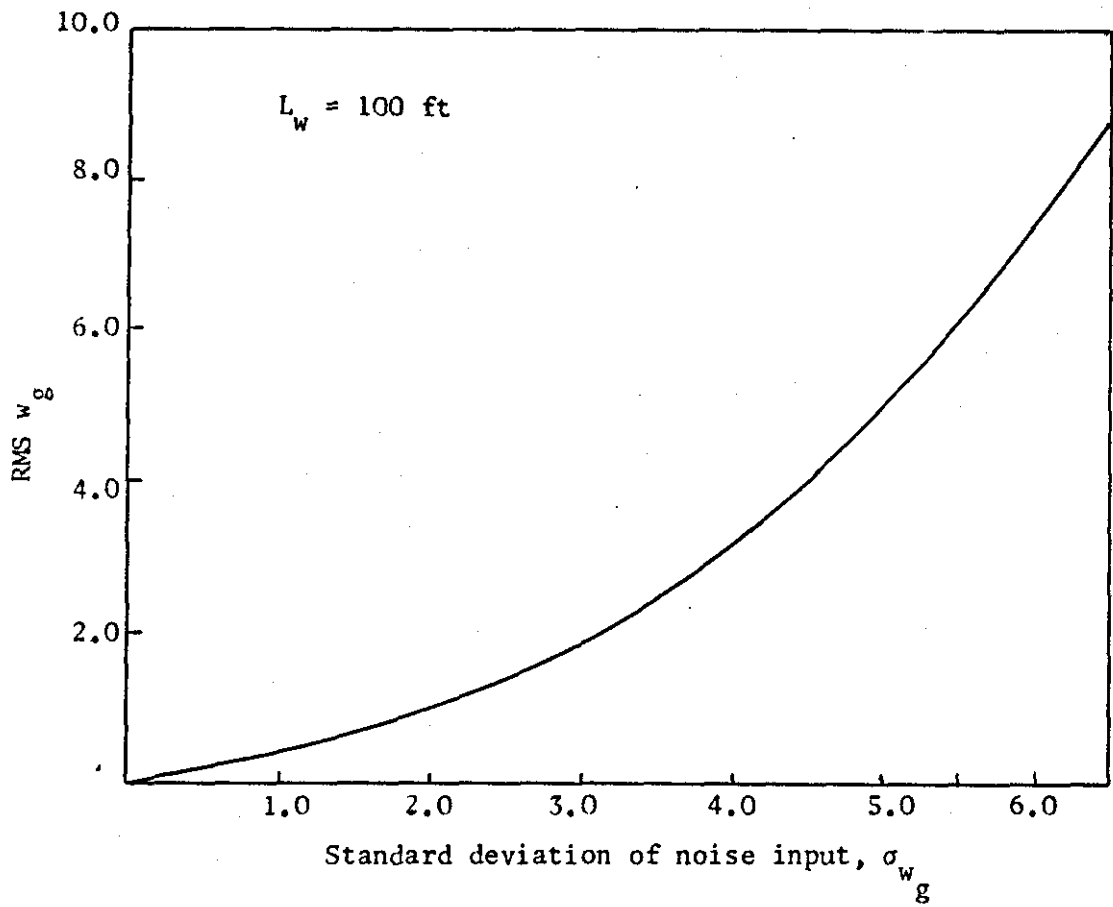


FIGURE 3.5: RMS w_g against σ_{w_g}

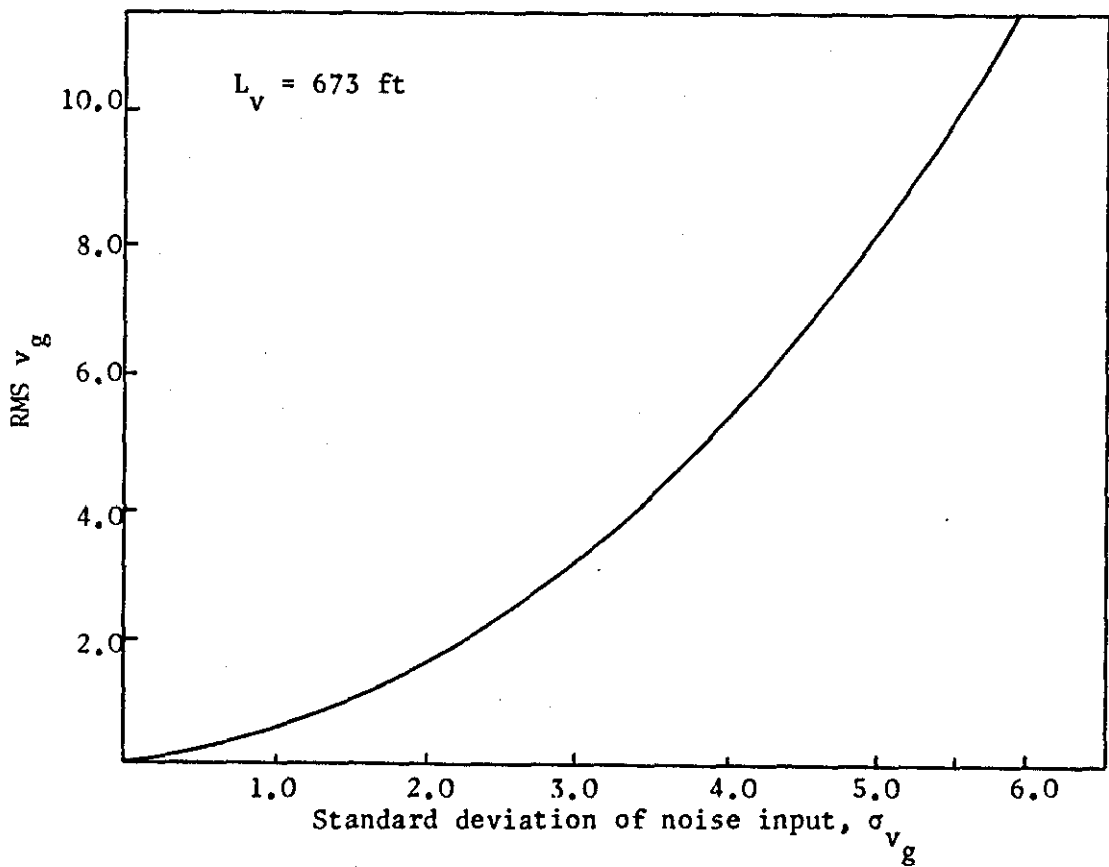


FIGURE 3.6: RMS v_g against σ_{v_g}

Then $H_{wg}(s)$ can be expanded by partial fractions:

$$H_{wg}(s) = k_1 \left[\frac{1}{s+a} + \frac{b-a}{(s+a)^2} \right] \quad (3.62)$$

(3.62) represents the transfer function of the following system

$$\dot{\underline{x}} = \begin{bmatrix} -a & 1 \\ 0 & -a \end{bmatrix} \underline{x} + \begin{bmatrix} 0 \\ 1 \end{bmatrix} n \quad (3.63)$$

$$w_g = k_1 [(b-a) \cdot 1] \underline{x} \quad (3.64)$$

Then

$$\dot{w}_g = k_1(b-a)\dot{x}_1 + k_1\dot{x}_2 \quad (3.65)$$

$$= -aw_g + k_1(b-a)x_2 + k_1 n \quad (3.65)$$

Let

$$\underline{x} = \begin{bmatrix} x_2 \\ w_g \end{bmatrix} \quad (3.66)$$

Then

$$\begin{bmatrix} \dot{x}_2 \\ \dot{w}_g \end{bmatrix} = \begin{bmatrix} -a & 0 \\ k_1(b-a) & -a \end{bmatrix} \begin{bmatrix} x_2 \\ w_g \end{bmatrix} + \begin{bmatrix} 1 \\ k_1 \end{bmatrix} n \quad (3.67)$$

In a similar manner the state representation of the transfer function,

H_{β_g} , can be obtained thus

$$H_{\beta_g}(s) = \frac{\sigma_v \beta_g}{u_0} \sqrt{\frac{L_v}{\pi u_0}} \frac{(1 + \frac{\sqrt{3}L_v}{u_0} s)}{(1 + \frac{L_v}{u_0} s)^2} \quad (3.68)$$

Therefore

$$\begin{bmatrix} \dot{x}_2 \\ \dot{\beta}_g \end{bmatrix} = \begin{bmatrix} -a' & 0 \\ k'(b'-a') & -a' \end{bmatrix} \begin{bmatrix} x_2 \\ \beta_g \end{bmatrix} + \begin{bmatrix} 1 \\ k' \end{bmatrix} n \quad (3.69)$$

where

$$\left. \begin{aligned} k' &= \frac{\sigma_{vg}}{u_0} \sqrt{\frac{3u_0}{\pi L_V}} \\ a' &= u_0/L_V \\ b' &= u_0/\sqrt{3} L_V \end{aligned} \right\} (3.70)$$

With the Dryden model defined for the simulation it remains only to decide upon the flight conditions to be used so that appropriate values of the scale length, L , and the gust intensity, σ , may be specified.

Selection of L and σ_{ig}

The flight conditions of the transport aircraft used for this research are assumed to be relating to a straight and level flight at low altitude and moderate speed. According to Taylor's theory (1937) the scale of turbulence can be regarded as constant for an isotropic environment for small intervals of time. A table giving the scale of turbulence L as a function of altitude is given here (R. Heath [1972])

$h(\text{ft})^\dagger$	L_w	L_V	L_u
$h > 1750$	1750	1750	1750
$100 < h \leq 1750$	h	$145h^{1/3}$	$145h^{1/3}$
$h < 100$	100	$145h^{1/3}$	$145h^{1/3}$

*. For $h=100\text{ft}$, $L_w=100\text{ft}$ and $L_V=673\text{ft}$.

These scale lengths were used when the vertical and horizontal turbulence models were employed. The choice of σ_{wg} and σ_{vg} was based on probability

[†]Since height is expressed in feet it has been appropriate in the work to use the scale length in feet

density curves. For vertical component of gust a choice of $\hat{\sigma}_{wg} = 7.6$ was made which, according to Figure 3.7, corresponds to a probability density of 6×10^{-3} . The lateral intensity $\hat{\sigma}_{vg}$, corresponding to the same probability density was found to be equal to 8.4ft/s. The values of $\hat{\sigma}_{wg}$ and $\hat{\sigma}_{vg}$ corresponded to noise standard deviations of 6.0 and 5.0 which were obtained from Figure 3.5 and Figure 3.6 respectively. The values chosen for the vertical and lateral r.m.s. components correspond to moderate-to-heavy turbulence.

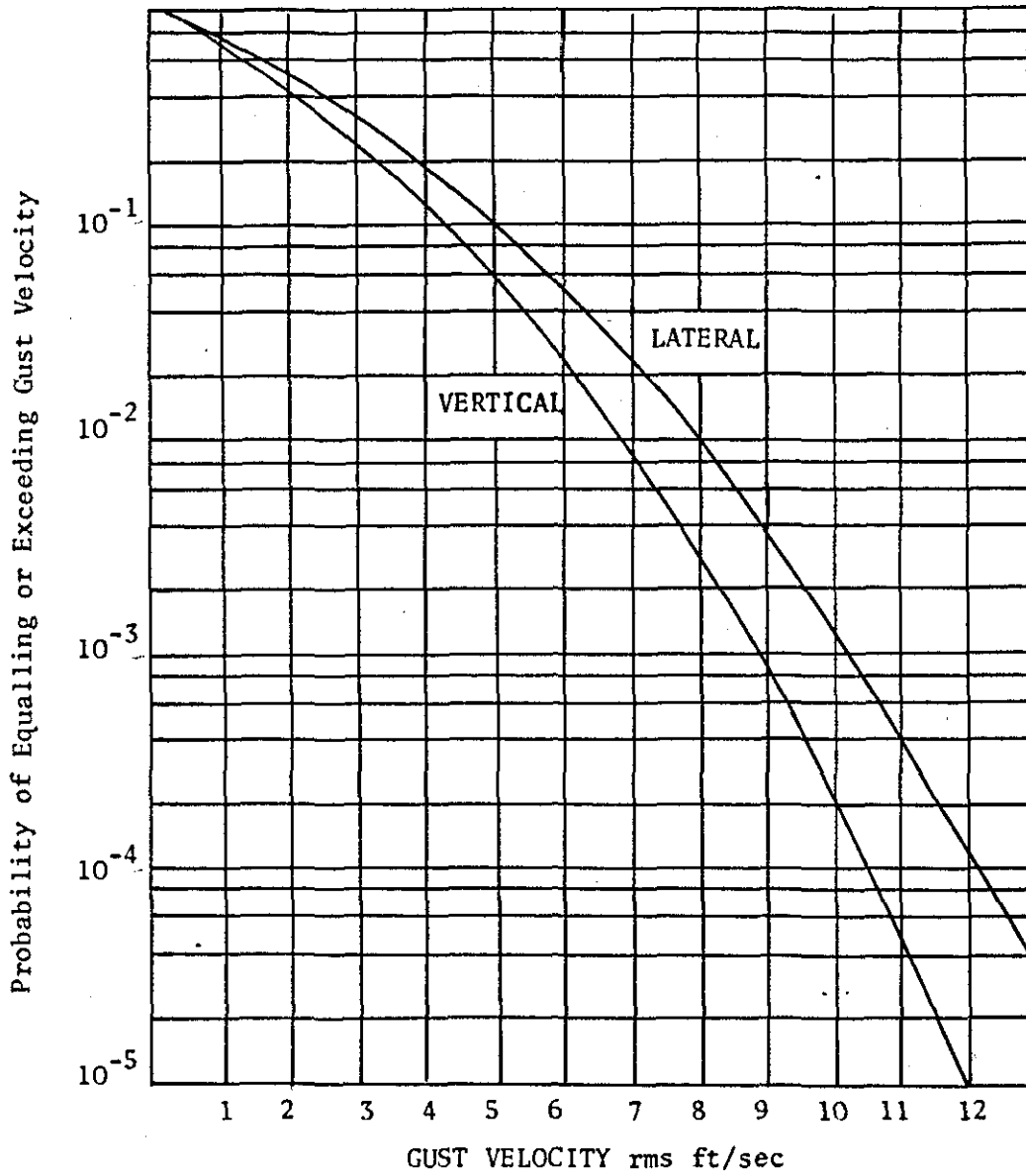


FIGURE 3.7: Probability of Equalling or Exceeding Gust Velocity

3.4 SOME CONCLUDING NOTES

In this chapter it has been demonstrated how atmospheric turbulence may be described by means of models based upon power spectral densities. It was also shown how atmospheric turbulence can be directly implemented in digital simulation by means of the Dryden filter, which is the most convenient way to simulate continuous atmospheric turbulence.

A noise generator was used to generate a pseudo-random number sequence with a zero mean Gaussian probability distribution. The output of this generator was fed to a particular Dryden filter to shape the random signal appropriately to represent those components of atmospheric turbulence which were regarded as being important for the simulation. To simplify the representation of atmospheric turbulence, only the vertical (w_g) and lateral (β_g) components of atmospheric turbulence were incorporated in the simulation. The other components of atmospheric turbulence were not considered because they were regarded as being comparatively insignificant.[†]

In this section a short account of this technique will be presented together with the simulation results obtained for the components of atmospheric turbulence which were considered to be important.

3.4.1 Relative significance of u_g , p_g , r_g and q_g

The significance of the u_g component of atmospheric turbulence for an aircraft dynamics could be judged from the resulting effect which it has on the longitudinal motion of the aircraft. Since u_g is the component of atmospheric turbulence acting along the x-axis of an aircraft (for body

[†]*The relative amplitude of these other components was sufficiently small for this assumption to be acceptable.*

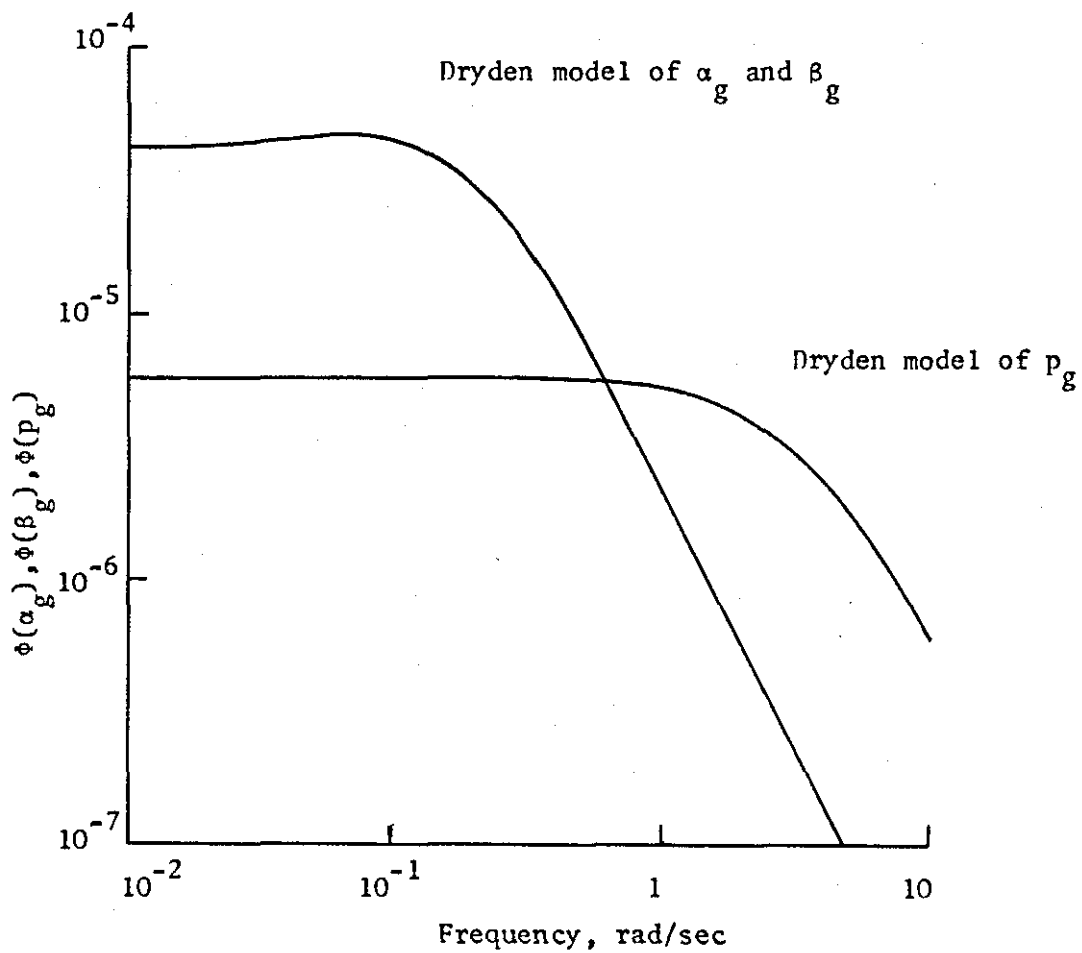


FIGURE 3.8: Comparison of $\phi(\alpha_g)$, $\phi(\beta_g)$ and $\phi(p_g)$

axis system) its significance may be estimated from the resulting induced drag variation in terms of the weight of the aircraft. It is possible to show (Houbolt [1972]) that the drag-to-weight variation due to the contribution of u_g is very small compared to that due to the flying speed of the aircraft. Hence, u_g may be ignored.

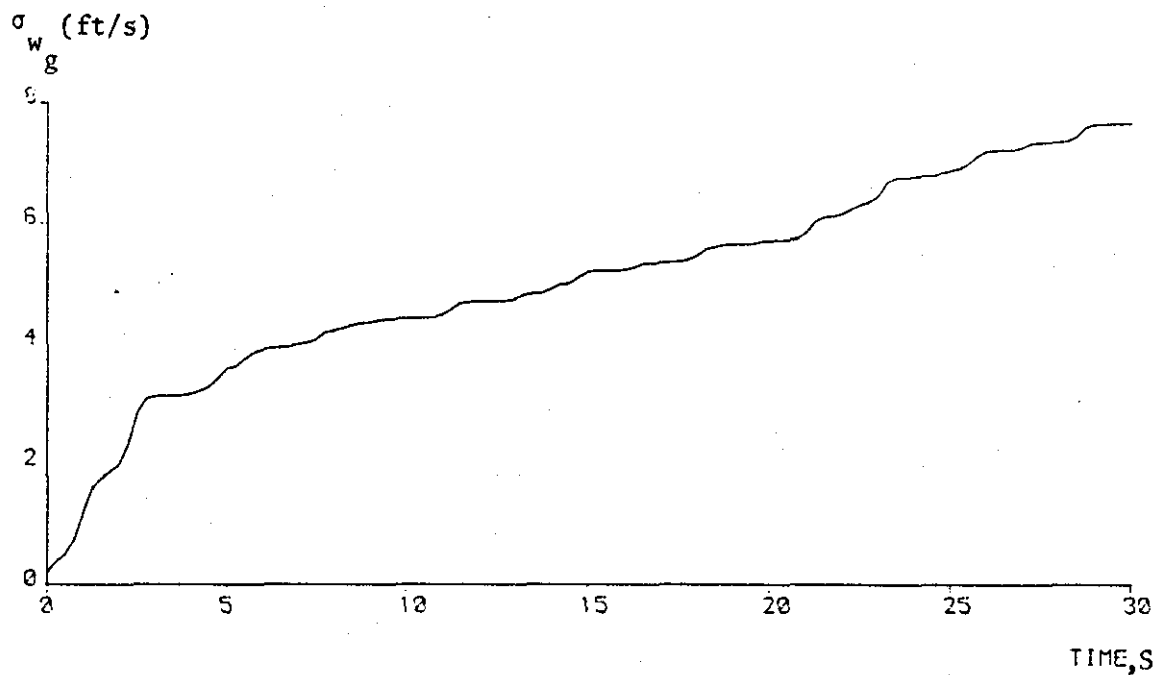
To investigate the significance of the p_g, r_g and q_g on the motion of an aircraft Figure 3.8 was employed. This figure shows the power spectra of the α_g, β_g and p_g components of the atmospheric turbulence for a wide range of frequencies. From this figure it can be deduced that the magnitude of $\phi_{(p_g)}$ is much smaller than that of $\phi_{(\alpha_g)}$ and $\phi_{(\beta_g)}$. Since $\phi_{(r_g)}$ and $\phi_{(q_g)}$ are of the same order of magnitude as $\phi_{(p_g)}$ due to the assumption of isotropy three components may be ignored due to their relatively small contribution as compared to β_g and α_g .

why not check p_g neglected by simulation

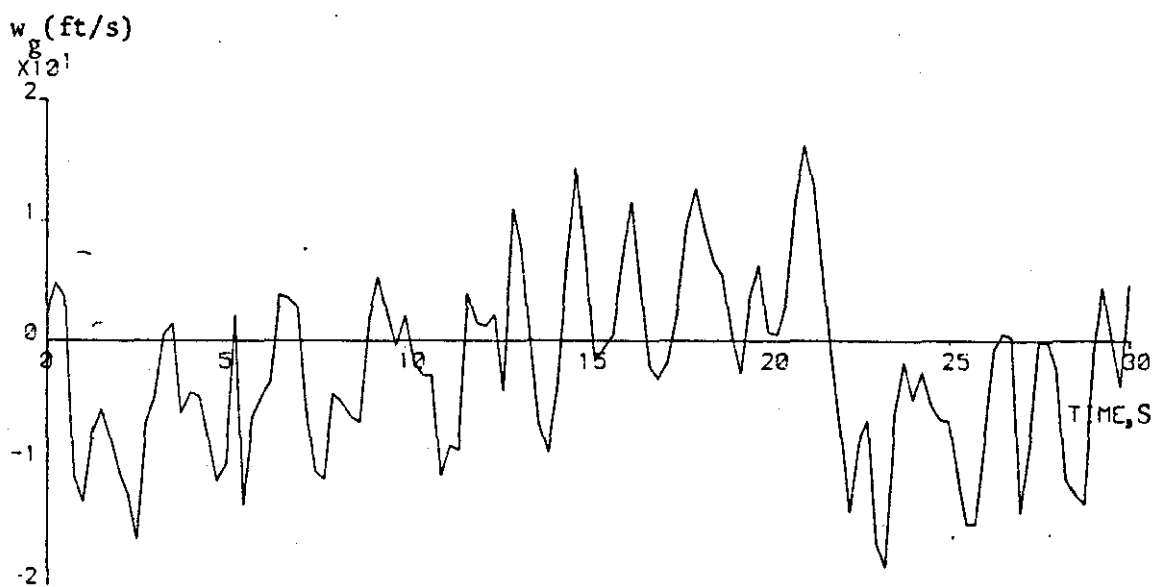
3.4.2 Results from the Simulation of Atmospheric Turbulence

Figures 3.9 and 3.10 illustrate the results obtained from the simulation of the vertical and lateral components of the atmospheric turbulence for 305 runs (w_g and β_g respectively). These figures represent turbulence with a probability of equalling or exceeding $\sigma_{w_g} = 7.6$ and $\sigma_{v_g} = 8.4$ ft/s of the order of 6×10^{-3} .

The sampling interval chosen to evaluate turbulence in the digital simulation was 0.25s. From Figure 3.9 it can be seen that the vertical gust w_g achieves a maximum value of 28 ft/s at about 20s. At the same time the lateral gust (v_g) achieves its maximum value which is approximately equal to 24 ft/s. ($\beta_g = 0.09$ rad). These peak gusts correspond to severe turbulence. However from closer inspection of Figure 3.10 it can be deduced that the sequence length of the random number generator (which is

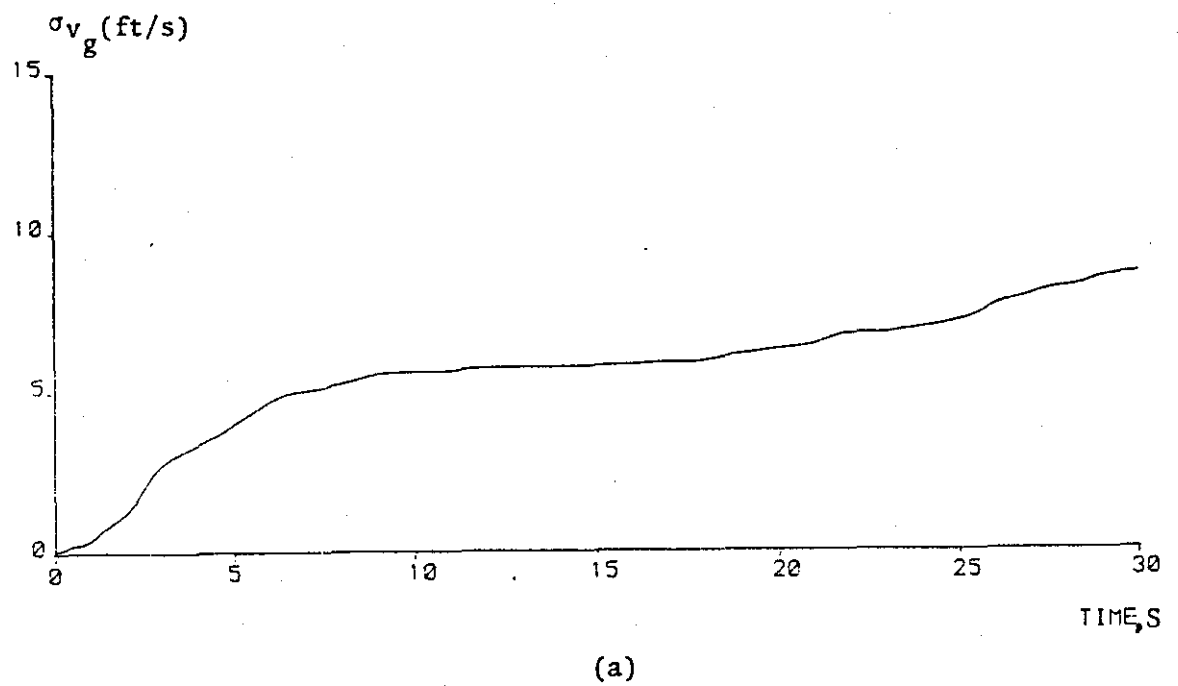


(a)

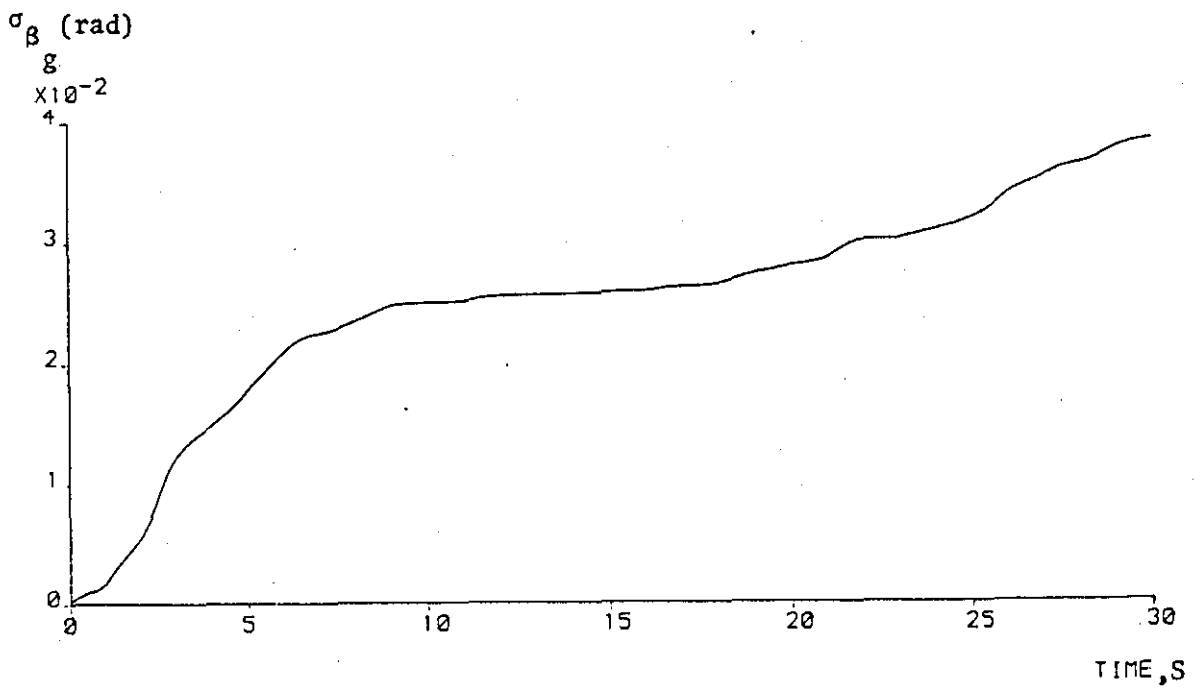


(b)

FIGURE 3.9: Variation of Vertical Gust Velocity (w_g) and σ_{w_g} with Time

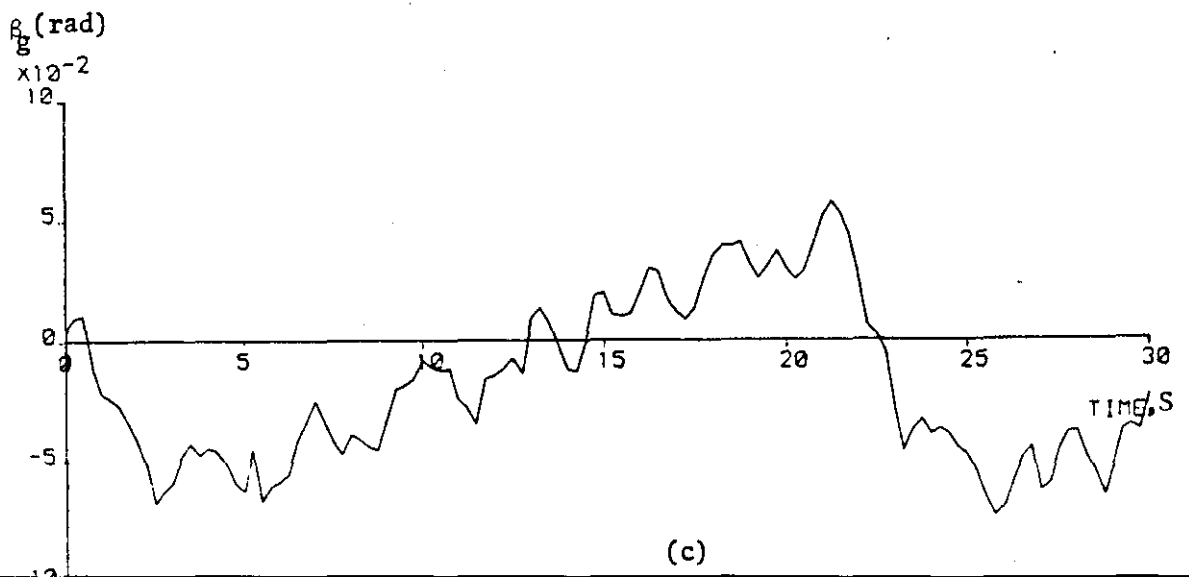


(a)



(b)

FIGURE 3.10: Variation of β_g , σ_{β_g} and σ_{v_g} with Time



(c)

a pseudo-random binary sequence (p.r.b.s.)) in SLAM has obviously been exceeded by 20 sec. and then the p.r.b.s. repeats and hence the r.m.s. turbulence levels will increase.

Due to this effect it would be expected that the peak gust encountered would scale up significantly the dynamic response of the aircraft at these peak gusts.

CHAPTER 4

OPTIMAL RIDE CONTROL SYSTEMS FOR AIRCRAFT

4.1 INTRODUCTION

In section 4 of Chapter 2 the relationship of different levels of acceleration to the ride quality provided by any aircraft was discussed and it was indicated there that both the normal and lateral accelerations due to rigid-body response are the principal constituents of the motion by which passengers or crew judge ride quality. The purpose of a ride quality control system (R.C.S.) must therefore be to reduce to acceptable levels those accelerations which give rise to discomfort. At the same time, of course, such reductions should not be achieved at the expense of excessive control surface activity for reasons of equipment reliability, life, and complexity. Nor must any ride control system result in the degradation of the handling qualities of the basic aircraft. If those were acceptable before the R.C.S. was fitted then they must remain so after it has been fitted. This requirement, of course, does not preclude the possibility of those handling qualities being enhanced by virtue of the R.C.S. action. Thus, it is evident from this brief introduction that the R.C.S. should be designed to reduce acceleration levels at specified fuselage stations, subject to constraints on the use of the control surfaces, and upon not degrading the handling qualities.

4.2 REPRESENTATION OF ACCELERATION IN TERMS OF STATE AND CONTROL VARIABLES

In order to study analytically the effects of the flight induced acceleration levels on the ride quality of an aircraft it is necessary first to define the equations which describe the normal and lateral accelerations and showing also the way that they vary at different fuselage stations.

The general equations that describe the normal and lateral equations for a rigid-body aircraft for any position along the fuselage are given by:

$$a_{z_x} = \ddot{w} - u_0 \dot{q} - x \dot{q} \quad (4.1)$$

and

$$a_{y_x} = u_0 \dot{\beta} - g\phi + u_0 r + x \dot{r} \quad (4.2) \quad \begin{matrix} \text{neglect} \\ z\dot{p} \end{matrix}$$

where a_{z_x} and a_{y_x} are the normal and lateral accelerations measured at a distance, x , from the centre of mass on the fuselage. The distance, x , is defined by convention as positive for any station forward of the centre of gravity (c.g.).

Normal and Lateral Accelerations at the c.g.

At the centre of gravity the distance, x , equals to zero and so from (4.1) the normal acceleration becomes:

$$a_{z_{c.g.}} = \ddot{w} - u_0 \dot{q} \quad (4.3)$$

Substituting for w from (2.66), (4.3) may be re-expressed as:

$$a_{z_{c.g.}} = Z_u u + Z_w w + Z_{\delta_E} \delta_E + Z_{\delta_{SP}} \delta_{SP} + Z_{\delta_{CH}} \delta_{CH} \quad (4.4)$$

(4.4) represents generally the variation of the c.g. acceleration when all the controls are activated. When a particular control is not

activated then the coefficient associated with the specific control in the above expression is assigned the value zero.

The lateral acceleration at the c.g. is given by putting $x=0$ to (4.2). Thus:

$$a_{y_{c.g.}} = u_0 \dot{\beta} - g\phi + u_0 r \quad (4.5)$$

Substituting for $\dot{\beta}$, from (2.68) yields:

$$a_{y_{c.g.}} = u_0 Y_v \beta + u_0 Y_{\delta_R}^* \delta_R + u_0 Y_{\delta_{CV}}^* \delta_{CV} \quad (4.6)$$

Both (4.4) and (4.6) may be expressed in a matrix form as follows:

$$y \triangleq a_{z_{c.g.}} = \begin{bmatrix} Z_u & Z_w & 0 & 0 \end{bmatrix} \begin{bmatrix} u \\ w \\ q \\ \theta \end{bmatrix} + \begin{bmatrix} Z_{\delta_E} & Z_{\delta_{SP}} & Z_{\delta_{CH}} \end{bmatrix} \begin{bmatrix} \delta_E \\ \delta_{SP} \\ \delta_{CH} \end{bmatrix} \quad (4.7)$$

which has the form

$$y = Cx + Du \quad (4.8)$$

Also,

$$y \triangleq a_{y_{c.g.}} = \begin{bmatrix} u_0 & Y_v & 0 & 0 & 0 & 0 \end{bmatrix} \begin{bmatrix} \beta \\ p \\ r \\ \phi \\ \psi \end{bmatrix} + \begin{bmatrix} Y_{\delta_R}^* u_0 & Y_{\delta_{CV}}^* u_0 \end{bmatrix} \begin{bmatrix} \delta_R \\ \delta_{CV} \end{bmatrix} \quad (4.9)$$

which can also be described in the form of (4.8).

Therefore for each axis the acceleration is a function of both state and control vectors.

The R.C.S. may sometimes be required to minimize levels of acceleration at particularly sensitive fuselage stations other than the c.g. In that case the distance, x , will not then be zero and (4.1) and (4.2) will represent the acceleration at the station of interest.

Normal and Lateral Accelerations at Other Fuselage Stations

As has been explained already (4.1) and (4.2) represent the normal and lateral accelerations at other fuselage stations.

Substituting in (4.1) for q from (2.66) and arranging the result in a matrix form, the following expression is obtained:

$$y \triangleq a_{z_x} = \begin{bmatrix} (Z_u - xM_u - xZ_u M_w) \\ (Z_w - xM_w - xZ_w M_w) \\ (-xM_w u_0 - xM_q) \\ 0 \end{bmatrix}^T \begin{bmatrix} u \\ w \\ q \\ \theta \end{bmatrix} + \begin{bmatrix} (Z_{\delta_E} - xZ_{\delta_E} M_w - xM_{\delta_E}) \\ (Z_{\delta_{SP}} - xZ_{\delta_{SP}} M_w - xM_{\delta_{SP}}) \\ (Z_{\delta_{CH}} - xZ_{\delta_{CH}} M_w - xM_{\delta_{CH}}) \end{bmatrix}^T \begin{bmatrix} \delta_E \\ \delta_{SP} \\ \delta_{CH} \end{bmatrix} \quad (4.10)$$

$$\text{i.e.} \quad y = \tilde{C}x + \tilde{B}u \quad (4.11)$$

For the lateral acceleration, substituting \dot{r} from (2.68) in (4.2), results in the following matrix equation:

$$y \triangleq a_{y_x} = \begin{bmatrix} u_0 Y_v + xN_\beta \\ xN_p \\ xN_r \\ 0 \\ 0 \end{bmatrix}^T \begin{bmatrix} \beta \\ p \\ r \\ \phi \\ \psi \end{bmatrix} + \begin{bmatrix} u_0 Y_{\delta_R}^* + N_{\delta_R} x \\ u_0 Y_{\delta_{CV}}^* + N_{\delta_{CV}} x \\ xN_{\delta_A} \end{bmatrix}^T \begin{bmatrix} \delta_R \\ \delta_{CV} \\ \delta_A \end{bmatrix} \quad (4.12)$$

which is also of the form of (4.11).

(4.10) and (4.12) show clearly that \tilde{C} and \tilde{D} are strongly related to the fuselage station which indicates that for different fuselage locations and for the same disturbance different acceleration levels can be expected.

Evidently from (4.10) and (4.12) any control system designed

to minimize accelerations must involve the minimization of both state and control variables. Such minimization accords with these requirements for an R.C.S. outlined in the Introduction 4.1.

The need to minimize the control variables to ensure reduction of acceleration also directly assists in achieving the aim of reducing control surface activity. Consequently a suitable method for designing an optimal R.C.S. is one which will involve the simultaneous reduction of the state vector and the control vector.

110
11/11/57

4.3 LINEAR QUADRATIC PROBLEM (L.Q.P.) FORMULATION

One of the modern methods of optimal control design which has found considerable practical application is that to obtain the solution which is known as the linear quadratic problem (L.Q.P.). The method of design is based on the minimization of a quadratic performance index by a suitable choice of the optimal control, $u^0(t)$, which, it turns out, is obtained as a feedback control.

A performance index (P.I.) is a single measure of the performance of a system. It can be chosen to emphasize those characteristics of the response that are considered to be particularly important. In optimal control design, the performance index, J , replaces the design criteria used in conventional control, such as peak overshoot, damping ratio, gain margin, phase margin, etc. A designer must be able to select the P.I. properly so that the resulting system will perform satisfactorily according to physical criteria, which are generally interpreted more easily by means of the performance criteria used in conventional control.

Although various forms of performance index have been used in the past the quadratic form has been found to be most useful in the design of aircraft control systems. The general form of a quadratic P.I. has been found most acceptable because for linear systems there exists a solution which can be readily obtained numerically by means of digital computation. Furthermore, the control itself is linear and the method is very readily applied to multivariable systems.

Since the solution of the optimal control problem is wholly analytic in its development the problem is stated here formally:

"Find the control, $\underline{u}^0(t)$, that will minimize the performance index

$$J = \int_{t_0}^{t_f} F[\underline{x}(t), \underline{u}(t), t] dt \quad (4.13)$$

given the initial state $\underline{x}_0(t_0) = \underline{x}_0$ and that the solution is subject to the constraint of the dynamic process to be controlled which is described in the most general way by:

$$\dot{\underline{x}}(t) = \underline{f}[\underline{x}(t), \underline{u}(t), t] \quad (4.14)$$

(4.14) is the state equation and describes the dynamics of the system to be controlled."

For a completely controllable, linear, time-invariant system the state equation is given by:

$$\dot{\underline{x}}(t) = A\underline{x}(t) + B\underline{u}(t) \quad (4.15)$$

where $A(n \times n)$ and $B(n \times m)$ are constant matrices. The state vector $\underline{x}(t)$ has dimension, n , and it represents an array of the state variables of the system. The control vector $\underline{u}(t)$ of dimension, m , is to be selected to minimize a weighted sum of the square values of the state variables and the squared values of the control variables. The quadratic performance index is merely a mathematical statement of the preceding 'least squares' requirement and is expressed thus:

$$J = \frac{1}{2} \underline{x}^T(t_f) S \underline{x}(t_f) + \frac{1}{2} \int_{t_0}^{t_f} \{ \underline{x}^T(t) Q \underline{x}(t) + \underline{u}^T(t) G \underline{u}(t) \} dt \quad (4.16)$$

where the matrices S, Q and G are generally symmetric.

The matrix, G , which weights the control vector must be positive definite; the matrix Q which weights the elements of the state vector needs only to be positive semi-definite. S can be a null matrix

when it is not important that the error at the end of the interval should be carefully controlled.

When the interval of the performance index is semi-infinite the problem is referred to as the Linear Quadratic Problem (L.Q.P.) and the P.I. is then defined as:

$$J = \frac{1}{2} \int_0^{\infty} \{ \underline{x}^T(t) Q \underline{x}^T(t) + \underline{u}^T(t) G \underline{u}(t) \} dt \quad (4.17)$$

It has been shown (Kalman [1960]) that an optimal control exists, is unique, is stabilizing and is given by:

$$\underline{u}^o(t) = K^o \underline{x}(t) \quad (4.18)$$

where
$$K^o = -G^{-1} B^T K \quad (4.19)$$

K is a constant $n \times n$ positive definite matrix which may be obtained by solving the equation (4.20) known as the algebraic Riccati equation (A.R.E.) viz:

$$0 = -K(t)A - A^T K(t) + K(t)BG^{-1}B^T K(t) - Q \quad (4.20)$$

Figure 4.1 gives a block diagram representation of the L.Q.P. K matrix can also be evaluated by using eigenanalysis (Marshal and Nicholson [1970]). The eigenanalysis method is superior with regard to computational time and therefore as such it was preferred for digital programming.

Solution of L.Q.P. by Eigenanalysis

The Hamiltonian associated with the performance index described by (4.17)

$$J = \frac{1}{2} \int_{t_0}^{t_f} (\underline{x}^T Q \underline{x} + \underline{u}^T G \underline{u}) dt \quad (4.17a)$$

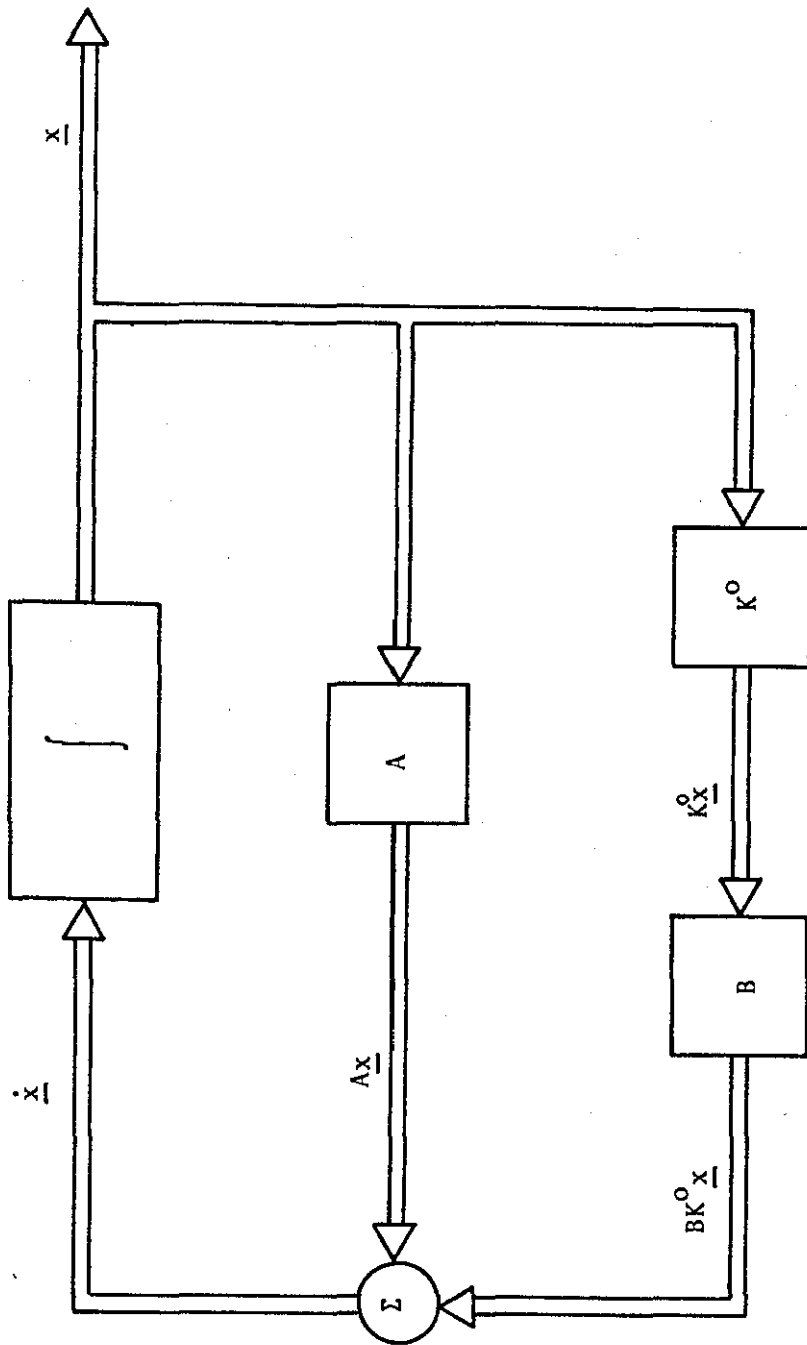


FIGURE 4.1: Block Diagram Representation of the LQP

is given by

$$\mathcal{H} = \frac{1}{2}(\underline{x}^T Q \underline{x} + \underline{u}^T G \underline{u}) + \underline{\psi}^T \{A \underline{x} + B \underline{u}\} \quad (4.21)$$

where $\underline{\psi}$ is the co-state vector. Hence, since

$$\dot{\underline{\psi}} \triangleq - \frac{\partial \mathcal{H}}{\partial \underline{x}} \quad (4.22)$$

$$\dot{\underline{\psi}} = -Q \underline{x} - A^T \underline{\psi} \quad (4.23)$$

Also

$$\frac{\partial \mathcal{H}}{\partial \underline{u}} = G \underline{u} + B^T \underline{\psi} \quad (4.24)$$

If \mathcal{H} is to be minimized (hence minimizing J) by a choice of \underline{u} , then

$$\frac{\partial \mathcal{H}}{\partial \underline{u}} \triangleq 0 \quad (4.25)$$

Therefore, from (4.24) and (4.25),

$$\underline{u}^0 = -G^{-1} B^T \underline{\psi} \quad (4.26)$$

For G^{-1} to exist it is necessary to restrict G to be positive definite (p.d.).

Now, from (4.15), (4.23) and (4.26), the following set of vector differential equations is obtained

$$\left. \begin{aligned} \dot{\underline{x}} &= A \underline{x} - B G^{-1} B^T \underline{\psi} \\ \dot{\underline{\psi}} &= -Q \underline{x} - A^T \underline{\psi} \end{aligned} \right\} \quad (4.27)$$

These vector equations can be written in a matrix form, viz.

$$\begin{bmatrix} \dot{\underline{x}} \\ \dot{\underline{\psi}} \end{bmatrix} = \begin{bmatrix} A & -B G^{-1} B^T \\ -Q & -A^T \end{bmatrix} \begin{bmatrix} \underline{x} \\ \underline{\psi} \end{bmatrix} \quad (4.28)$$

If a new composite vector $\underline{\zeta}$ is employed and is defined as

$$\underline{\zeta} \triangleq \begin{bmatrix} \underline{x} \\ \underline{\psi} \end{bmatrix} \quad (4.29)$$

then

$$\dot{\underline{\zeta}} = M \underline{\zeta} \quad (4.30)$$

where

$$M = \begin{bmatrix} A & -BG^{-1}B^T \\ -Q & -A^T \end{bmatrix} \quad (4.31)$$

(4.30) is the canonical equation of the optimal system. The optimal solution is given by the solution of (4.28) with the known boundary conditions $\underline{x}(t_0)=0$ and $\underline{\psi}(T)=0$. An explicit solution of (4.28), based on the condition of asymptotic stability, may be obtained in the form of two single-point boundary-value problems using eigenanalysis.

The time response of the system described by (4.30) can be defined for distinct eigenvalues in terms of the eigenvector components of the matrix, M . Thus

$$\underline{y} = Ue^{A\tau}U^{-1}\underline{y}_0 \quad (4.32)$$

where

$$\tau = t_f - t_0 \quad (4.33)$$

and U is the $2n \times 2n$ modal matrix of eigenvector columns associated with the shape of each system mode, and $e^{A\tau}$ is a diagonal matrix with elements $e^{\lambda_1\tau}, e^{\lambda_2\tau}, \dots, e^{\lambda_{2n}\tau}$. The corresponding equation relating the eigenvectors is

$$MU = UA \quad (4.34)$$

The matrix M possesses convergent and divergent mode pairs, with eigenvalues equal in magnitude and opposite in sign. Partitioning the eigenvalues of A into two sets of n eigenvalues, namely $\Lambda_1 = [\lambda_i]$, with $i=1,2,\dots,n$ and negative real parts, $\Lambda_2 = [\lambda_i]$, with $i=n+1,n+2,\dots,2n$ and positive real parts. Similarly, partitioning the solution of (4.32), results in

$$\begin{bmatrix} \underline{x} \\ \underline{\psi} \end{bmatrix} = \begin{bmatrix} U_{11} & U_{12} \\ U_{21} & U_{22} \end{bmatrix} \begin{bmatrix} e^{\Lambda_1\tau} & 0 \\ 0 & e^{\Lambda_2\tau} \end{bmatrix} \begin{bmatrix} V_{11} & V_{12} \\ V_{21} & V_{22} \end{bmatrix} \begin{bmatrix} \underline{x}_0 \\ \underline{\psi}_0 \end{bmatrix} \quad (4.35)$$

where V_{11}, V_{12}, V_{21} and V_{22} represent the components of the inverse matrix U^{-1} . The time solution of (4.35) for the state variables is then given by

$$\underline{x} = U_{11} e^{\Lambda_1 \tau} \{V_{11} \underline{x}_0 + V_{12} \underline{\psi}_0\} + U_{12} e^{\Lambda_2 \tau} \{V_{21} \underline{x}_0 + V_{22} \underline{\psi}_0\} \quad (4.36)$$

The divergent modes, which correspond to the unstable roots, must now be eliminated to satisfy the assumed condition of asymptotic stability.

From (4.36), this requires the condition that

$$\underline{\psi}_0 = -V_{22}^{-1} V_{21} \underline{x}_0 \quad (4.37)$$

$$= U_{21} U_{11}^{-1} \underline{x}_0 \quad (4.38)$$

(using the relationship $VU=I$).

Hence from (4.36),

$$\begin{aligned} \underline{x} &= U_{11} e^{\Lambda_1 \tau} (V_{11} - V_{12} V_{22}^{-1} V_{21}) \underline{x}_0 \\ &= U_{11} e^{\Lambda_1 \tau} U_{11}^{-1} \underline{x}_0 \end{aligned} \quad (4.39)$$

Similarly, from (4.35)

$$\begin{aligned} \underline{\psi} &= U_{21} e^{\Lambda_1 \tau} U_{11}^{-1} \underline{x}_0 \\ &= U_{21} U_{11}^{-1} \underline{x} \end{aligned} \quad (4.40)$$

(4.39) and (4.40) define the optimal solution as two single-point boundary-value problems in terms of the partitioned eigenvector components associated with the n stable modes of the $2n \times 2n$ matrix M . The optimal control law to be applied for all time, t , may now be obtained directly from (4.26) and (4.40). Thus,

$$\underline{u}^0 = G^{-1} B^T U_{21} U_{11}^{-1} \underline{x} \quad (4.41)$$

The optimal-control law for the linear system, with quadratic performance and asymptotic-stability conditions, can thus be determined explicitly using the maximum principle of Pontryagin.

4.4 THE OUTPUT REGULATOR PROBLEM

It was shown earlier, in section 4.2, that any aircraft acceleration of interest can be represented as an output equation of the form:

$$\underline{y} = \underline{C}\underline{x} + \underline{D}\underline{u} \quad (4.42)$$

\underline{y} is the output vector of dimension, p . C and D are matrices of the order $(p \times n)$ and $(p \times m)$ respectively. The minimization of acceleration can be attempted implicitly by minimizing a performance index involving the states and the control inputs in the manner described in the preceding section. Direct minimization of acceleration involves minimizing a performance index described in terms of acceleration only. However it is usual still to add to the index a term which governs the use of control.

Under the assumption that all sensing elements needed to measure the required state variables at any given time are available, the quadratic performance index used in minimizing the acceleration i.e. the output vector (4.42) is given as:

$$J_0 = \frac{1}{2} \int_0^{\infty} \{ \underline{y}^T \underline{Q} \underline{y} + \underline{u}^T \underline{G} \underline{u} \} dt \quad (4.43)$$

Substituting (4.42) in (4.43) yields

$$J_0 = \frac{1}{2} \int_0^{\infty} \{ (\underline{C}\underline{x} + \underline{D}\underline{u})^T \underline{Q} (\underline{C}\underline{x} + \underline{D}\underline{u}) + \underline{u}^T \underline{G} \underline{u} \} dt \quad (4.44)$$

which can be shown (Annex A) to reduce to

$$J_0 = \frac{1}{2} \int_0^{\infty} \{ \underline{x}^T \hat{\underline{Q}} \underline{x} + \hat{\underline{u}}^T \hat{\underline{G}} \hat{\underline{u}} \} dt \quad (4.45)$$

where

$$\hat{\underline{Q}} = \underline{C}^T \{ [\underline{I}] - \underline{Q}\underline{D} [\underline{D}^T \underline{Q}\underline{D} + \underline{G}]^{-1} \underline{D}^T \} \underline{Q} \underline{C} \quad (4.46)$$

and

$$\hat{\underline{G}} = \underline{D}^T \underline{Q}\underline{D} + \underline{G}$$

and

$$\hat{\underline{u}} = \underline{u} + \hat{\underline{G}}^{-1} \underline{W}^T \underline{x} \quad (4.47)$$

where

$$\underline{W}^T = \underline{C}^T \underline{Q}\underline{D} \quad (4.48)$$

From (4.15) and (4.47) the following equation may be obtained:

$$\begin{aligned}\dot{\underline{x}} &= \underline{A}\underline{x} + \underline{B}(\underline{\hat{u}} - \underline{G}^{-1}\underline{W}^T\underline{x}) \\ &= (\underline{A} - \underline{B}\underline{G}^{-1}\underline{W}^T)\underline{x} + \underline{B}\underline{\hat{u}}\end{aligned}\quad (4.49)$$

or

$$\dot{\underline{x}} = \underline{\hat{A}}\underline{x} + \underline{B}\underline{\hat{u}} \quad (4.50)$$

where

$$\underline{\hat{A}} = \underline{A} - \underline{B}\underline{G}^{-1}\underline{W}^T = \underline{A} - \underline{B}\underline{G}^{-1}\underline{C}^T\underline{Q}\underline{D} \quad (4.51)$$

According to (4.18) and (4.19) the optimal control $\underline{\hat{u}}^0(t)$ which minimises the P.I., given as (4.45) is obtained from the following equation:

$$\underline{\hat{u}}^0(t) = -\underline{G}^{-1}\underline{B}^T \underline{K} \underline{x}(t) \quad (4.52)$$

where \underline{K} may be found from an algebraic Riccati equation of the following form:

$$0 = -\underline{\hat{K}}\underline{A} - \underline{A}^T\underline{\hat{K}} + \underline{\hat{K}}\underline{B}\underline{G}^{-1}\underline{B}^T\underline{\hat{K}} - \underline{\hat{Q}} \quad (4.53)$$

However, \underline{K} was evaluated by eigenanalysis as it was shown in section 4.3.

Therefore the optimal control $\underline{u}^0(t)$ is obtained from (4.47)

and (4.52) as:

$$\begin{aligned}\underline{u}^0 &= \underline{\hat{u}}^0 - \underline{G}^{-1}\underline{W}^T\underline{x} \\ &= -\underline{G}^{-1}(\underline{B}^T\underline{K} + \underline{W}^T)\underline{x}\end{aligned}\quad (4.54)$$

Hence,

$$\underline{u}^0 = \underline{\hat{K}}^0 \underline{x} \quad (4.55)$$

where

$$\underline{\hat{K}}^0 = -\underline{G}^{-1}(\underline{B}^T\underline{K} + \underline{W}^T) \quad (4.56)$$

Figure 4.2 gives a block diagram representation of the output regulator problem.

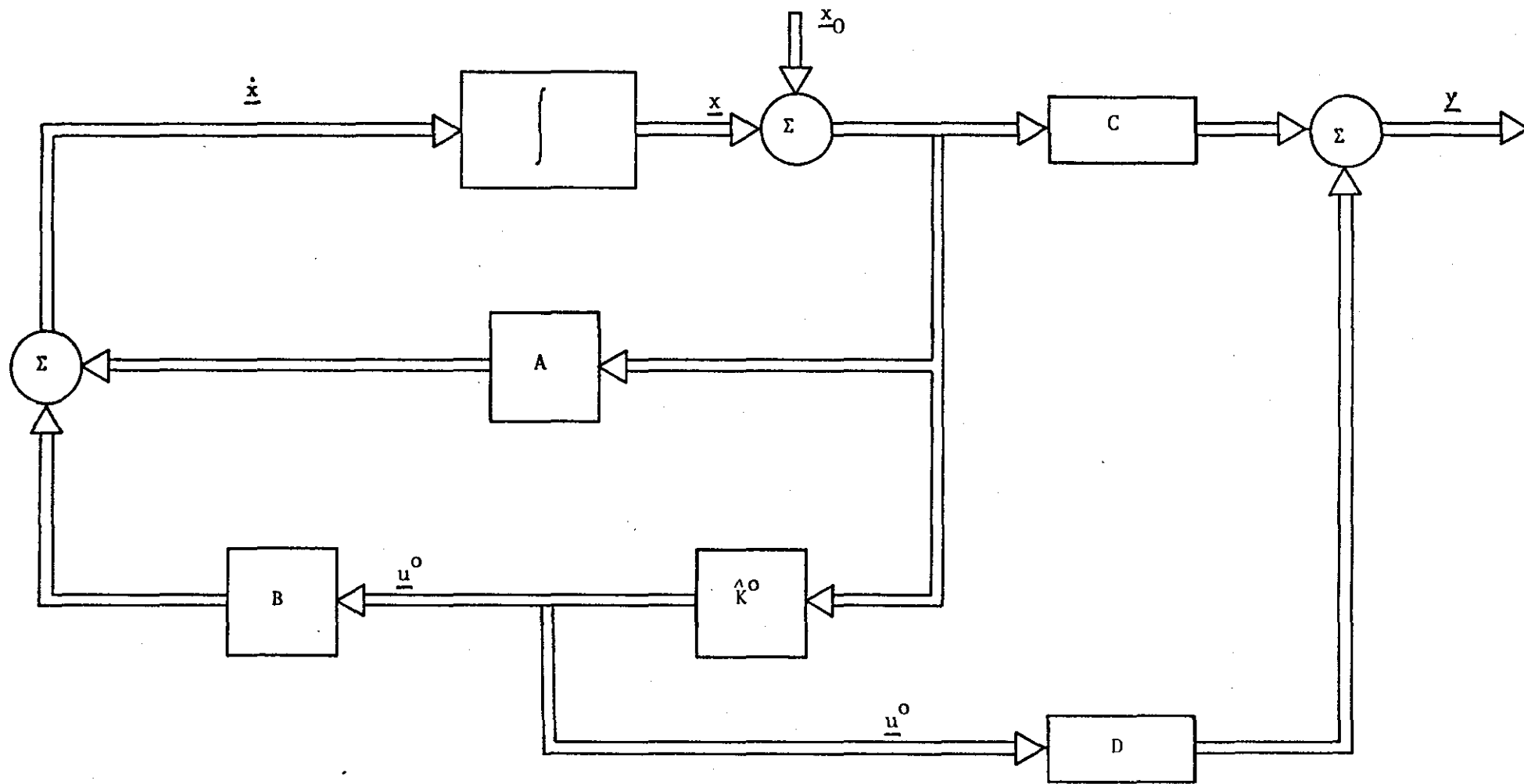


FIGURE 4.2: Block Diagram Representation of the Optimal Output Regulator

4.5 DESCRIPTION OF THE DIGITAL PROGRAMS 'WAYMX' AND 'OUTREG'

In order to derive the optimal feedback matrix for the output regulator two digital programs were employed. These were 'WAYMX' which was used to provide the elements of the diagonal weighting matrices Q and G, and the 'OUTREG' which was used to determine the optimal feedback laws for the output regulator problems for some specific choice of matrices Q and G. A short description of these two digital programs follows.

4.5.1 Determination of Appropriate Q and G Matrices

In order to minimize the performance index, J_0 , described by (4.43) it is necessary first to choose the matrices Q and G. There is however no theoretical method available to date for obtaining appropriate matrices Q and G and the choice must therefore be made such that the resulting feedback control produces acceptable levels of \underline{y} and \underline{u} . A choice (Bryson and Ho [1969]) which turns out to be quite acceptable is,

$$Q^{-1} = n(t_f - t_0) \times \text{maximum acceptable value of} \\ \text{diag}\{\underline{x}(t)\underline{x}^T(t)\} \quad (4.57)$$

and

$$G^{-1} = m(t_f - t_0) \times \text{maximum acceptable value of} \\ \text{diag}\{\underline{u}(t)\underline{u}^T(t)\} \quad (4.58)$$

By specifying the maximum values of the state and control vectors it is then possible to evaluate the Q and G matrices to ensure that when the resulting optimal control law is applied to the system the resulting states and control inputs in the closed-loop system never exceed the specified limits.

Let

$$t_f - t_0 = \tau \quad (4.59)$$

Then Q and G matrices are given by

will there ever be?

$$Q = \begin{bmatrix} \frac{1}{n\tau (x_{1,\max})^2} & & & 0 \\ & \ddots & & \\ & & \ddots & \\ 0 & & & \frac{1}{n\tau (x_{n,\max})^2} \end{bmatrix} \quad (4.60)$$

and

$$G = \begin{bmatrix} \frac{1}{m\tau (u_{1,\max})^2} & & & 0 \\ & \ddots & & \\ & & \ddots & \\ 0 & & & \frac{1}{m\tau (u_{m,\max})^2} \end{bmatrix} \quad (4.61)$$

where $x_{1,\max}, \dots, x_{n,\max}$ and $u_{1,\max}, \dots, u_{m,\max}$ represent the maximum possible values of the elements of the state and control vectors respectively. Hence for this specific choice of weighting the quadratic performance index which was to be minimized had the following form

$$J_0 = \int_0^{\infty} \left\{ \frac{1}{n\tau} \left[\frac{(x_1)^2}{(x_{1,\max})^2} + \dots + \frac{(x_n)^2}{(x_{n,\max})^2} \right] \right\} dt + \left\{ \frac{1}{m\tau} \left[\frac{(u_1)^2}{(u_{1,\max})^2} + \dots + \frac{(u_m)^2}{(u_{m,\max})^2} \right] \right\} dt \quad (4.62)$$

Hence, the weighting corresponding to each element of the state and control vectors was inversely proportional to its maximum value and the time of interest. However the relative weighting of state and control vectors further depended on the dimensions corresponding vectors.

4.5.1.1 Choice of the Maximum Values for the State and Control Vectors for Longitudinal Motion

The maximum values chosen for the elements of the state and control vectors in this work were the following:

$$\underline{x}_{\max} = \begin{bmatrix} u_{\max} \\ w_{\max} \\ q_{\max} \\ \theta_{\max} \end{bmatrix} = \begin{bmatrix} \pm 25 \text{ ft/s} \\ \pm 4 \text{ ft/s} \\ \pm 2^\circ/\text{s} \\ \pm 2^\circ \end{bmatrix} \quad (4.63)$$

and

$$\underline{u}_{\max} = \begin{bmatrix} \delta E_{\max} \\ \delta SP_{\max} \\ \delta CH_{\max} \end{bmatrix} = \begin{bmatrix} \pm 23^\circ \\ \pm 7.5^\circ \\ \pm 5^\circ \end{bmatrix} \quad (4.64)$$

The reasons for these choices are briefly discussed here.

Choice of maximum denation of forward speed u_{\max}

The stalling speed of the aircraft for the flying conditions considered was $u_s = 160$ ft/s. The equilibrium airspeed of the aircraft was $u_0 = 224$ ft/s. Hence, a choice of the perturbed velocity $u = \pm 25$ ft/s would be a reasonable figure since the resulting total velocity would remain well above the stalling speed and the variation on equilibrium speed remains within 10% thus obeying the assumptions involved in the small perturbation theory used in deriving the equations of motion.

Choice of w_{\max} , q_{\max} and θ_{\max}

The choice of the maximum values of the perturbed q , w and θ was based on the control anticipation parameter (C.A.P.) and the maximum value of the parameter N_{z_α} which determines the maximum acceptable values

of induced accelerations for changes in the angle of attack (see Annex D2).

The C.A.P. was found to be $25^{\circ}/s/g$. Hence for normal acceleration of $0.1g$, which was considered to be an acceptable level, the maximum corresponding value for q would most likely be

$$q_{\max} = 2.5^{\circ}/s \quad \text{also} \quad \theta_{\max} = 2.5^{\circ}.$$

The parameter $N_{z\alpha}$ was equal to 6.32 g/rad .

Therefore

$$N_{z\alpha} \triangleq \frac{\partial N_z}{\partial \alpha} = 6.32 \quad (4.63.1)$$

hence for $1g$ the maximum angle of attack is

$$\alpha = \frac{1}{6.32} \quad \text{or} \quad \frac{w_{\max}}{u_0} = \frac{1}{6.32} \quad (4.63.2)$$

Thus,

$$w_{\max} = 40 \text{ ft/s} \quad (4.63.3)$$

Hence, for $0.1g$, w_{\max} would be 4 ft/s .

Choice of $\delta_{E_{\max}}$, $\delta_{SP_{\max}}$, and $\delta_{CH_{\max}}$

A maximum deflection angle of 23° was chosen for elevator ($\delta_{E_{\max}}$) since it was assessed that it was the most effective control surface for ride control for the Jetstar aircraft. The drag penalty due to the use of elevator is less than spoilers and so it could be used more. However the choice of $\delta_{E_{\max}}$ was such that it would allow the elevator to be used for other flight tasks. The maximum deflection allowed for spoilers ($\delta_{SP_{\max}} = 7.5^{\circ}$) was low mainly due to the high drag penalty which their use imposes on the aircraft, since spoilers have to operate from a biased position. Finally, horizontal canards were allowed to deflect by a maximum of $\pm 5^{\circ}$ so that their use would not significantly affect the airflow over the wings nor disturb the inlet airflow to the engines of the aircraft.

how?

st

4.5.1.2 Choice of the maximum values for the state and control vectors for lateral motion

The maximum values chosen for the elements of the state and control vectors associated with the lateral motion were the following,

$$\underline{x}_{\max} = \begin{bmatrix} \beta_{\max} \\ p_{\max} \\ r_{\max} \\ \phi_{\max} \\ \psi_{\max} \end{bmatrix} = \begin{bmatrix} \pm 5^{\circ} \\ \pm 20^{\circ}/s \\ \pm 20^{\circ}/s \\ \pm 30^{\circ} \\ \pm 50^{\circ} \end{bmatrix} \quad (4.65)$$

and

$$\underline{u}_{\max} = \begin{bmatrix} \delta_{R_{\max}} \\ \delta_{CV_{\max}} \\ \delta_{A_{\max}} \end{bmatrix} = \begin{bmatrix} \pm 10^{\circ} \\ \pm 5^{\circ} \\ \pm 25^{\circ} \end{bmatrix} \quad (4.66)$$

Choice of β_{\max} , r_{\max} and ϕ_{\max}

From the aircraft specifications it was indicated that the maximum excursion of β at the c.g. occurring within two seconds was 20° .

Hence,

$$\beta_{\max} = 20^{\circ} \quad (4.65.1)$$

and

$$r_{\max} = 10^{\circ}/s \quad (4.65.2)$$

The absolute ratio of $|\phi/\beta|$ for dutch roll mode was given by

$$|\phi/\beta| = 1.22 \quad (4.65.3)$$

Hence from (4.65.1)

$$\phi_{\max} = 25^{\circ} \quad (4.65.4)$$

Thus the choice of β_{\max} , r_{\max} , ϕ_{\max} described by (4.65) would be reasonable for the ride control scheme.

Choice of p_{\max} and ψ_{\max}

From the handling qualities requirements for the type of aircraft and mission chosen for this research (Class I, flight phase B

Level 1) acceptable roll performance is roll angle of 60° in 1.7s.

Hence the maximum value for the roll rate was chosen to be

$$p_{\max} = 20^\circ/\text{s} \quad (4.65.5)$$

The value of ϕ_{\max} was chosen arbitrarily and was

$$\phi_{\max} = 50^\circ \quad (4.65.6)$$

Choice of $\delta_{R_{\max}}$, $\delta_{A_{\max}}$ and $\delta_{CV_{\max}}$

A maximum deflection angle of 10° was chosen for the rudder ($\delta_{R_{\max}}$) since the fin is the main source of the induced lateral acceleration on the aircraft and hence it would be desirable to use as little rudder activity as possible in the ride control scheme. Compared to rudder use, a choice of higher maximum deflection for aileron of 25° was made. The reason for such a choice was that if rudder activity was reduced the aircraft requires more aileron activity to compensate for the reduced contribution of the rudder. However, the maximum values for both these controls were restricted so that they would allow sufficient control activity to be available for other flight tasks.

The maximum deflection angle allowed for vertical canard was only $\pm 5^\circ$. This choice was based on the high drag effects which would be expected to result due to higher angles of incidence of the vertical canard.

Hence from knowledge of the specified values for x_{\max} , u_{\max} , n , m and τ , 'WAYMX' was simply evaluating the matrices Q and G described by (4.60) and (4.61).

4.5.2 Determination of the Optimal Feedback Matrix (\hat{K}^0) for the Output Regulator

The matrix \hat{K}^0 was obtained by using the digital program 'OUTREG'. From the weighting matrices Q and G, the corresponding matrices \hat{Q} and \hat{G} were obtained by means of (4.46). Once \hat{Q} and \hat{G} were determined then the canonical matrix \hat{M} , for the system could be determined provided \hat{A} is known. i.e. from (4.31)

$$\hat{M} = \begin{bmatrix} \hat{A} & -\hat{B}\hat{G}^{-1}\hat{B}^T \\ -\hat{Q} & -\hat{A}^T \end{bmatrix} \quad (4.67)$$

A numerical procedure to determine the eigenvectors of (4.67) was used and then these eigenvectors were adjusted so that they comprised appropriate columns of the modal matrix, \hat{U} . This matrix was then partitioned as in (4.35). Once the sub-matrices \hat{U}_{11} , \hat{U}_{12} , \hat{U}_{21} and \hat{U}_{22} of the modal matrix were defined then by forming the inverse of \hat{U}_{11} , (\hat{U}_{11}^{-1}) it was possible to determine the matrix product $\hat{U}_{21}\hat{U}_{11}^{-1}$ and hence, according to (4.41) the optimal feedback law \hat{K}^0 , was obtained from

$$\hat{K}^0 = \hat{G}^{-1}\hat{B}^T\hat{U}_{21}\hat{U}_{11}^{-1} \quad (4.68)$$

By setting $D=[0]$ and allowing $C=[I]$ in (4.42) (4.43) becomes

$$J_0 = \frac{1}{2} \int_0^{\infty} \{ \underline{x}^T \hat{Q} \underline{x} + \underline{u}^T \hat{G} \underline{u} \} dt \quad (4.69)$$

where

$$\hat{Q} = C^T Q C = Q \quad (4.70)$$

Therefore, from (4.69) and (4.70) it can be seen that the output regulator reduces in this case to the L.Q.P. Then any minimization of acceleration is achieved implicitly.

4.6 HANDLING QUALITIES REQUIREMENTS FOR AN EXECUTIVE JET AIRCRAFT

An automatic flight control system (a.f.c.s.) designed to perform a particular task for an aircraft should always be assessed in terms of the effect it has on the handling qualities of the aircraft. An a.f.c.s. which is found to be successful, for example, in terms of the operational task for which it has been designed, may possibly be unacceptable for use if its operation results in the handling qualities of the aircraft being degraded.

Handling qualities criteria which define the flying characteristics of an aircraft are not objective functions and depend upon the opinions of test pilots. The assessment of the handling qualities of an aircraft by its pilot depends on a large number of factors including: stability and control characteristics of the aircraft, the type of mission being undertaken; the cockpit layout, the external environment, etc.

To be able to assess the handling qualities of an aircraft there must be available a suitable technique by which it will be possible to make appropriate judgements. For this purpose there exist rating scales which classify an aircraft according to the handling qualities they are adjudged to possess. One of the most widely known rating scales is that suggested by Cooper and Harper [1966]. This employs a pilot rating scale from 1 to 10 where 1 corresponds to excellent, i.e. pilot compensation is not considered to be a factor for desired performance and 10 indicates major deficiencies i.e. the aircraft is considered uncontrollable. Other techniques have also been applied to the rating of handling qualities. The rating scales are generally taken to correspond to some of the dynamic parameters of aircraft motion such as damping, natural frequency, stick force, etc.

Extensive research in this field has been summarized in the USAF military specification document MIL-F-8785 (A.S.G.) which was first adopted in 1954 and subsequently revised in 1959 and 1968. The latest version (Chalk and Wilson [1968]) has provided a framework which permits tailoring each requirement according to:

- (a) the kind and mission of an aircraft (class)
- (b) the different control tasks required from an aircraft (flight phase)
- (c) the degree of acceptability of the dynamic characteristics of an aircraft for some specified mission (levels)

In Annex B a detailed classification of a military aircraft according to the type of mission and flight phase is given (MIL-F-8785 revision). From Tables B1, B2, the NASA Jestar may be classified as class I, in flight phase B, which represents a small light airplane in cruise. To meet airworthiness requirements three distinct specified values of stability, or control, parameters, must be achieved. Each value is a limiting condition to satisfy one of three levels of acceptability. These levels are related to the ability of the aircraft to complete the missions for which it is designed. The levels are defined as follows:

Level	Definition
1	Flying qualities clearly adequate for the mission flight phase.
2	Flying qualities adequate to accomplish mission flight phase, but with some degradation in mission effectiveness, or increase in pilot workload, or both.

Level	Definition
3	Flying qualities such that the aircraft can be controlled, but the mission effectiveness is clearly inadequate, or the total workload of the pilot is approaching the limit of his capacity.

Level 1 was adopted in order to represent acceptable flying qualities of the NASA Jetstar in cruise flight phase. Table 4.1 gives a description of the specified flying qualities.

TABLE 4.1: Handling qualities for an aircraft of class I,
in flight phase B with acceptable level 1

LONGITUDINAL MOTION	
Phugoid response	$\zeta_p \geq 0.04$
Short period response	$0.3 < \zeta_{sp} < 2.0$
	$\omega_p / \omega_{sp} \leq 0.1$
LATERAL MOTION	
Roll Mode Time Constant (T_R)	$T_R < 1.4$
Spiral Mode Time for Bank Angle of 20° to double (sec.)	$> 20 \text{ s}$
Dutch Roll Mode	
Damping Ratio, (ζ_d)	$\zeta_d \geq .19$
Damping factor, ($\zeta_d \omega_d$)	$\zeta_d \omega_d \geq .35$
Natural frequency (ω_d)	$\omega_d \geq 1.0$

4.7 CLOSED-LOOP RESPONSE

In the earlier section 4.3 it was shown how the linear quadratic regulator theory was able to be used to provide an optimal feedback control law for some specific choice of the weighting matrices, Q and G . When applied to an aircraft such a feedback control ensures the stability of the aircraft and also minimizes its mean square values of the state deviation and control variables. As a result of such minimization the acceleration levels will be minimized too. Although minimizing the acceleration levels will provide a better ride quality for the aircraft, as described in section 2.4 such a result does not ensure that the handling qualities of the aircraft have not been degraded. In other words, the optimal solution obtained from the L.Q.P. will not guarantee that desirable aircraft handling qualities (acceptable to the pilot) will result.

In order to incorporate the need to attain good flying qualities simultaneously with improved ride and to investigate how the optimal control affects the performance of the aircraft in terms of its handling qualities, it is convenient to use the state representation of the equations of motion of the aircraft. Thus,

$$\dot{\underline{x}} = \underline{A}\underline{x} + \underline{B}\underline{u} \quad (4.71)$$

where the nature of this equation in respect of aircraft dynamics has been discussed in Chapter 2.

Using state feedback gives

$$\underline{u}^o = \hat{K}^o \underline{x} \quad (4.72)$$

where \hat{K}^o is obtained from (4.56). The closed loop system may then be described by

$$\dot{\underline{x}}_c = \underline{A}\underline{x}_c + \underline{B}\hat{K}^o \underline{x}_c + \underline{H}\underline{r} \quad (4.73)$$

where the subscript c , represents the closed loop situation. The

vector \underline{r} , of dimension q is a command or reference vector, representing the command inputs from the pilot or his navigation systems. $H(n \times q)$ is the coefficient matrix of the command vector. (4.73) then reduces to:

$$\dot{\underline{x}}_c = (A + BK^0)\underline{x}_c + Hr \quad (4.74)$$

The characteristic equation of the open loop system described by (4.71) is given by,

$$|\lambda I - A| = 0 \quad (4.75)$$

For the closed loop system, however, the characteristic equation is

$$|\lambda I - (A + BK^0)| = 0 \quad (4.76)$$

From a comparison of (4.75) and (4.76) it can be seen that the resulting eigenvalues will not be identical. Such differences will affect these dynamic characteristics that describe the handling qualities of the aircraft. The way in which the handling qualities for the closed loop controlled system will be affected depend on the feedback matrix K^0 which in turn is dependent on the particular choice of the weighting matrices Q and G . In order to obtain desirable handling qualities for the aircraft when using an L.Q.P. solution the selection of the matrices, Q and G should be made with care. A trial and error procedure could prove to be very laborious and inefficient since there does not exist a method of obtaining appropriate Q and G matrices which are unique.

A variety of methods of obtaining suitable weighting matrices for the L.Q.P. have been proposed (e.g. Bryson and Ho [1969], Harvey and Stein [1978]). However no explicit method is yet available by means of which Q or G may be selected so that specified handling qualities are obtained. In an effort to overcome this difficulty it was ^{designed} designed to make use of the model-matching, or as it is often referred to in the literature, model-following technique.

4.8 A MODEL MATCHING METHOD FOR HANDLING QUALITIES IMPROVEMENT

The use of the theory of model-matching makes it possible to provide for an aircraft a control law which will force its output variables to follow closely the output variables of some designer-specified model. Such a model is an idealization and is generally chosen to provide flight characteristics which are stable and invariant throughout the flight envelope.

There exist several methods that can be used to achieve model matching between the model of the aircraft and the desired, or ideal, model. The two most widely-used methods are explicit (or model-in-the-system) and implicit model following (or model-in-the-P.I.). Explicit model-following uses the desired model in the control system as a prefilter ahead of the dynamics of the aircraft (Tyler [1964]). Implicit model-following uses optimal feedback gains to modify the characteristics of the uncontrolled aircraft such that they approach the model characteristics. In this method the model is usually incorporated into the performance index. Generally explicit model-following needs the synthesis of input derivatives and for this reason the method of implicit model-following is more effective in aeronautical engineering.

4.8.1 Implicit Model Following

For the reasons explained briefly above the implicit model-following was found to be more appropriate for the purpose of this work.

Implicit model-following requires a solution that produces a perfect match between the output variables of the models representing the aircraft and the ideal dynamics. Instead of minimizing directly the error between the motion variables of the aircraft and the model states implicit model-following imposes a somewhat weaker condition which in mathematical

terms is stated as follows (Erzberger [1968]). Let the aircraft dynamics be described by

$$\dot{\underline{x}} = A\underline{x} + B\underline{u} \quad (4.77)$$

$$\underline{y} = C\underline{x} \quad (4.78)$$

where \underline{x} is an n -dimensional state vector;
 \underline{u} is an m -dimensional control vector;
 \underline{y} is a p -dimensional output vector.

The matrices A, B and C are invariant and have dimensions $n \times n$, $n \times m$ and $p \times n$ respectively.

Also, it is assumed that $n \geq m$ and $n \geq p$. The mathematical description of the model aircraft dynamics is taken to be

$$\dot{\underline{z}} = L\underline{z} \quad (4.79)$$

where L is the model matrix of order $(\ell \times \ell)$
and \underline{z} is an ℓ -dimensional vector.

The objective of implicit model following is to find a feedback law, $\underline{u} = S\underline{x}$ to be placed around the aircraft dynamics so that its output vector \underline{y} approximates as closely as possible over some specified time interval to

$$\dot{\underline{y}} = L\underline{y} \quad (4.80)$$

In contrast to Kalman who proposed to achieve this objective by the use of the optimal control law which minimized the quadratic performance index of the following form

$$J = \int_{t_0}^{t_f} [(\dot{\underline{y}} - L\underline{y})^T Q (\dot{\underline{y}} - L\underline{y}) + \underline{u}^T R \underline{u}] dt \quad (4.81)$$

Erzberger suggested the algebraic solution which was employed in this work.

Using (4.77) and (4.78) and requiring that (4.80) be a strict equality, then

$$\dot{\underline{y}} = LC\underline{x} \quad (4.82)$$

and
$$\dot{\underline{y}} = C\dot{\underline{x}} = CA\underline{x} + CB\underline{u} \quad (4.83)$$

Therefore equating the right hand sides of (4.82) and (4.83) provides:

$$LC\underline{x} = CA\underline{x} + CB\underline{u} \quad (4.84)$$

or
$$CB\underline{u} = (LC-CA)\underline{x} \quad (4.85)$$

Hence,
$$\underline{u}^0 = [CB]^\dagger (LC-CA)\underline{x} \quad (4.86)$$

where $[CB]^\dagger$ represents the pseudo-inverse of the matrix $[CB]$. Its evaluation is possible by using any of several available algorithms.

If perfect matching is achieved then from (4.85) and (4.86)

$$\begin{aligned} (LC-CA)\underline{x} &= [CB][CB]^\dagger (LC-CA)\underline{x} \\ &\rightarrow \{[CB][CB]^\dagger - I\} \{(LC-CA)\underline{x}\} = [0] \end{aligned} \quad (4.87)$$

For perfect matching (4.87) is zero for any \underline{x} . If perfect matching is not achieved then, because of the properties of the pseudo-inverse, the feedback matrix $[CB]^\dagger (LC-CA)$, is guaranteed to yield a weighted least-squares match between the response of the resulting controlled system and that of the model.

4.8.2 Selection of the Model Matrix (L)

If it is possible to specify the eigenvalues of a closed-loop system which result in some desired output characteristics then it is possible to derive the matrix L which is characterised by these eigenvalues. In this work the L matrix was selected empirically to provide reasonable dynamic characteristics to the model, by basing the choice on coefficient matrices associated with aircraft dynamics which are known to provide acceptable handling qualities.

what is
good
L

4.8.2.1 Selection of a model for longitudinal motion

The selection of the model for longitudinal motion was based on the criteria for acceptable handling qualities (Table 4.1). Approximate expressions describing the dynamic characteristics of the sp and phugoid modes of the aircraft were employed for the selection of corresponding model parameters which would result in desirable handling qualities for the aircraft.

From the two degree of freedom approximation for the short period motion ω_{sp} and ζ_{sp} may be described (McRuer et al [1973]) as

$$\omega_{sp} = \sqrt{M_q Z_w - M_w U_0} \quad (4.88)$$

and

$$\zeta_{sp} = -(Z_w + M_q + U_0 M_w) / 2\omega_{sp} \quad (4.89)$$

From the three degree of freedom approximation for phugoid motion ω_p and ζ_p may be described as follows:

$$\omega_p^2 = -\frac{g}{U_0} \left(Z_u + \frac{M_u Z_w}{M_w} \right) \quad (4.90)$$

and

$$\zeta_p = \left\{ -X_u + \frac{M_u (U_0 X_w - g)}{M_w U_0} \right\} / 2\omega_p \quad (4.91)$$

If some appropriate choice of the stability derivatives viz. $X_w, Z_w, M_w, M_q, X_u, Z_u, M_u$ and M_w is made to ensure that ζ_{sp}, ζ_p and ω_{sp}/ω_p are within the ranges specified for acceptable handling qualities, then these parameters may be used to construct the model matrix for longitudinal motion.

In section 2.3.1 of Chapter 2 in which the ride discomfort index was presented, the ride comfort of an aircraft was shown to be directly proportional to either Z_w or M_w . The smaller the values of these derivatives the less is the resulting ride discomfort index and hence better ride comfort will result.

However, since the primary aim of the implementation of model-matching theory was to provide acceptable handling qualities, an initial choice of a model matrix was made to satisfy the handling qualities requirements for the aircraft. Table 4.2 shows the choice of the stability derivatives for the model.

TABLE 4.2

	BASIC AIRCRAFT	MODEL
$\checkmark X_w$.108	.1
$\checkmark Z_w$	-1.01	-1.65
$\checkmark M_w$	-.0099	-.02
$\checkmark X_u$	-0.166	-0.136
$\checkmark Z_u$	-.175	-0.0305
$\checkmark M_u$.00131	.000727
$\checkmark M_q$	-.546	-1.33
M_w	-.00091	-.000906

ie does it need RCS?

The model stability derivatives are very nearly identical to those of the aircraft flying at sea level, at a somewhat higher speed and increased all-up weight (and correspondingly higher wing-loading).

4.8.2.2 Selection of a model for lateral motion

In a similar fashion the lateral motion model was chosen to satisfy the handling qualities criteria presented in Table 4.1.

The selection of parameters the model was based on the description of the lateral motion characteristics by means of the following approximate expressions (McRuer et al [1973]).

From the three degree of freedom approximation for dutch roll ω_d and ζ_d may be defined as follows:

$$\omega_d = \sqrt{N'_\beta + N'_R Y_v} \quad (4.92)$$

and

$$\zeta_d = (-Y_v - N'_R) / 2\omega_d \quad (4.93)$$

For the same equations of motion the solution of the following equations give the time constants of the spiral and roll subsidence modes (T_S and T_R respectively).

$$T_S \cdot T_R = 1 / \left\{ \frac{g}{U_0} \left(\frac{L'_\beta}{N'_\beta} N'_R - L'_R \right) \right\} \quad (4.94)$$

$$\frac{1}{T_S} + \frac{1}{T_R} = L'_P - \frac{L'_\beta}{N'_\beta} (N'_P - g/U_0) \quad (4.95)$$

If an appropriate choice of the stability derivatives $Y_v, L'_\beta, N'_\beta, L'_P, N'_P, L'_R$ and N'_R is made, to ensure that the resulting handling qualities agree with the requirements presented in Table 4.1, then these derivatives may be used to construct an appropriate model matrix. Table 4.3 shows the values which are more chosen for the stability derivatives of the model.

TABLE 4.3

	BASIC AIRCRAFT	MODEL
Y_v	-.14	-.229
L'_β	-4.05	-7.28
N'_β	1.34	5.47
L'_P	-1.85	-2.0
N'_P	-.245	-1.87
L'_R	.517	.17
N'_R	-.19	-2.4

Since no ride discomfort index has been proposed for a lateral motion the choice of the model was made in the absence of any possible constraints for ride comfort.

Table 4.4 summarizes the dynamic characteristics of the basic aircraft and the models for both the longitudinal and lateral motions.

TABLE 4.4

Handling Qualities Characteristics for Basic Aircraft and Model

LONGITUDINAL MOTION			
	Acceptable handling qualities (H.Q.)	Basic Aircraft H.Q.	Model H.Q.
ζ_p	>0.04	0.0087^\dagger	0.059
ζ_{sp}	$0.3 < \text{ and } < 2.0$	0.5	0.616
ω_p/ω_{sp}	≤ 0.1	0.11^\dagger	0.035
LATERAL MOTION			
	Acceptable handling qualities (H.Q.)	Basic Aircraft H.Q.	Model H.Q.
ζ_d	$\geq .19$	0.0247^\dagger	0.465
ω_d	≥ 1.0	1.397	2.35
$\zeta_d \omega_d$	$\geq .35$	0.034^\dagger	1.09
T_R	< 1.4	0.474	0.444

† denotes unacceptable handling qualities

CHAPTER 5

MATHEMATICAL MODELS OF THE ACTUATING ELEMENTS

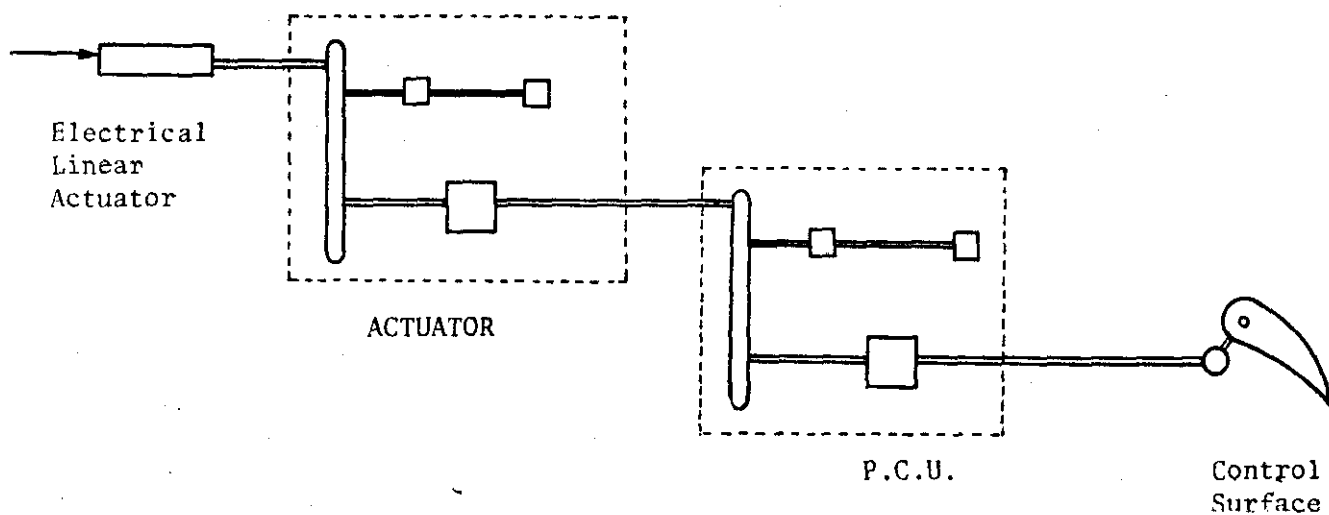
5.1 INTRODUCTION

The operation of a control system consists of three elemental processes: sensing, signal processing, and actuation. In any aircraft flight control system sensing elements are employed to sense (or measure) the absolute or relative value of particular motion variables. The output from such sensors will be signals which have to be processed by some on-board controller, or computer, according to a predetermined flight control program. At the same time the controller will also process the command signals from the pilot, or any automatic guidance system, to drive the actuating element(s).

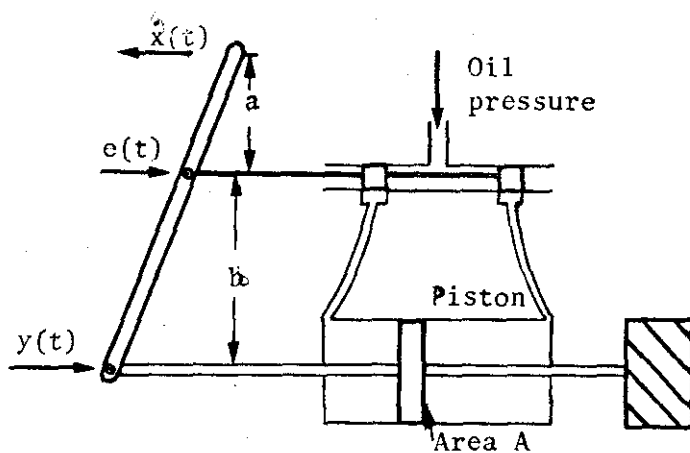
The actuating elements (A.E.) for an aircraft are those system components which drive the prime movers (i.e. engines, control surfaces, etc.) in response to commands. The A.E. required to move an aerodynamic control surface usually consists today of an hydraulic actuator and associated powered flying control unit (P.C.U.). Figure 5.1 illustrates the control activity of a typical two-stage hydraulic actuating element. The command signal from the pilot or from an on-board controller activates an electrical linear actuator which moves the control valve of the hydraulic actuator accordingly. The flow from the hydraulic power supply generates a force which acts on the piston of the actuator and this force then moves the piston which is connected with the valve of the P.C.U. The same procedure is then repeated for the P.C.U. component which gives rise to a force which finally moves the control surface through appropriate mechanical linkages.

The selection of an actuating device is determined primarily by the power required to drive the load. Other factors to be considered include the dynamic characteristics, the existing power supplies available, the physical and economic limitations of the equipment as well as the complexity and the likely reliability of the resulting system. For modern high

a. Control configuration of the A.E.



b. Position feedback control for actuator and P.C.U.



c. Block diagram representation of A.E.

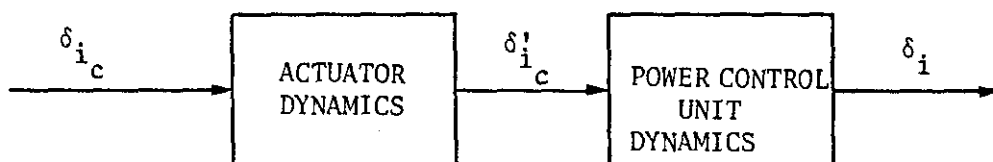


FIGURE 5.1: Two stage hydraulic actuating element

performance aircraft it is required that continuous control of the motion variables should be achieved easily and rapidly with precision. The continuous, rapid and accurate response of the A.E. to a command signal imposes very serious "life" constraints on the actuating system. Consequently the design of a hydraulic actuator and the associated mechanical linkage stages should be very carefully considered in the early designing of an automatic control system in order to achieve an acceptable fatigue life of the actuating elements.

In this work no attempt was made to design such actuating systems but the models of the actuators and power control units were chosen such that they represented realistic actuating systems. Special consideration of the limited power capabilities available for use was made in terms of imposing displacement rate limits upon the actuating element and this is discussed in Section 5.3. In Section 5.2 the mathematical models employed to represent the considered control surfaces are described.

5.2 MATHEMATICAL MODELS FOR THE ACTUATING ELEMENTS EMPLOYED

The dynamic response of an aerodynamic control surface to a command signal depends upon both the dynamic characteristics of the A.E.s composing the actuating system and the nature of the hinge moment. Generally such hinge moments are non-linear and depend to a considerable degree upon the mechanical arrangements adopted in the design of each aircraft. However, the non-linearity can often be represented as a saturation characteristic. Therefore it was decided in this work to account for such characteristic implicitly by the imposition of displacement limits. As a result, the analysis remained linear with due note rate being taken, when appropriate, of response degradation due to existence of these limits.

An actuating element can be classified as a first, second, etc., order system depending on its dynamic response characteristics. Consider the following configuration for a simple ram

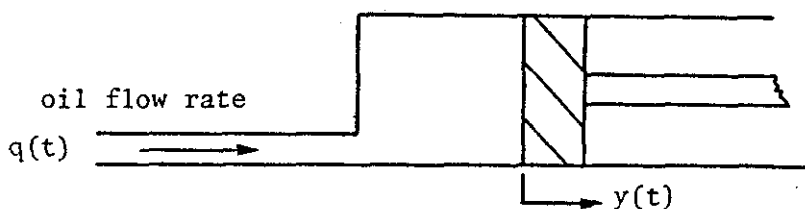


FIGURE 5.2: Simple ram

It can be shown (Schwarzenbach and Gill [1978]) if ram inertia, viscous forces and compressibility effects are considered then the following equation for flow rate input may be obtained.

$$q(t) = \frac{\nu M}{k_B A} \frac{d^3 y(t)}{dt^3} + \left(\frac{k_L M}{A} + \frac{\mu \nu}{k_B A} \right) \frac{d^2 y(t)}{dt^2} + \left(\frac{k_L \mu}{A} + A \right) \frac{dy(t)}{dt} \quad (5.1)$$

where v : volume of trapped fluid
 M : total mass being moved
 A : effective ram area
 K_B : bulk modulus of the fluid
 K_L : leakage coefficient
 μ : friction coefficient

For a hydraulic servomechanism with mechanical feedback control as shown in Figure 5.1b the rate of flow through the valve is proportional to the area of opening, say,

$$q(t) = c e(t) \quad (5.2)$$

where c is a constant and $e(t)$ can be found by geometry, viz.

$$e(t) = \frac{b}{a+b} x(t) - \frac{a}{a+b} y(t) \quad (5.3)$$

if $a=b$ then

$$e(t) = \frac{x(t)-y(t)}{2} \quad (5.4)$$

and (5.2) becomes

$$q = c \frac{(x(t)-y(t))}{2} \quad (5.5)$$

from (5.1) and (5.5) the following transfer function may be obtained

$$\frac{Y(s)}{X(s)} = \frac{c/2}{s \left\{ \frac{vM}{K_B A} s^2 + \left(\frac{K_L M}{A} + \frac{\mu v}{K_B A} \right) s + \left(\frac{K_L \mu}{A} + A \right) \right\} + c/2} \quad (5.6)$$

If leakage is assumed to be negligible then the transfer function described by (5.6) simplifies to

$$\frac{Y(s)}{X(s)} = \frac{c/2}{s \left\{ \frac{vM}{K_B A} s^2 + \frac{\mu v}{K_B A} s + A \right\} + c/2} \quad (5.7)$$

For an actuator or a small power unit the trapped volume v and μ , will be small and compared to the high bulk modulus of oil it can be

eliminated from (5.7). Hence,

$$\frac{Y(s)}{X(s)} = \frac{c/2}{sA+c/2} \quad (5.8)$$

Hence, for an actuator and a small power control unit which could be used to drive a small control surface a first order representation would be a good approximation. For a larger power control unit (5.7) gives a third order system. Experimental testing can be used to prove (Schwarzenbach and Gill [1978]) that a second order approximation for such a system would be adequate for representing the dynamic characteristics of the P.C.U.

In choosing the A.E.s it is important to consider the range of frequencies over which they operate, so that their natural frequencies will not interfere with the rigid-body motion and the natural frequencies of the structural modes of the aircraft. In the case of a STOL aircraft, assumed to be perfectly represented by its rigid-body motion alone, this constraint on the natural frequencies of the actuating system is translated according to section 2.2 as

$$\omega_{n \text{ A.E.}} \geq 63 \text{ rad/s} \quad (5.8)$$

From the Bode diagram (see Annex C) of the dynamics of the actuator and power unit associated with particular control surfaces it can be seen that (5.8) is satisfied, indicating that little interference with the aircraft response by the actuator dynamics will occur.

The actuating element is considered to comprise (Fig.5.1) an actuator, which may be, depending on type, 1st or 2nd order system and the power unit, which is regarded as being a 1st order system.

The following models were used to represent the actuating elements for the control surfaces considered.

*disorder numbers*LONGITUDINAL MOTION

ACTUATOR

POWER CONTROL UNIT

ELEVATOR

$$\frac{\delta_E(s)}{\delta_{E_C}(s)} = \frac{1}{0.08s+1} \frac{1}{0.25 \times 10^{-4} s^2 + 0.75 \times 10^{-2} s + 1} \quad (5.9)$$

SPOILER

$$\frac{\delta_{SP}(s)}{\delta_{SP_C}(s)} = \frac{1}{0.8s+1} \frac{1}{0.5 \times 10^{-2} s + 1} \quad (5.10)$$

HORIZONTAL CANARD

$$\frac{\delta_{CH}(s)}{\delta_{CH_C}(s)} = \frac{1}{0.08s+1} \frac{1}{0.02s+1} \quad (5.11)$$

LATERAL MOTION

RUDDER

$$\frac{\delta_R(s)}{\delta_{R_C}(s)} = \frac{1}{0.04s+1} \frac{1}{0.2777 \times 10^{-4} s^2 + 0.75 \times 10^{-2} s + 1} \quad (5.12)$$

AILERON

$$\frac{\delta_A(s)}{\delta_{A_C}(s)} = \frac{1}{0.033s+1} \frac{1}{0.01s+1} \quad (5.13)$$

VERTICAL CANARD

$$\frac{\delta_{CV}(s)}{\delta_{CV_C}(s)} = \frac{1}{0.04s+1} \frac{1}{0.02s+1} \quad (5.14)$$

STATE REPRESENTATION

For a second order actuator transfer function of the following form

$$\frac{\delta_i}{\delta_{i_C}} = \frac{1}{T_1 s^2 + T_2 s + 1} \cdot \frac{1}{T_3 s + 1} \quad (5.15)$$

the equivalent state representation may be given by

$$\dot{\underline{x}} = \underline{A}\underline{x} + \underline{B}u \quad (5.16)$$

$$\dot{\underline{y}} = \underline{C}\underline{x} \quad (5.17)$$

in which

$$A = \begin{bmatrix} 0 & 1 & 0 \\ 0 & 0 & 1 \\ -\frac{1}{T_3 T_1} & -\frac{(T_2 + T_3 + T_2 T_3)}{T_3 T_1} & -\frac{1}{T_3} \end{bmatrix}$$

$$B = \begin{bmatrix} 0 \\ 0 \\ \frac{1}{T_3 T_1} \end{bmatrix}, \text{ and } C = [1 \quad 0 \quad 0]$$

An actuating system with a first order actuator has a transfer function of the form:

$$\frac{\delta_i}{\delta_{i_c}} = \frac{1}{T_1 s + 1} \frac{1}{T_2 s + 1} \quad (5.18)$$

Hence,

$$A = \begin{bmatrix} 0 & 1 \\ -\frac{1}{T_1 T_2} & -\frac{(T_1 + T_2)}{T_1 T_2} \end{bmatrix}, \quad B = \begin{bmatrix} 0 \\ \frac{1}{T_1 T_2} \end{bmatrix}$$

$$C = [1 \quad 0].$$

5.3 POWER LIMITATIONS OF THE ACTUATING ELEMENT

The consideration of the actuator and power unit dynamics in the simulation is necessary when a realistic knowledge of the aircraft's behaviour is required. But once realism and therefore applicability is considered the assumption of complete linearity of the control system should be doubted.

Independent of its dynamic characteristics a physical system is constrained by specific design limitations which in effect have the result that particular tasks commanded from a linear automatic control system cannot be performed within the linear range of the system. A common problem of this nature is that the maximum rate at which the A.E. can move, in order to follow a command signal is limited. The displacement rates of A.E.'s characterize the power demanded from the actuating system. These physical limitations are mainly imposed upon the weight and volume of the fitted system. Currently the power/weight ratio of an hydraulic A.E. is about $2W/N$ and the best available ratio for an electric A.E. is about $0.5W/N$.

As a result of such power limitations a control system could prove to be unusable on an aircraft because it would then degrade the performance by being unable to perform the commands from the linear control law. To prevent, and cure, if needed, a similar situation rate limits of the A.E.s were considered in the simulation. Figure 5.3 gives a block diagram representation of the actuating system with rate constraints.

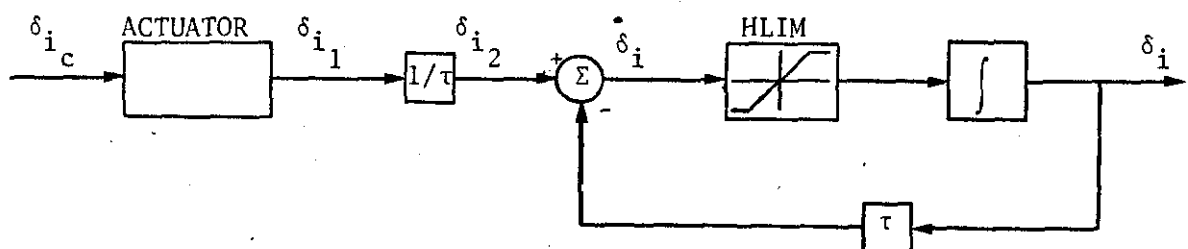


FIGURE 5.3: Actuating system with rate constraints

The function HLIM ensures that the rate limits will not be exceeded at any time. Whenever the linear control law demanded from the A.E. rates larger than could be provided, the HLIM function allowed only the maximum available rate to act on the control surface. The rate limits were chosen to represent for this work realistic models and they were as follows:

Elevator	25 ⁰ /s	(0.436 rad/s)
Spoilers	180 ⁰ /s	(3.141 rad/s)
H.Canards	140 ⁰ /s	(2.443 rad/s)
Rudder	70 ⁰ /s	(1.222 rad/s)
V.Canard	120 ⁰ /s	(2.094 rad/s)
Aileron	140 ⁰ /s	(2.443 rad/s)

How chosen?

Deflection angle limits were also employed to account for non-linearities due to hinge moment saturation. Figure 5.4 gives a block diagram representation of the actuating system with deflection angle constraints.

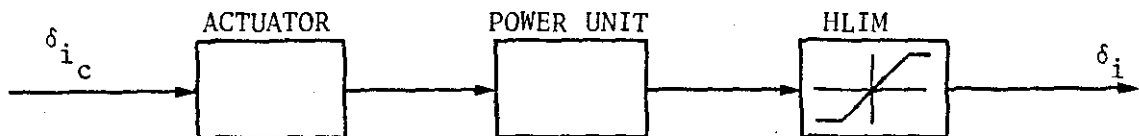


FIGURE 5.4: Actuating system with deflection angle constraints

The deflection limits employed for this research for the considered aerodynamic control surface configurations were chosen to be

$$\begin{aligned}
 -23^{\circ} &< \delta_E < 23^{\circ} \\
 -7.5^{\circ} &< \delta_{SP} < 7.5^{\circ} \\
 -5^{\circ} &< \delta_{CH} < 5^{\circ} \\
 -10^{\circ} &< \delta_R < 10^{\circ} \\
 -25^{\circ} &< \delta_A < 25^{\circ} \\
 -5^{\circ} &< \delta_{CV} < 5^{\circ}
 \end{aligned}$$

Figure 5.5 gives a full block diagram representation of the control system with actuators and rate and deflection angle limits included.

ACTUATORS INCLUDED IN THE LOOP

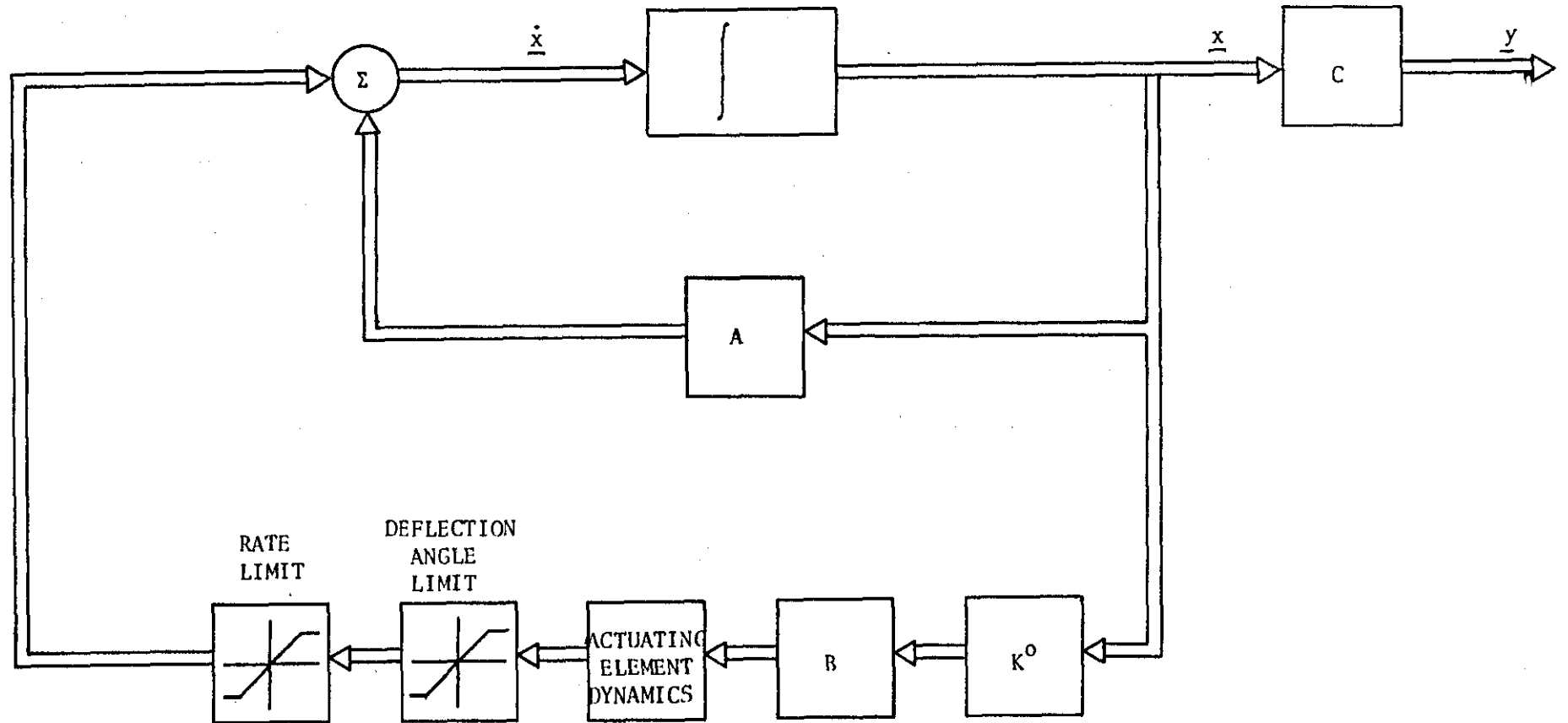


FIGURE 5.5

CHAPTER 6

ANALYSIS OF THE DYNAMIC RESPONSE
OF THE MODIFIED JETSTAR AIRCRAFT

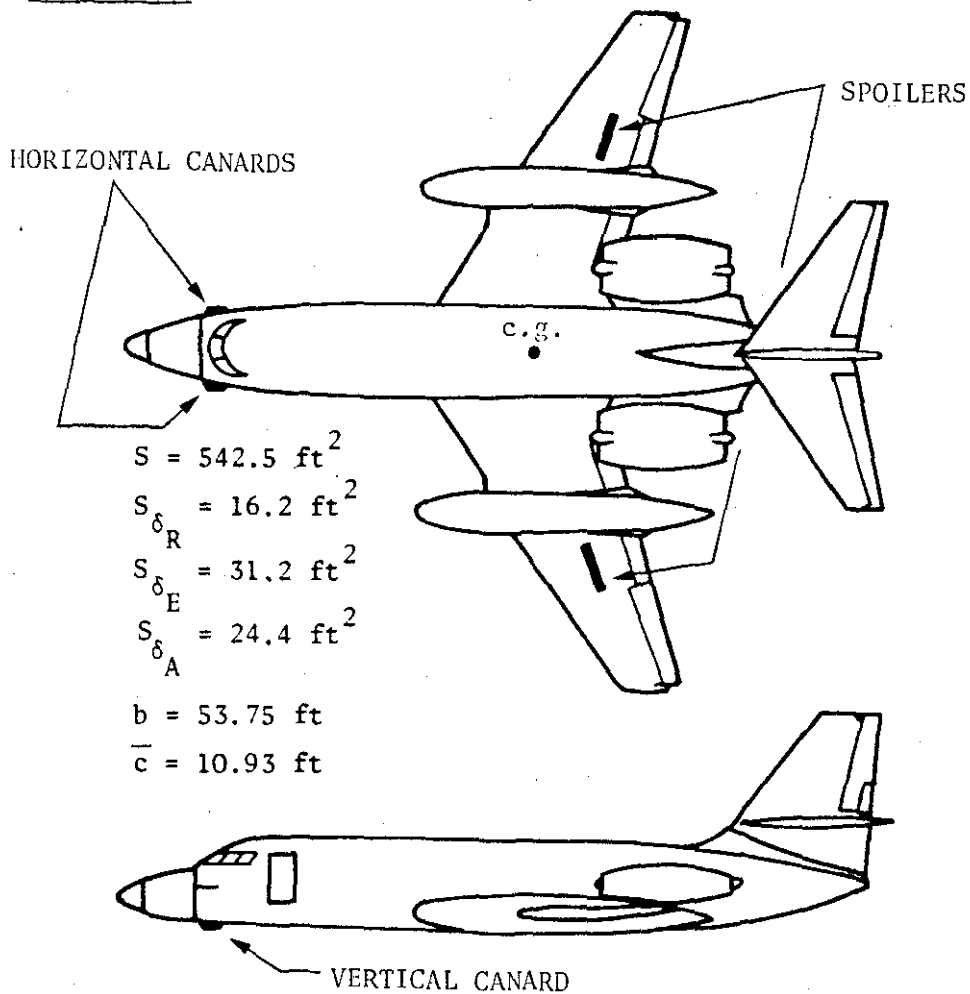
6.1 INTRODUCTION

The analysis of the dynamic performance of the modified Jetstar was based on the results obtained from digital simulation and frequency response analysis. The modified Jetstar aircraft used in this ride quality study is presented in Figure 6.1. The table presented in this figure summarises all possible combinations of the conventional and the auxiliary aerodynamic control surfaces which were investigated in this research. The dynamic response of the aircraft was studied separately for deterministic and stochastic (turbulence) inputs.

Deterministic analysis was used to determine the dynamic characteristics of the aircraft due to the activity of different control surface combinations for different types of deterministic inputs and optimal feedback control laws. In the deterministic analysis the dynamic responses of the uncontrolled and controlled aircraft were studied separately. The dynamics of the uncontrolled aircraft were investigated by using both frequency response analysis and digital simulation.

Stochastic inputs were used to evaluate the ride quality performance of the modified Jetstar in turbulent flight. The same optimal feedback control laws which were used in the deterministic analysis were also employed. However, a nonlinear controller was also considered in the stochastic analysis.

FIGURE 6.1: Jetstar Modification



INVESTIGATED CONTROL SURFACE CONFIGURATIONS

	LONGITUDINAL MOTION			LATERAL MOTION		
	ELEVATOR	SPOILER	HORIZONTAL CANARD	RUDDER	VERTICAL CANARD	AILERON
OPTION.1	X			X		
OPTION.2		X			X	
OPTION.3			X			X
OPTION.4	X	X		X	X	
OPTION.5	X		X	X		X
OPTION.6		X	X		X	X
OPTION.7	X	X	X	X	X	X

6.2 ANALYSIS OF THE DYNAMIC RESPONSE OF THE AIRCRAFT SUBJECTED TO COMMAND INPUTS

The deterministic analysis was developed by studying the dynamics of the uncontrolled and optimally controlled aircraft separately. In each of these studies the dynamic characteristics of the longitudinal and lateral motions were also investigated separately.

6.2.1 Dynamics of the Uncontrolled Aircraft

The general transient characteristics of the dynamic response of an aircraft may be inferred from frequency response analysis. In this research Bode diagrams were employed to illustrate the characteristics of the modes of motion of the aircraft for different aerodynamic control surface inputs. Bode diagrams show how both the amplitude ratio and the phase difference between an input and output variable change over a wide range of frequencies. From these frequency response diagrams it is possible to judge the relative effectiveness of the considered control surfaces on each motion variable of the aircraft. The frequency response analysis using Bode diagrams provides valuable information for single-input, single-output (S.I.S.O.) systems and for systems where sinusoidal excitation is physically realizable. However, such an approach cannot provide information for multivariable control systems other than indicate a general knowledge of the effectiveness of each control acting alone. In order to obtain better information about each control and any possible combination of controls on the dynamic response of an uncontrolled aircraft, time-domain analysis and simulation should be employed. In this research both step function deflections of the controls and initial conditions were used to provide the required excitation.

The use of a step function as the reference variable is very useful as it represents an instantaneous jump in amplitude which provides a lot of information about the system's dynamic characteristics. Further since a step function, in principle, contains a wide band of frequencies in its spectrum as a result of the jump discontinuity it is equivalent to the application of an infinite frequency series of sinusoidal functions. Another way of testing the dynamics of an uncontrolled aircraft is by releasing it from initial conditions. Bode diagrams, step inputs, and initial conditions were all used to determine the relative effectiveness of the control surfaces employed and the transient characteristics of the uncontrolled aircraft for both longitudinal and lateral motions.

6.2.1.1 Longitudinal Motion Analysis

The Bode diagrams of the open loop transfer functions of the aircraft were established for an appropriate range of frequencies. Figures 6.2(a),(b),(c) and (d) represent the Bode diagrams of the motion variables u, w, q and θ in response to elevator input. From these figures the two basic modes of longitudinal motion, the phugoid and the short period oscillation, (s.p.o.) may be identified. The phugoid lies in the low frequency range and its natural frequency is $\omega_p = 0.19$ rad/s. The s.p.o. lies at higher frequencies and has a natural frequency $\omega_{sp} = 1.7$ rad/s. Also the damping ratio of the phugoid and s.p.o. are $\zeta_p = 0.009$ and $\zeta_{sp} = 0.5$ respectively (see Annex D). From comparison of the damping factors it can be said that the phugoid is a very lightly damped low frequency mode while the s.p.o. is a well-damped, high-frequency mode. These dynamic characteristics correspond to the phugoid and s.p. modes of the basic Jetstar at low, straight and level, flight conditions. Figure 6.2(a) shows that the amplitude ratio $|u/\delta_E|$ is much smaller at the natural

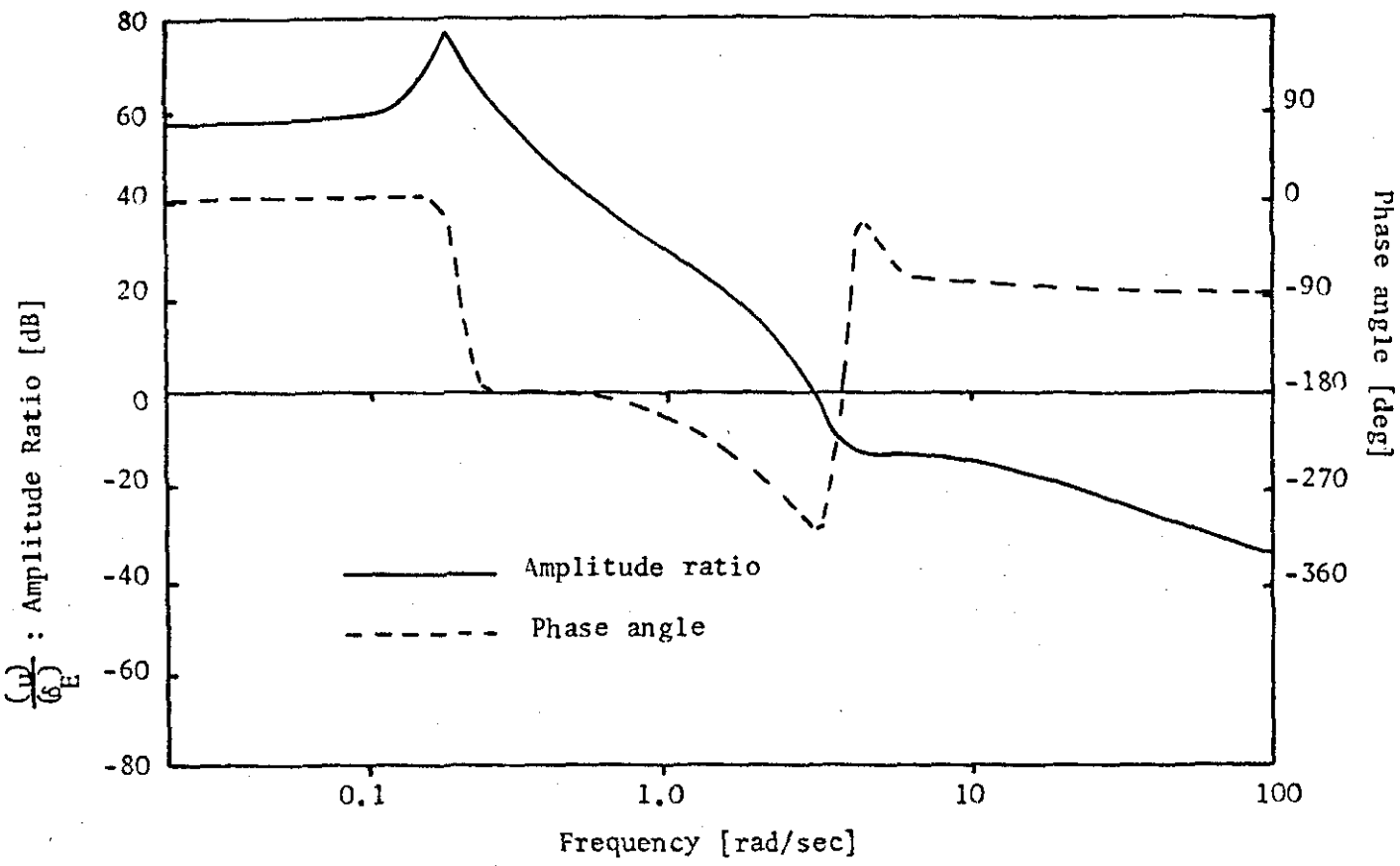


FIGURE 6.2(a)

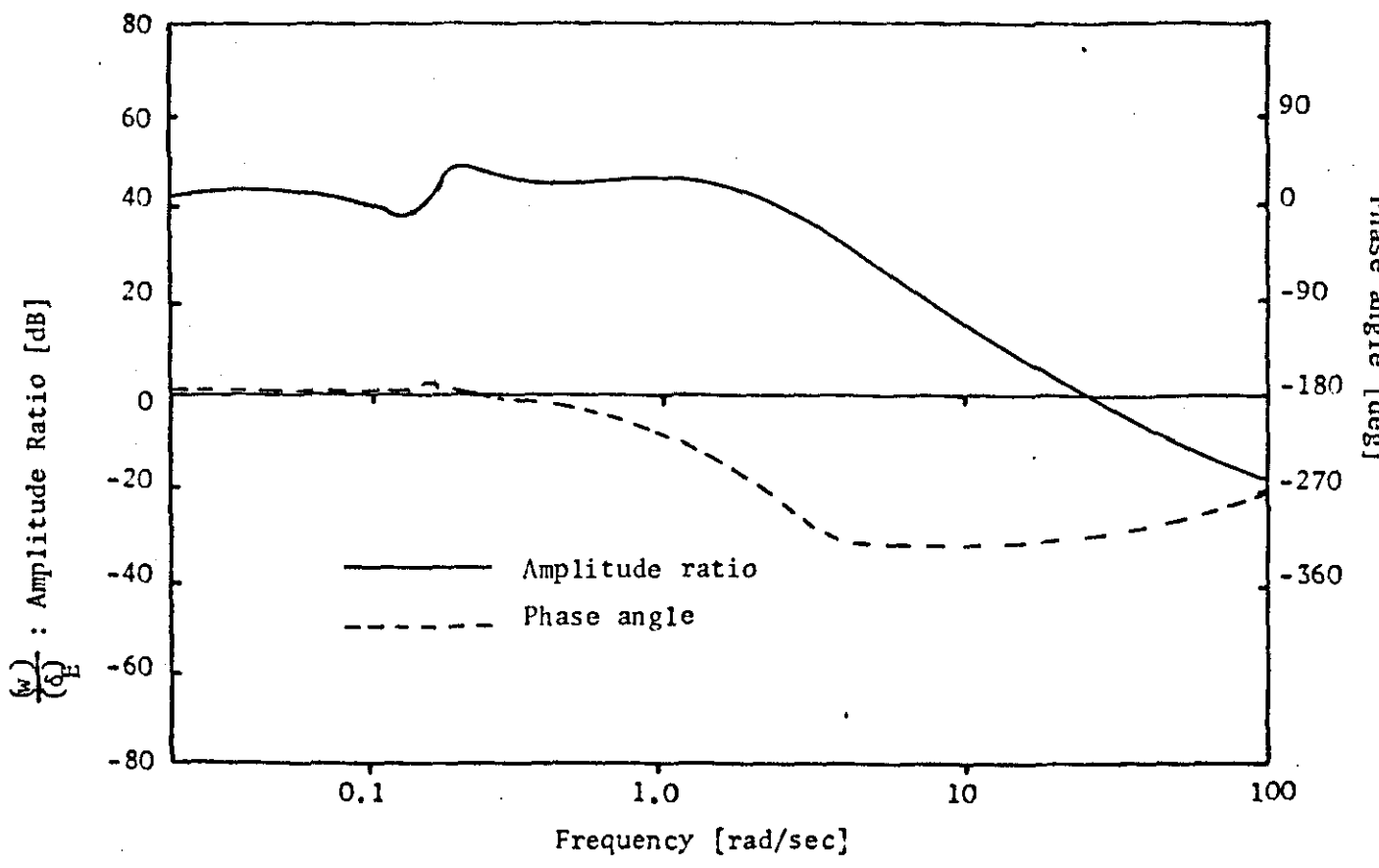


FIGURE 6.2(b)

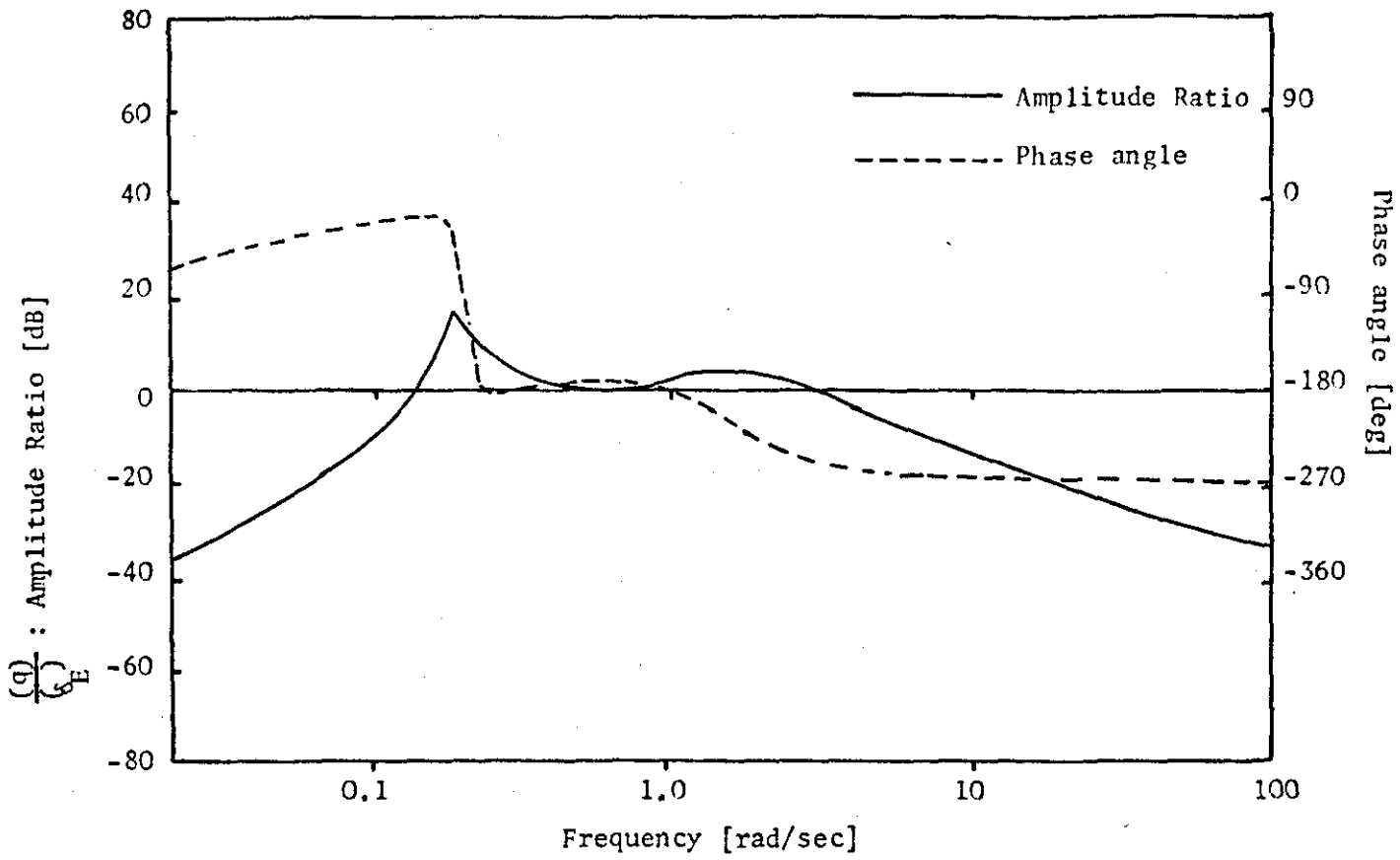


FIGURE 6.2(c)

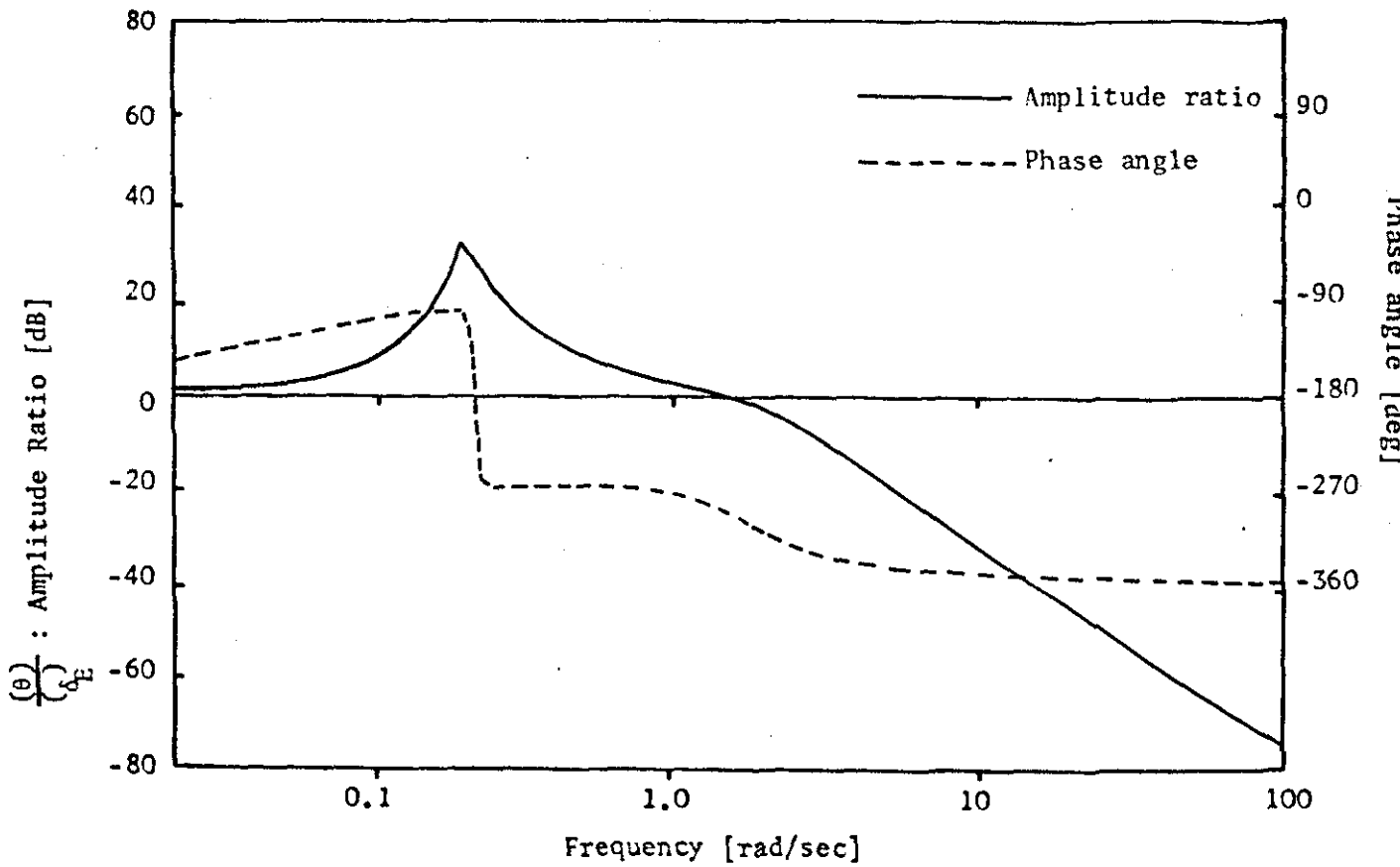


FIGURE 6.2(d)

frequency of the s.p.o. than at that of the phugoid. In other words, phugoid introduces the largest forward speed changes. Figures 6.2(b), (c) and (d) show that the values of the amplitudes $|w/\delta_E|$, $|q/\delta_E|$ and $|\theta/\delta_E|$ for the s.p.o. and phugoid are of nearly the same magnitude.

Figures 6.2(a) and (b) illustrate the strong effect which elevator has on u and w motion variables. From equation (4.4) it can be seen that the normal acceleration at the c.g. of an aircraft depends on these two motion variables. According to Figures 6.2(a) and (b) elevator will be expected to be an important contributor to normal acceleration. From comparison of 6.2(a) and (b) it may be deduced that the normal acceleration contribution, due to phugoid is slightly higher than that due to the s.p. mode. ?

Figure 6.2(c) indicates that the aircraft exhibits a relatively slow pitch response to elevator commands which is a desirable feature for a transport aircraft. Similar shapes of amplitude ratio variations, over the same frequency range, were obtained for the same motion variables when spoilers and horizontal canards were used for inputs. Figure 6.3 illustrates the amplitude ratio and the phase change of the normal acceleration transfer functions a_z/δ_E , a_z/δ_{SP} and a_z/δ_{CH} over the same range of frequencies. ?

Figure 6.3(a) confirms the prediction that the acceleration induced on the aircraft due to the phugoid is higher from that due to the s.p. mode. From the same figure the relative effectiveness of the selected longitudinal control surfaces on normal acceleration may be judged. It can be seen that the acceleration due to elevator input is by approximately 10db higher from that due to spoiler which in turn is approximately 1.5db higher from that due to horizontal canards. Hence it *which prediction*

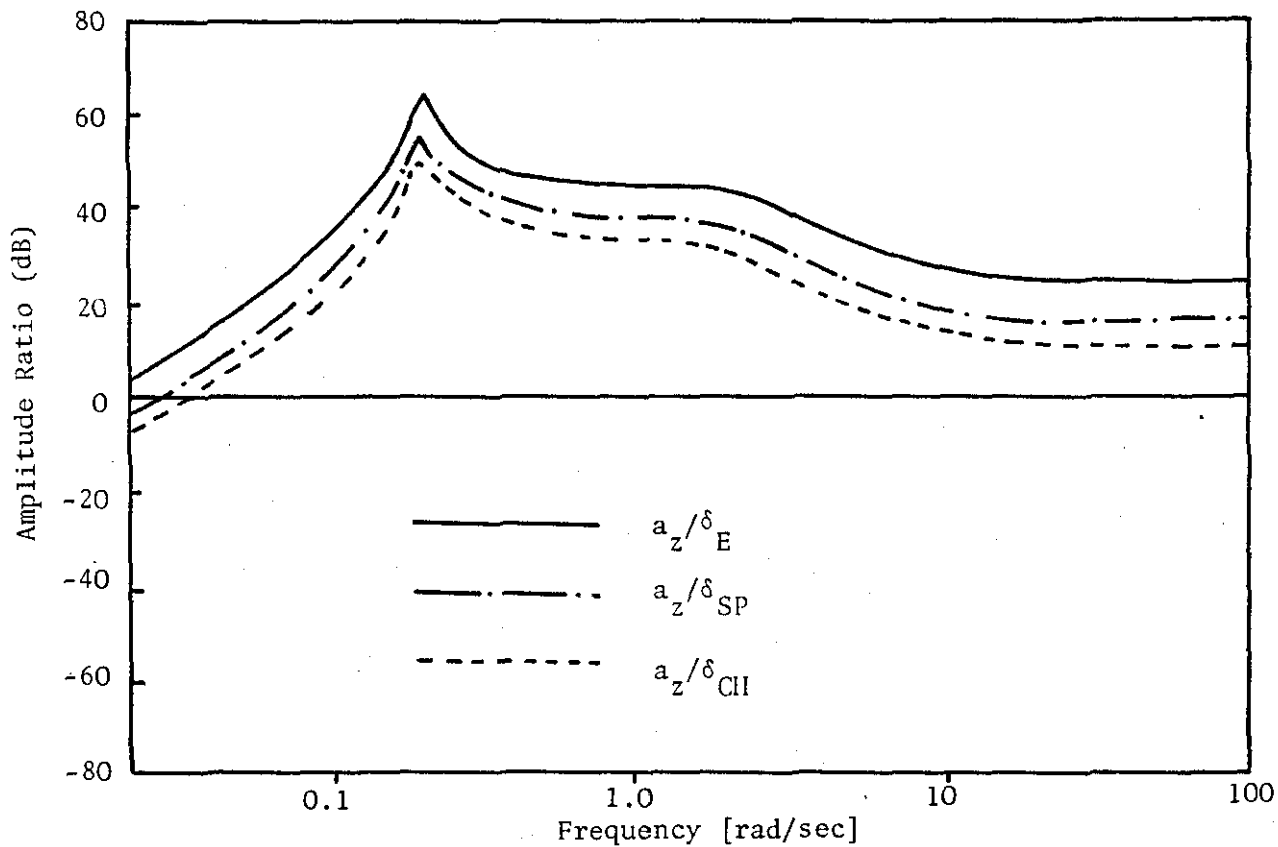


FIGURE 6.3(a)

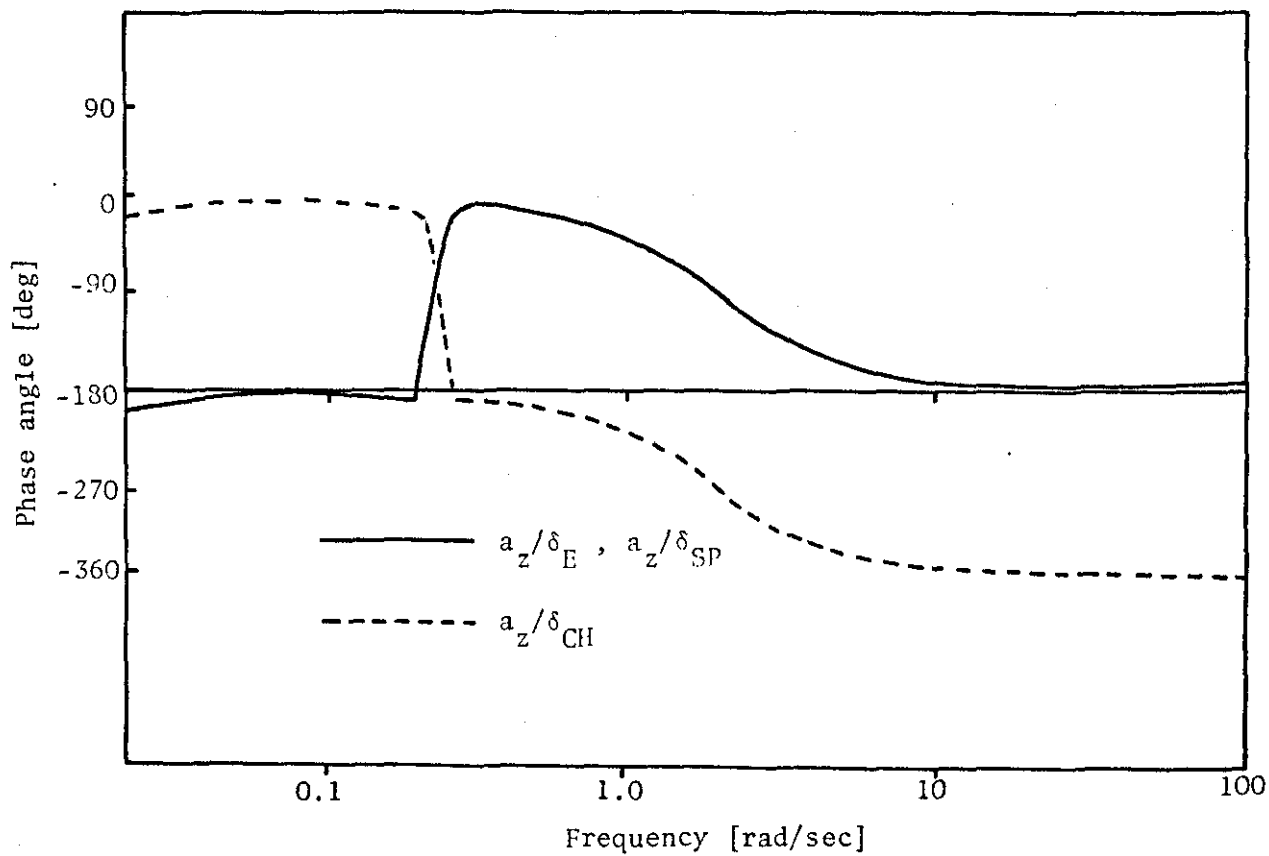
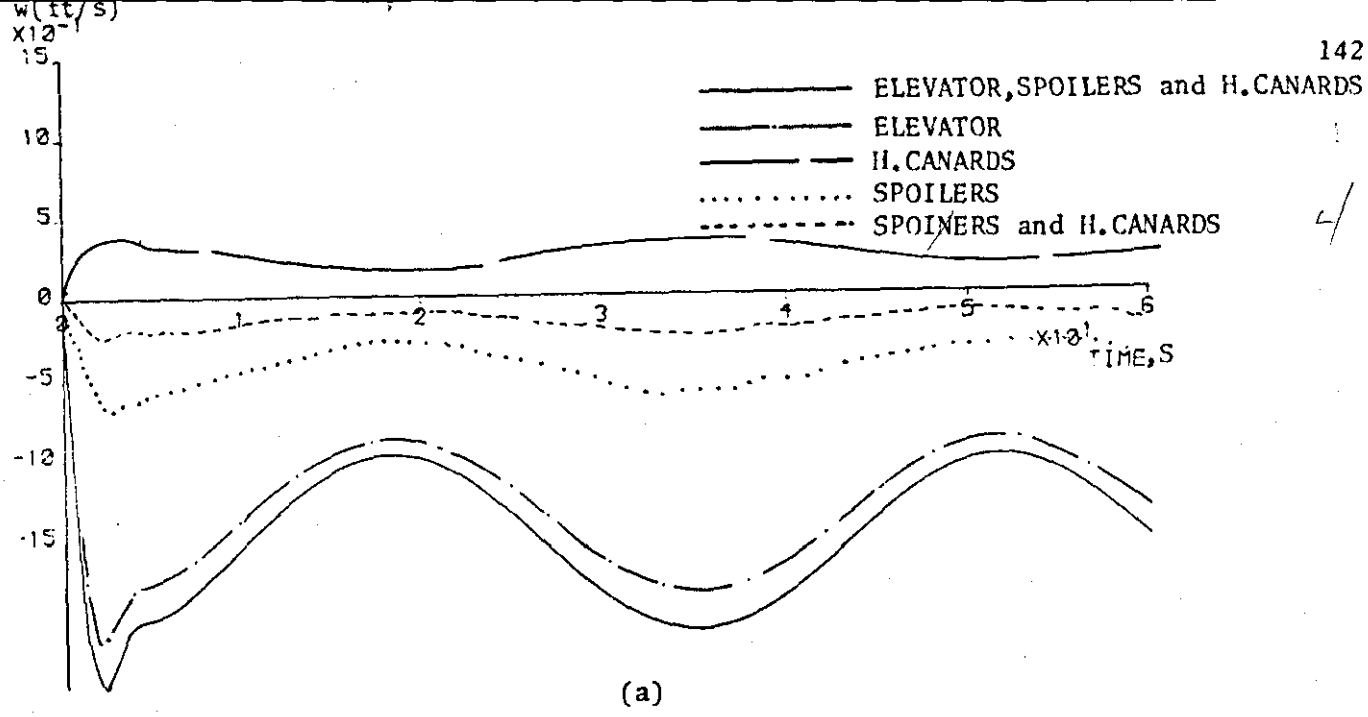
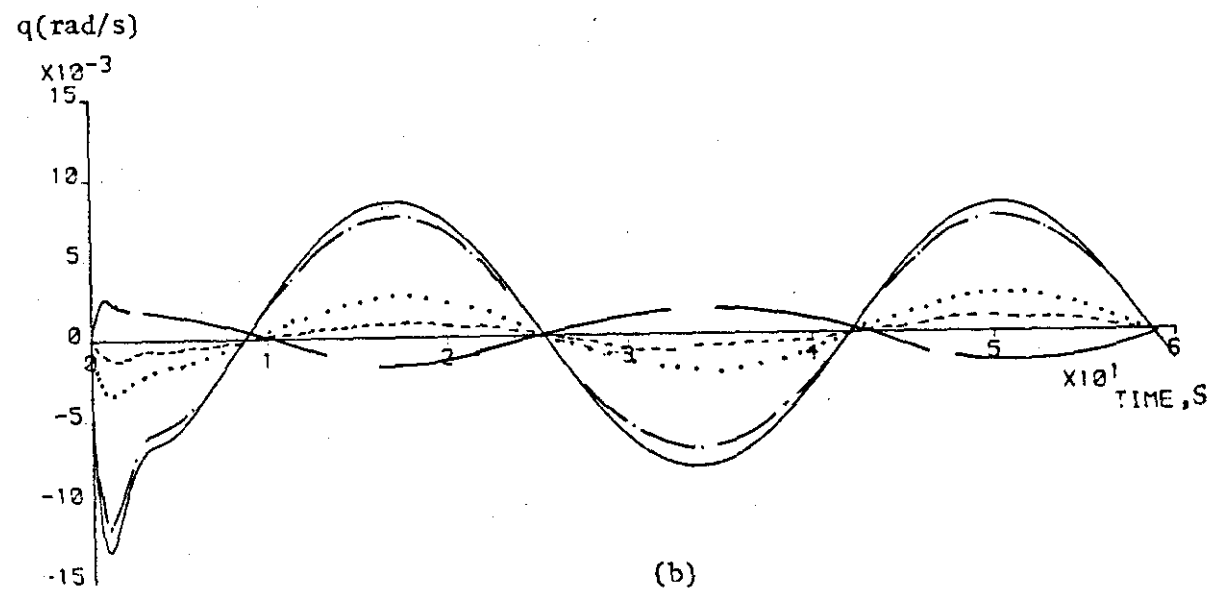


FIGURE 6.3(b)

could be said that the elevator is more effective from spoilers by a factor of 3 and from horizontal canards by a factor of 4.5. It should be noticed that these factors correspond to the ratios by which the force and moment coefficients of elevator is related to the spoilers and horizontal canards respectively. From the phase angle change diagram the canard is seen to be 180° out of phase with elevator and spoilers for the frequency range of interest. This property of horizontal canards could be proved to be very important in terms of normal acceleration control when they are considered to act in conjunction with elevator or spoilers in a controlled situation. In order to investigate the combinational effectiveness of the considered control surfaces and to verify the results obtained from frequency response analysis time domain analysis should be employed. Figure 6.4 illustrates the dynamic responses of the modified Jetstar aircraft subjected to 0.01 rad. step input commands. From this figure the two longitudinal modes of motion may be easily identified. The high frequency mode (s.p.o.) dies out in the first 5 sec. indicating that it is a well damped mode while the low frequency mode (phugoid) will take a long time before it will die out (lightly damped). From 6.4(c) it can be concluded that the normal acceleration due to phugoid dominates the average value of acceleration which accords with the frequency response analysis conclusion. In terms of the control surface effectiveness it can be seen that horizontal canards are 180° out of phase with the elevator and spoilers. Also the horizontal canards are less effective than spoilers as may be seen when they are applied simultaneously on the aircraft. An important conclusion which may be drawn from Figure 6.4 is the dominance of the elevator which was also shown in the frequency response analysis. Elevator dominates the

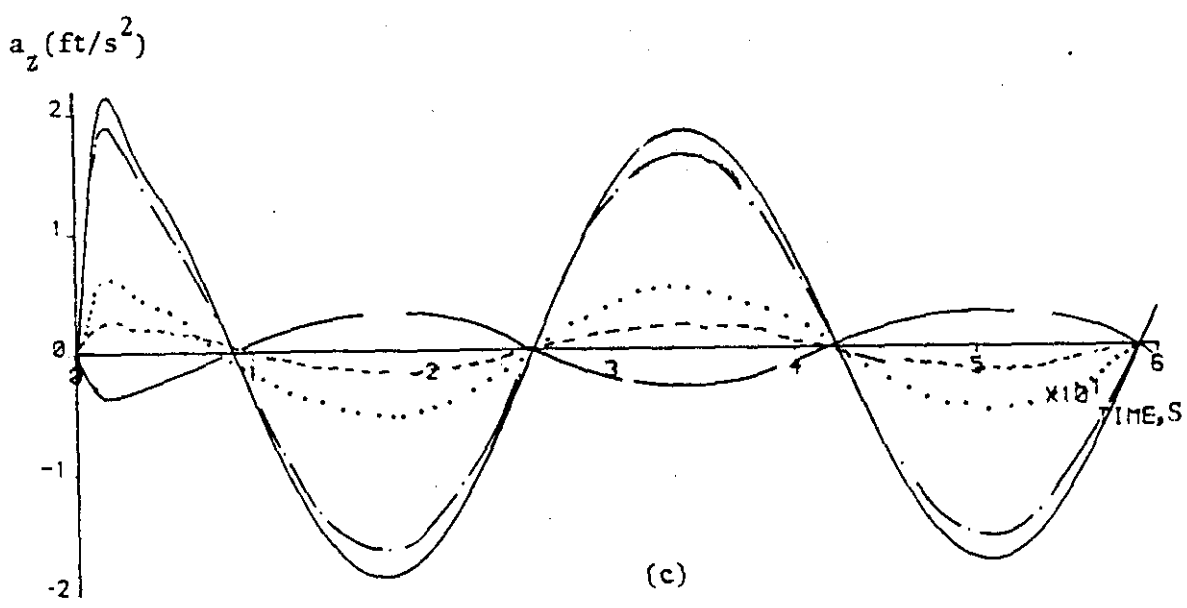


(a)



(b)

FIGURE 6.4: Dynamic Responses of the Uncontrolled Jetstar Aircraft for 0.01 rad step Commands of the Longitudinal Control Surfaces



(c)

longitudinal motion when equally used as the other controls. As it can be seen from 6.4(b) elevator induces comparatively high pitch rates which in turn (6.4(a)) results in changes in heave motion and hence induces normal accelerations on the aircraft. The same effect on acceleration is achieved in smaller scale by the spoilers indicating that they act more like conventional flaps rather than 'pure direct lift' control as defined by Pinsker (Section 2.6.1).

t.c. fms

6.2.1.2 Lateral Motion Analysis

The same procedure, as in the analysis of the longitudinal motion, was followed for the investigation of the lateral dynamics of the modified Jetstar aircraft. The frequency response analysis by Bode diagrams was based on Figures 6.5 and 6.6. Figures 6.5(a), (b), (c) and (d) illustrate the variation of amplitude ratio and phase angle of the motion variables β , p , r , and ϕ for rudder input over a wide range of frequencies. From these figures it can be seen that the dutch roll mode dominates the lateral response of the aircraft. This mode has a natural frequency $\omega_d = 1.4$ rad/s and damping ratio, $\zeta_d = 0.025$ which indicates that it is a high frequency response with low damping (see Annex D). Comparison of the phase angle of p and r (obtained from figures 6.5(b) and 6.5(c) respectively) indicates that these two motion variables are 180° out of phase. This is a typical characteristic of the dutch roll mode showing the strong coupling of the directional and pure lateral motion.

Spiral and roll subsidence are of minor importance as one can infer from their small contribution to the frequency response diagrams. The time constants of the spiral and roll subsidence modes are $T_S = 370$ s and $T_R = 0.5$ s (Annex D). From equation (4.6) it can be deduced that sideslip, β , is an effective contributor to the lateral acceleration measured at the c.g. of the aircraft. Figure 6.5(a) shows that dutch roll considerably affects the sideslip and hence the lateral acceleration. Whenever other modes make insignificant contributions to the motion compared to that of the dutch roll only the dutch roll mode will be considered therefore to represent lateral motion. The relative effectiveness of the rudder, aileron and vertical canard on lateral acceleration can be assessed from

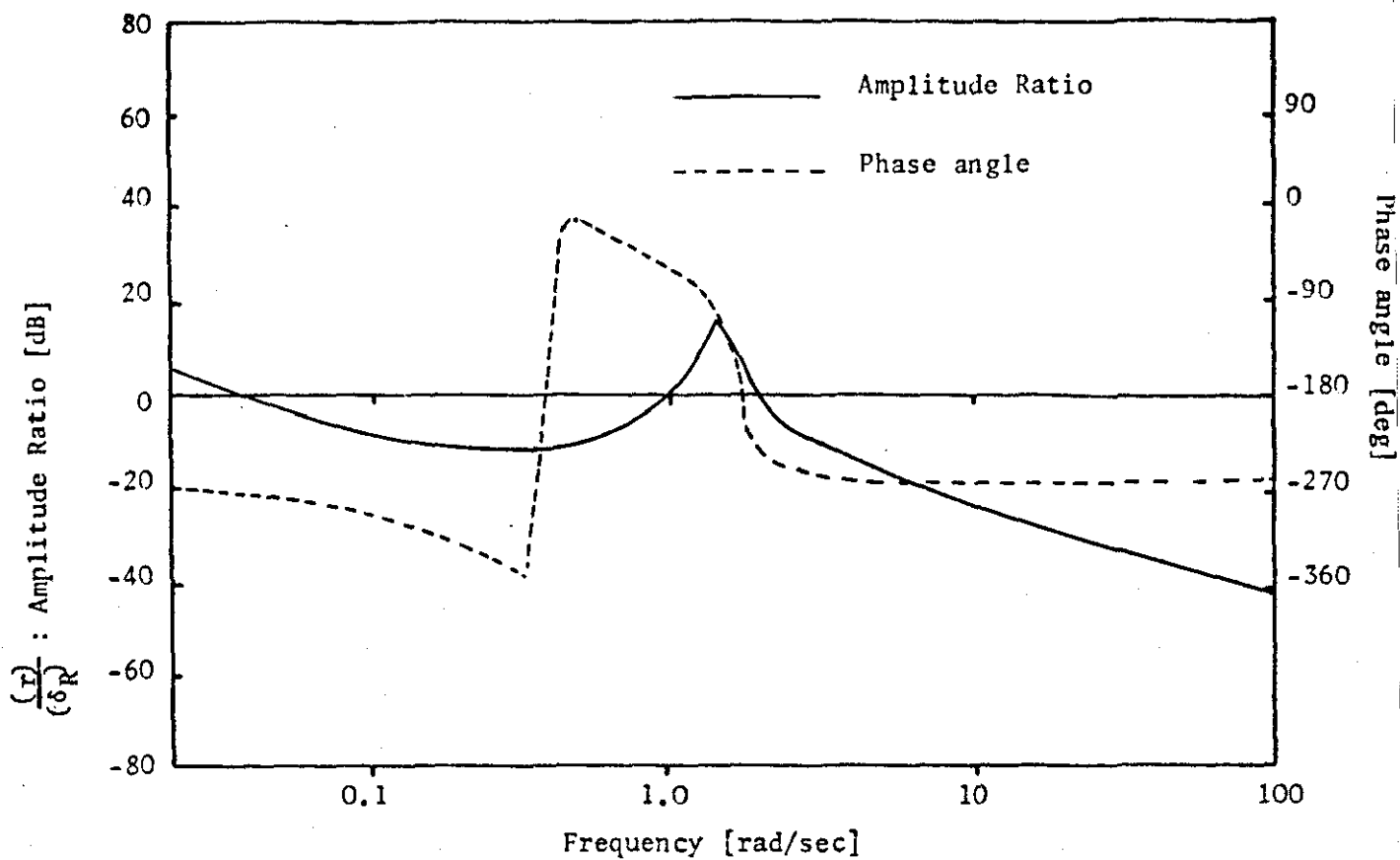


FIGURE 6.5(c)

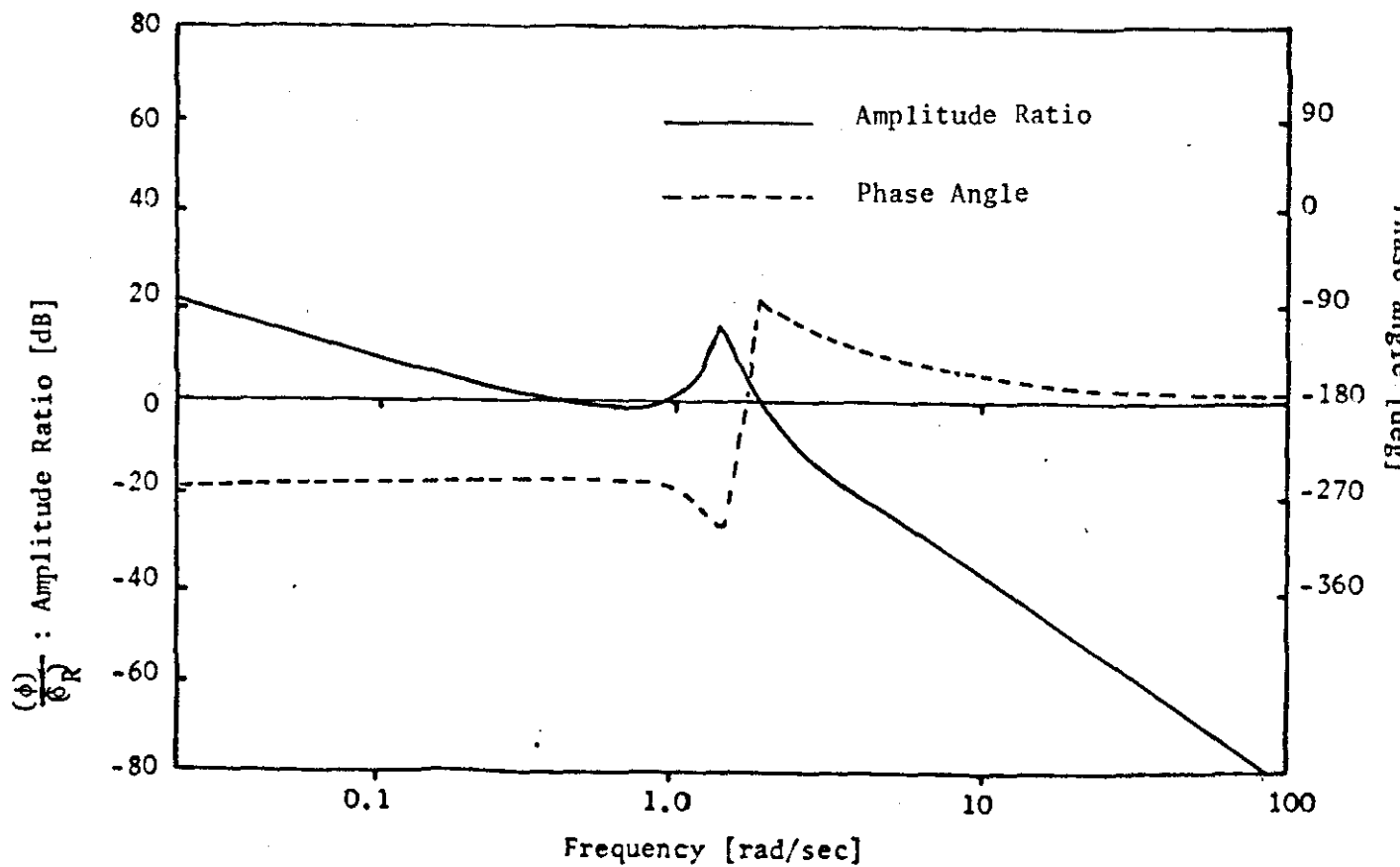


FIGURE 6.5(d)

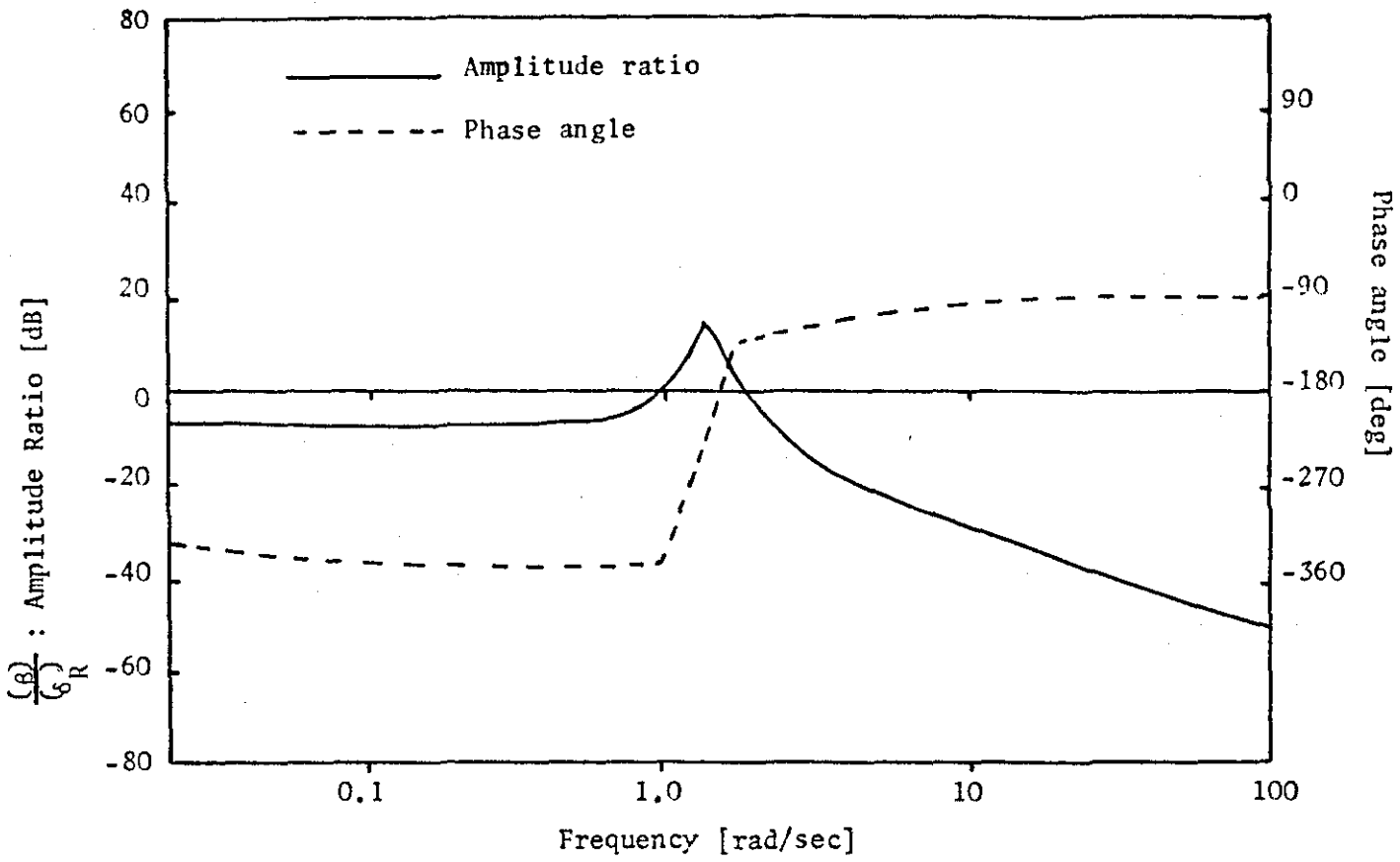


FIGURE 6.5(a)

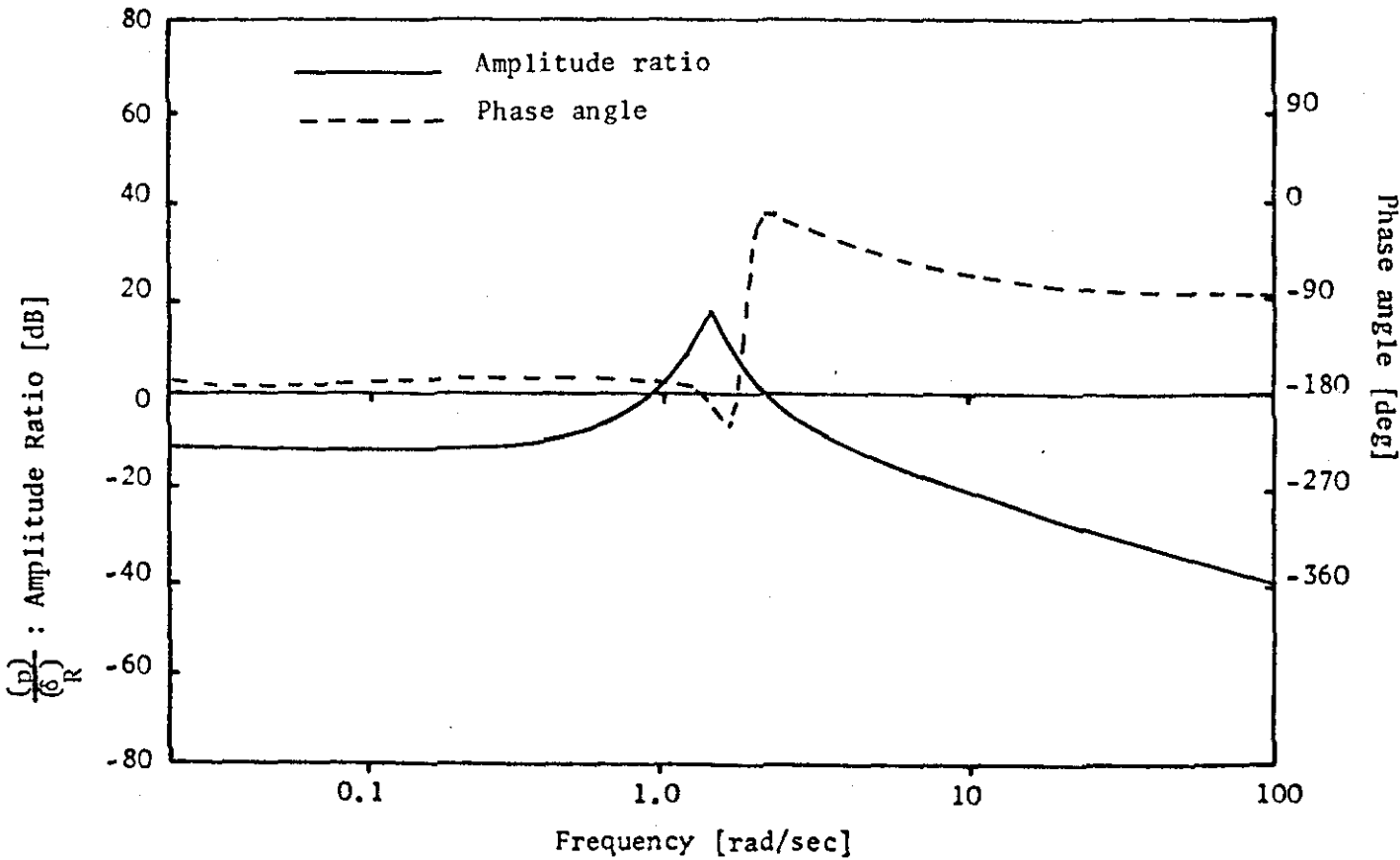


FIGURE 6.5(b)

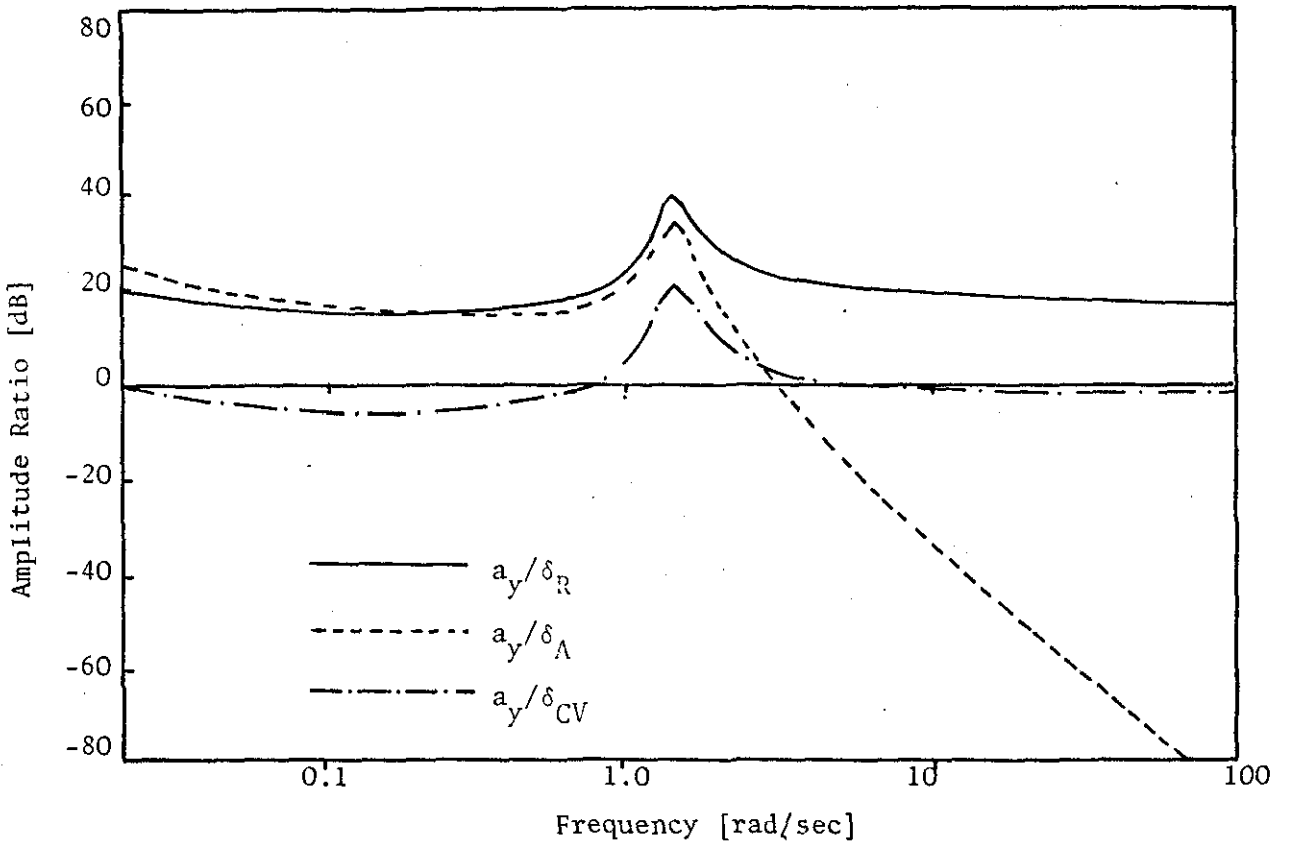


FIGURE 6.6(a)

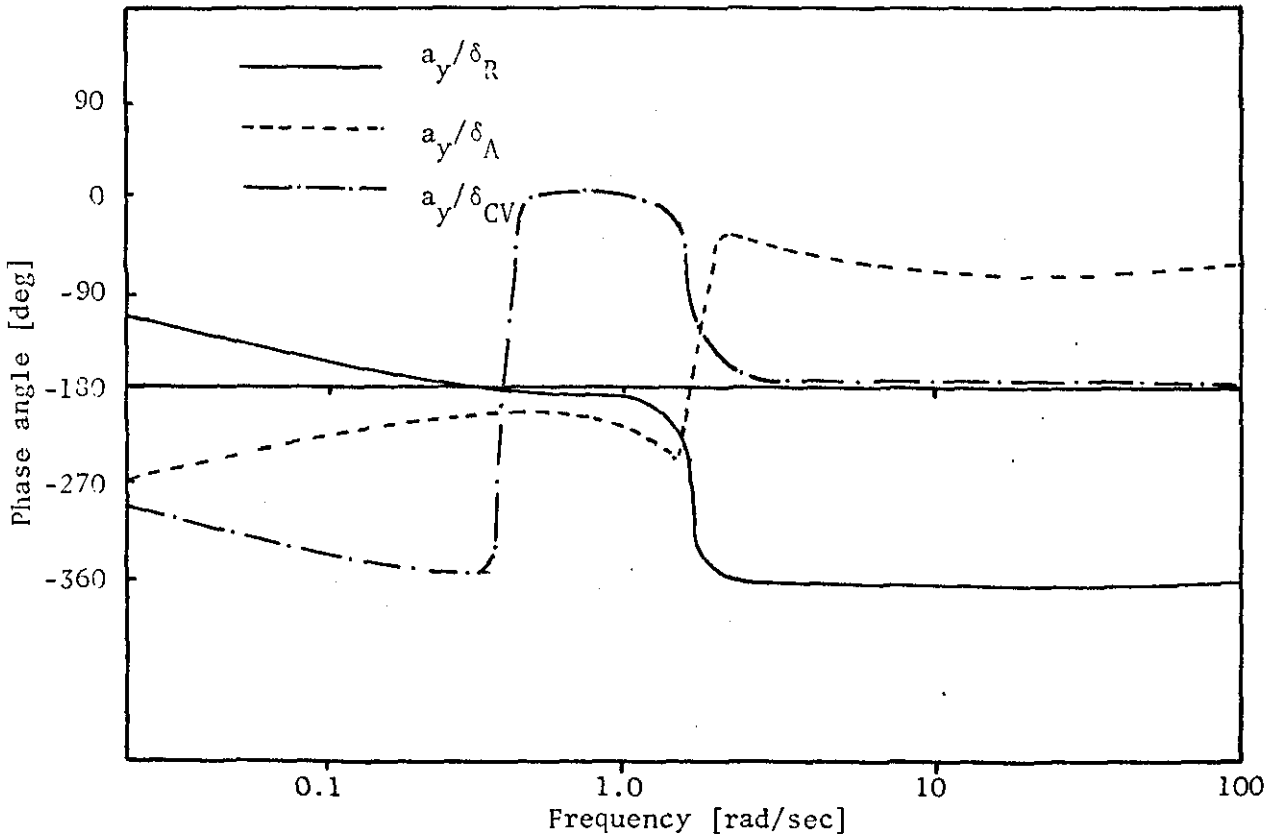


FIGURE 6.6(b)

Figure 6.6. From Figure 6.6(a) it can be seen that the rudder is more effective at all frequencies about 0.2 rad/s than the aileron which, in turn, is more effective than the vertical canard, particularly in the low frequency region. From Figure 6.6(a) it can be seen that the rudder is more effective by approximately 20db from vertical canard which corresponds to a factor of 10 equivalent to the ratio of the force and moment coefficient of these two control surfaces. From the phase angle of the Bode diagram (6.6(b)) it can be seen that the vertical canard is 180° out of phase with the rudder (compare the situation of the horizontal canards in relation to elevator). It can be also seen that rudder and aileron are out of phase.

} does this mean anything?

For the same reason as in the case of longitudinal motion time-domain analysis of the lateral motion of the aircraft was employed. Figure 6.7 shows how the lateral motion variables β, p, r, ϕ, ψ , and a_y vary with time when the aircraft is subjected to input step commands of 0.01 radians to the lateral aerodynamic control surfaces. The dominant role of the dutch roll mode which was determined in the frequency response analysis can also be detected by inspection of Figure 6.7. However, from Figures 6.7(b), (e) and (f) the presence of the spiral mode can also be detected. It may be deduced (from Figures 6.7(b), (e) and (f)) that it is the ailerons more than any other control surface which excite the spiral mode. As a result of the action of the ailerons yaw rate, r , bank angle, ϕ , and heading angle, ψ , build up faster than when the use of the rudder or vertical canard is considered. Due to the spiral mode the

?

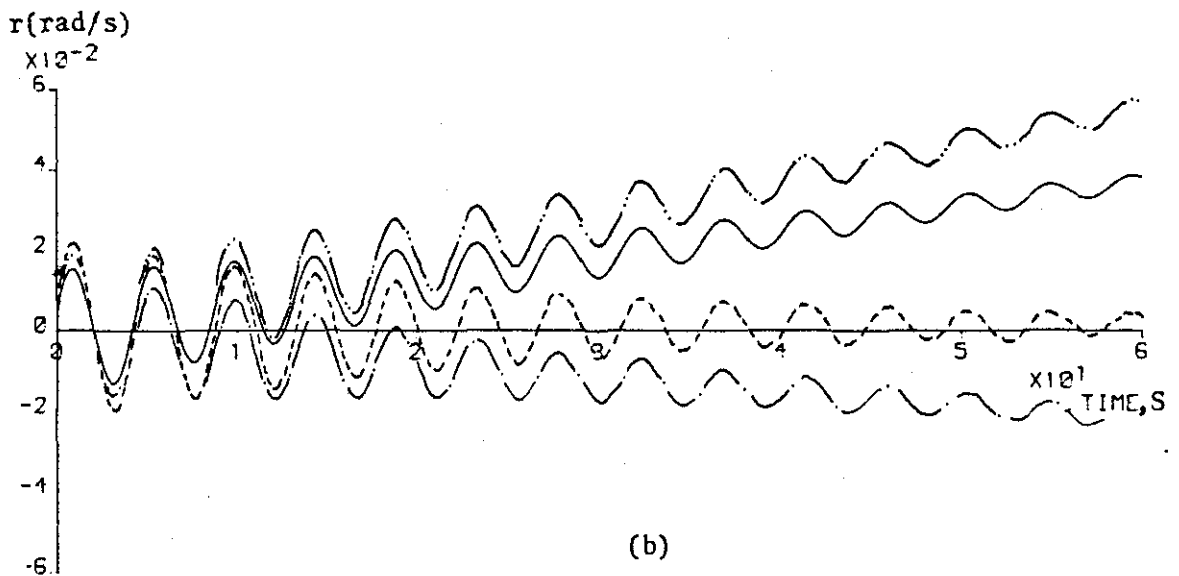
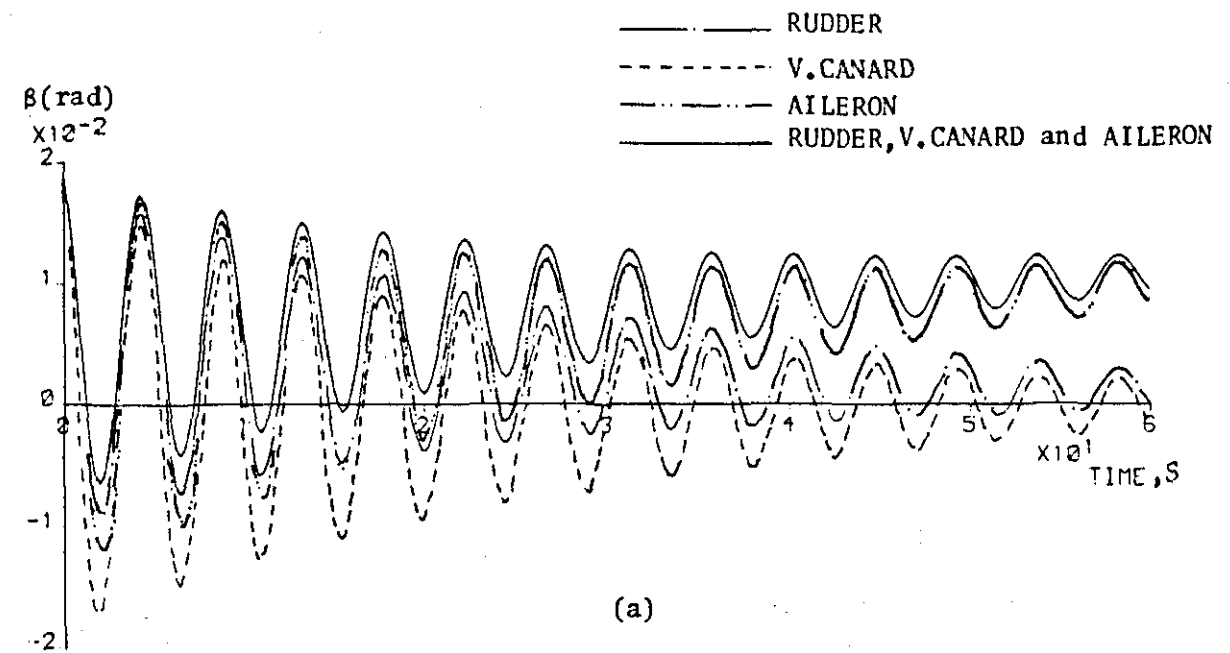
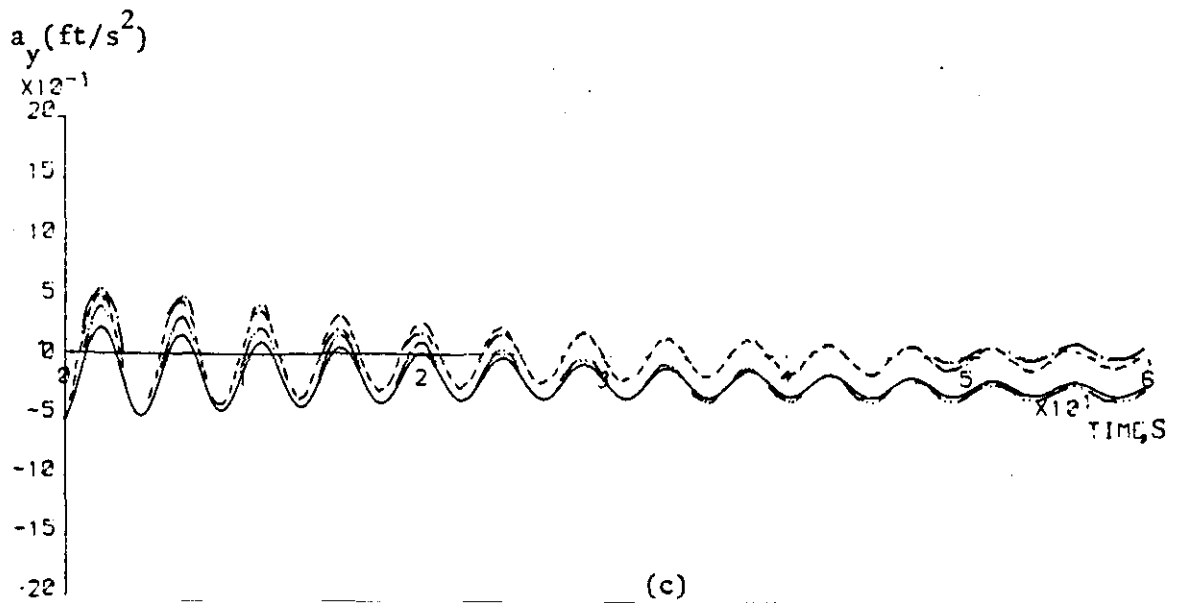


FIGURE 6.7: Dynamic Responses of the Uncontrolled Jetstar Aircraft for 0.01 rad Step Commands to the Lateral Control Surfaces



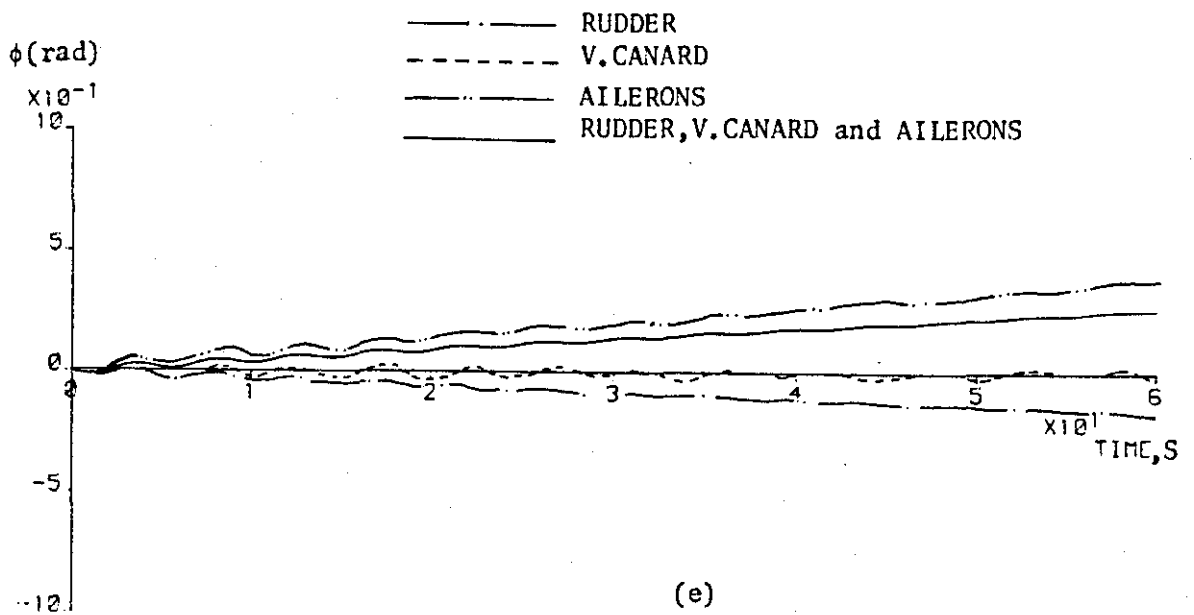
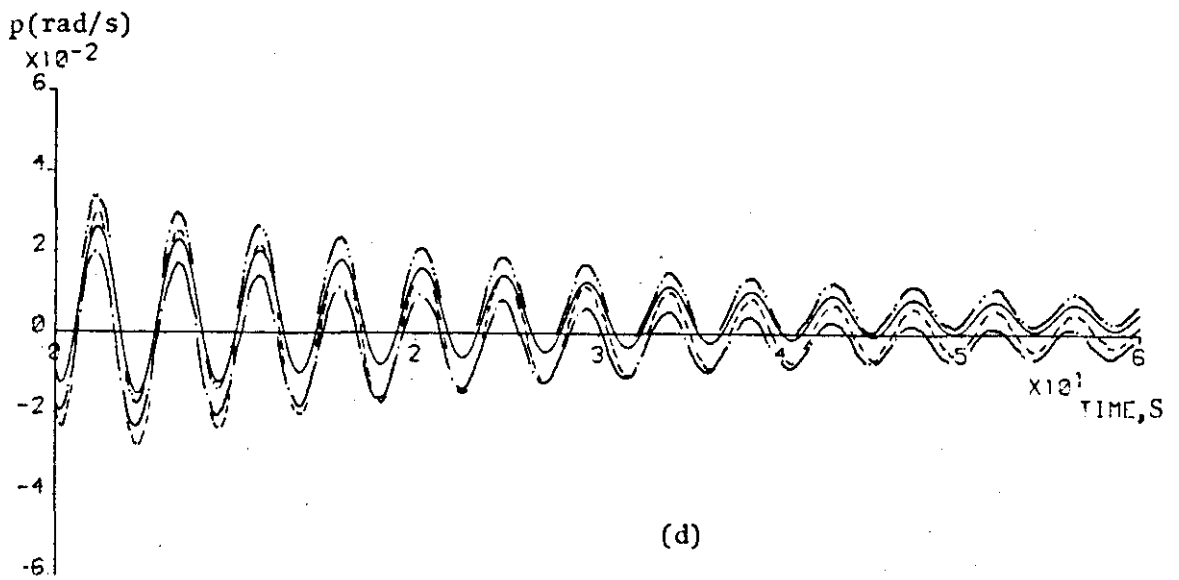
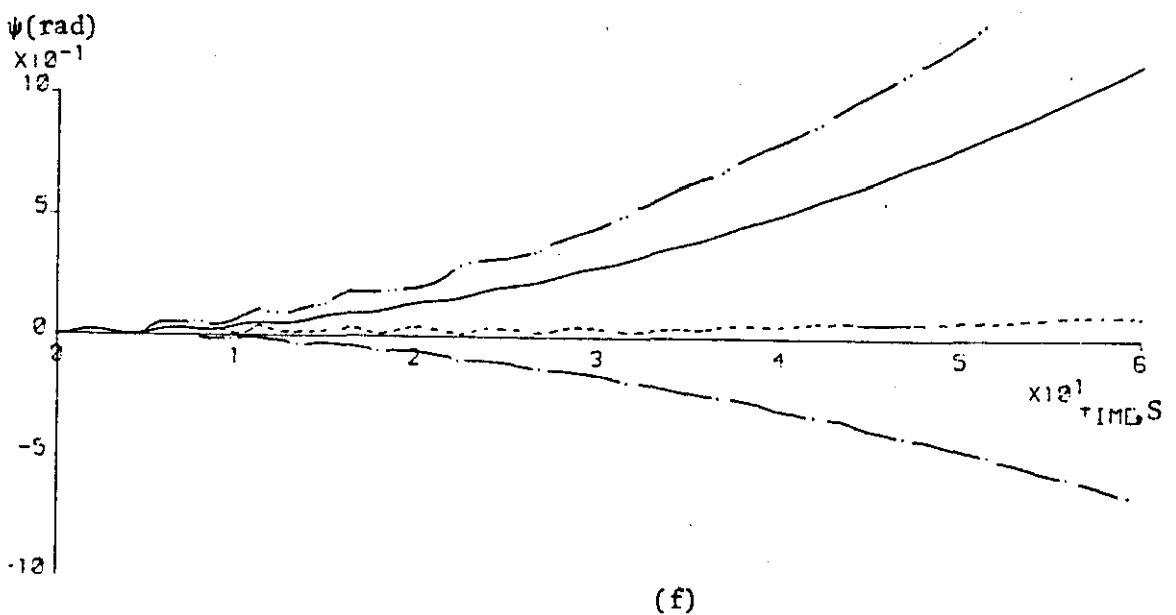


FIGURE 6.7: (Continued)



aircraft behaves as if performing an uncoordinated turn with increasing bank and yaw angle which gives rise to the comparatively higher levels of sideslip angle, β , and, in turn, higher levels of lateral acceleration (See Figure 6.8).

From Figures 6.7 and 6.8 it may be deduced that the ailerons were not as effective as the rudder or vertical canard in controlling lateral acceleration since they excited the spiral mode of the aircraft. However, no definite conclusions about the relative effectiveness of the control surfaces employed can be drawn from the analysis of the lateral motion of the uncontrolled aircraft, unless the controlled aircraft is considered where it is expected that the slow dynamic effects due to the spiral mode, as well as to the weakly damped dutch roll, will be eliminated.

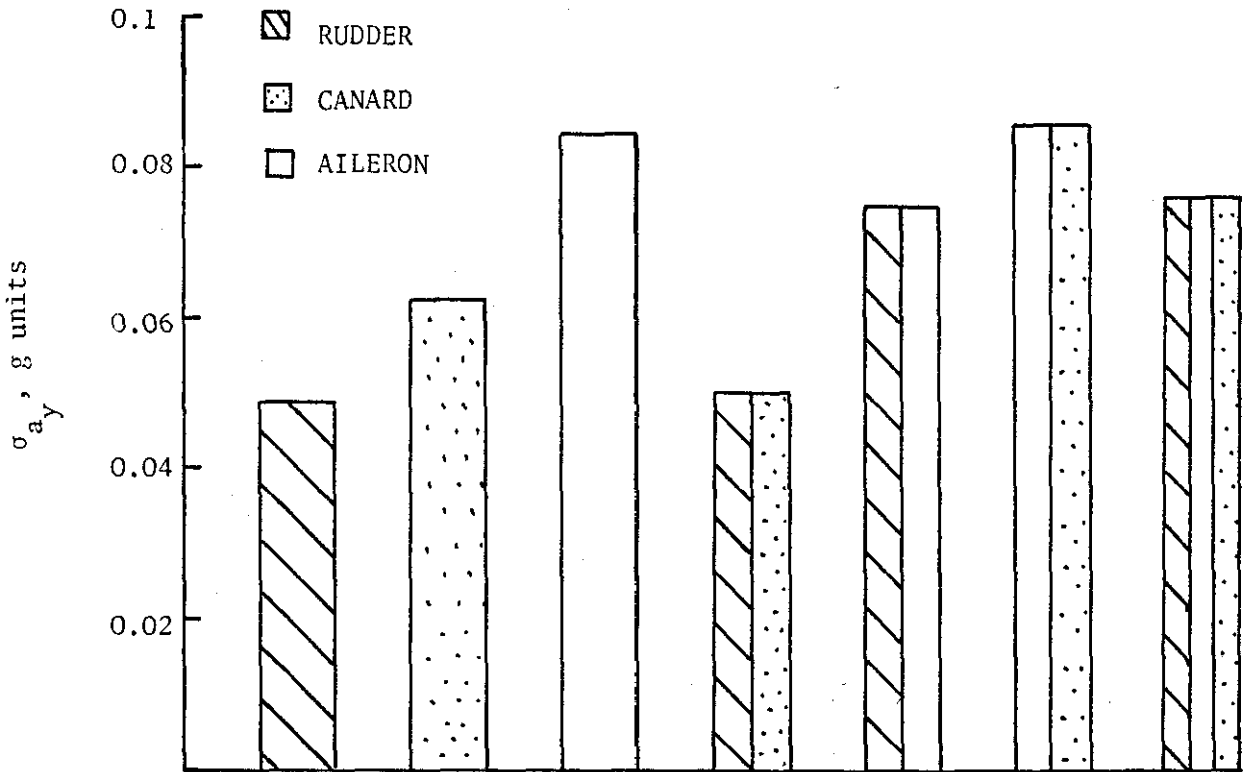


FIGURE 6.8: σ_{a_y} Resulting from 0.01 rad Step Commands to Lateral Control Surfaces (60s flight)

6.2.2 Dynamics of the Optimally Controlled Aircraft

In Chapter 4 the theories of optimal control and model matching were employed to derive feedback control laws for the modified Jetstar aircraft. These feedback control laws were used to minimize the acceleration levels induced on the aircraft and also to improve the handling qualities of the aircraft. The minimization of the acceleration was attempted 'implicitly' and 'explicitly' as described in sections 4.3 and 4.4 of Chapter 4, but which are summarized here for convenience:

'implicit' minimization means here the indirect minimization of acceleration which is achieved by means of minimizing a performance index which consists of elements comprising the state and the control vector of the aircraft.

'explicit' minimization means here the direct minimization of acceleration by minimizing a performance index whose elements are the acceleration and the control vector.

The optimal feedback laws derived for the 'implicit' minimization of the acceleration were those principally used in the simulation and those for 'explicit' minimization were employed for comparison. The optimal feedback control laws which were considered for handling qualities improvement were examined in terms of their effect on acceleration (Section 4.8). The effectiveness of these control laws on the motion variables of the aircraft was judged by comparison with the uncontrolled aircraft response for the same initial conditions. Table 6.1 summarizes the three optimal feedback control laws which were investigated in this research.

TABLE 6.1

OPTIMAL FEEDBACK CONTROL LAWS	FUNCTION
Control Law I	Implicit minimization of acceleration
Control Law II	Explicit minimization of acceleration
Control Law III	Handling qualities improvement

The CONTROL LAW I was tested for command signals which would result in the same steady state response like those obtained from step input commands to the uncontrolled aircraft. The ride quality performance due to each of these feedback control laws was judged according to the resulting acceleration levels. All possible control surface configurations were examined for the CONTROL LAWS I and III. The relative effectiveness of each control surface configuration was evaluated. Actuator dynamics, power and hinge moment limits were also considered and included in the feedback loop.

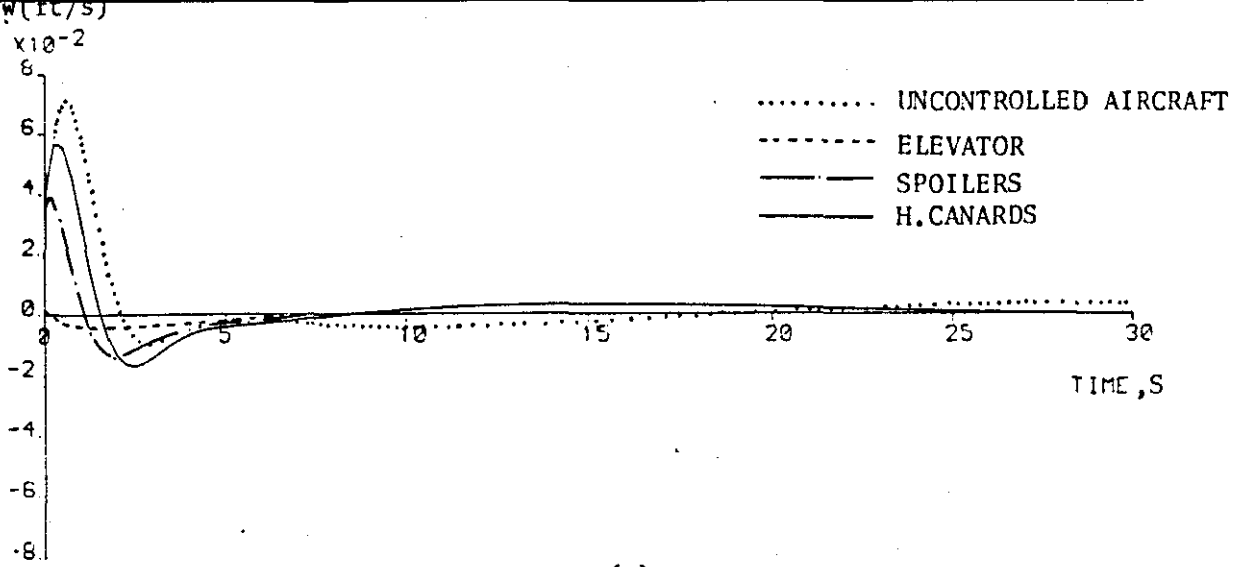
However, it is important to emphasize that the relative effectiveness of each control surface activity, in the optimally controlled aircraft analysis, is a factor depending significantly on the particular weighting of the control vector elements in the performance index which is chosen to be minimized. In this research the weighting corresponding to each component of the control and state vectors was determined from the digital program WAYMX (Section 4.5). Different weighting matrices, G , other than

those obtained from WAYMX were also investigated for specific control surface configurations.

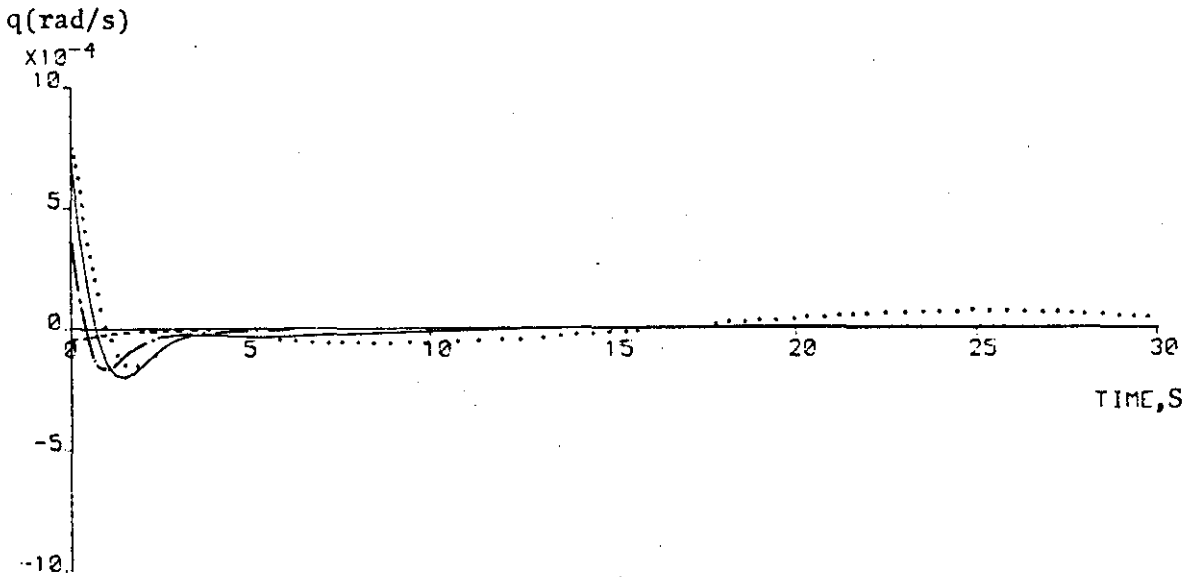
The analysis of results was based on the dynamic response of the aircraft obtained for 30s digitally simulated flight.

6.2.2.1 Longitudinal Motion Analysis

The optimal CONTROL LAWS I obtained from the digital program OUTREG were applied to all the possible control surface configurations of the modified Jetstar aircraft. Figure 6.9 illustrates the effect of the optimal CONTROL LAWS I on the motion variables w, q and a_z for various configurations. From this figure it can be seen that the long period dynamics of the aircraft (phugoid) have been eliminated in less than 8 sec. and the short period dynamics have been effectively damped out. The most effective minimization of the motion variables has been achieved when the elevator was involved. From 6.9(a), (b) and (c) it can be seen that spoiler is more effective than horizontal canards but both of them, even if acting together, are not as effective as when the elevator is acting on its own. It is evident therefore that the elevator is the most important control surface for longitudinal ride control. In order to investigate the ride quality effects of any possible combination of the elevator with the other control surfaces and to examine the relative advantages of each configuration in terms of r.m.s. deflection angles Figure 6.10 was employed. Figure 6.10(a) represents the r.m.s. acceleration levels for all configurations without and with the consideration of the actuators dynamics in the feedback loop. From this figure it can be seen that whether or not the actuators are considered in the digital simulation the elevator alone provides the best result in terms of acceleration reduction. The reduction of acceleration r.m.s., value when elevator acts alone is of the order of 76.7% compared to the uncontrolled aircraft. When the actuator dynamics of the control surface are considered the acceleration r.m.s. value is increased but still elevator alone achieves the best result which is a reduction of 70%. Figure 6.10(b) also shows the favourable effect of using only the elevator.

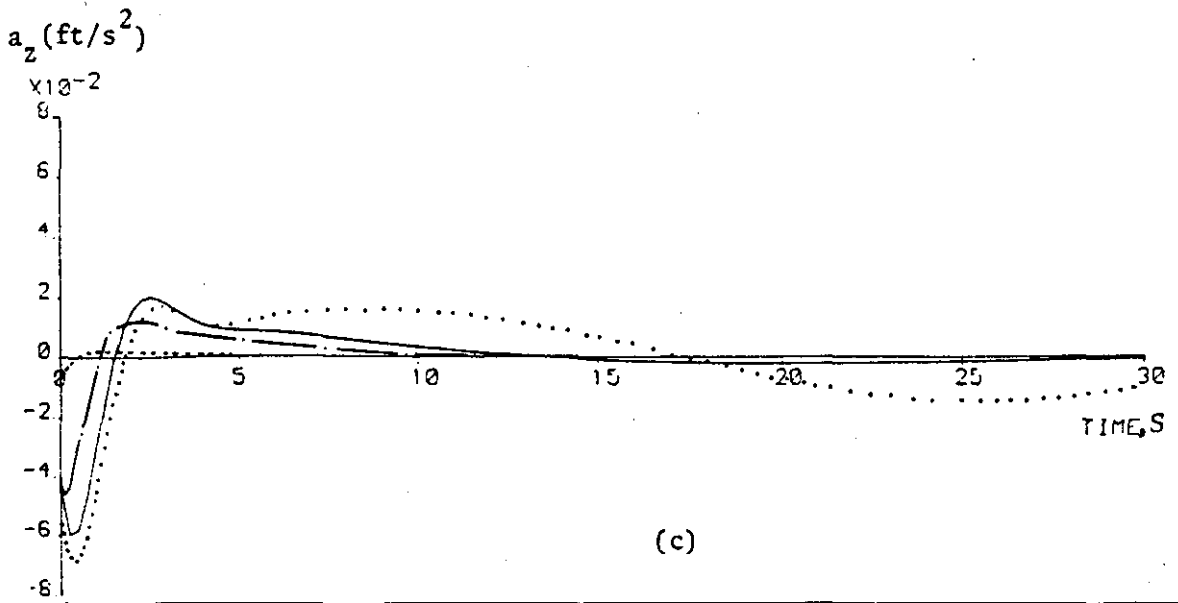


(a)



(b)

FIGURE 6.9: Dynamic Responses of the Aircraft when CONTROL LAW I was considered



(c)

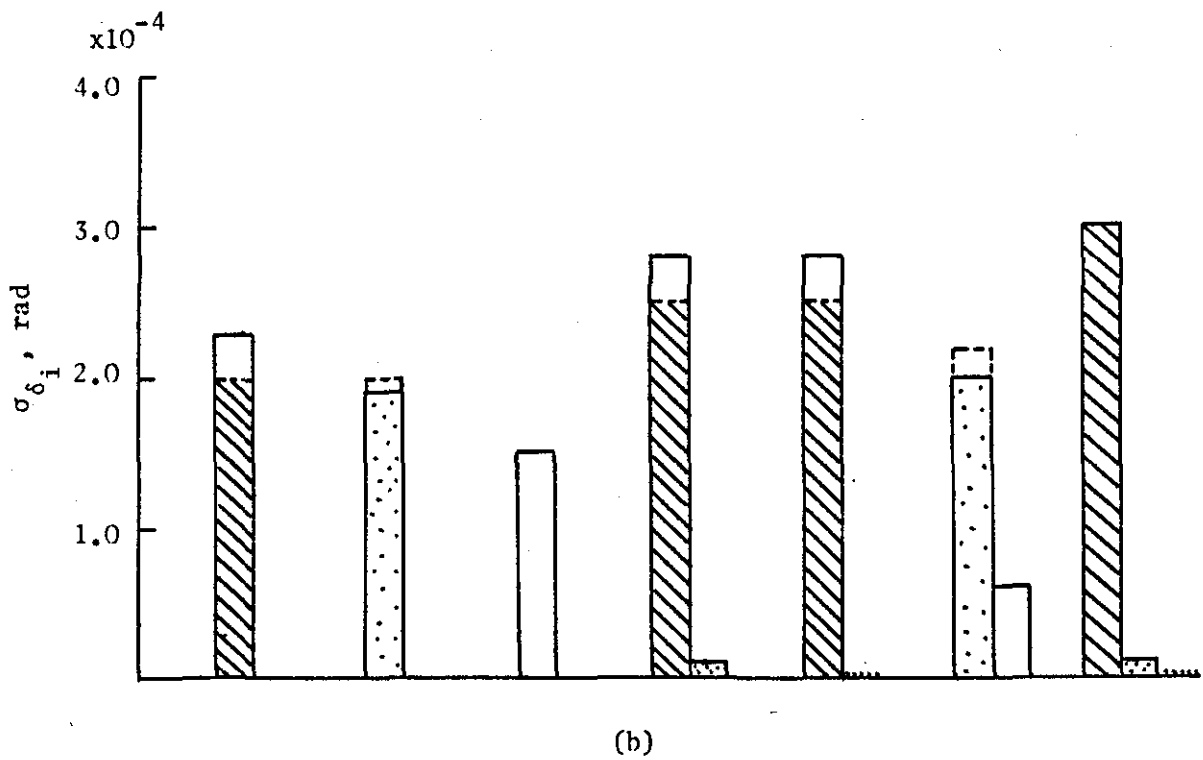
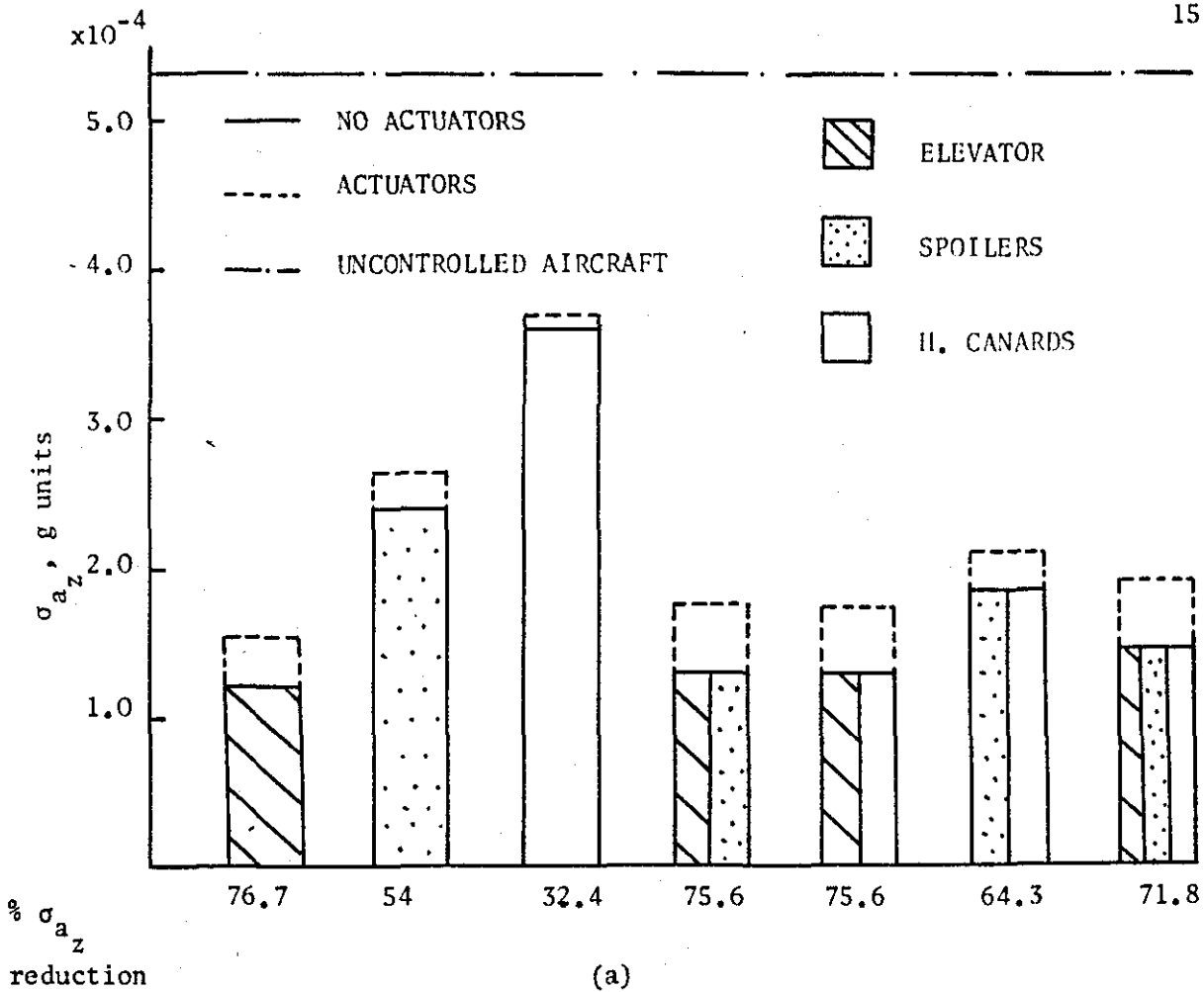
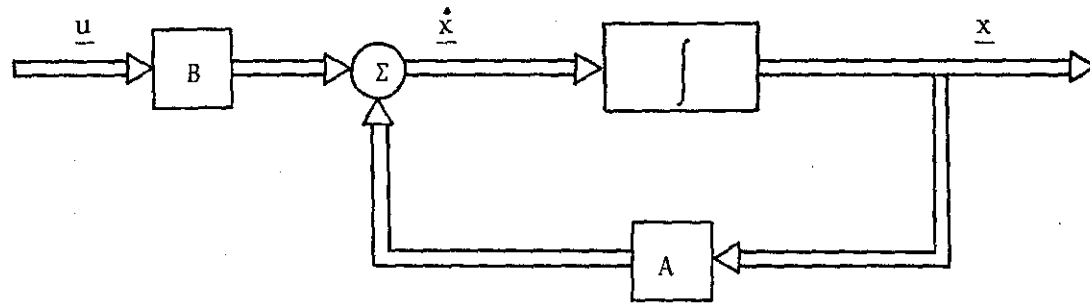


FIGURE 6.10: Optimally Controlled (CONTROL LAW I) Longitudinal Motions

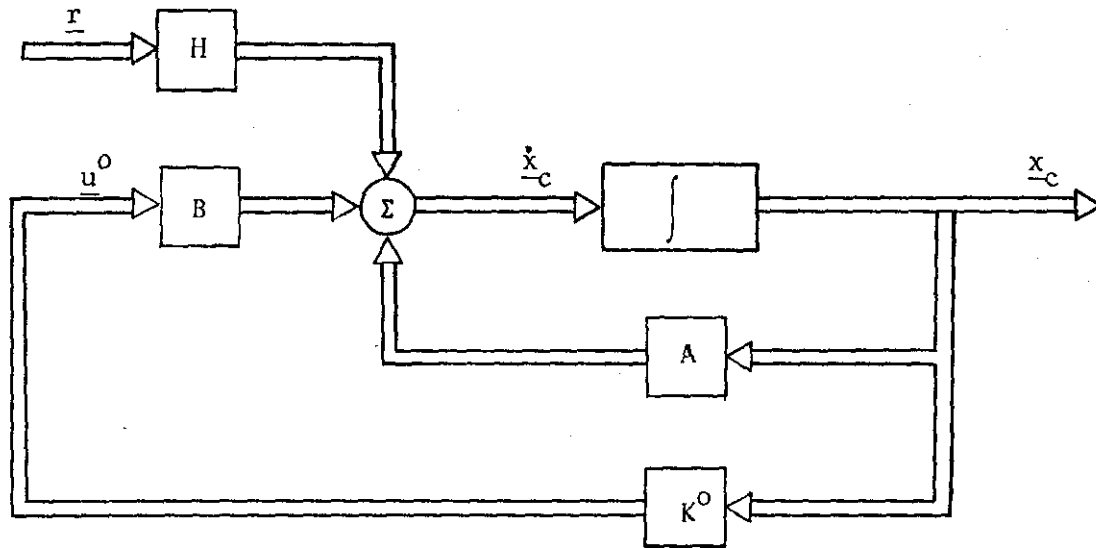
The combined use of the elevator with spoilers or horizontal canards results in an increase in the activity required from the elevator. This conclusion reinforces the inference drawn from Figure 6.10(a) that the lower the degree of activity required from the elevator the more it may be used for other flight purposes such as trim or flight path adjustments. The power limitations of the actuators and the surface deflection limits were considered but it was found that they did not materially affect the response. This implies that the CONTROL LAW I in these conditions did not require rates or deflections exceeding the available capabilities.

From Figure 6.10(a) it is evident that second order actuators (as in the case of the elevator) result in levels of acceleration higher than when first order actuators are employed (spoilers and horizontal canards). However a general conclusion which could be drawn including actuator dynamics in the feedback loop is that their presence results in time lag of the control surface activity which in turn decreases the effectiveness of the control law.

In order to investigate the dynamic characteristics of the aircraft when using the optimal feedback CONTROL LAW I a digital program called SSCOM (steady state command) was developed. This digital program could be used to determine a command vector \underline{r} which when used as input to the optimally controlled aircraft would result in appropriate steady state values of the output vector for comparison purposes. Figure 6.11 illustrates the block diagram for the above situation. The requirement to evaluate the command vector \underline{r} of dimension p for a fixed coefficient matrix $H(n \times p)$ was formulated mathematically as follows:



(a) Open Loop



(b) Closed Loop with a Command Vector \underline{r}

FIGURE 6.11: Block diagram representation of:

(a) $\dot{\underline{x}} = A\underline{x} + B\underline{u}$

(b) $\dot{\underline{x}}_c = (A+BK^0)\underline{x}_c + H\underline{r}$

$$\dot{\underline{x}}_c = (A+BK)\underline{x}_c + H \underline{r} \quad (6.1)$$

at steady state $\dot{\underline{x}}_{c_{ss}} = 0$.

Hence (6.1) becomes

$$0 = (A+BK)\underline{x}_{c_{ss}} + H \underline{r} \quad (6.2)$$

solving for $\underline{x}_{c_{ss}}$ (6.2) yields

$$\underline{x}_{c_{ss}} = -(A+BK)^{-1}H \underline{r} \quad (6.3)$$

But

$$\underline{y}_{ss} = C\underline{x}_{ss} \quad (6.4)$$

hence (6.4) by using (6.3) gives:

$$\underline{y}_{ss} = -C(A+BK)^{-1}H \underline{r} \quad (6.5)$$

solving (6.5) for \underline{r}

$$\underline{r} = -[C(A+BK)^{-1}H]^{-1}\underline{y}_{ss} \quad (6.6)$$

By using this program it was possible to determine the command vector required to produce the same steady states of the output variables as when step inputs of 0.01 rad were applied to the uncontrolled aircraft. In this way the uncontrolled aircraft dynamics presented in Figure 6.4 could be directly compared to the optimally controlled aircraft dynamics.

Figure 6.12 illustrates the favourable effect of the optimal feedback CONTROL LAW I as compared with the uncontrolled aircraft excited from step command of elevator. Similar responses were obtained when the rest of the control surfaces were considered. Figure 6.13 compares the r.m.s acceleration levels induced by the uncontrolled and controlled aircraft due to the action of elevator, spoiler canard and their combination. From this figure the favourable effectiveness of CONTROL LAW I on r.m.s. normal accelerations as compared to the uncontrolled aircraft is evident.

explain

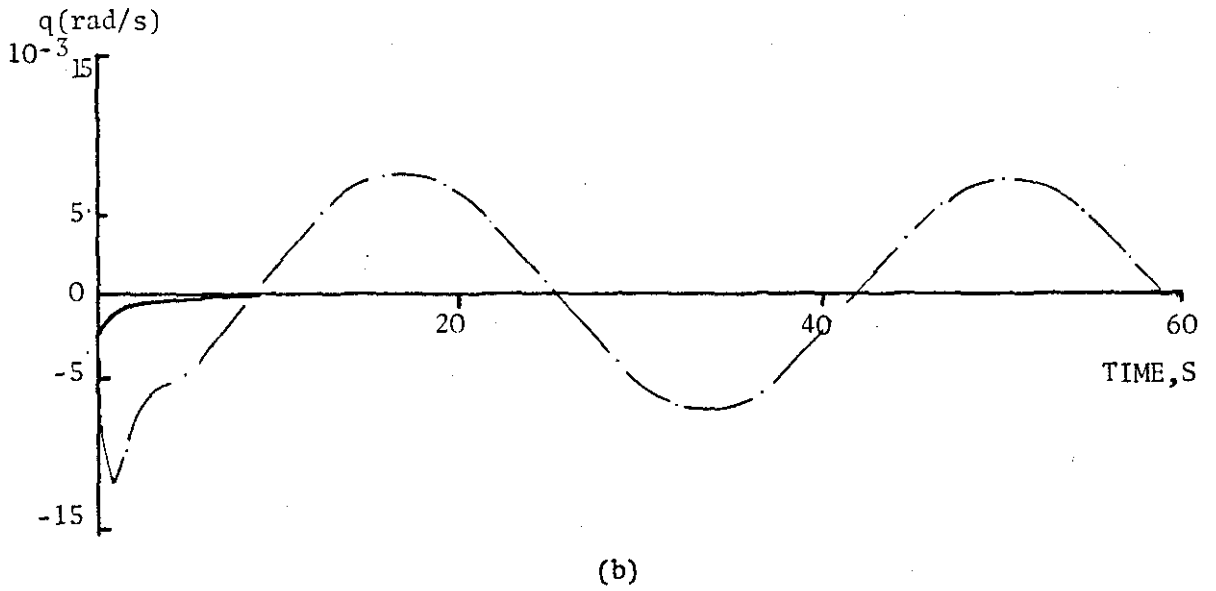
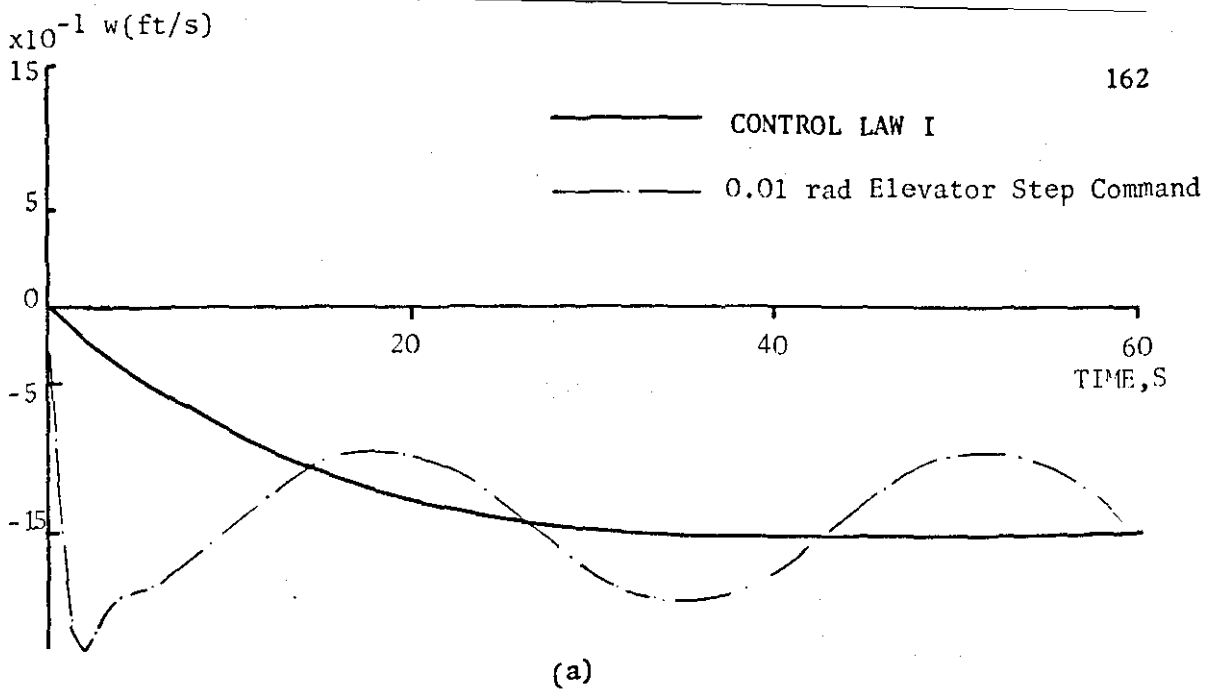
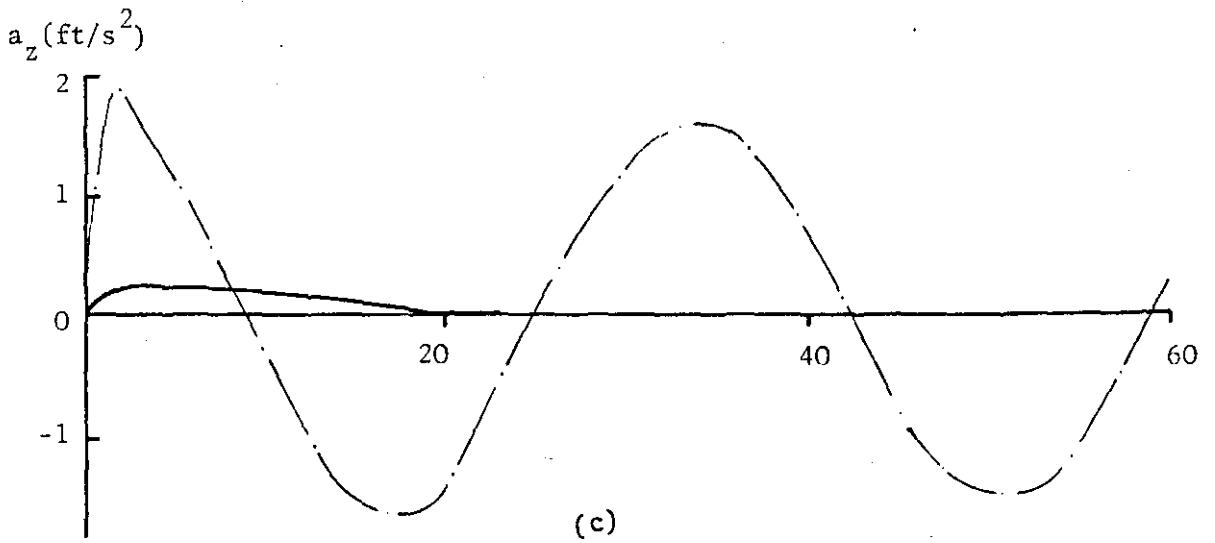


FIGURE 6.12: The Effect of CONTROL LAW I for Desirable Steady State Commands



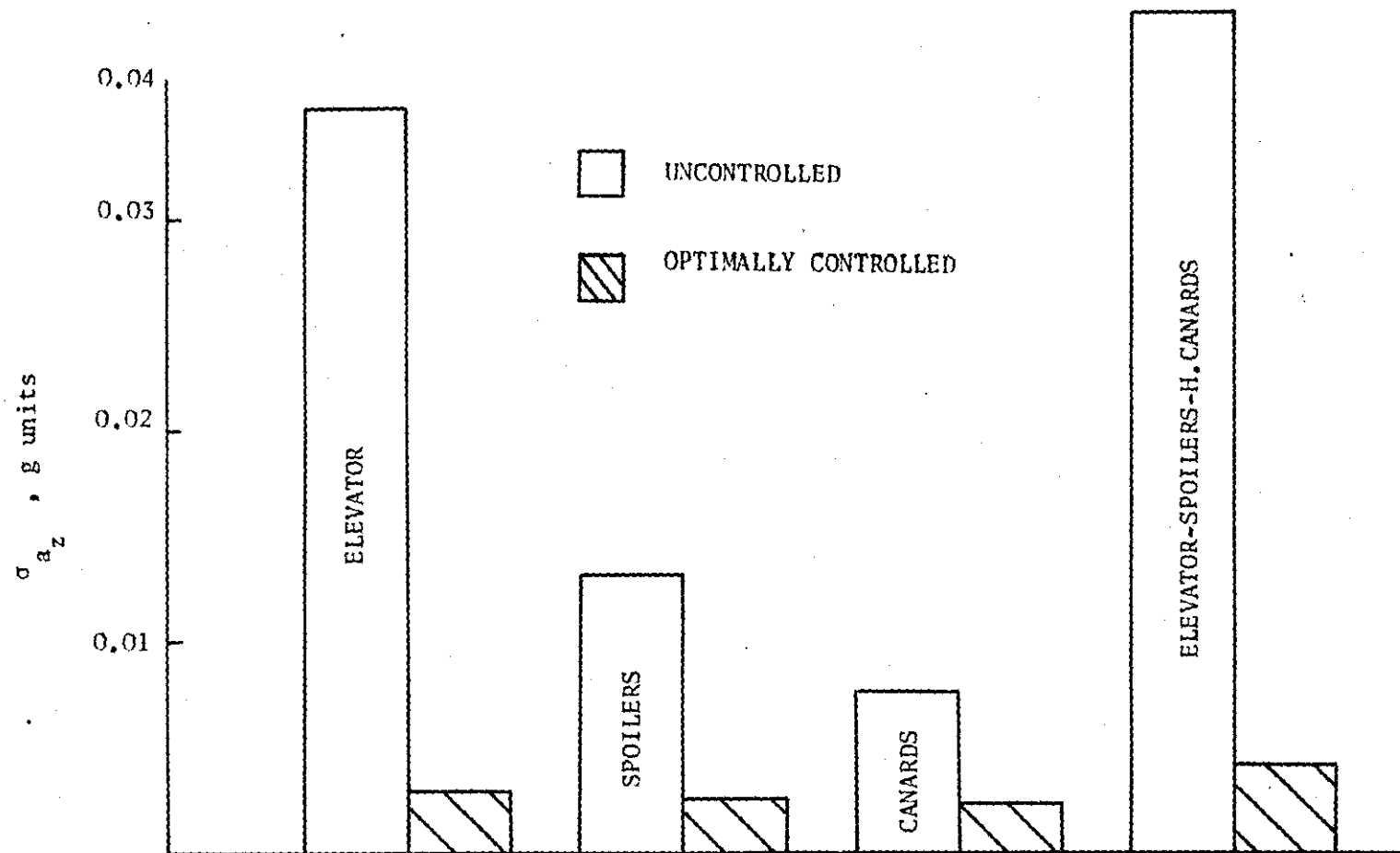


FIGURE 6.13: Comparison of the r.m.s. Acceleration Levels between Uncontrolled and Optimally Controlled Aircraft for a 60s run

From Figure 6.10(a) it is apparent that the surface configuration using only elevator provided the best results in terms of ride quality performance. It was therefore decided to consider CONTROL LAW II for this case only. The optimal feedback CONTROL LAW II was obtained from the digital program OUTREG. Figure 6.14 illustrates the dynamic response of the aircraft employing elevator and using this feedback control law. With this control law an r.m.s. acceleration reduction of 78% resulted. Figure 6.17(a) illustrates the effect of CONTROL LAW II compared with CONTROL LAWS I AND II.

From Figure 6.14(a) it can be seen that the use of CONTROL LAW II introduces secondary effects on the aircraft dynamics. It may be inferred from this figure that although the variations in the vertical velocity, w , of the aircraft has been minimized effectively for the s.p. mode it increased gradually in the phugoid mode. This small effect occurred because of the absence of q and θ from the performance index for the 'explicit' minimization of acceleration. However this slow building up of vertical velocity of the aircraft would be easily controlled by the pilot or by a control system. Note too that the use of the controls for the ride quality system involves small surface deflections which allows adequate control authority for other flying tasks.

The optimal feedback CONTROL LAWS I, for various combinations of the longitudinal control aerodynamic surfaces, improve the performance in terms of r.m.s. normal acceleration. Although these control laws did not improve the handling qualities of the aircraft, it was desirable to examine how the feedback control laws could affect the aircraft's handling qualities. Model-matching was employed to derive the optimal feedback control laws for

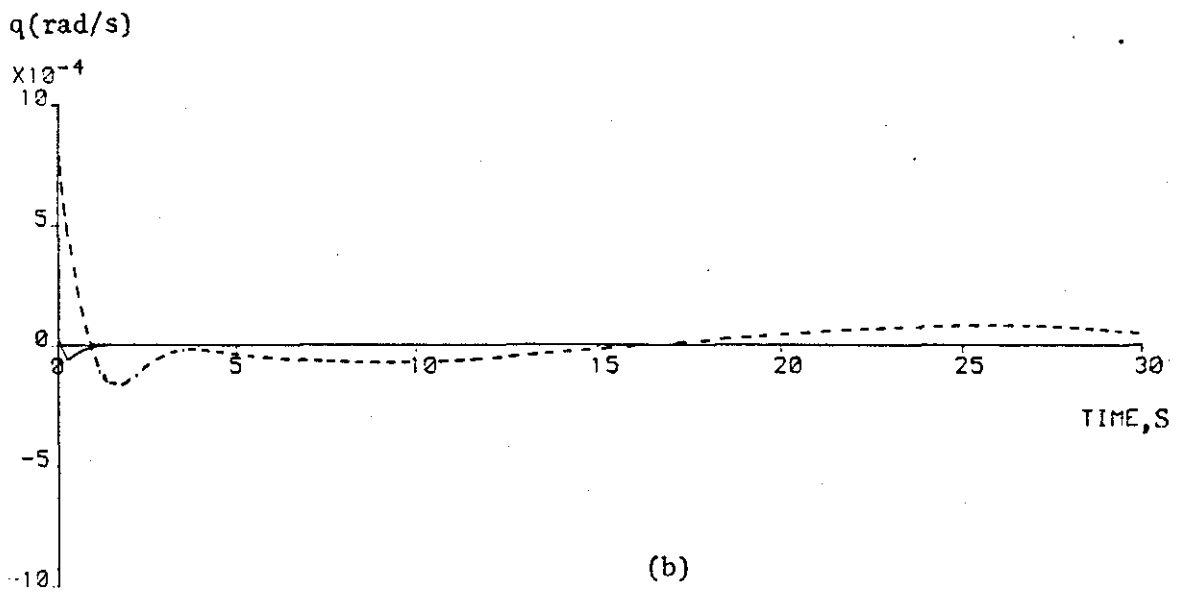
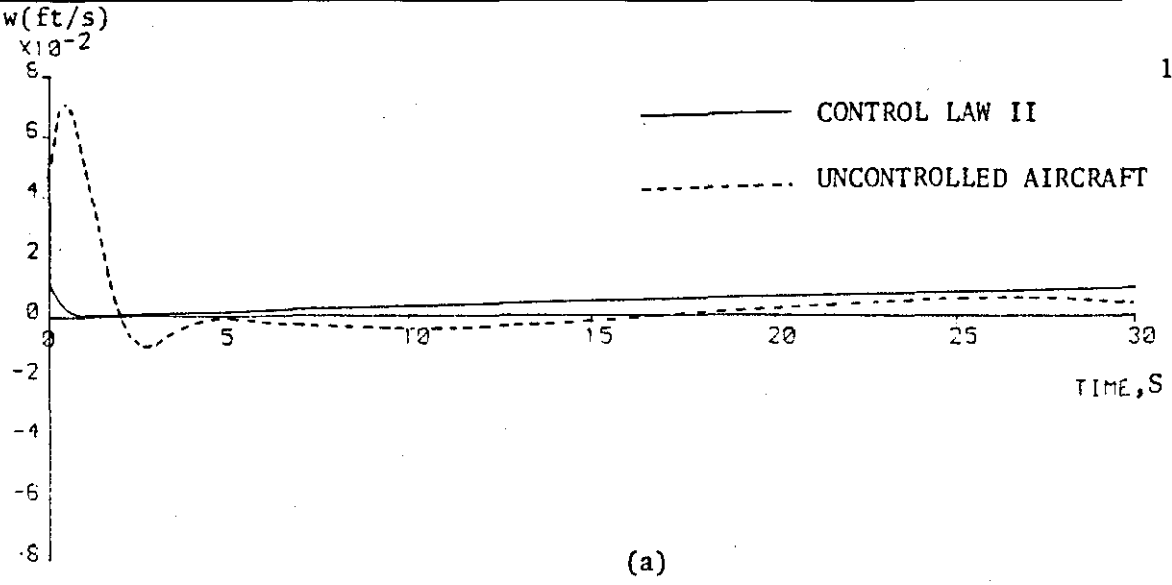
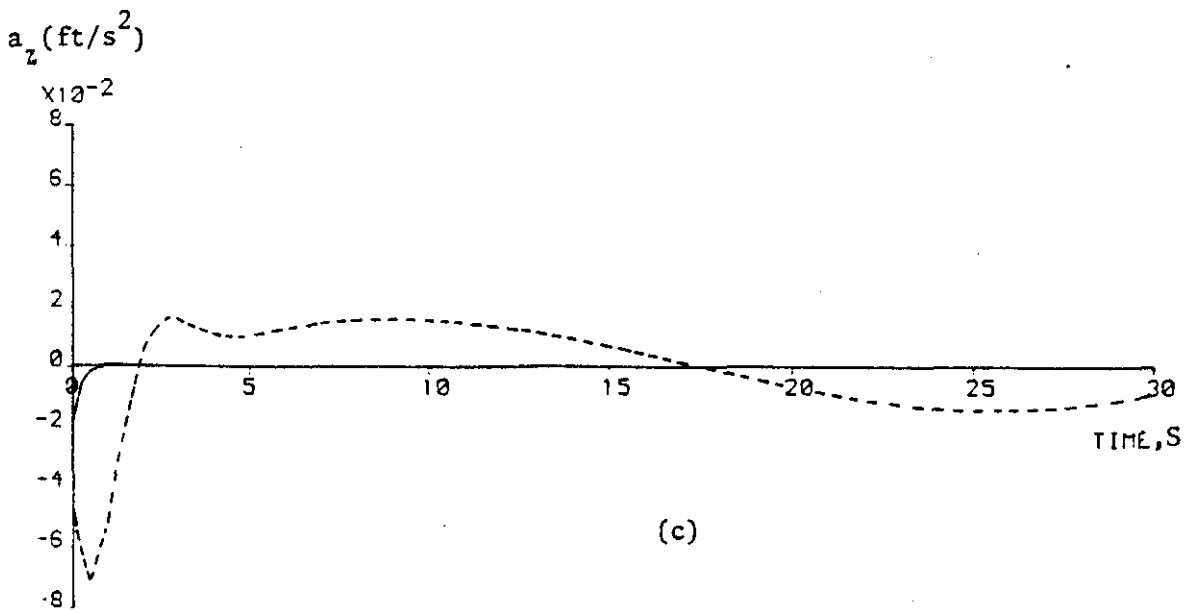


FIGURE 6.14: Effect of CONTROL LAW II for Longitudinal Motion when Elevator Only was considered



handling qualities. Use of CONTROL LAWS III was intended to result in dynamic response characteristics of the modified Jetstar similar to those of the idealized model specified in Section 4.7.

Figure 6.15 shows the dynamic responses of the modified Jetstar when it was forced to follow the dynamics of the model. The same dynamic responses were obtained for all the possible control surface configurations of the aircraft. From Figure 6.15 it can be seen that the dynamic response of the aircraft for the control laws being considered exhibits a more lightly damped response compared to Figure 6.9. The light damping results in a higher level of acceleration than than obtained from the optimal feedback control laws (CONTROL LAW II) for the 'implicit' minimization of acceleration. Figure 6.16(a) illustrates the induced r.m.s. acceleration levels on the aircraft for the different control surface configurations when the feedback control laws for handling qualities were employed. From this figure it can be seen that about the same reduction in r.m.s. acceleration of 60% results from any aerodynamic control surface configuration. In Figure 6.16(b) is shown the r.m.s. deflection angles required for any possible combinations; from this figure it is evident that the control law requires less control surface activity for those cases when the control surfaces are used alone than for those when they were used in combination. The least control surface activity was required when elevator was used alone, which suggests that this is the best control surface configuration.

Table 6.2 shows the effect of the control laws I, II and III on the handling qualities of the aircraft.

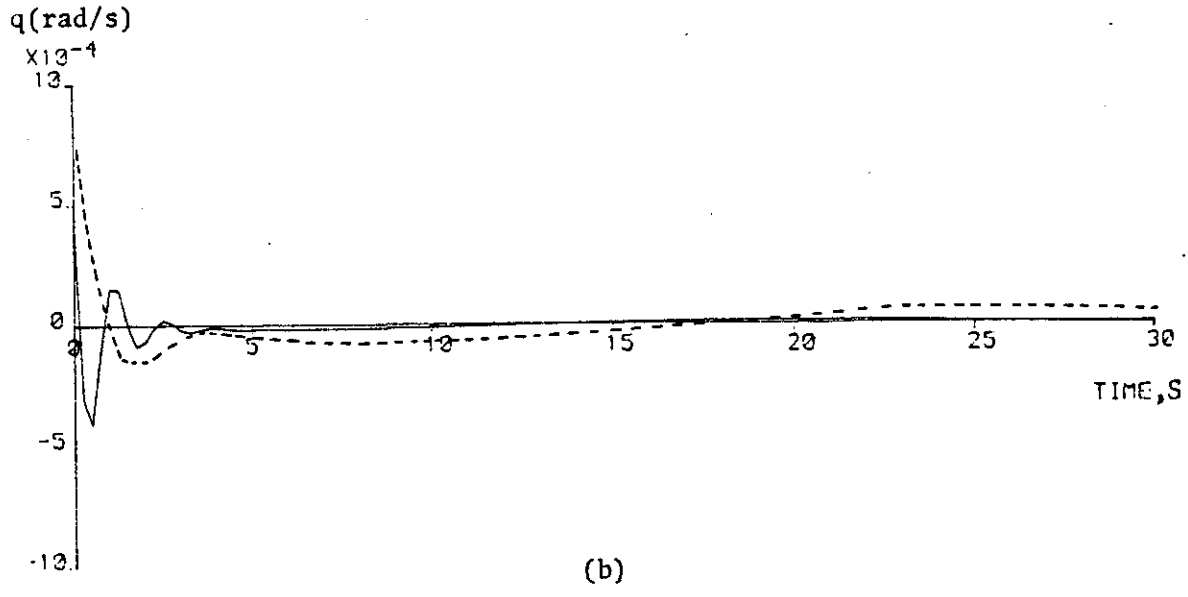
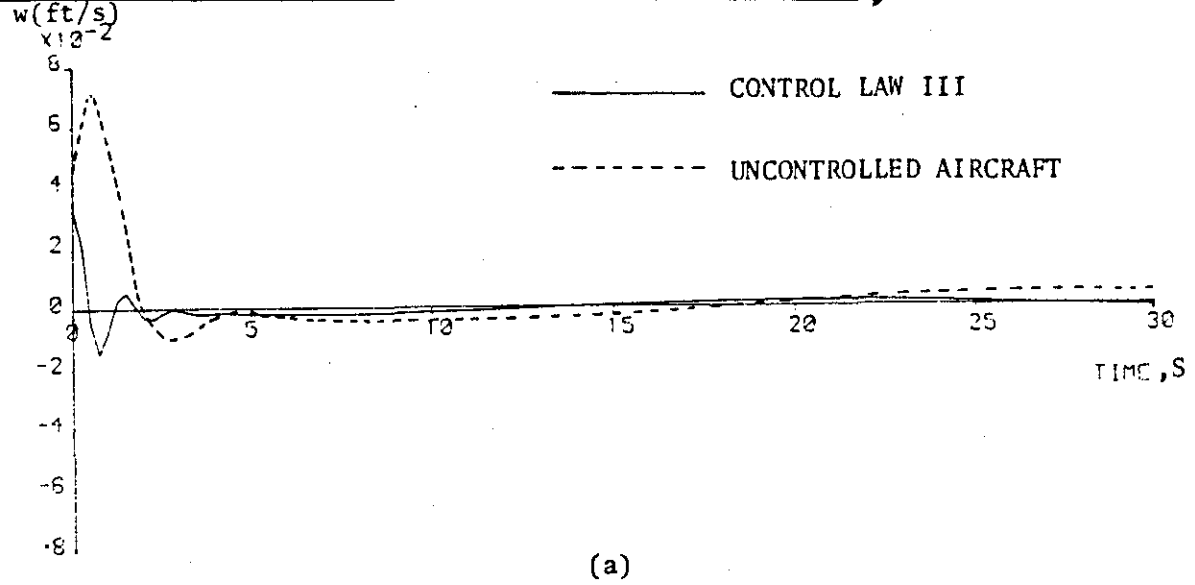
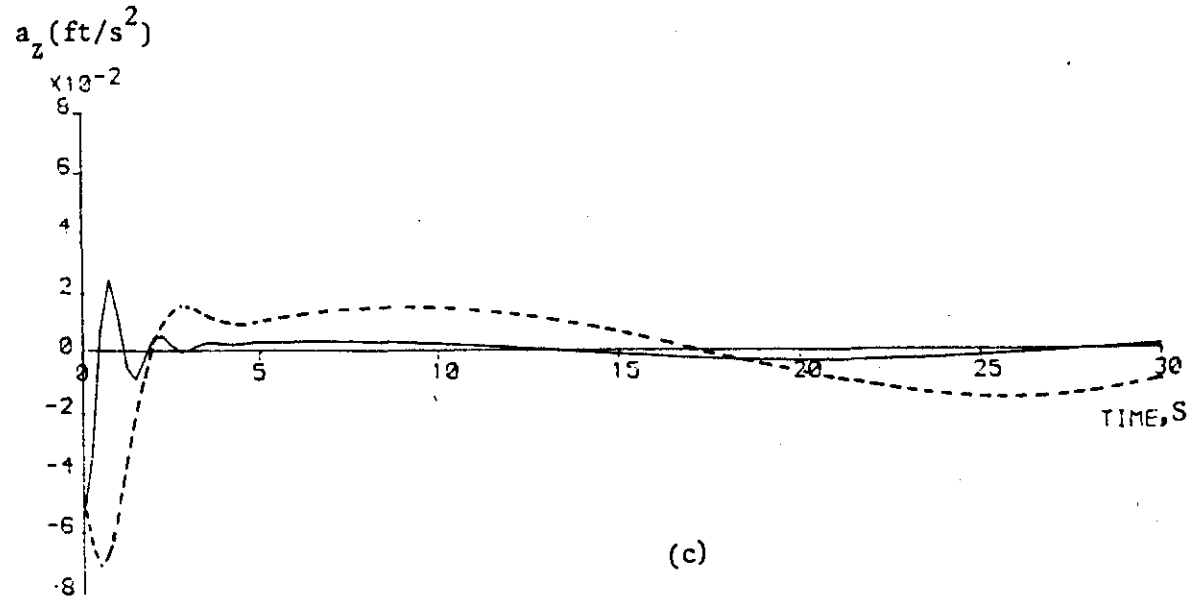
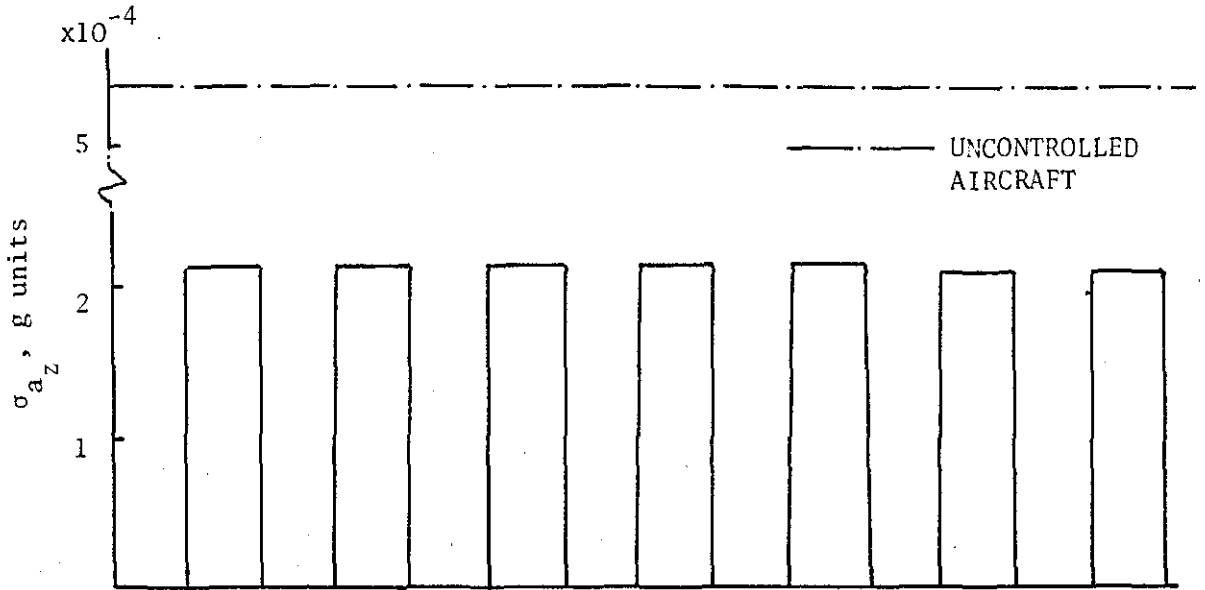


FIGURE 6.15: Effectiveness of CONTROL LAW III for Longitudinal Motion





(a)

OPTION	1	2	3	4	5	6	7
σ_{δ_E}	.00014			.013	.014		.0146
$\sigma_{\delta_{SP}}$.0004		.039		.901	.953
$\sigma_{\delta_{CH}}$.0007		.066	1.43	1.58

(b)

FIGURE 6.16: Effectiveness of CONTROL LAW III for Longitudinal Motion

TABLE 6.2

Comparison of the effect of the three control laws on the handling qualities of the aircraft for the elevator spoilers and h. canards configuration

	ζ_p	ζ_{sp}	ω_p/ω_{sp}
UNCONTROLLED AIRCRAFT	0.0087 [†]	0.5	0.11 [†]
CONTROL LAW I	3.181	14.9 [†]	0.58 [†]
CONTROL LAW II	2.058	2.0 [†]	0.00085
CONTROL LAW III	0.059	0.616	0.036
ACCEPTABLE HANDLING QUALITIES	>0.04	>0.3 or <2.0	≤.1

From Table 6.2 it can be deduced that the use of CONTROL LAW I results in over-damped dynamic characteristics for the longitudinal motion. Although it results in appropriate damping of the phugoid motion it over-damps the s.p. mode of the aircraft and degrades the ratio of the natural frequencies of the two modes. In the contrary CONTROL LAW II achieves better dynamic characteristics for the aircraft although the short period mode is slightly over-damped. CONTROL LAW III achieves identical dynamic characteristics with the ones intended and it results in acceptable handling

[†] denotes unacceptable handling qualities characteristics.

qualities for the aircraft.

However, as it has been discussed in Section 4.7 of Chapter 4, the handling qualities characteristics of the aircraft for CONTROL LAWS I and II could be improved if different choice of the Q and G matrices could be made. Since a procedure to derive appropriate weighting matrices Q and G for handling qualities does not exist and a trial and error method which would determine optimal Q and G matrices for handling qualities and ride performance simultaneously would require long time of investigation, it was decided that this problem should be considered in future research.

Figure 6.17 summarizes the results achieved by the three control laws in terms of r.m.s. normal accelerations reductions and deflection angles for the configuration employing only elevator. It is evident from this figure that CONTROL LAW II achieves the best results in terms of ride quality performance in the deterministic analysis of the optimally controlled aircraft.

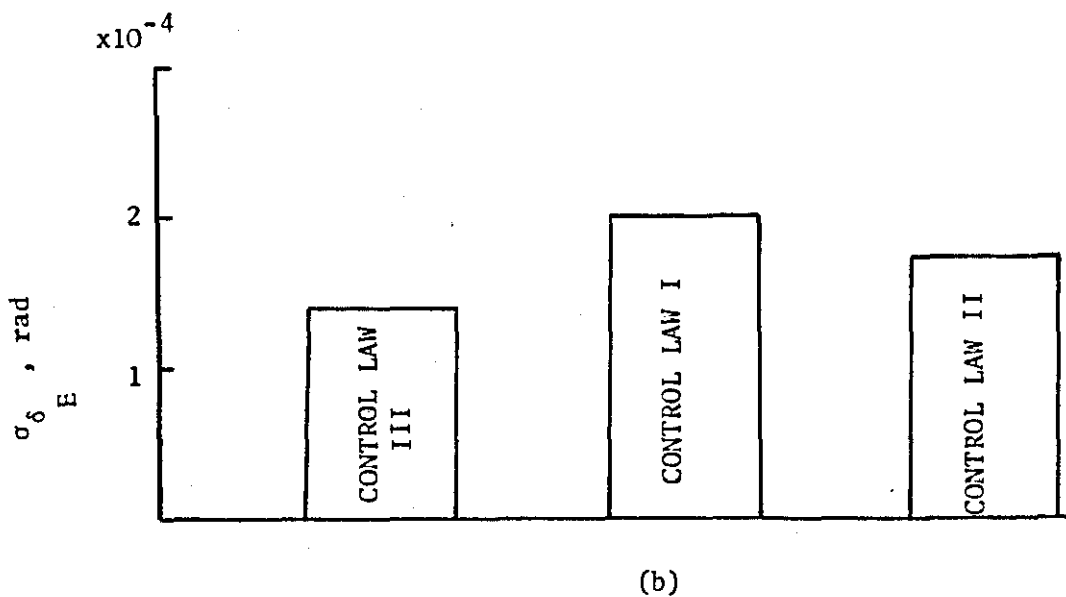
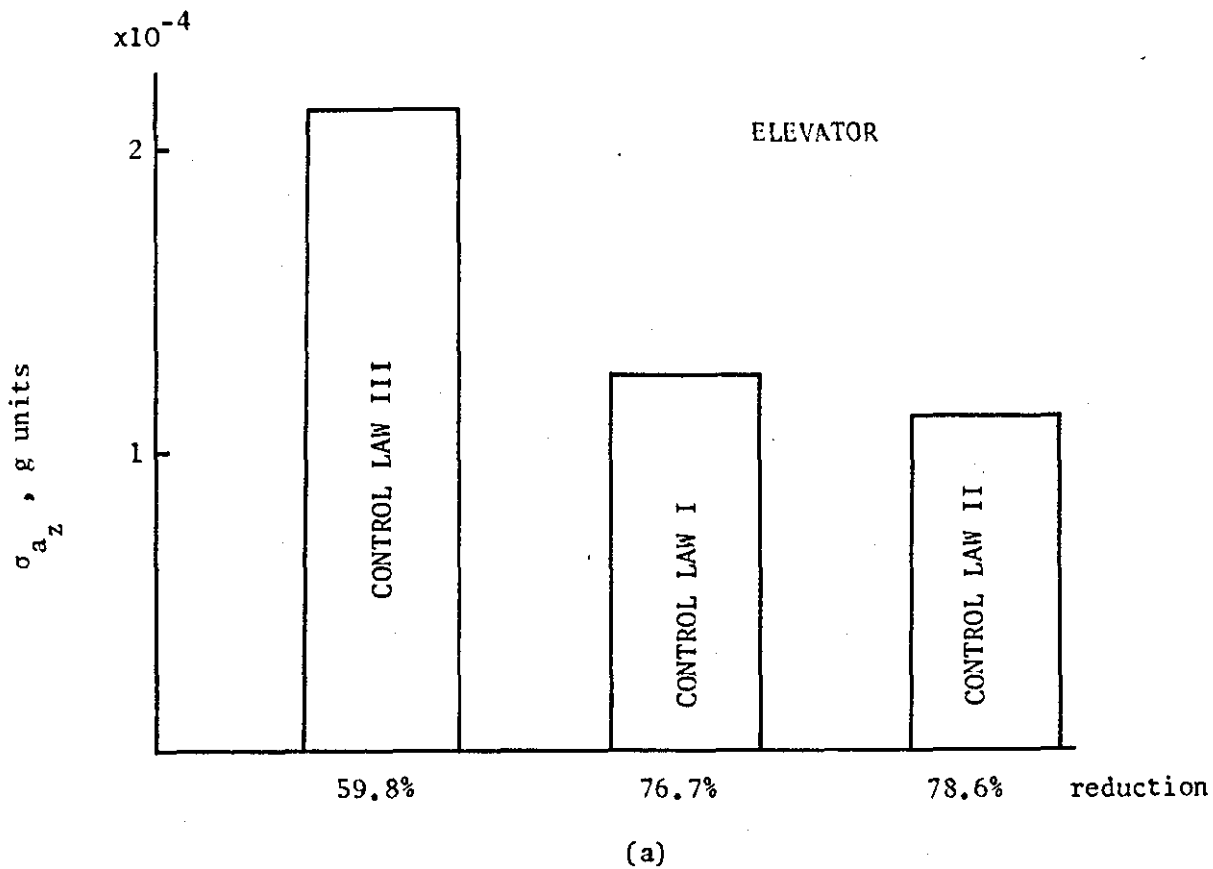


FIGURE 6.17: Effectiveness of CONTROL LAWS I, II and III where only elevator is involved for longitudinal ride control

6.2.2.2 Lateral Motion Analysis

The same procedure used for the deterministic analysis of the longitudinal motion was also adopted for lateral motion. As in the analysis of the longitudinal motion three separate optimal feedback control laws for the lateral motion were examined. The digital program OUTREG was employed to obtain the optimal feedback CONTROL LAWS I and II. CONTROL LAW I was used principally to determine and then to assess the dynamic characteristics of the controlled aircraft for all possible combinations of the lateral control surfaces. CONTROL LAWS II and III were employed in the same manner as for longitudinal motion.

Figure 6.18 illustrates the dynamic responses achieved by CONTROL LAW I for various lateral control surface configurations. The effectiveness of each control surface configuration can be judged by comparison to the uncontrolled aircraft dynamics when released from the same initial conditions.

From this figure it can be seen that the transient response of the aircraft dies out after 20 sec. except for the case when the vertical canard acts alone, a case which does not result in any significant improvement in the dynamic response of the controlled aircraft. To illustrate the effect of each control surface configuration on the r.m.s. levels of lateral acceleration of the modified aircraft Figure 6.19 should be considered. The best result was obtained when all the lateral control surfaces were employed simultaneously. A reduction of 65% in the r.m.s. value of lateral acceleration has been achieved in this case. Approximately the same reduction (64.5%) was achieved when the aileron and rudder combination was employed. In Figure 6.19(b) it is shown that aileron-rudder-vertical canard

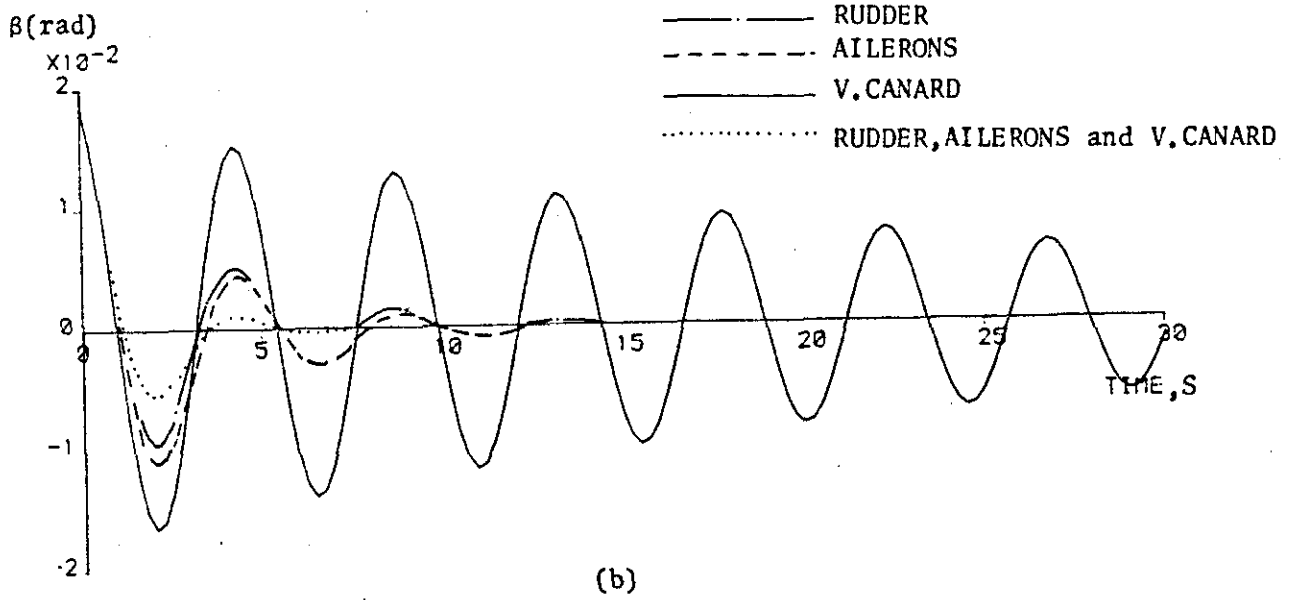
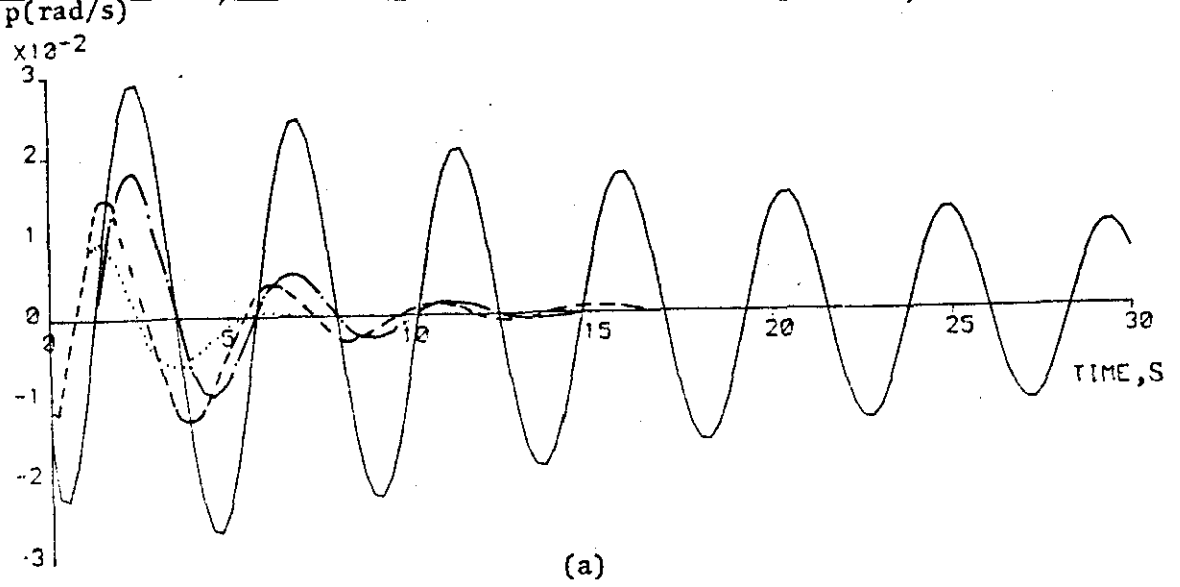
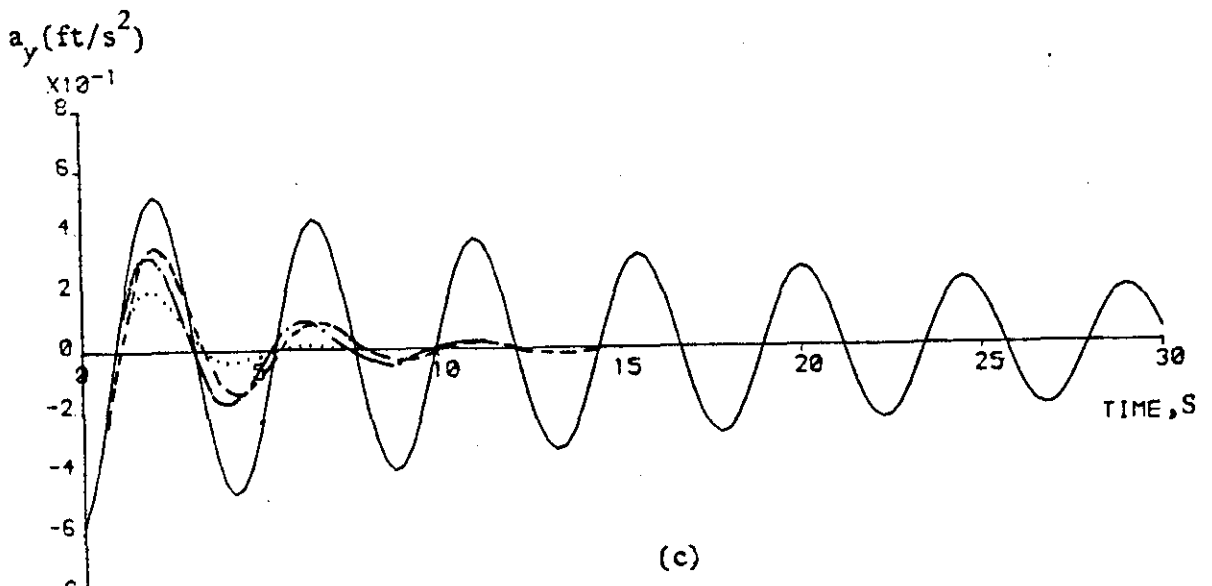
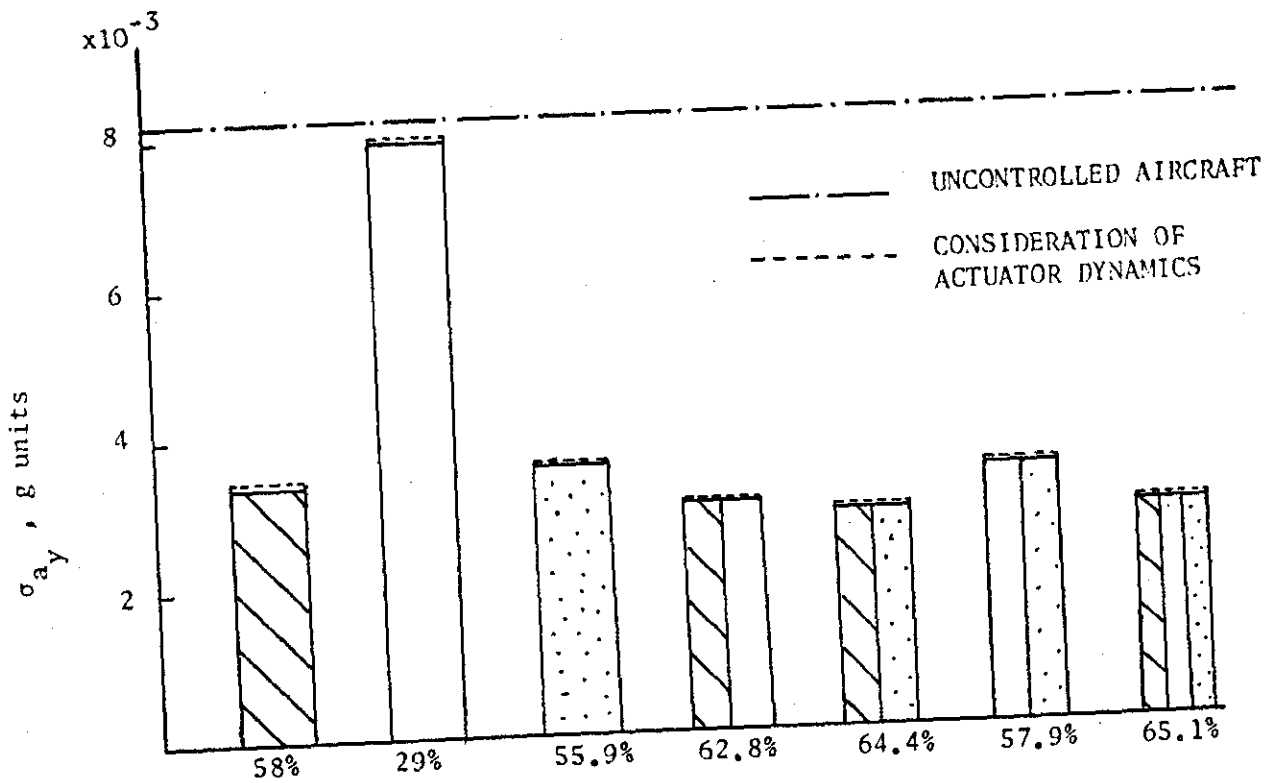


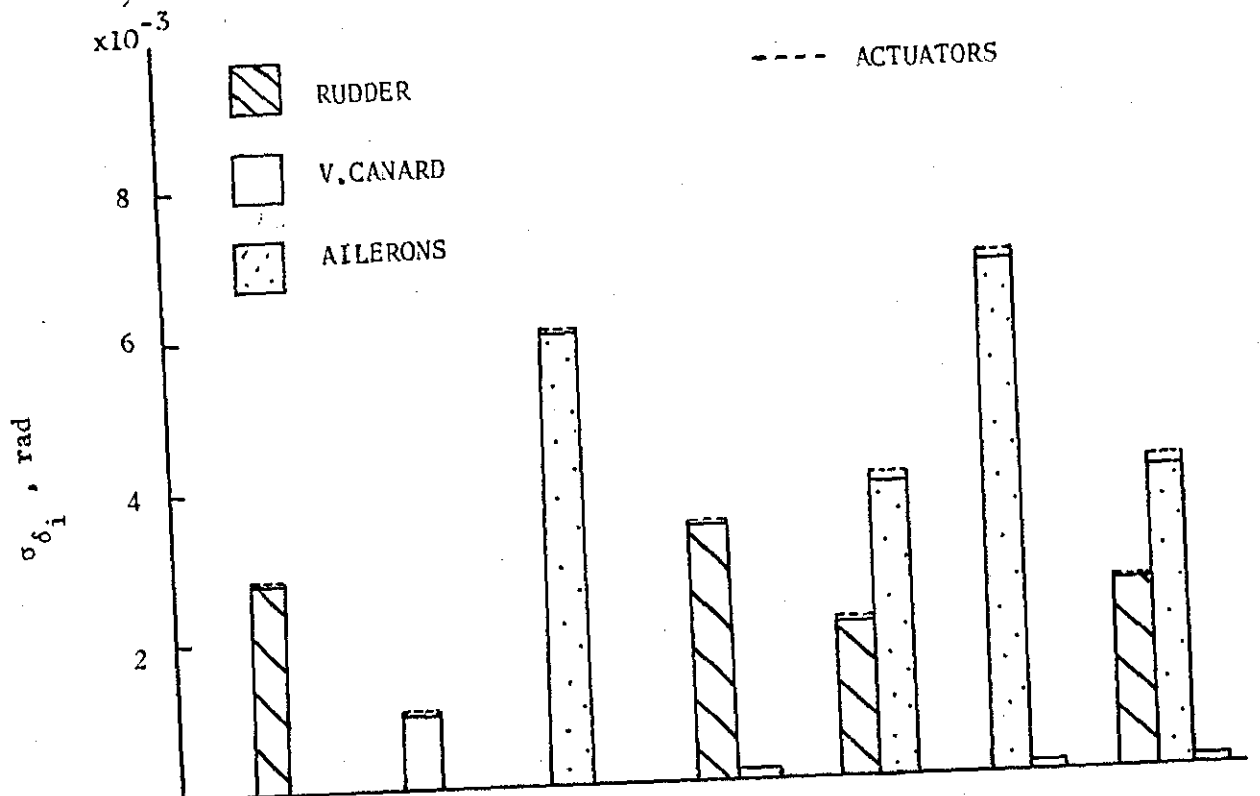
FIGURE 6.18: Effectiveness of CONTROL LAW I for Lateral Motion





% reduction of σ_{a_y}

(a)



(b)

FIGURE 6.19: Optimally Controlled (CONTROL LAW I) Lateral Motion

and aileron-rudder configurations use the least r.m.s. deflections of the control surfaces. When the actuator dynamics were included in the feedback loop the levels of acceleration did not increase significantly. It was found in the deterministic case that the rate and deflection limits associated with the control surfaces were never exceeded. To obtain better information about the relative effectiveness, of each single control surface and when they act all together, for the weighting found from WAYMX the digital program SSCOM was used to evaluate the command inputs required for each modification to achieve a steady bank angle of $\phi_c = 2^\circ$. The results obtained when using this command vector with the optimally controlled aircraft are shown in Figure 6.20 from where it can be seen ((a) and (b)) that when all the controls are used the transients associated with the sideslip angle and the roll rate, decay in less time than when all the controls were used together. From the curve (c) in Figure 6.20 it can be seen that rudder induces the highest r.m.s. values of lateral acceleration on the aircraft while aileron, vertical canard, and all three combined, result in about the same r.m.s. level of lateral acceleration. The effectiveness of each possible combination of the controls for a bank angle manoeuvre (measured in terms of r.m.s. acceleration) is demonstrated by means of Figure 6.21, which shows that the combinations of rudder-aileron or rudder-canard result in least r.m.s. acceleration induced as a consequence of this particular command.

The optimal feedback CONTROL LAW II was tested for the complete lateral aerodynamic control surface configuration. The simulated results obtained from the use of this control law are illustrated in Figure 6.22. The favourable effect which this control law has on the ride quality performance of the aircraft is evident from this figure. When CONTROL LAW II

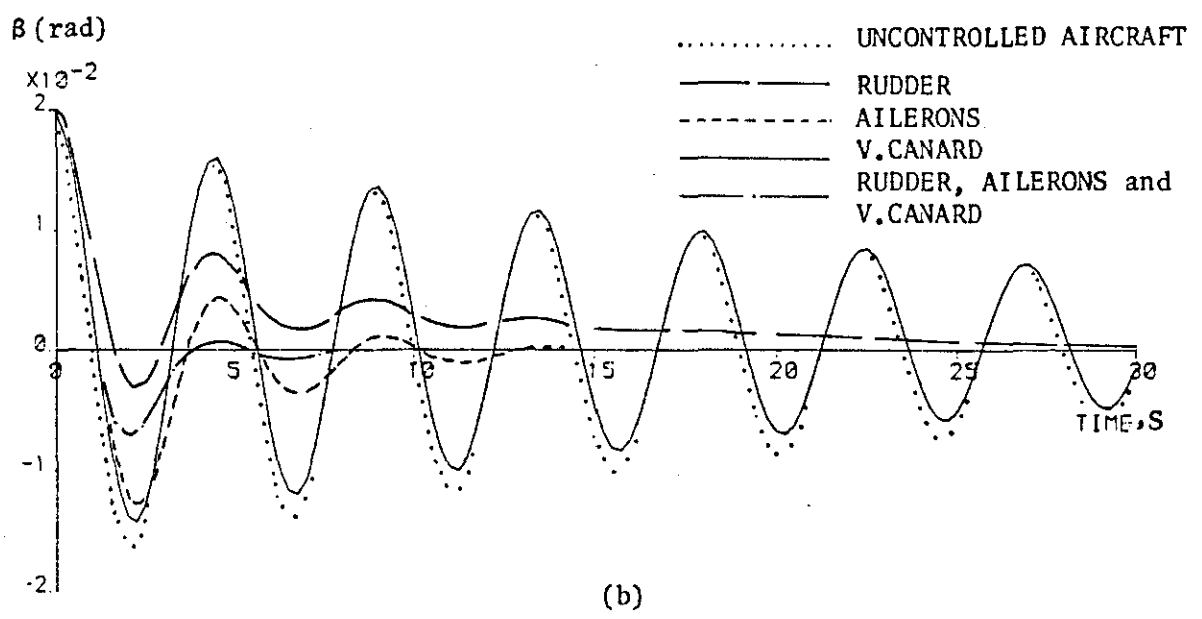
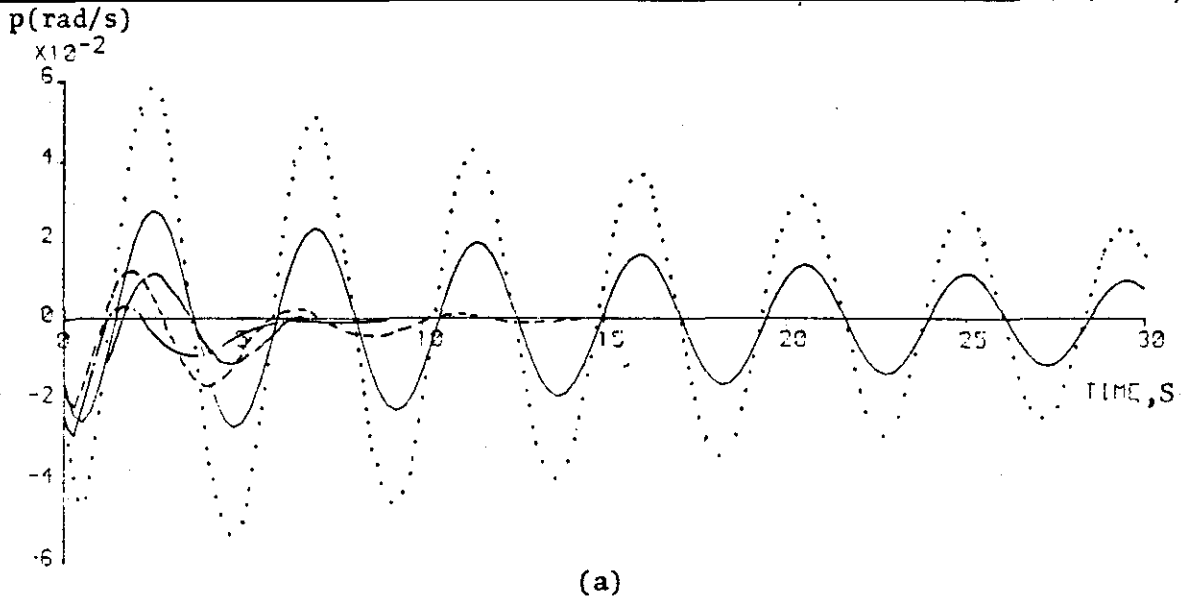
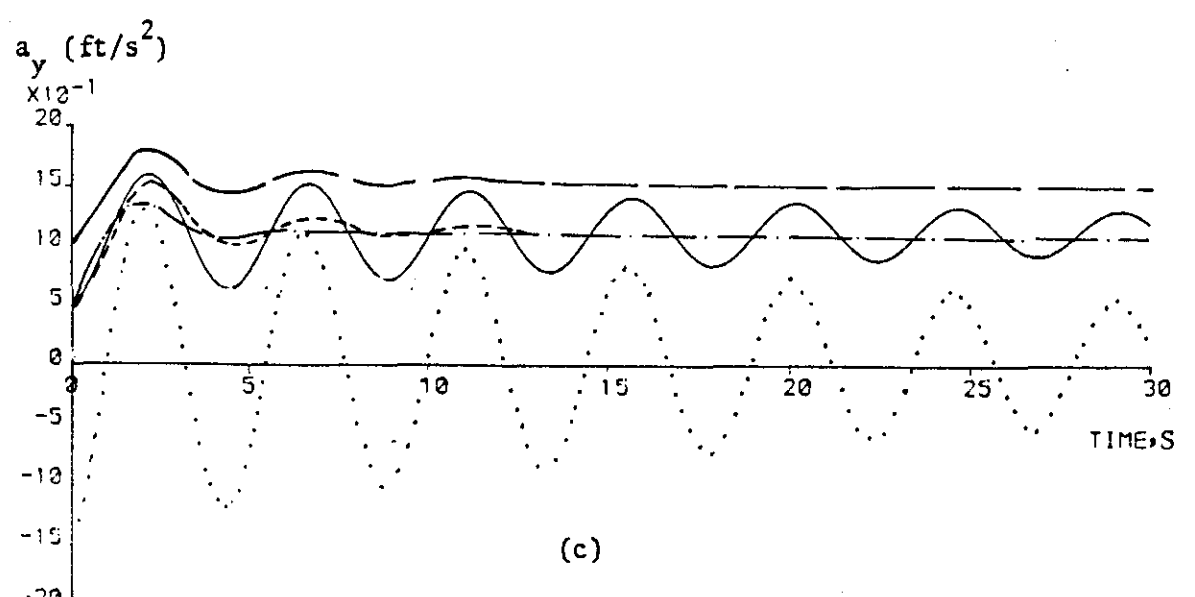


FIGURE 6.20: Dynamic Responses Resulting from a Command of Bank Angle of 2° (CONTROL LAW I)



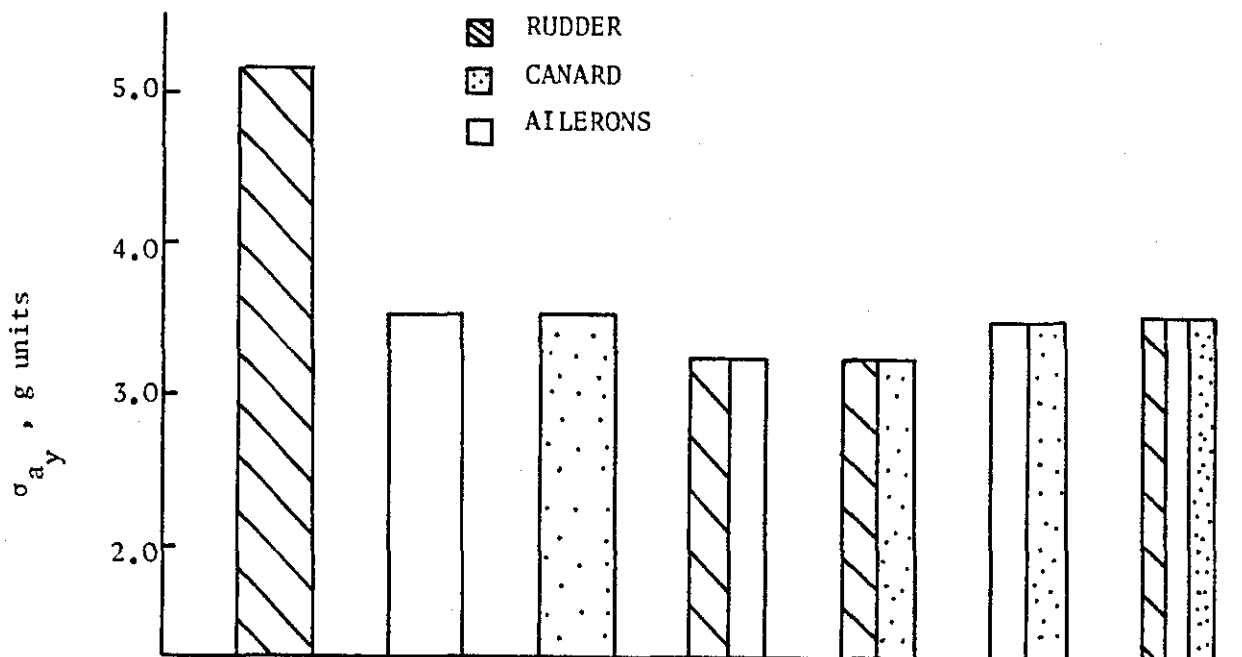


FIGURE 6.21: Resulting Lateral r.m.s. Acceleration when Different Combinations of the Controls are used to achieve a steady bank angle of 2° (CONTROL LAW I)

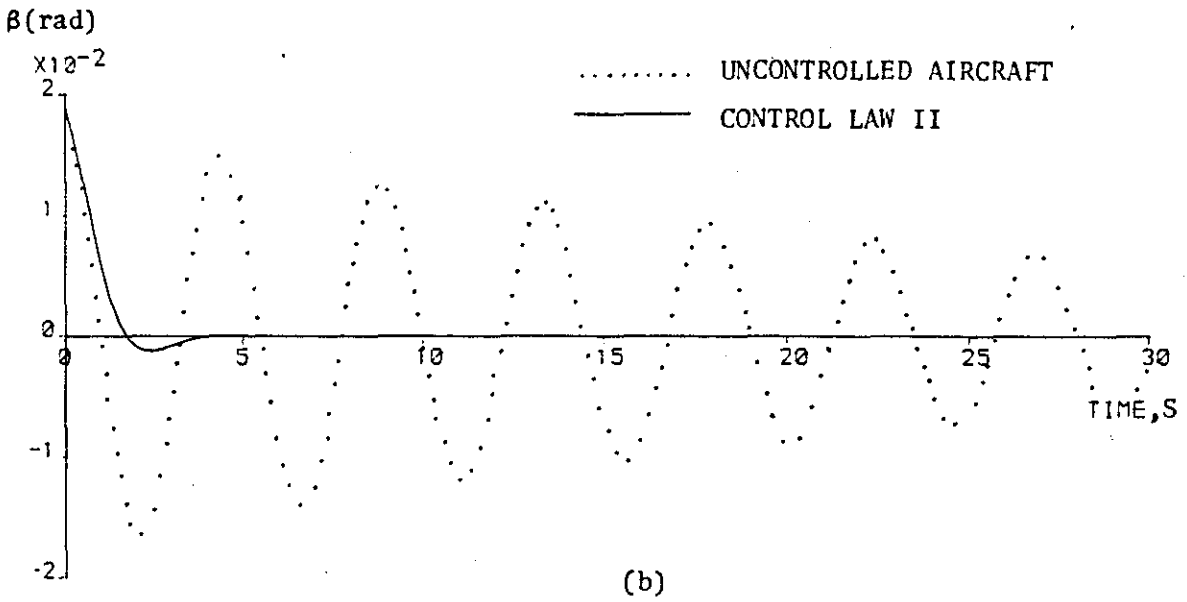
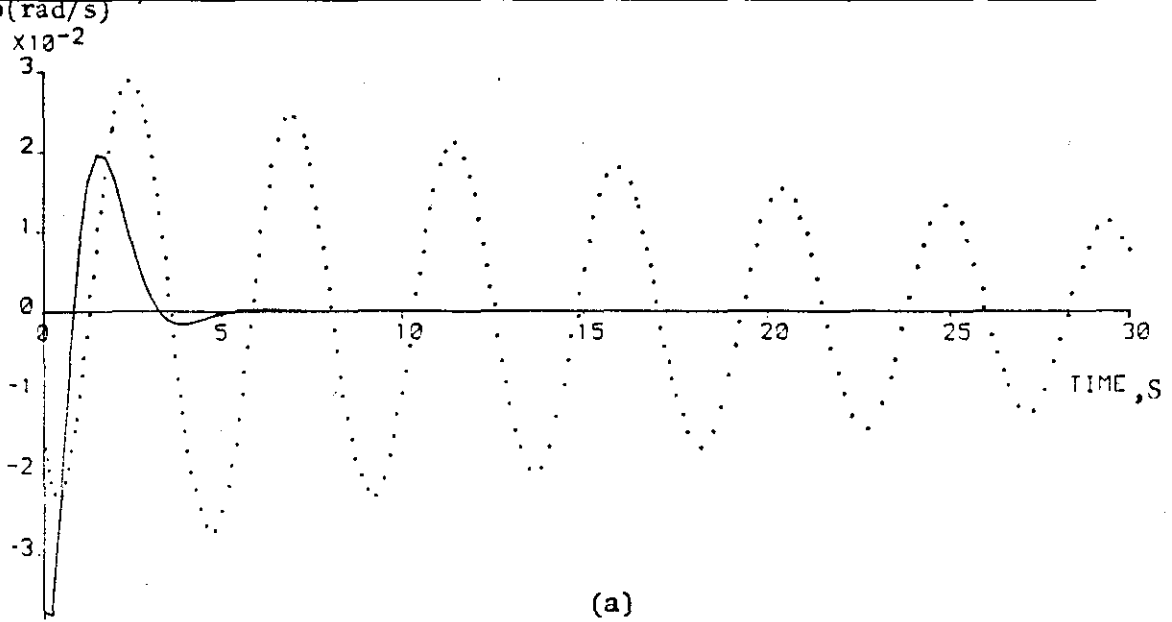
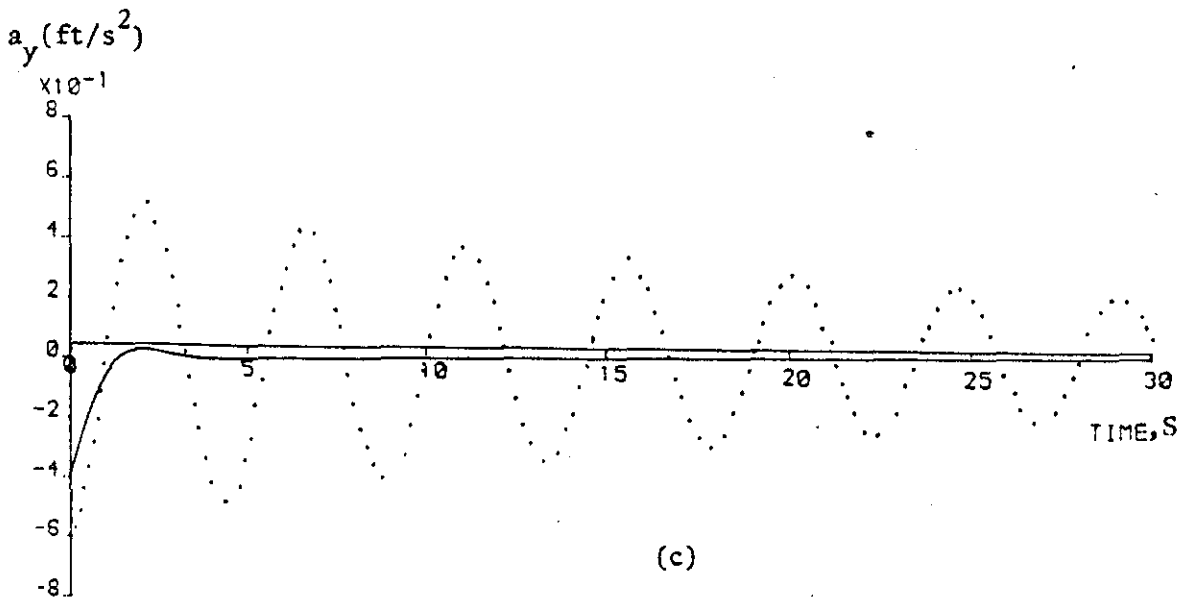


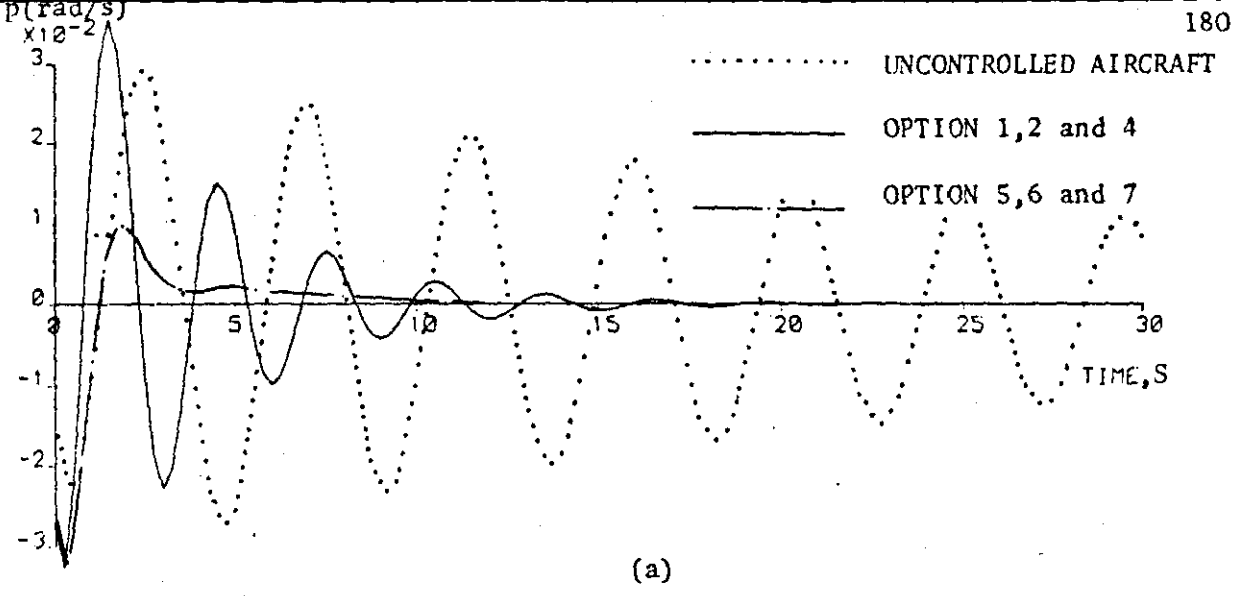
FIGURE 6.22: Effectiveness of CONTROL LAW II for Lateral Motion



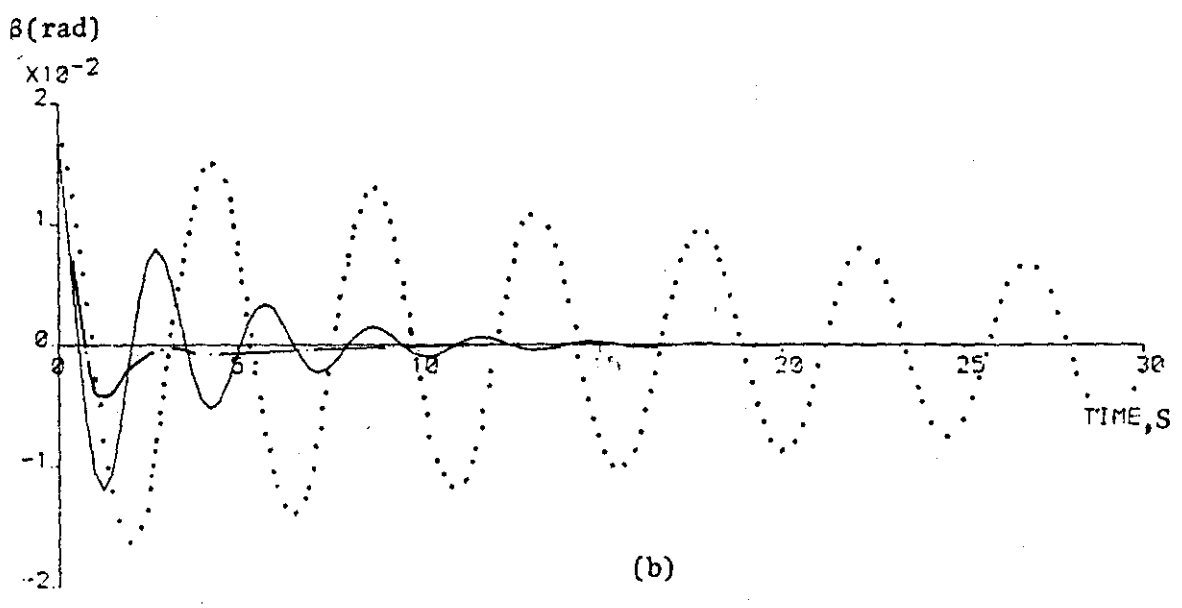
was used a reduction of 77.5% of r.m.s. lateral acceleration was achieved. For the same matrix G used for CONTROL LAW I, the CONTROL LAW II achieved the best reduction of lateral acceleration, as may be seen from Figure 6.26(a). However, the use of CONTROL LAW II also introduced secondary effects on the dynamic performance of the aircraft (rather like CONTROL LAW II for longitudinal motion). A slow, gradual increase of the heading angle, ϕ , was detected in the lateral dynamic response of the aircraft. This effect could be easily controlled by the pilot, or by a control system, provided the lateral control surfaces did not require too large a ride quality control of the lateral motion of the aircraft.

Optimal feedback control laws for lateral handling qualities (CONTROL LAW III) and for different control configurations were investigated in terms of their contribution to ride quality performance. Some typical responses obtained from application of different control surface configurations are given in Figure 6.23 from which it can be seen that combinations of aileron with rudder and canard result in a response which is more heavily-damped than that shown in Figure 6.20. For the remainder of the control surface configurations, except the aileron acting alone, a response more highly damped than that shown in Figure 6.20 results.

A very significant characteristic which results when only the aileron is used in the feedback control is shown in Figure 6.24. For this particular configuration CONTROL LAW III makes the aircraft unstable. This instability results from the positive real parts of two of the eigenvalues of the closed loop system. These are given by $0.05 \pm j(1.51)$. The instability which results from this aileron-alone situation conditions the use of this particular control law in case of failure of operation of the

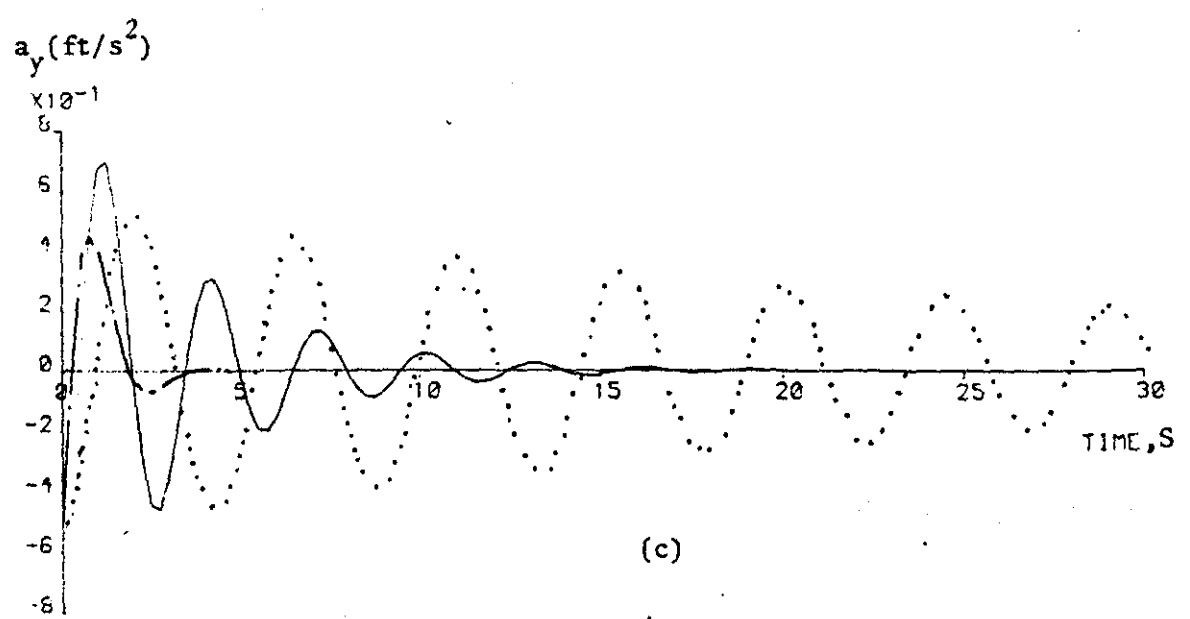


(a)



(b)

FIGURE 6.23: Effect of CONTROL LAW III for Lateral Motion



(c)

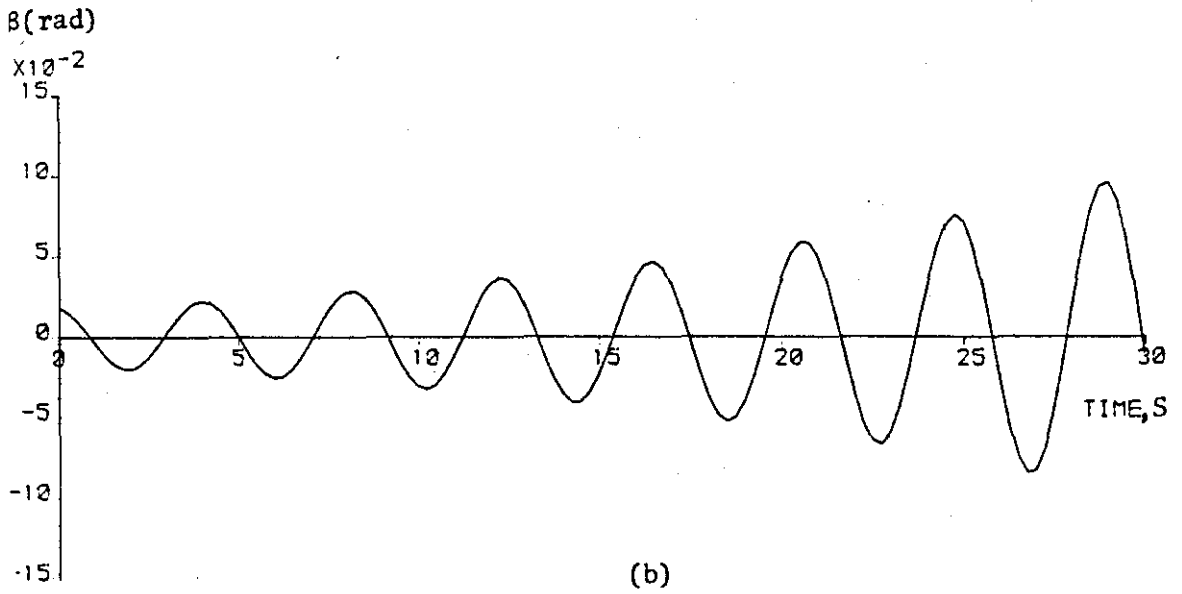
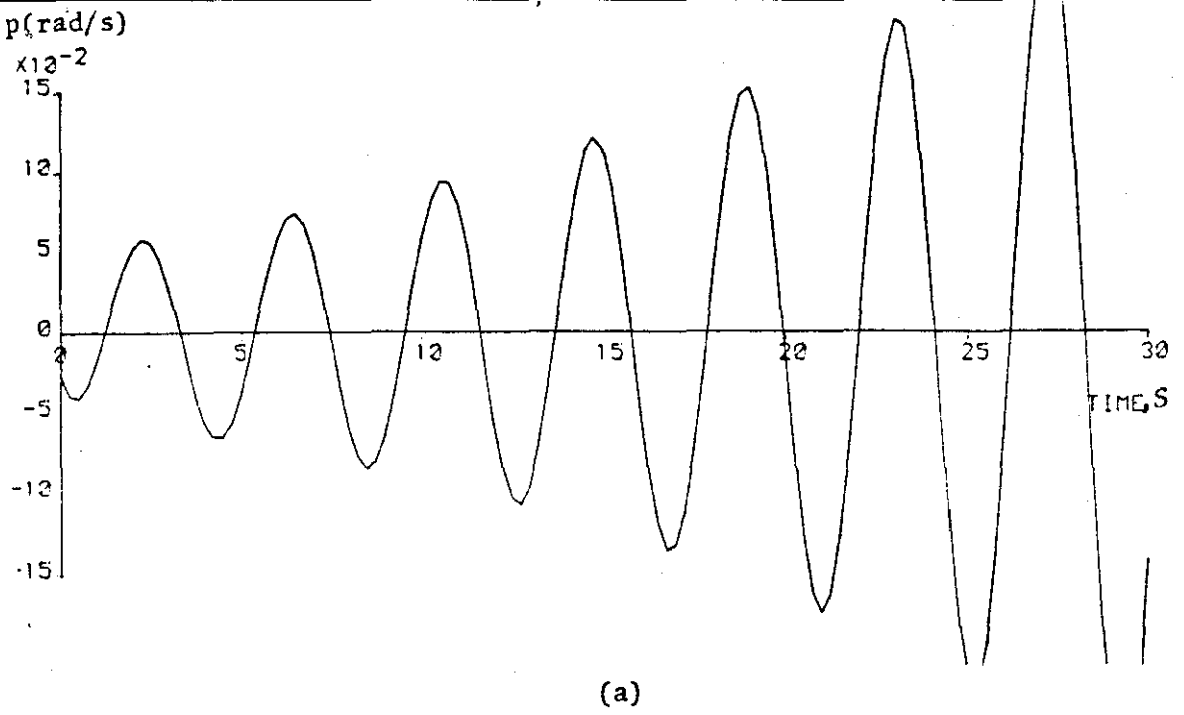
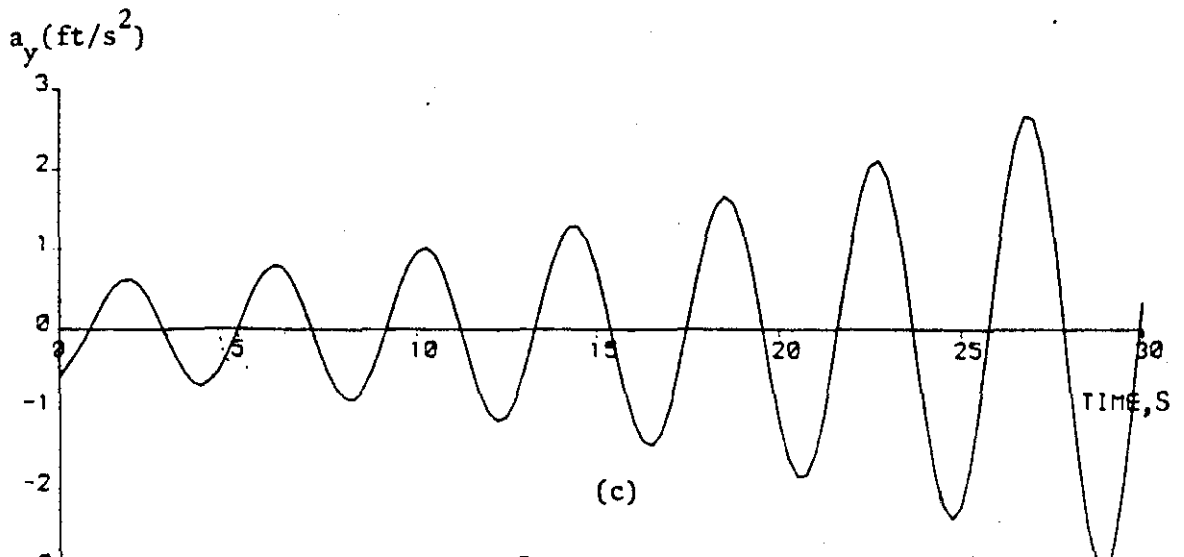


FIGURE 6.24: Instability Introduced by CONTROL LAW II when Aileron was considered alone



other control surfaces. Figure 6.25 shows the r.m.s. values of acceleration and control surface deflections which result when the feedback control law obtained from Model matching theory is used. From this figure it can be seen that the maximum reduction of acceleration (48.0%) is achieved when aileron is acting in combination with rudder or v. canard or both.

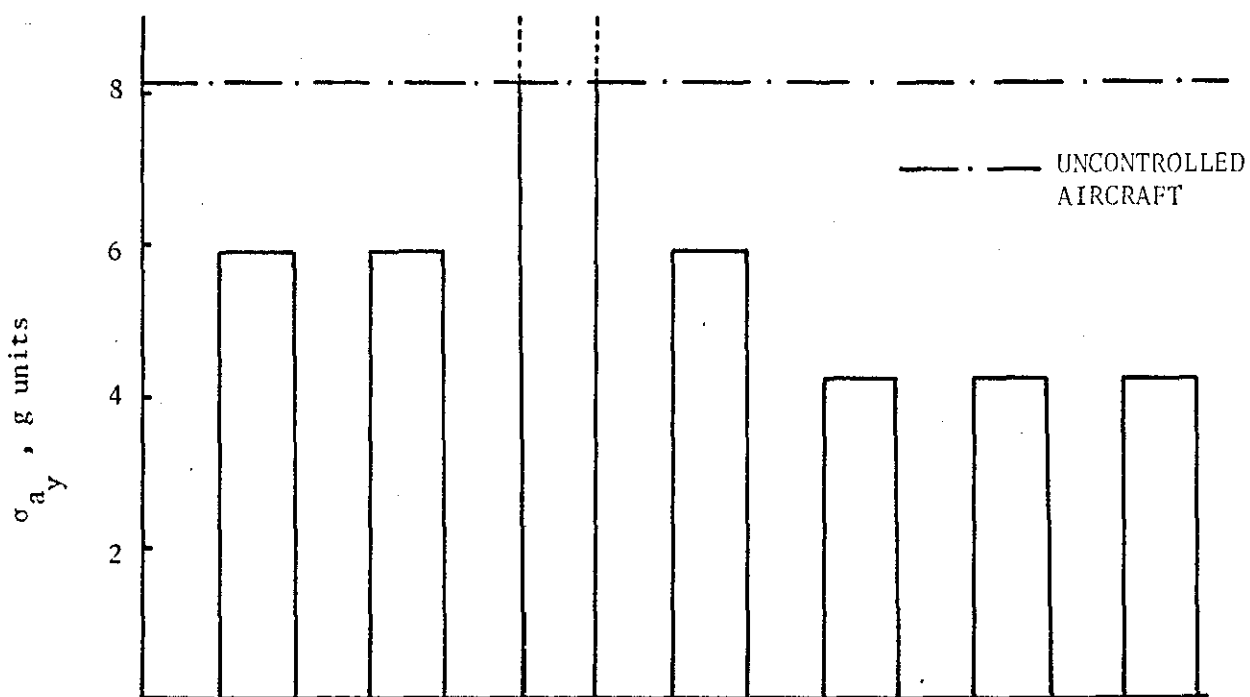
Table 6.3 shows the effect of the CONTROL LAWS I, II and III on the lateral handling qualities of the aircraft.

TABLE 6.3

Effects of CONTROL LAWS I, II and III on the lateral handling qualities of the aircraft with complete control surface configuration

	ζ_d	ω_d	$\zeta_d \omega_d$	T_R
UNCONTROLLED AIRCRAFT	0.0247 [†]	1.397	0.034 [†]	0.474
CONTROL LAW I	0.395	1.5	0.6	0.344
CONTROL LAW II	0.688	1.93	1.33	0.4013
CONTROL LAW III	0.5	2.25	1.1	0.444
ACCEPTABLE HANDLING QUALITIES	≥ 0.19	≥ 1.0	≥ 0.35	< 1.4

[†] denotes unacceptable handling qualities.



% reduction
of σ_{a_y}

(a)

OPTION	1	2	3	4	5	6	7
σ_{δ_R}	.011			.011	.0116		.011
σ_{δ_C}		.112		.0012		.111	.0012
σ_{δ_A}			.049		.005	.005	.005

(b)

FIGURE 6.25: Effectiveness of CONTROL LAW III for Lateral Motion

By comparing the resulting handling qualities for CONTROL LAWS I, II and III with Table 4.4, it may be inferred that CONTROL LAWS I and II improves the handling qualities of the uncontrolled aircraft while CONTROL LAW III achieves very similar handling qualities to those of the model.

Figure 6.26 summarizes the best results obtained for lateral motion for the three control laws considered.

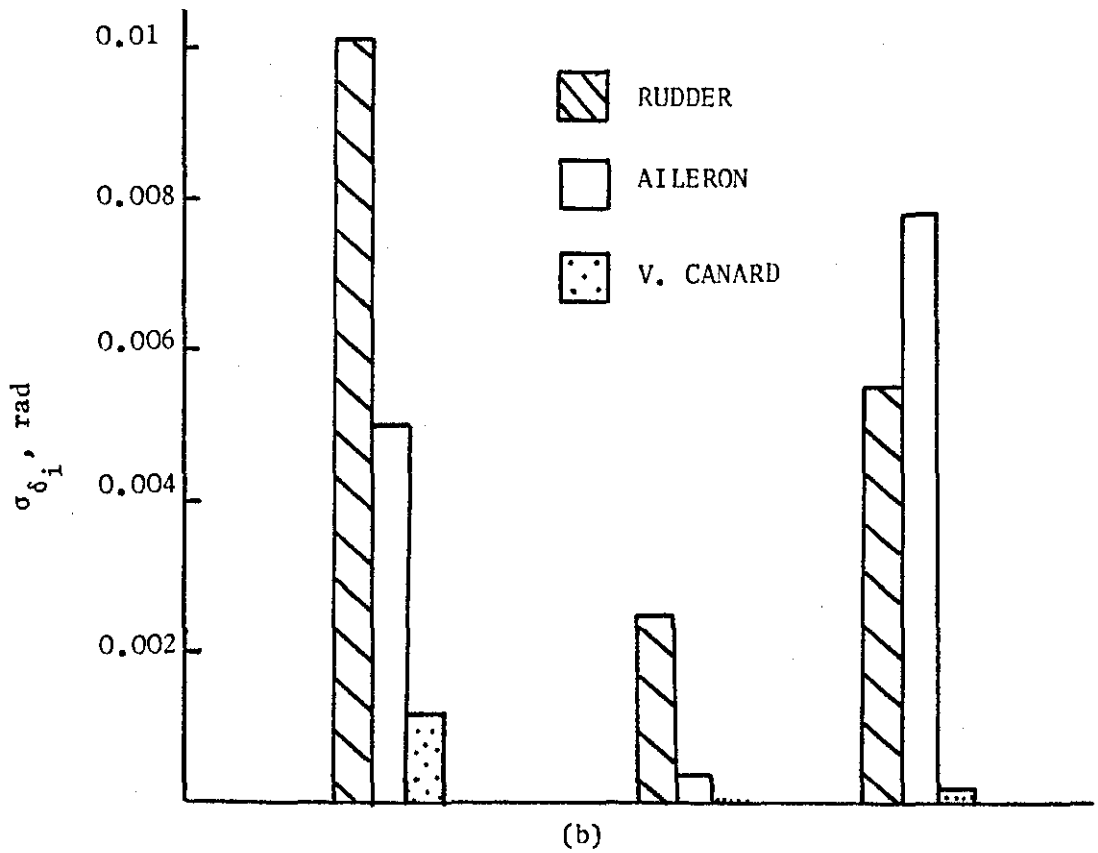
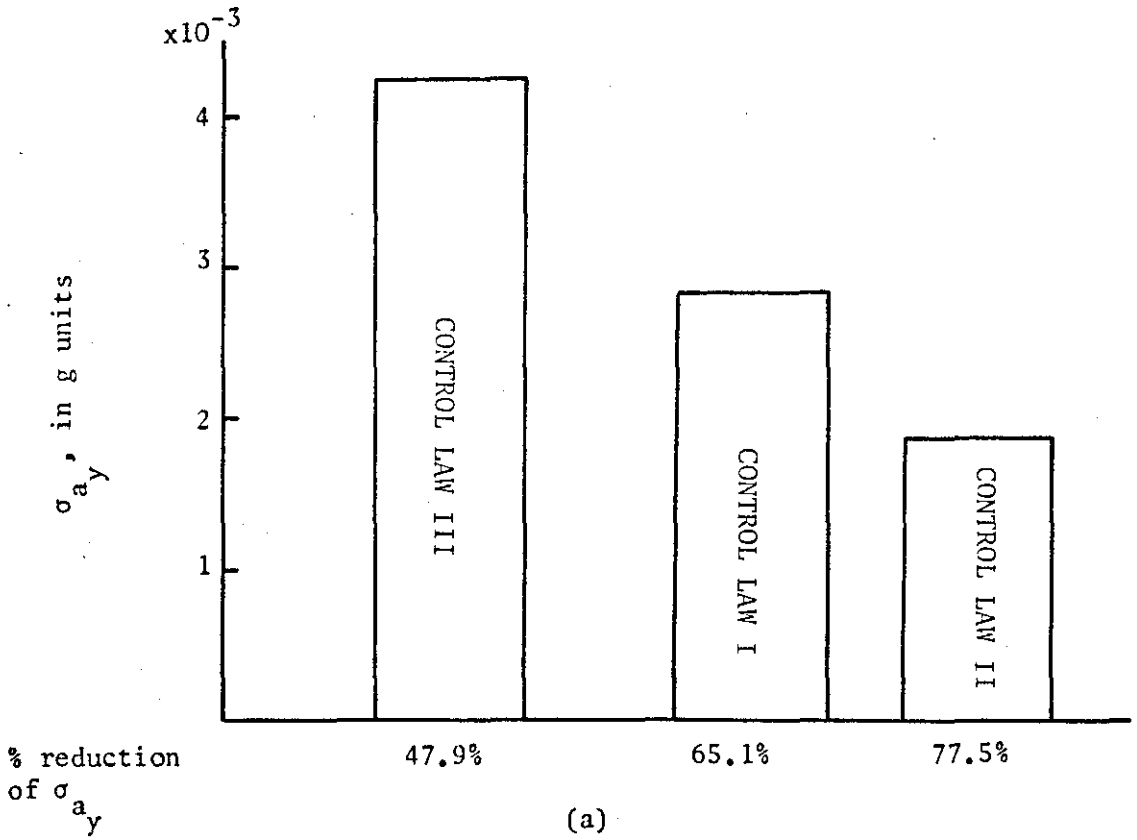


FIGURE 6.26: Effectiveness of CONTROL LAWS I,II and III when all Lateral Control Surfaces are Involved

6.3 ANALYSIS OF THE DYNAMIC RESPONSE OF THE MODIFIED JETSTAR AIRCRAFT IN TURBULENT FLIGHT

The digital simulation of atmospheric turbulence was achieved by means of the Dryden filter which was described in Chapter 3. The components of turbulence normal to the flight path of the aircraft were those considered. In particular the effect of turbulence upon the motion of the aircraft was introduced by means of force and moment coefficients. The r.m.s. values of the vertical and the lateral components of atmospheric turbulence were chosen to be 7.6 and 8.4 ft/s respectively. These values correspond to a probability of equalling or exceeding the given σ_w (or σ_v) once turbulence has been encountered of 6×10^{-3} and represent moderate to heavy turbulence.

The dynamic response of the aircraft was examined for all possible combinations of the considered aerodynamic control surfaces and for the three optimal feedback laws as described in earlier sections. The actuators dynamics and their nonlinearities due to power and control surface deflection angles limitations were also investigated. A non-linear controller was considered in order to improve one undesirable feature of the ride quality performance of the modified Jetstar. The analysis of the results was based on the r.m.s. values of both acceleration levels and control surface deflection angles obtained from turbulent flight. As in the deterministic analysis longitudinal and lateral motions were studied separately.

6.3.1 Longitudinal Motion Analysis

6.3.1.1 Effectiveness of CONTROL LAWS I,II and III

The same control laws and procedure which were employed in the deterministic analysis of the controlled aircraft were considered in the stochastic analysis. The effectiveness of the deterministic optimal feedback control laws was examined in the presence of digitally simulated atmospheric turbulence. CONTROL LAW I was used, like for the deterministic analysis, as the basis for the analysis of the longitudinal motion. The effectiveness of each optimal feedback control law was judged by comparison with the dynamic response of the aircraft with locked controls when disturbed by atmospheric turbulence. Figure 6.27 shows a typical result obtained when CONTROL LAW I was employed. In this case elevator is acting alone. From 6.27(a)(b) and (c) it can be seen that the absolute values of w , q and a_z have been effectively reduced compared to the uncontrolled aircraft. The strong effect of the elevator is evident from Figure 6.27(b). From this figure it may be inferred that the reduction of the r.m.s. value of pitch rate is accompanied by higher frequency components which in turn appear in the normal acceleration response. This particular type of small amplitude, high frequency dynamic response is known as 'cobblestone effect' and evidently it would be annoying for the passengers of a transport aircraft (see Figures 2.2 and 2.3 in section 2.2). As will be shown later a non-linear function could be used to reduce these high frequency effects. It can also be deduced from Figure 6.27(c) that CONTROL LAW I achieves a considerable reduction in the r.m.s. value of normal acceleration.

Figure 6.28 illustrates the effect of different control surface configurations and actuator dynamics on the character of the r.m.s.

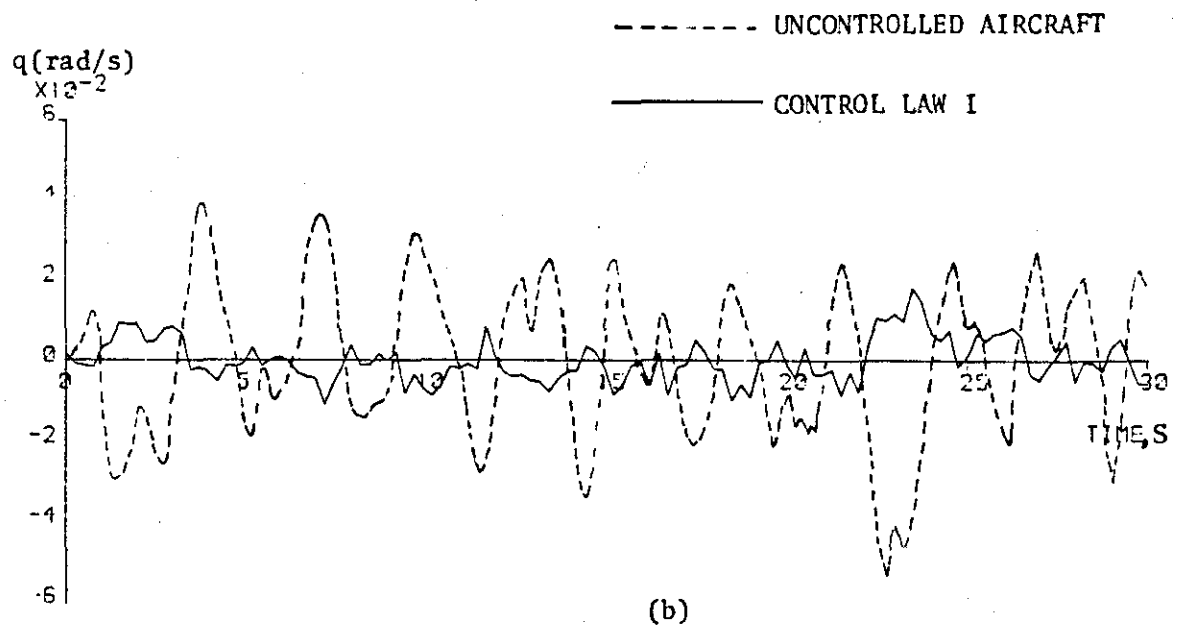
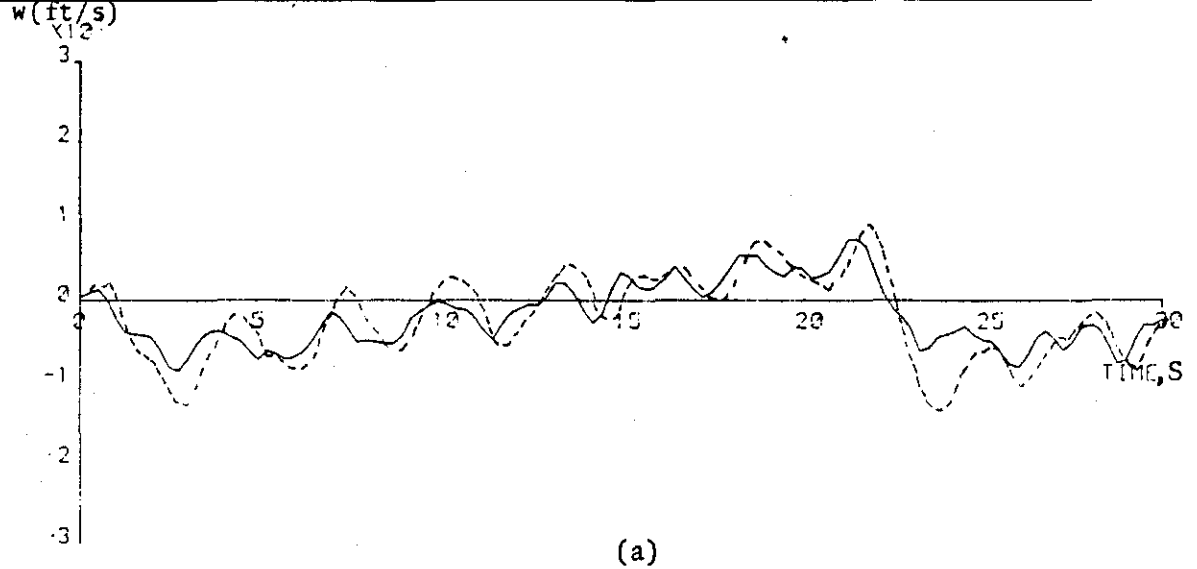
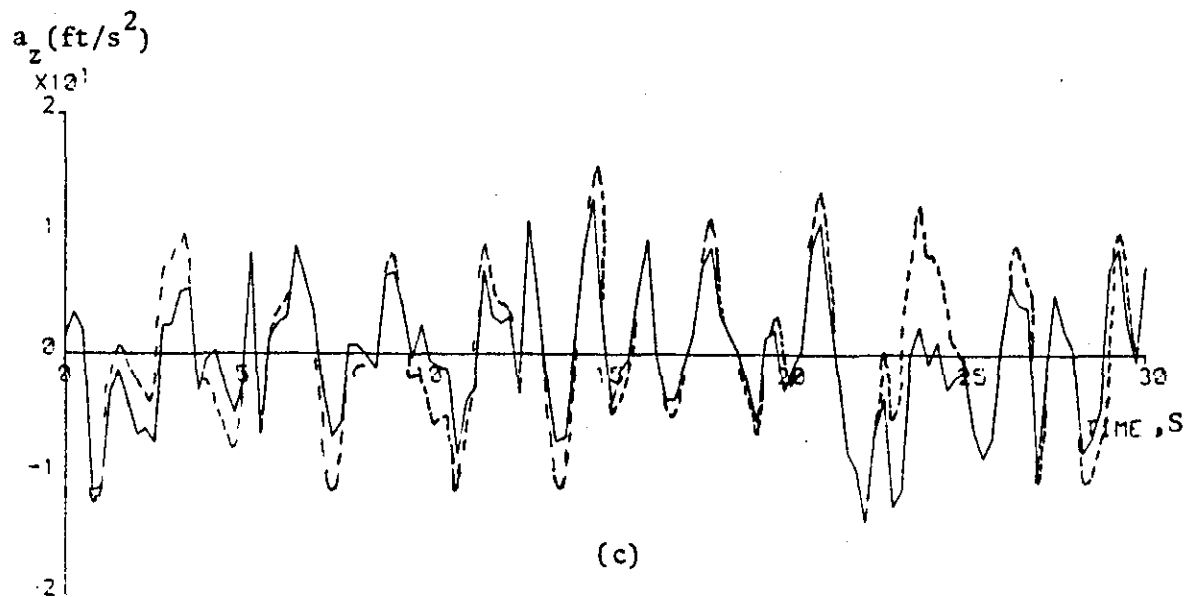
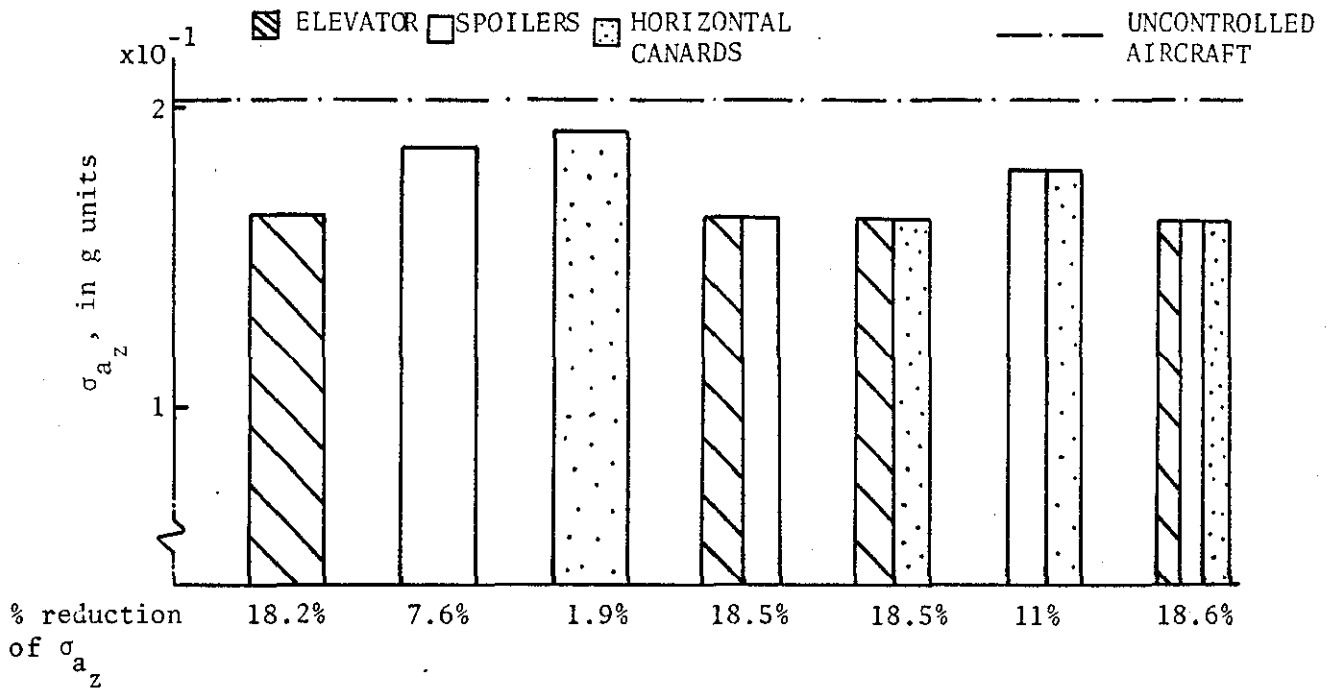


FIGURE 6.27: Effectiveness of CONTROL LAW I for Longitudinal Motion in Turbulent Flight

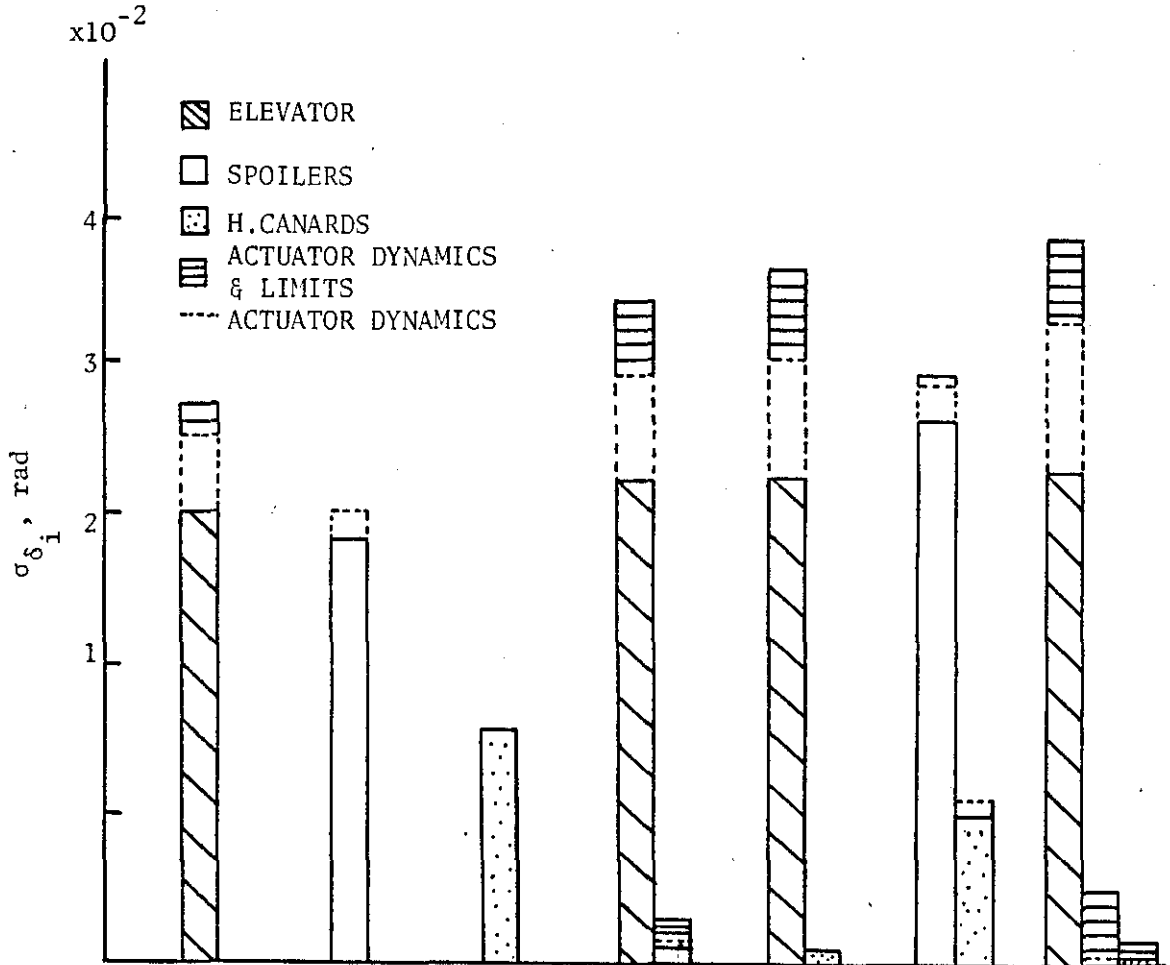


normal acceleration. The best results were obtained when the elevator was involved in the control surface configurations (see Figure 6.28(a)). However Figure 6.28(b) shows that the elevator was used more than any other control surface when it was acting in combination. The maximum reduction of r.m.s. normal acceleration (18.5%) was achieved when all the longitudinal control surfaces were acting simultaneously. When the actuator dynamics were considered the ride performance of the aircraft was slightly degraded for every configuration. Due to time lags introduced by the actuator dynamics the control law required more activity from the control surfaces (Figure 6.28(b)) and this extra activity in turn affected the acceleration levels induced on the aircraft. Whether the actuator dynamics were considered or not, the deflection angles of the control surfaces did not exceed the specified deflection limits, as can be seen from inspection of Figure 6.28(b). However, when the rate limits of the actuators were considered the control surface configurations employing elevator were affected favourably while for the other configurations the performance was unaltered. To account for this result consider Figure 6.29.1 which shows how the actuator rates required by the control law vary with time when all the control surfaces are used. It is evident from inspection of this figure that the elevator must act very fast in order to perform the commands from the control law. At the same time very slow performance is required from the spoilers, with even slower response needed from the horizontal canards, although these control surfaces are each capable of achieving much faster responses than the elevator. All these effects are a consequence of the choice of the control vector weighting matrix, G , which was derived from the program WAYMX (Section 4.5). However, consideration of the non-linearities of the actuators, due to inherent power limits, resulted in better ride



WITH ACTUATOR DYNAMICS	18.1%	6.9%	1.5%	17.7%	17.7%	10.3%	17.5%
WITH ACTUATOR DYNAMICS & LIMITS	18%	6.9%	1.5%	18.6%	18.9%	10.3%	19.8%

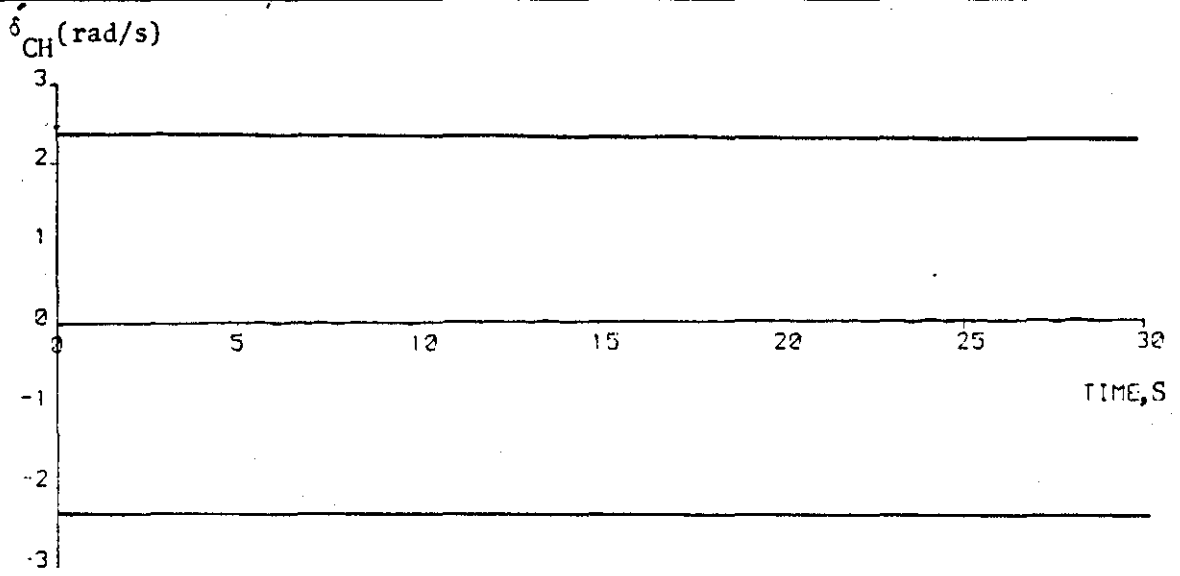
(a)



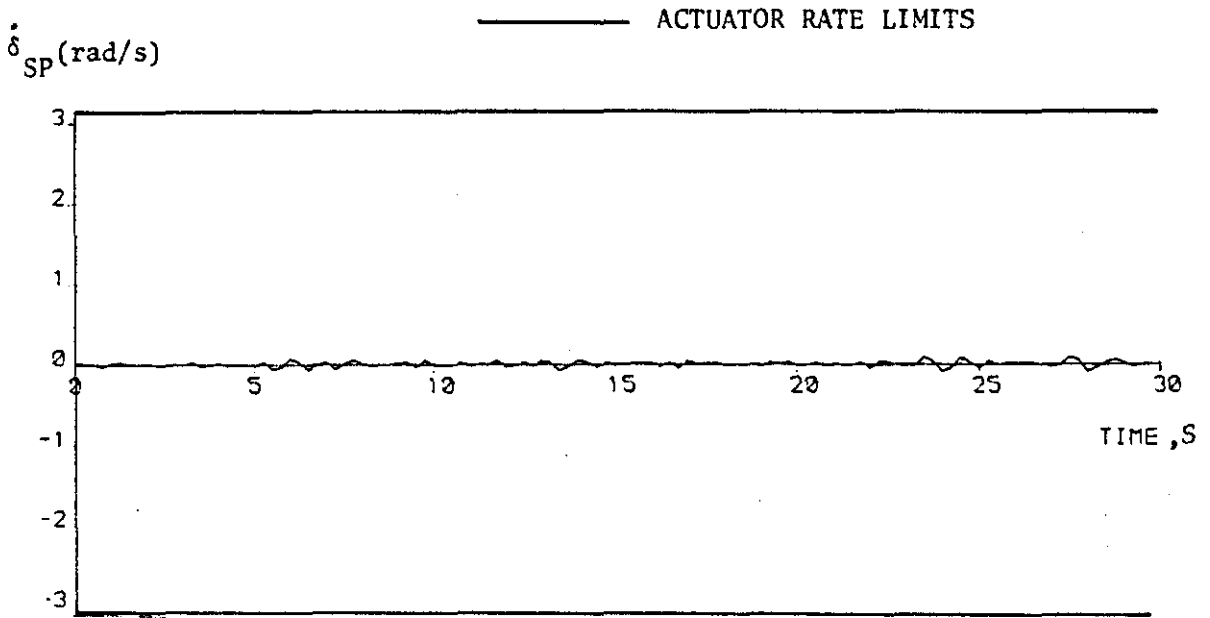
(b)

FIGURE 6.28: Effectiveness of CONTROL LAW I in Turbulent Flight for Different Control Surface Configurations

quality performance for configurations employing elevator in combination with spoilers, or canards, or both, than for the same configurations without considering actuator dynamics. Although no general conclusion can be drawn from this particular result an explanation can be offered. The consideration of the rate limits on the elevator activity resulted in higher r.m.s. values of deflection angles of the control surfaces employed in conjunction with the elevator (Figure 6.28(b)) which assisted in the reduction of the levels of the r.m.s. acceleration (20%). For this particular configuration, and weighting of the control vector, the rate limits effectively result in approximately on/off activity of the elevator (See Figure 6.29.1(c)). It could therefore be possible to achieve similar results if instead of using the linear control law, an on/off controller for the elevator was employed. However such an investigation was outside the scope of this research and therefore further investigation was pursued. To use the dynamic characteristics of spoilers and horizontal canards more effectively some different choices of the matrix G , which were empirical in nature, were investigated. From these investigations few conclusions could be drawn; however, for any attempt to reduce the relative effectiveness of the elevator resulted in higher levels of acceleration emphasising once more the major importance of the elevator in any ride quality control configuration. The same effects in smaller scale were identified when the relative effectiveness of the spoilers was reduced. On the contrary when the relative effectiveness of the canards was increased degradation of the ride quality performance ensued. This particular result indicates that horizontal canards do not necessarily improve the ride performance of this aircraft. These results reinforced some conclusions drawn so far in respect of the significance of horizontal canards in the ride quality control system.

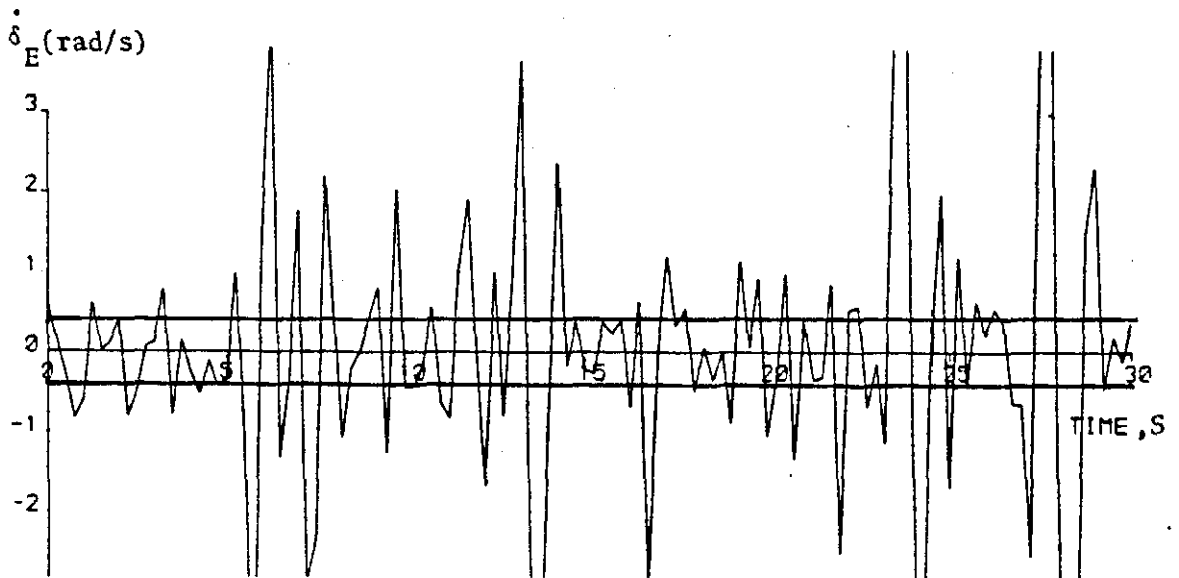


(a)

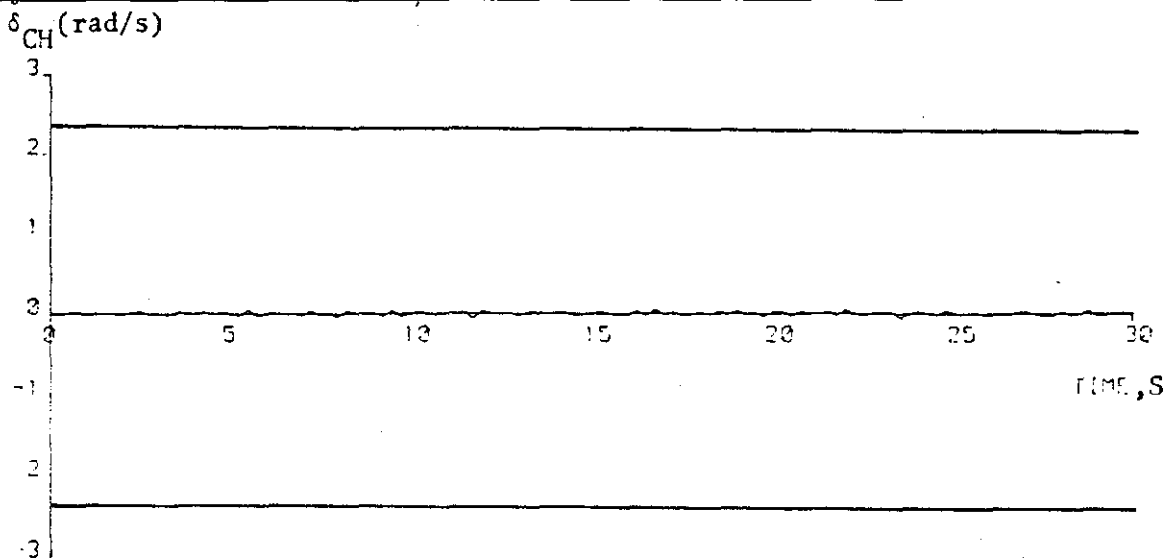


(b)

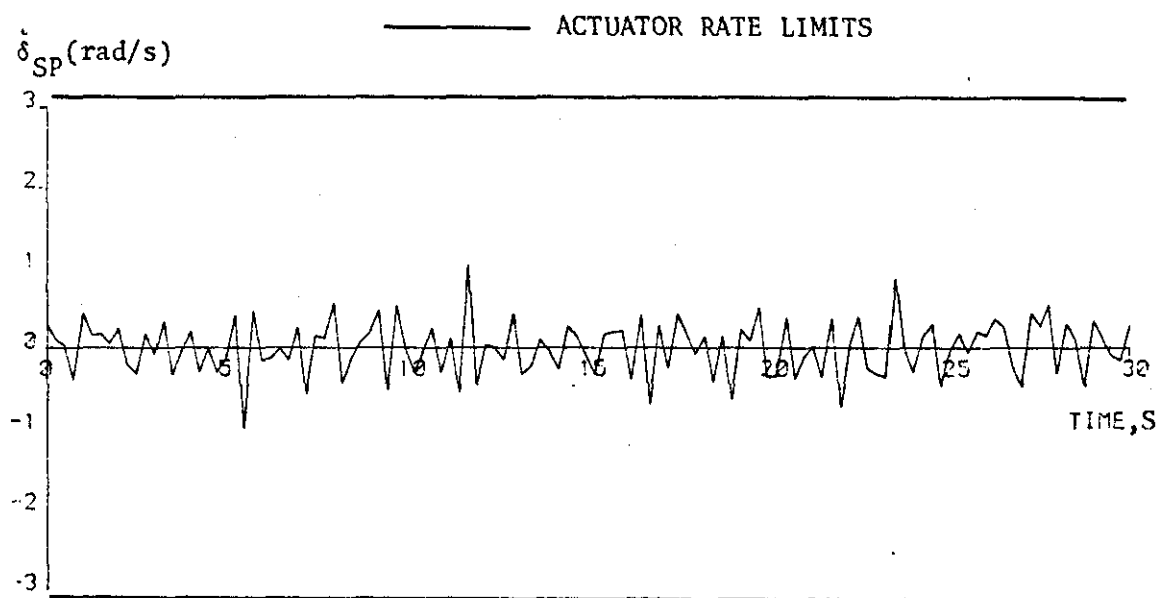
FIGURE 6.29.1: Deflection Angle Rates Required from CONTROL LAW I due to the 'WAYMX' Weighting of the State and Control Vectors



(c)

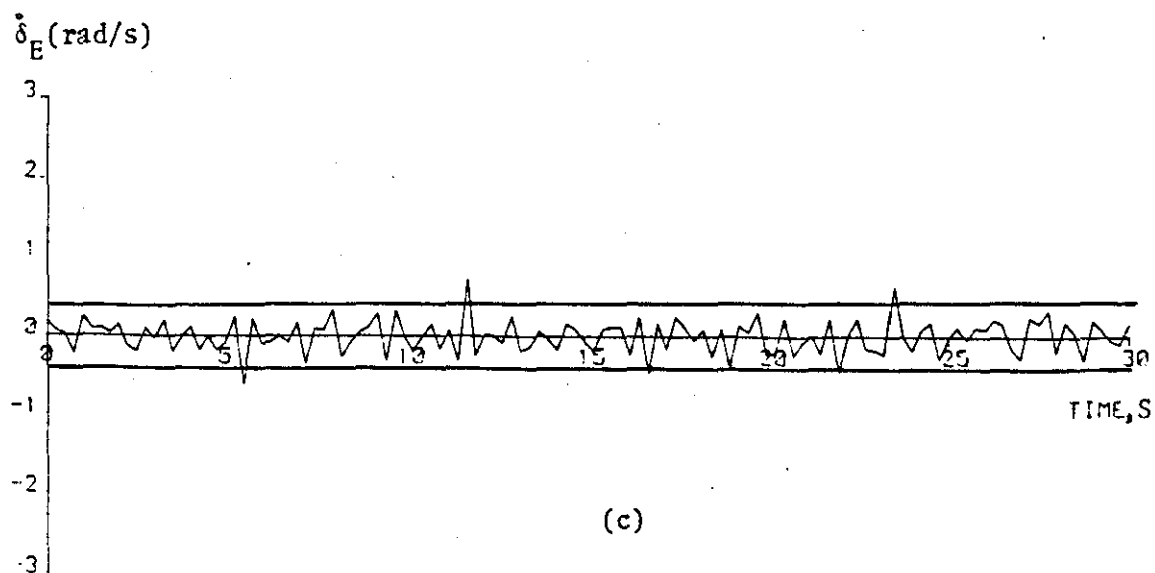


(a)



(b)

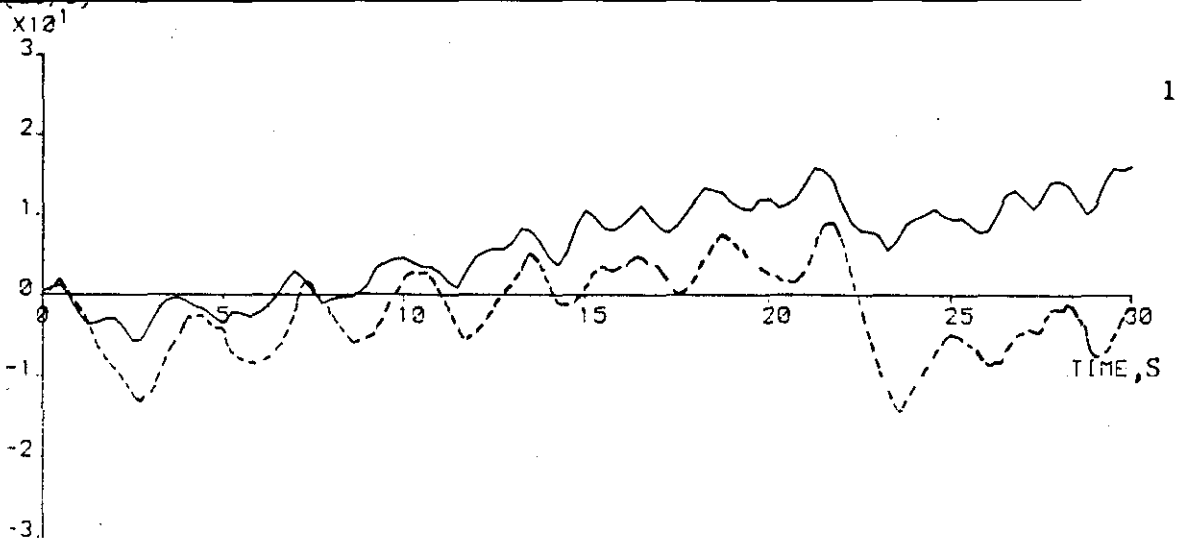
FIGURE 6.29.2: Deflection Angle Rates Required from CONTROL LAW I due to Different to 'WAYMX' Weighting of the Control Vector



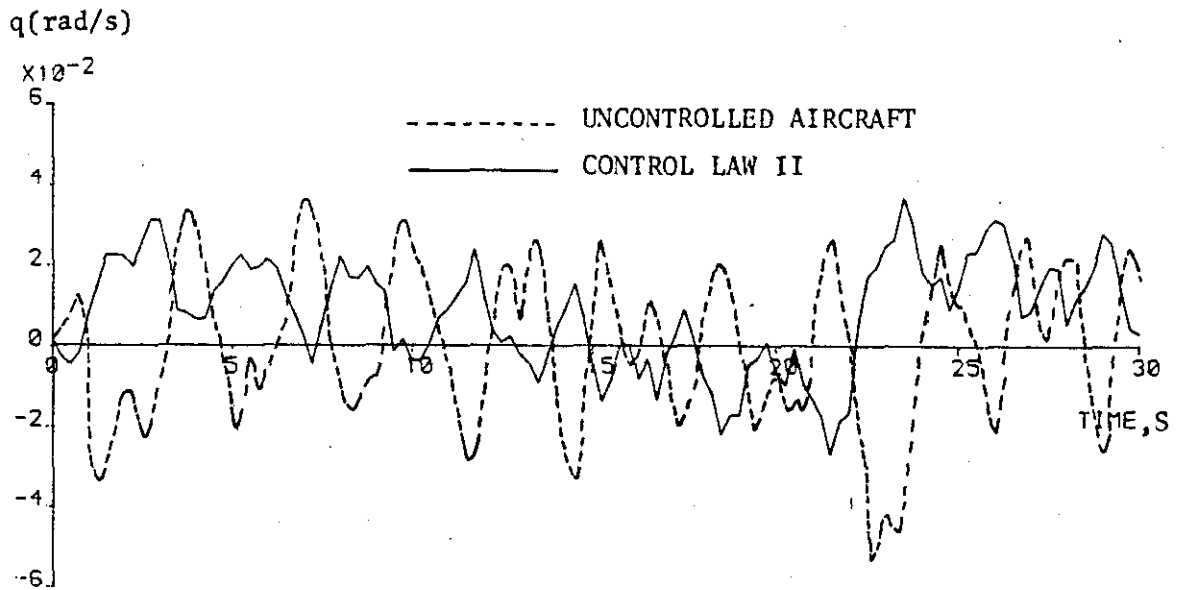
(c)

Figure 6.29.2 shows the results obtained for the rates of activity for a control surface configuration which employed all the controls and in which they were weighted such that the relative effectiveness of spoilers increased while that of the elevator decreased. At the same time canards effectiveness was kept low. From the same figure it is apparent that the elevator acted within its rate limits while the spoilers were capable of even higher rates. Although the 18.2% reduction of r.m.s. acceleration relative to the uncontrolled aircraft was not as high as that obtained when the weighting (from WAYMX) corresponding to the results shown in Figure 6.29.1 was employed a better weighting of the state vector would undoubtedly improve the results.

The optimal feedback CONTROL LAW II was investigated for two configurations (elevator alone and elevator-spoilers-h.canards) in turbulent conditions. Figure 6.30 shows the dynamic response of the aircraft as a result of this control law when elevator was used as a control surface. From the figure it can be deduced that although the overall effect is favourable in terms of acceleration, both the pitch and heave responses of the aircraft do not achieve the dynamic performance which was obtained when CONTROL LAW I was considered (see Figure 6.27). A 18.5% reduction of r.m.s. acceleration was achieved with CONTROL LAW II for both elevator alone and elevator-spoiler-h.canards configurations. However, by employing this control law it is expected that the dynamic response of the aircraft will not be the 'best' as far as the motion variables, apart from acceleration, are concerned. This is because not all the state variables are included in the performance index when "explicit" minimization of acceleration is considered. The same effect on w as for the deterministic analysis (viz. the progressive but small increase in w with time) was also detected when gust effects were considered.

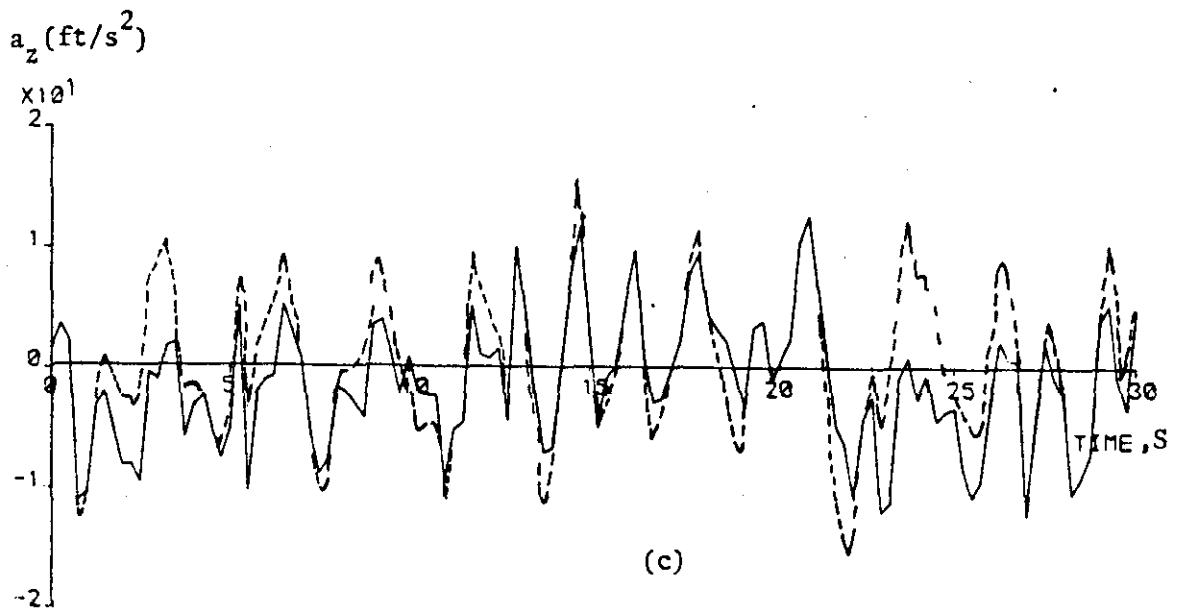


(a)

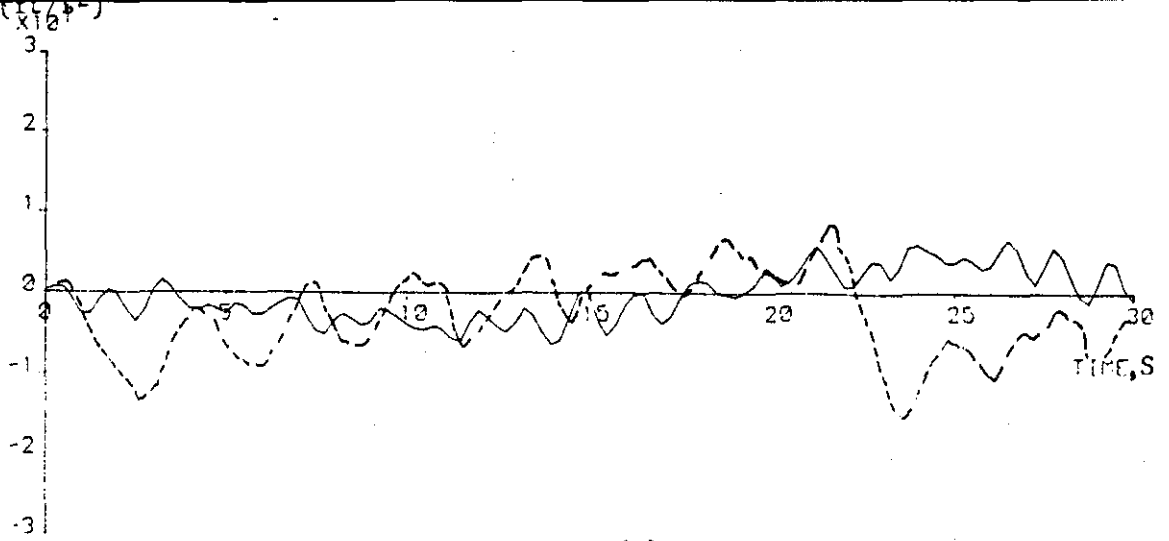


(b)

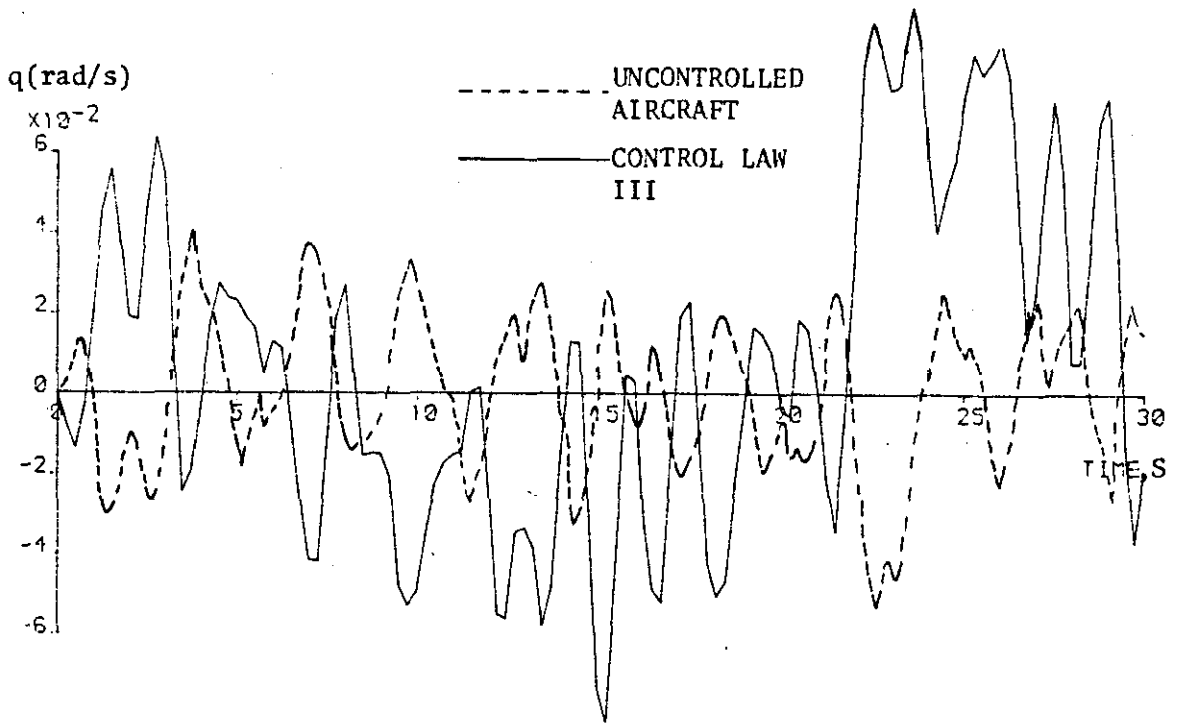
FIGURE 6.30: Effectiveness of CONTROL LAW II for Longitudinal Motion when Elevator Only is considered



(c)

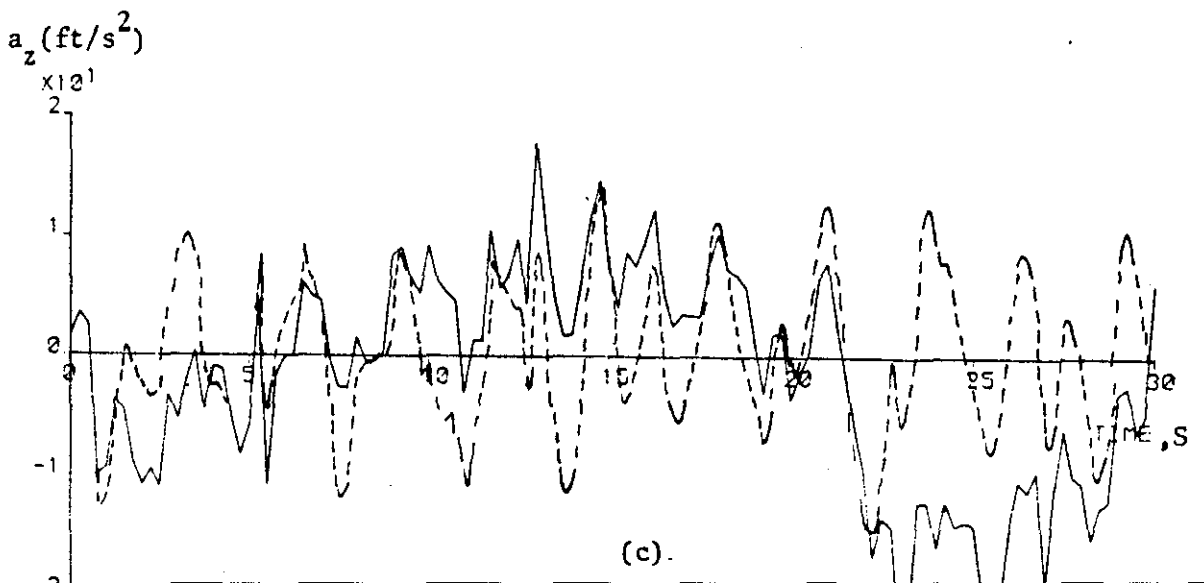


(a)

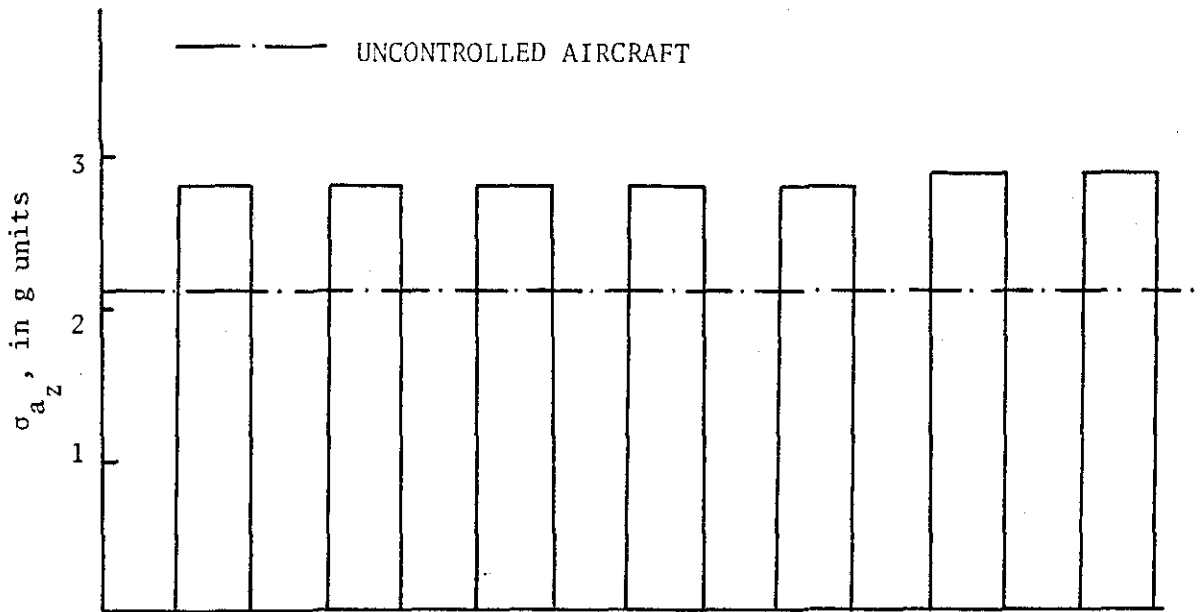


(b)

FIGURE 6.31: Effectiveness of CONTROL LAW III for Longitudinal Motion



(c)



OPTION	1	2	3	4	5	6	7
δ_E (rad)	0.0615			8.031	8.9		8.69
δ_{SP} (rad)		0.184		23.93		435	466
δ_{CH} (rad)			0.293		39.78	691.9	780

FIGURE 6.32: Effectiveness of CONTROL LAW III for Longitudinal Control in Turbulent Flight

When the optimal feedback control law for handling qualities improvement (CONTROL LAW III) was tested for turbulent flight it did not provide any ride quality performance improvement. On the contrary it resulted in the degradation of the dynamic performance compared with that of the uncontrolled aircraft. Figure 6.31 illustrates a typical dynamic response of the aircraft for this control law in turbulent flight conditions. From the figure it is evident that the use of CONTROL LAW III results in excessive levels of pitch rate and acceleration compared to those associated with the uncontrolled aircraft. The results obtained for different control surface configurations are presented in Figure 6.32. From 6.32(a) it is evident that the r.m.s. acceleration levels due to the application of the control law obtained from model matching theory are higher than those of the uncontrolled aircraft for every combination of the control surfaces. From Figure 6.32(b) it can be seen that the deflection angles required from the control law, when the control surfaces were considered to act in combination, are unrealistically high due to the absence of weighting in the derivation of the control law. It is apparent from this figure that the control law derived for the particular model chosen for handling qualities improvement failed to provide acceptable ride quality performance when gusts affected the aircraft.

6.3.1.2 Non-Linear Controller

It was mentioned in the previous section 6.3.1.1 that the use of the optimal feedback CONTROL LAW I resulted in high frequency components in the dynamic response of the aircraft which is referred to as 'cobblestone effect'. To remove such an effect from the dynamic response of the R.C.S. a non-linear function was included in the feedback path of

the optimally controlled aircraft. The non-linear function used was that suggested by FRY and WINTER [1978] and is represented by (6.7) viz:

$$\ddot{x}_0 = |x_i - x_0| (x_i - x_0) \tau_f \quad (6.7)$$

This function is represented in the block diagram of Figure 6.33.

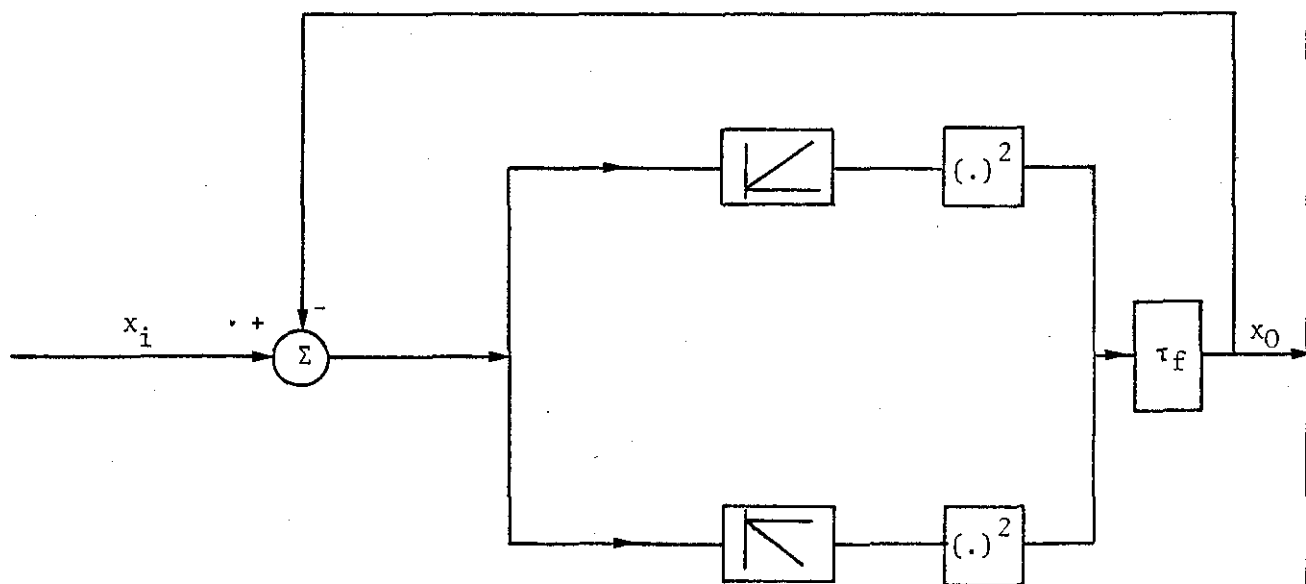


FIGURE 6.33: Non-linear function block diagram

From equation (6.7) the non-linear function can be considered as having parabolic properties with positive values of \dot{x}_0 for positive error between input and output $(x_i - x_0)$ and negative values of \dot{x}_0 for negative error. The characteristic of the non-linear function is shown in Figure 6.34.

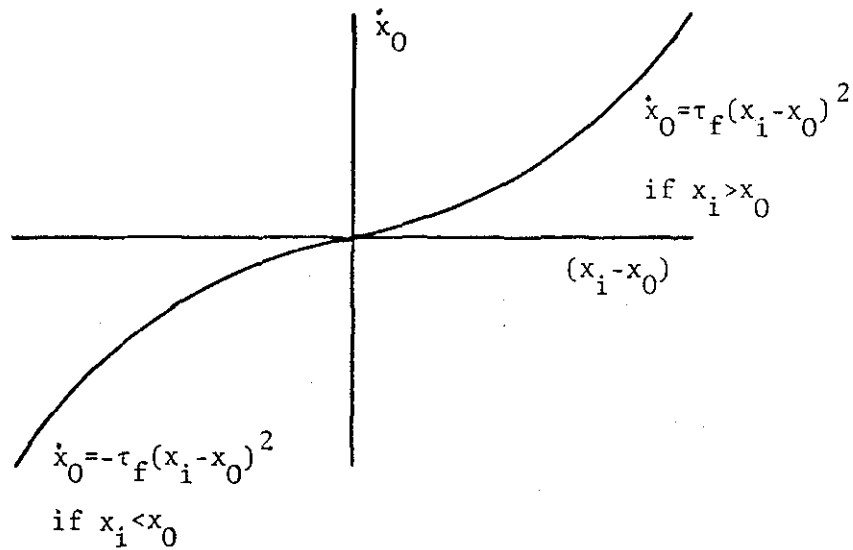


FIGURE 6.34: The non-linear function characteristic

The outputs rate of change is low for small changes between input and output, while for larger changes it is intensified. In other words the non-linear function is essentially an amplitude-dependent gain function and as the gain reduces for low errors so too does the associated natural frequency of a closed-loop system. Hence, the use of the non-linear function should result in elimination of the high frequency components and at the same time in a reduction of the absolute values of the state variables employed; provided that the scaling factor τ_f , of the parabola is chosen correctly. For any particular motion variable the value of the scaling factor of the parabola (τ_f) should be chosen such that it will account for maximum deviations from the mean.

The implementation of this non-linear function in the feedback loop of the optimally controlled aircraft is described in the following block diagram.

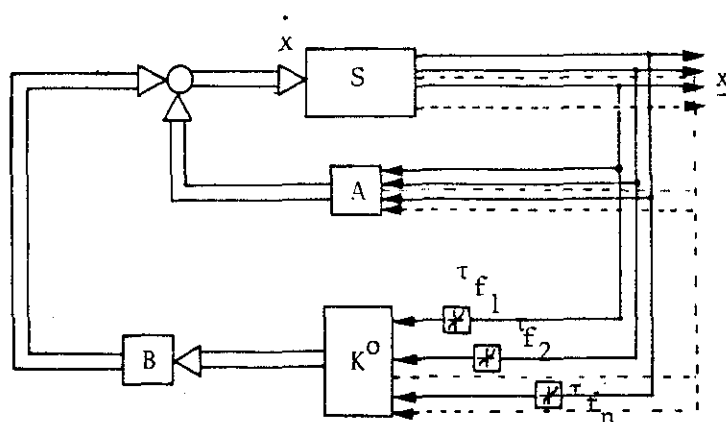


FIGURE 6.35: Block diagram of the non-linear controller in the ride control system

The non-linear function was tested for the CONTROL LAW I and was employed in the configurations of elevator only and elevator-spoilers-h.canards. The scaling factors $\tau_{f_1}, \tau_{f_2}, \dots, \tau_{f_n}$, were chosen to be equal for each state variable. Different values of τ_f were tested for the two control surface configurations. A typical result is illustrated in Figure 6.36 for $\tau_f=75$ which was obtained when elevator only configuration was considered. The figure demonstrates that the frequency was reduced and that acceleration was also reduced. Although the pitch rate r.m.s. level increased this nevertheless could be kept low if the value of τ_f was chosen appropriately. In this particular case a reduction of 20% of acceleration was achieved improving by 2% the reduction of acceleration achieved by CONTROL LAW I.

For the configuration of elevator acting in conjunction with spoilers and h.canards the non-linear controller did not offer any improvement on the r.m.s. levels of acceleration.

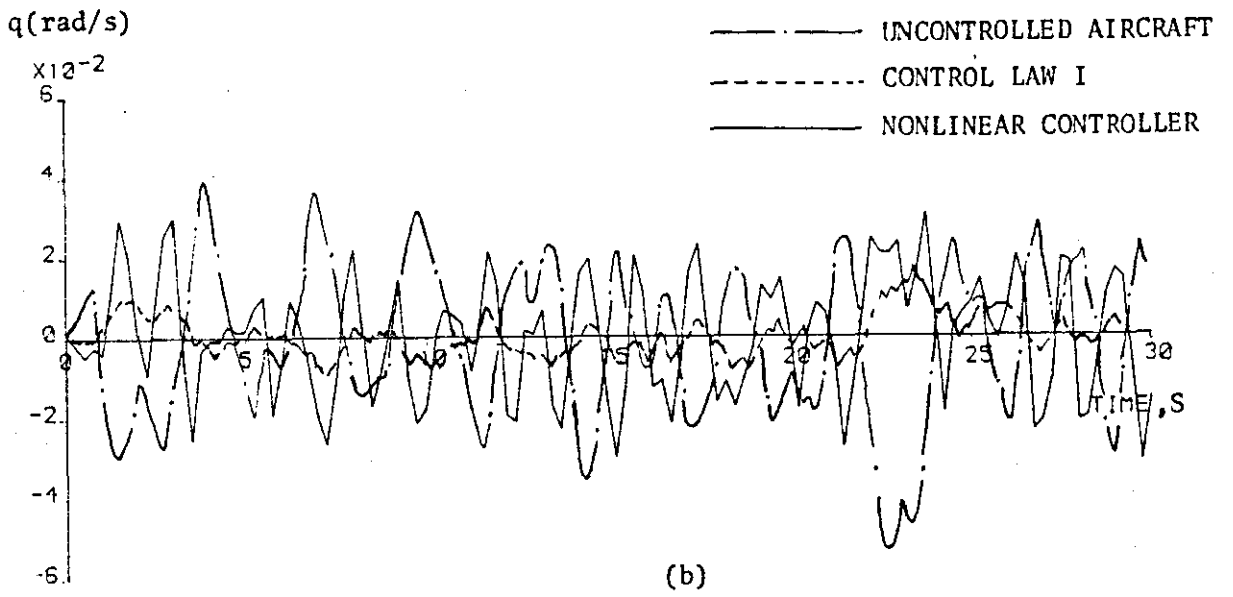
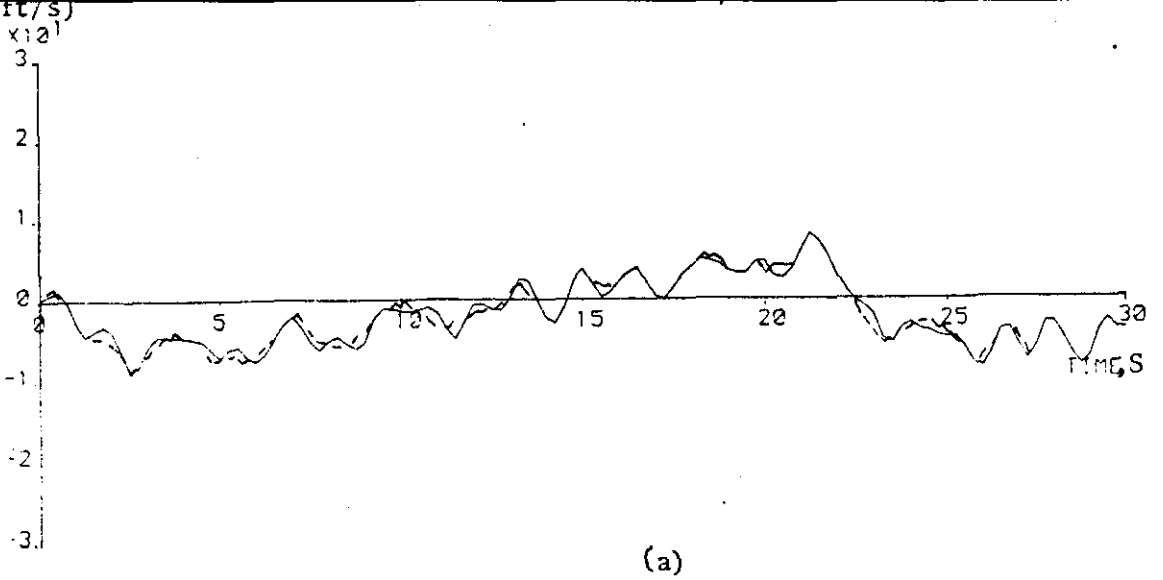
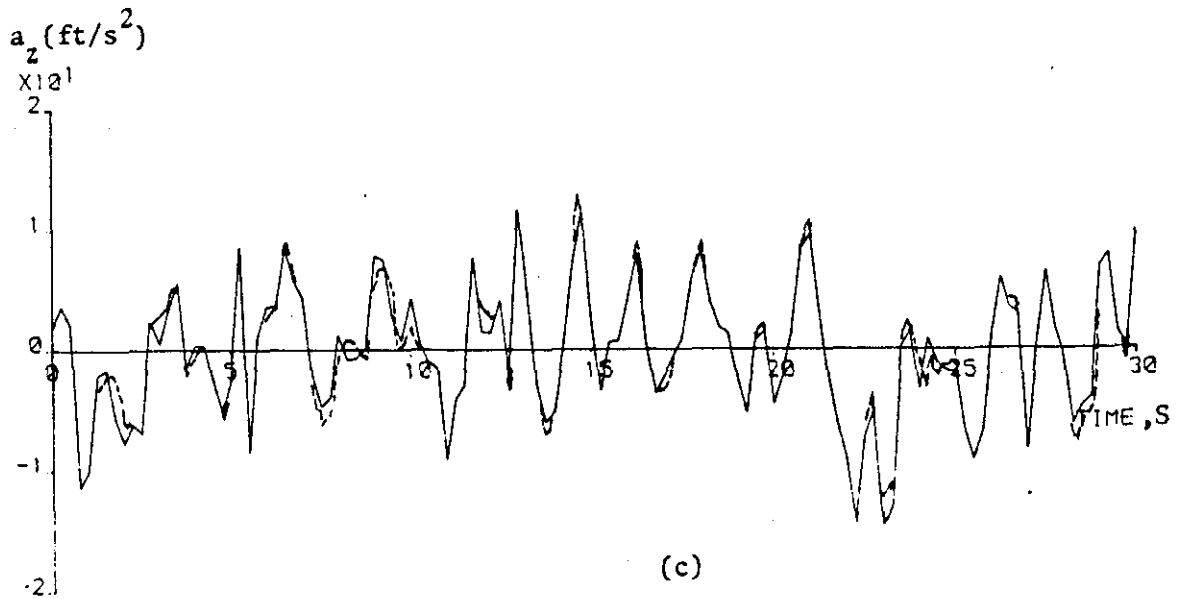


FIGURE 6.36: Effectiveness of Nonlinear Controller with $\tau_f=75$

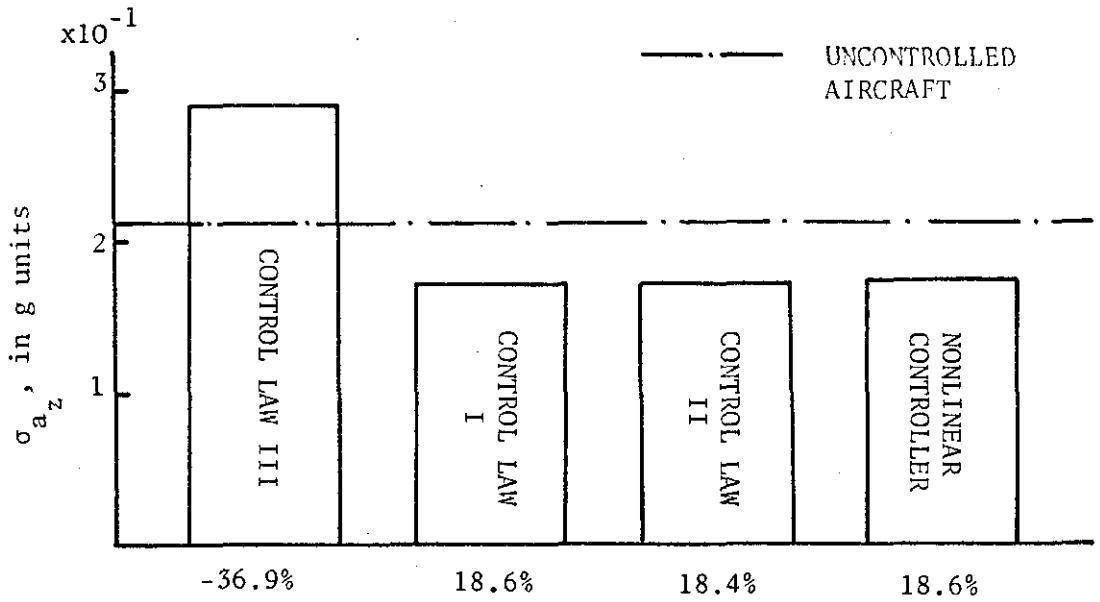


For the configuration of elevator acting alone the effect of the non-linear function was also evaluated from the number of exceedances of specific levels of acceleration. Table 6.2 shows the percentage of exceedance of representative acceleration levels achieved by CONTROL LAW I and non-linear controller.

TABLE 6.2

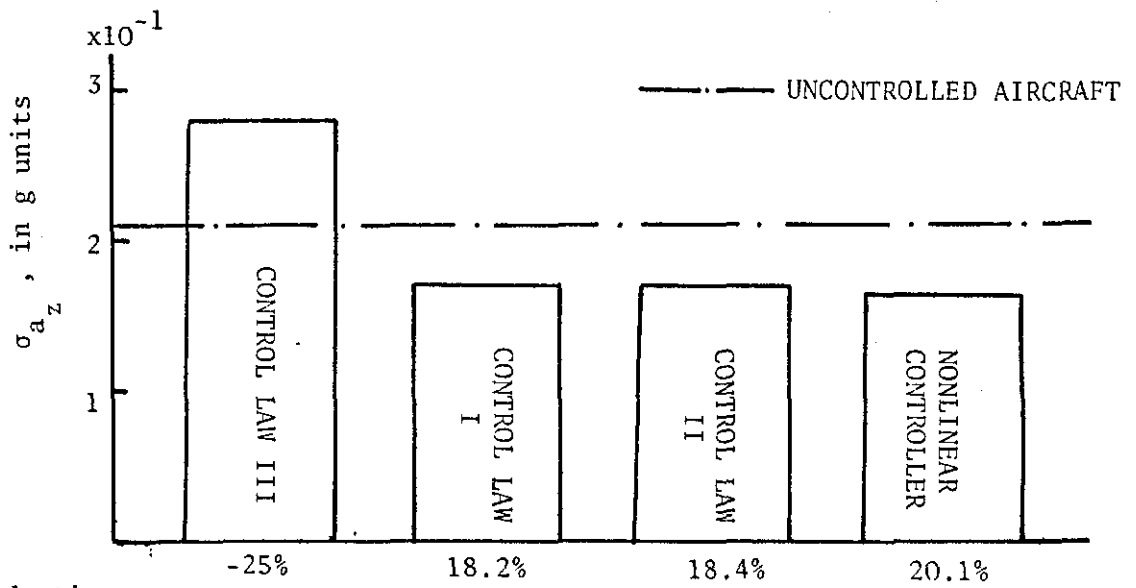
σ_{a_z} in g units	% of Exceedance	
	CONTROL LAW I	NON-LINEAR CONTROLLER
0.005	97.5%	98.3%
0.05	75.8%	70.8%
0.15	38.3%	35.8%

From Table 6.2 it can be deduced that the use of the non-linear function increase the number of exceedances of low values of acceleration and reduced the number of exceedances of higher acceleration levels. However from inspection it appears to have eliminated some of the high frequency components reducing the higher acceleration levels. Figure 6.37 summarizes the results obtained for the three control laws and the non-linear controller for the elevator on its own and elevator spoiler canards configurations.



% reduction of σ_{a_z}

(a) Elevator-Spoilers-H.Canards Control Surface Configuration for Longitudinal Ride Control



% reduction of σ_{a_z}

(b) Elevator Only Configuration for Longitudinal Ride Control

FIGURE 6.37: Effectiveness of the CONTROL LAWS I,II and III and of the Nonlinear Controllers for Longitudinal Ride Control

It can be seen by comparison of the results obtained for the two different configurations that very similar ride performance is achieved in both cases. However, consideration of the configuration of elevator and spoilers acting together could improve even further the results if the weighting of the control and state vectors is appropriately chosen.

6.3.2 Lateral Motion Analysis

The lateral dynamic response of the optimally controlled aircraft in turbulent flight was studied for the same control laws which were employed in the deterministic analysis. All the control surface configurations were investigated for the three optimal feedback control laws which were discussed earlier. The aircraft lateral dynamic responses due to turbulence were evaluated for 30s digitally simulated flights. The effectiveness of each control law was judged according to the resulting r.m.s. values of lateral acceleration and deflection angles activity of the considered control surfaces. CONTROL LAW I was also used as a basis in the analysis. CONTROL LAW II was used for comparison as in the longitudinal motion analysis. CONTROL LAW III was employed for all the configurations to show the ride quality effectiveness of the control law derived for handling qualities improvement, when turbulence is encountered.

Figure 6.38 illustrates the dynamic response of the aircraft in turbulence when CONTROL LAW I and all the lateral control surfaces were employed. From this figure it can be seen that CONTROL LAW I acts favourably by reducing the r.m.s. values of the motion variables p, β and a_y .

The results obtained with the same control law for all the possible combinations of the control surfaces are summarized in Figure 6.39. This figure shows that the maximum reduction of lateral acceleration (40%) was achieved when all the three control surfaces (rudder-aileron-v.canard) were used simultaneously. A comparable reduction of r.m.s. acceleration was achieved when ailerons and rudder were acting together (38%). However, it is important to emphasize the 'low' weighting of the canard which was derived from WAYMX. It is evident from Figure 6.39(b) that the v.canard has been

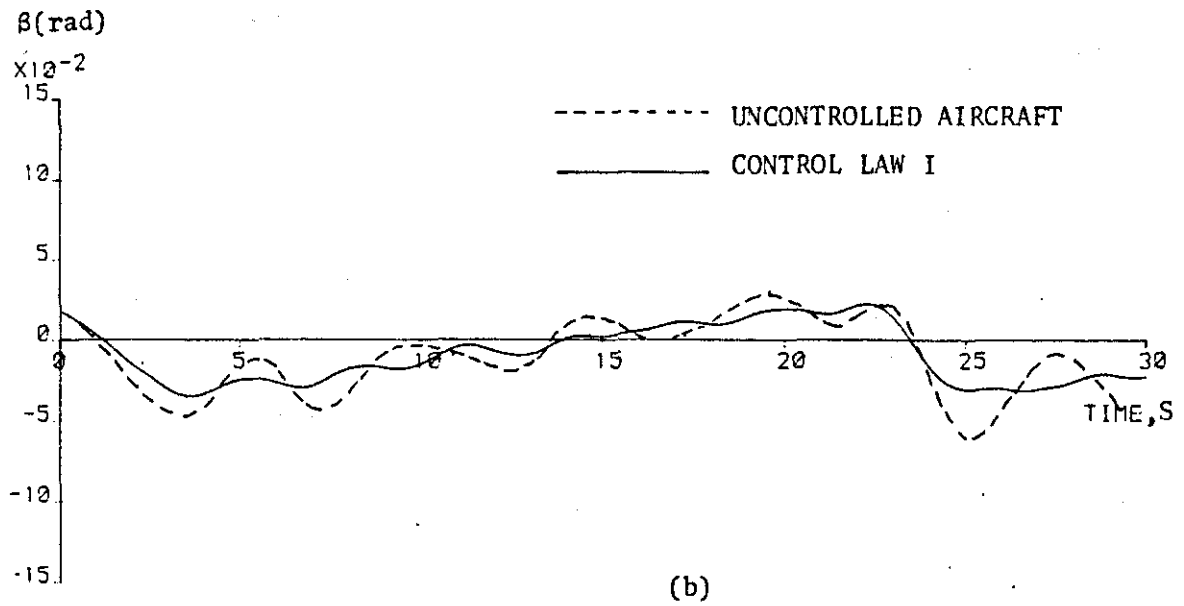
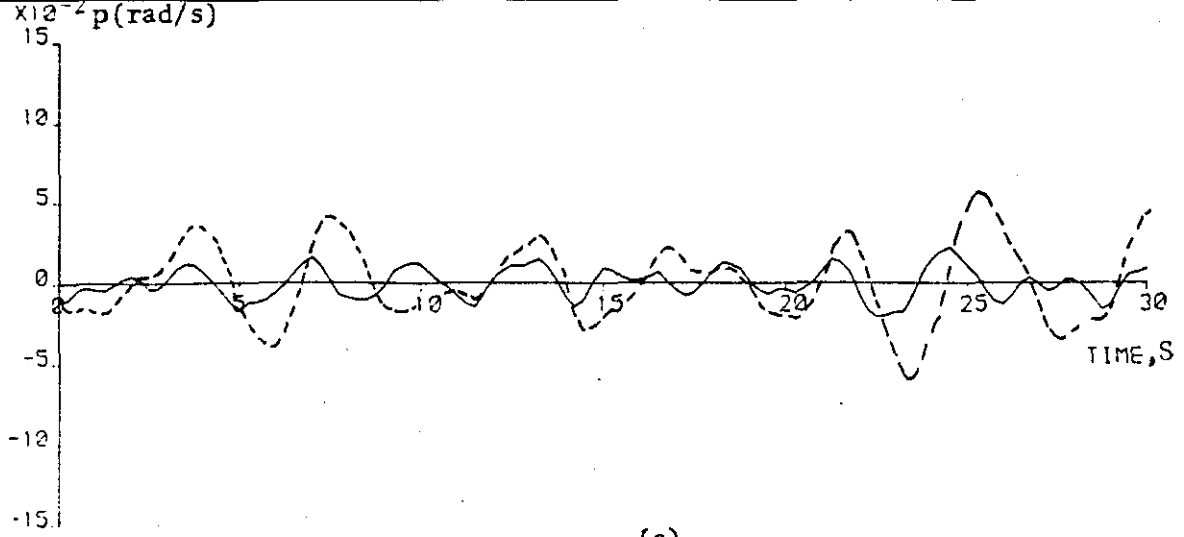
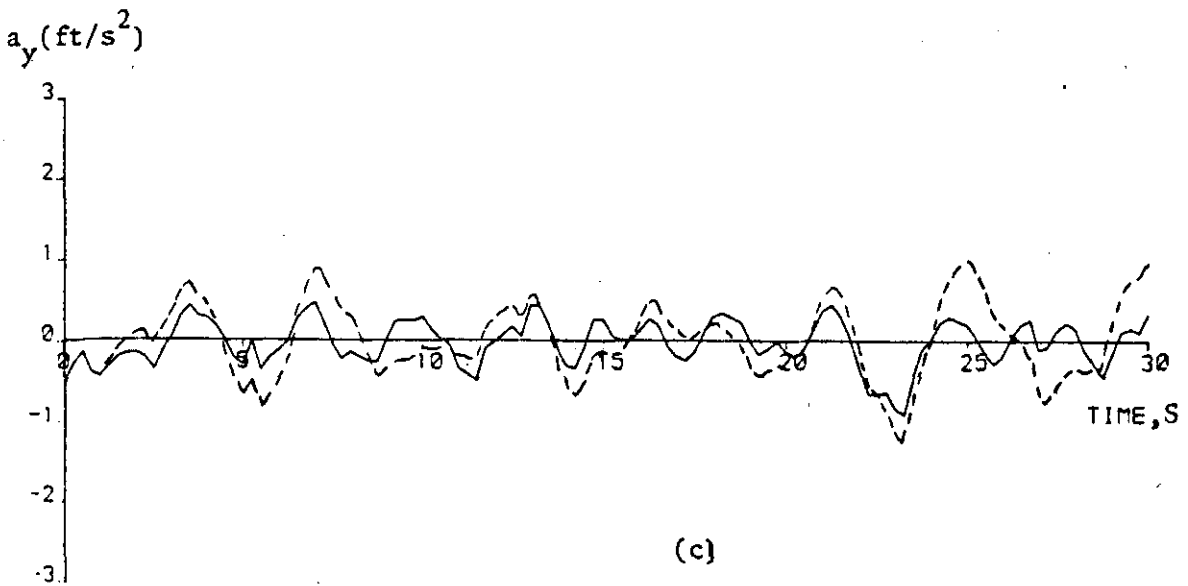


FIGURE 6.38: Effectiveness of CONTROL LAW I for Lateral Motion



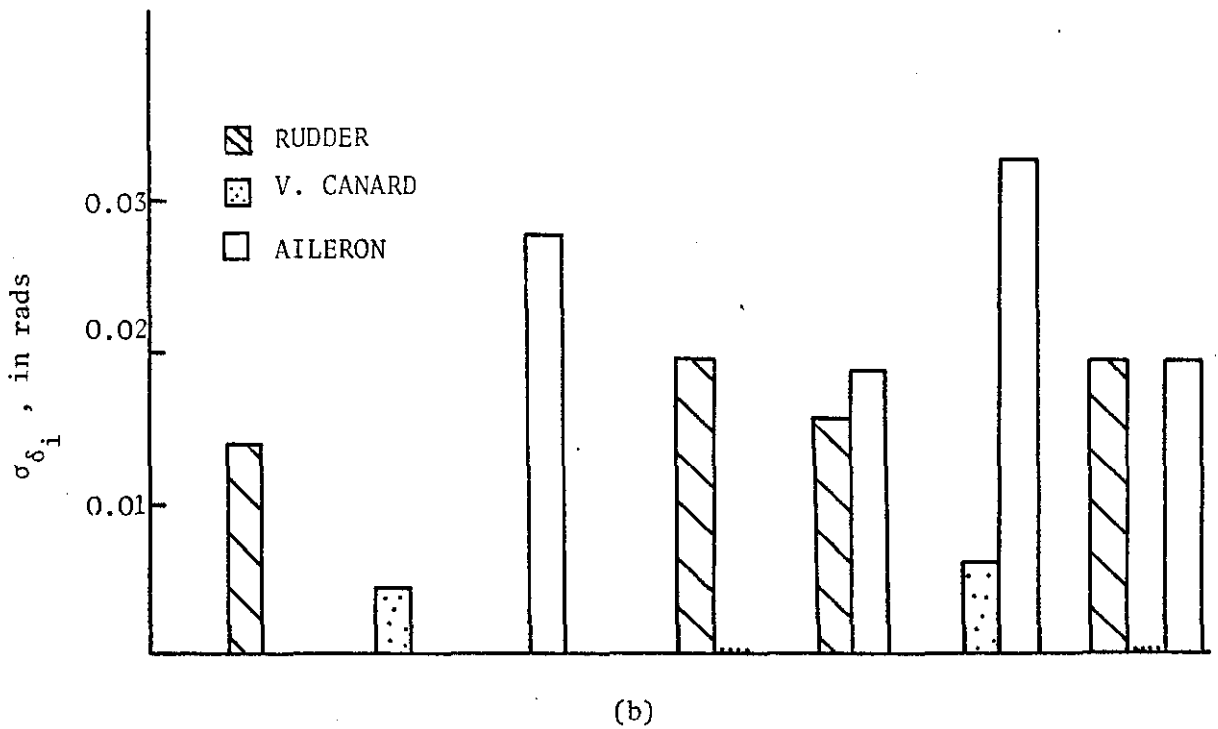
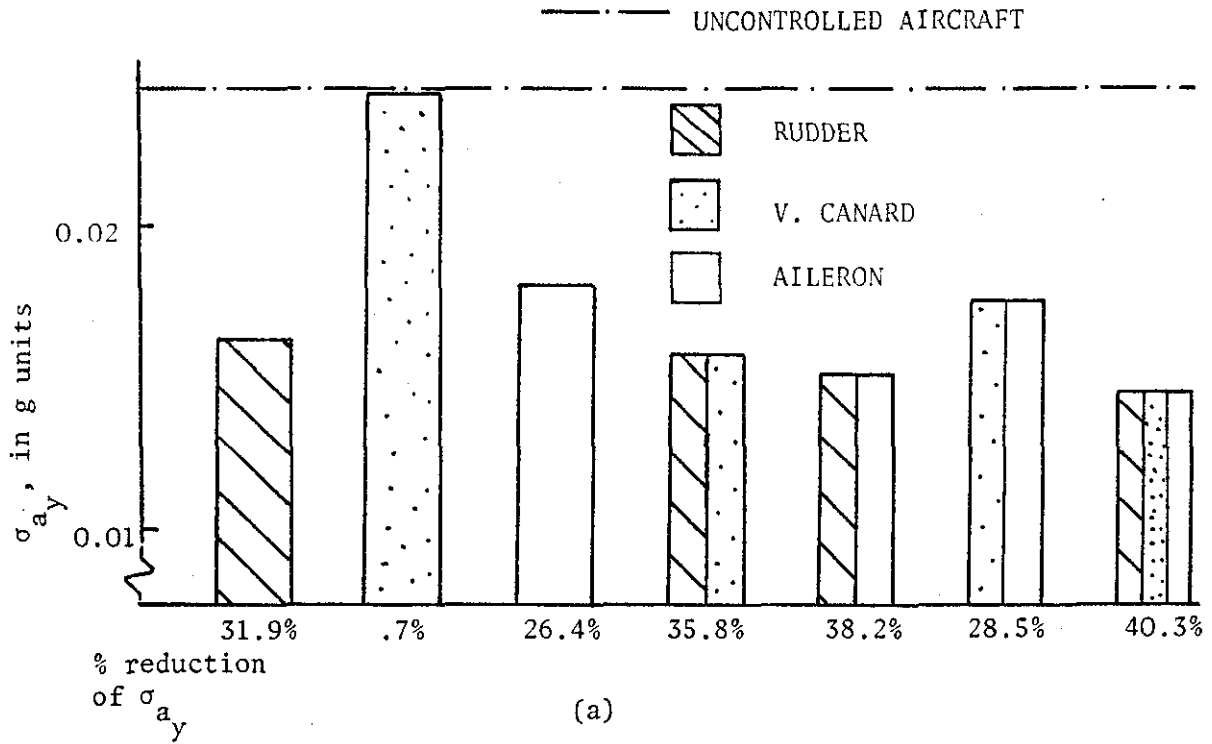


FIGURE 6.39: Effectiveness of CONTROL LAW I for Lateral Ride Control

used very little in all configurations and therefore its abilities could be underestimated from these results. In order to illustrate the effectiveness of v.canard in a configuration employing rudder and ailerons different empirical G matrices were investigated.

Figure 6.40 shows the rate of activity required from the control laws for each control surface when all were employed simultaneously. It may be seen that although the rudder and ailerons were activated by the control law equally the vertical canard was penalized. The use of WAYMX to derive the weighting elements of the control vector gave similar results for the vertical canard as for the horizontal canards used in the longitudinal motion. Although with this weighting this configuration provided the higher r.m.s. reduction of acceleration it was decided to investigate other weighting matrices giving more authority to the vertical canard. From the brief investigation which was carried out, it was determined that the weighting of the G matrix obtained from WAYMX was providing the best results. Hence, any further improvements of the ride performance of the aircraft should be achieved by appropriate manipulation of the Q and G matrices simultaneously.

For the configuration employing all the lateral control surfaces CONTROL LAW II was investigated for stochastic inputs. The weighting matrix Q was chosen by a trial and error method while G was derived from WAYMX ($G = \text{diag}\{0.5, 2.0, 0.08\}$). Figure 6.41 illustrates the dynamic response which resulted when CONTROL LAW II was employed. It can be seen that significant reduction of acceleration (35%) was achieved. However, the roll rate has been increased but by insignificant amount. The knowledge gained by manipulation of Q matrix was valuable. When Q was chosen to be equal to 1.0 it resulted in the degradation of the performance of the uncontrolled

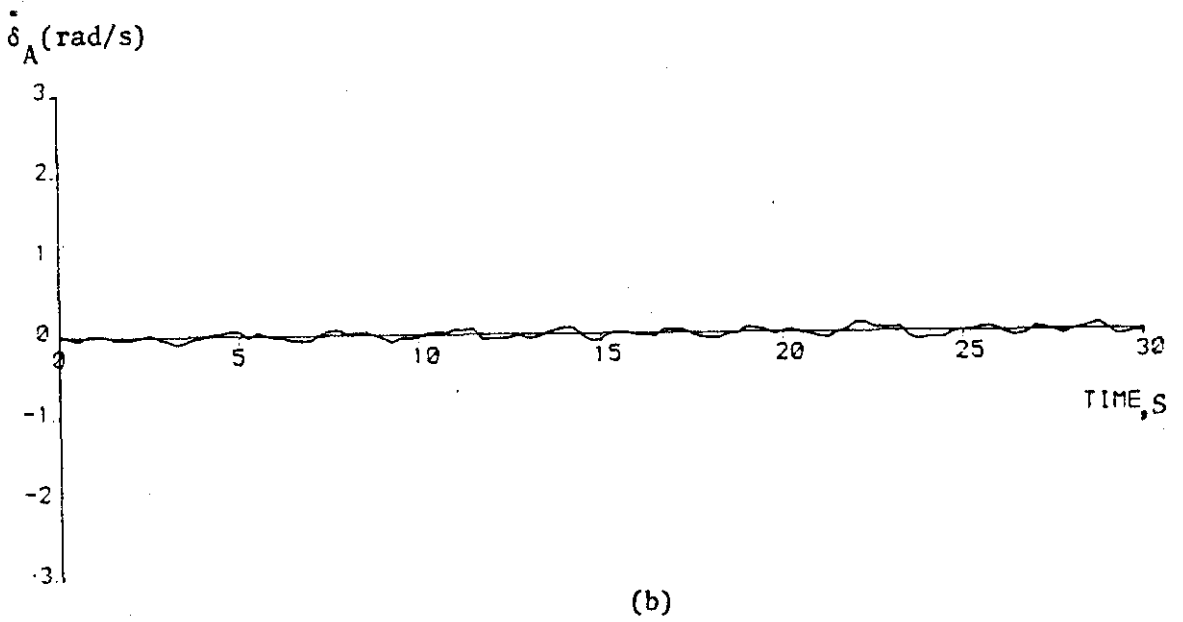
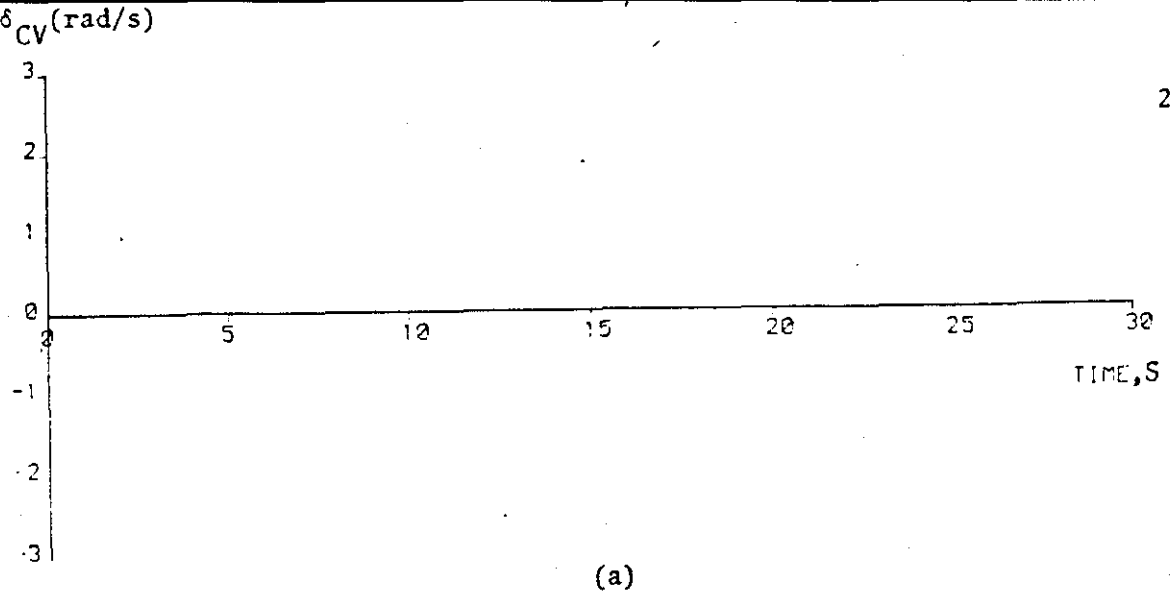
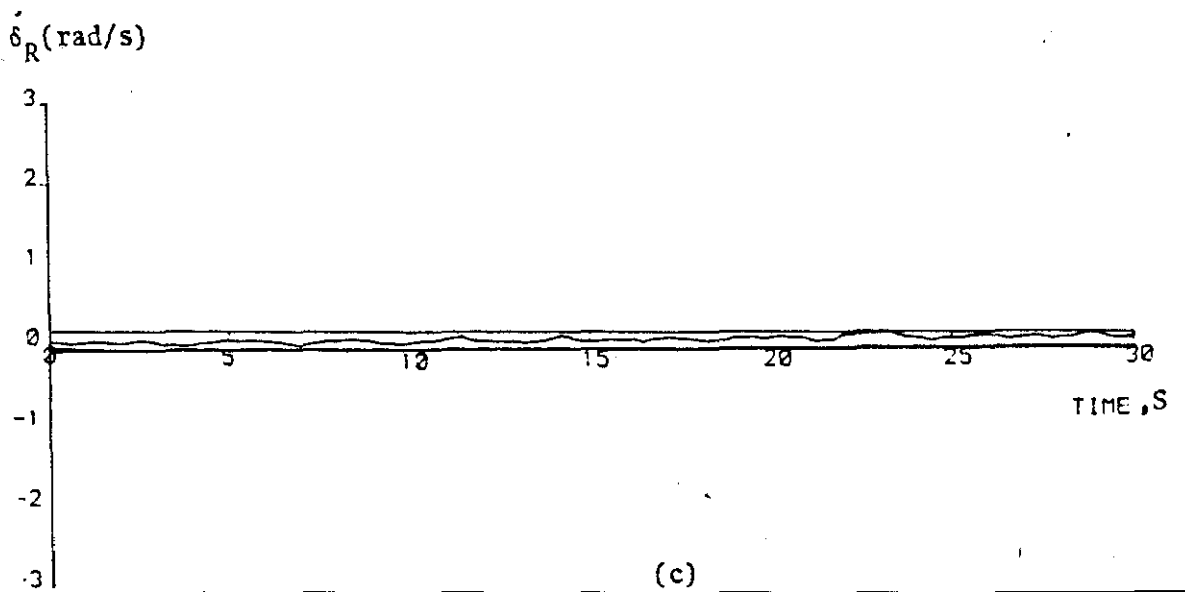


FIGURE 6.40: Deflection Angle Rates Required from CONTROL LAW I



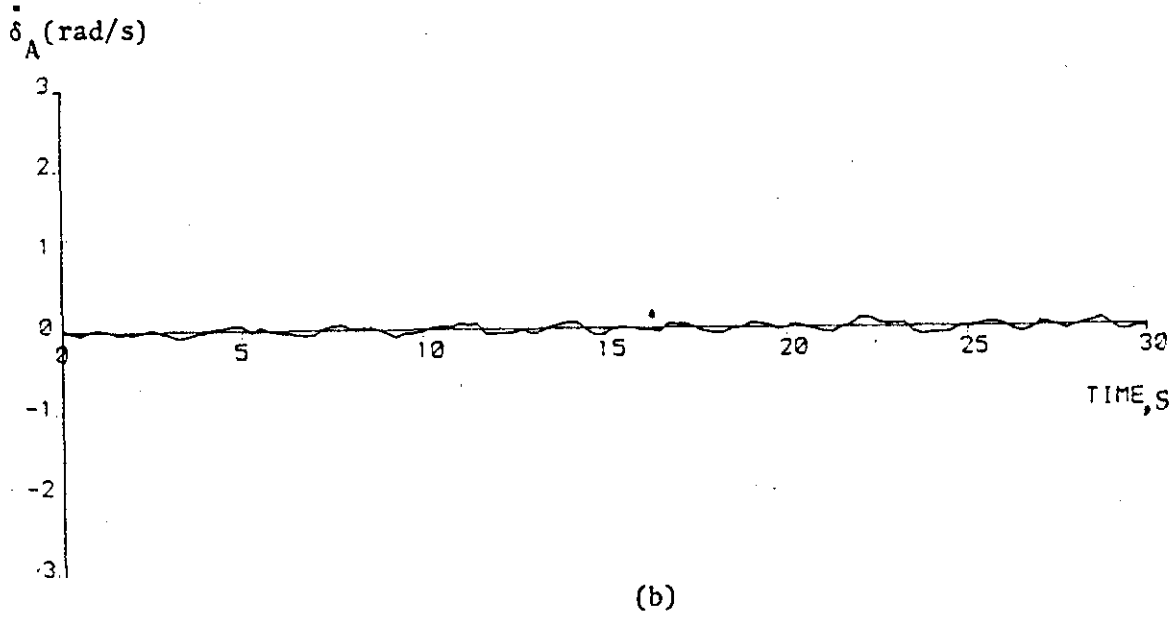
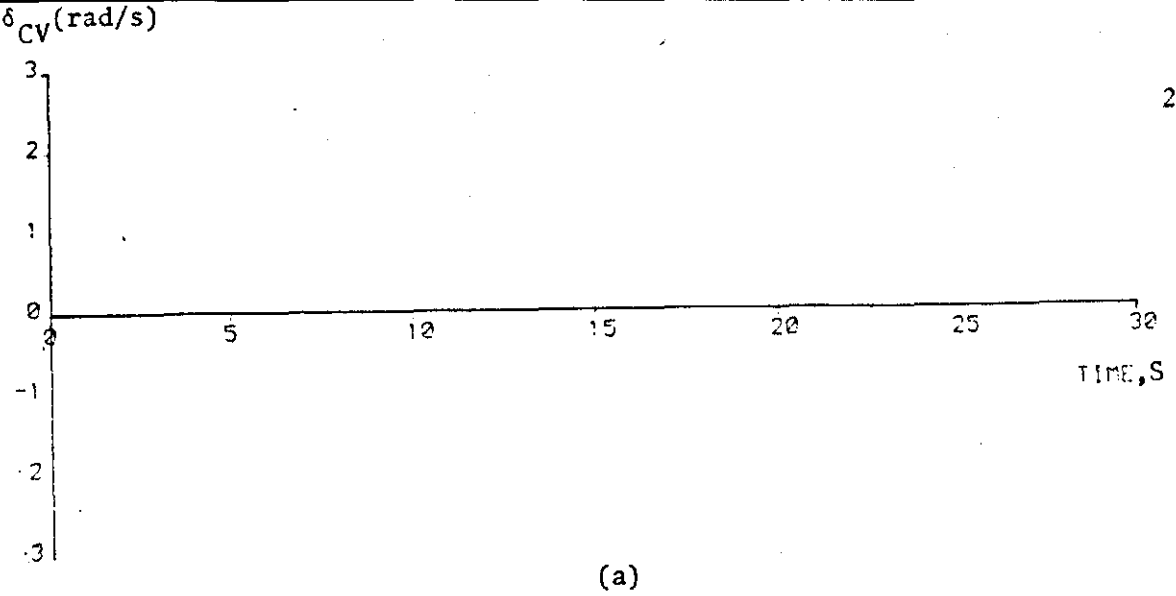
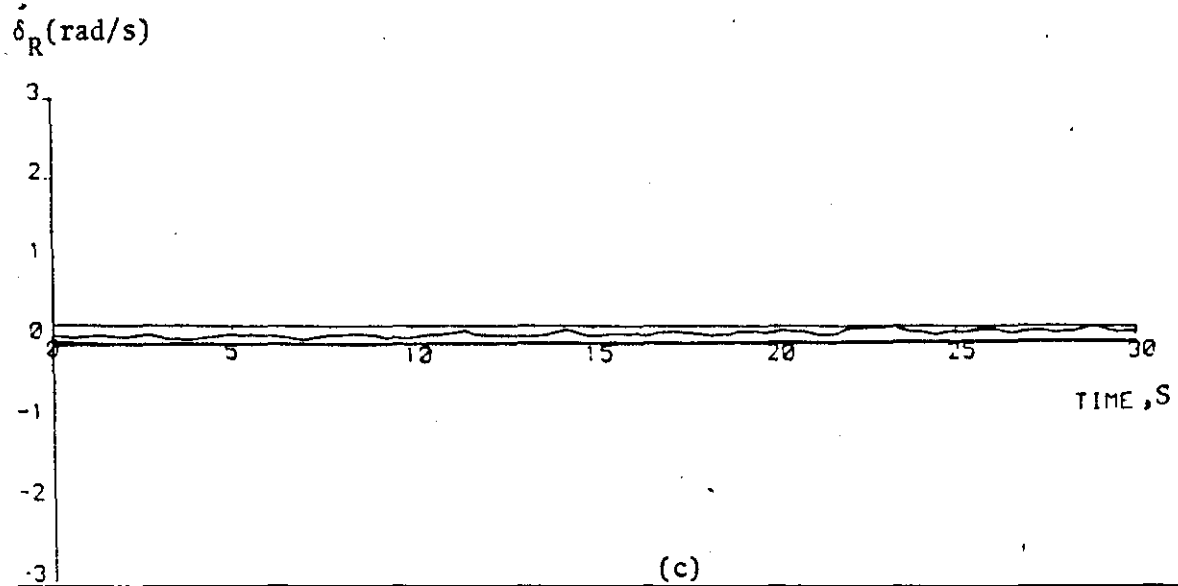


FIGURE 6.40: Deflection Angle Rates Required from CONTROL LAW I



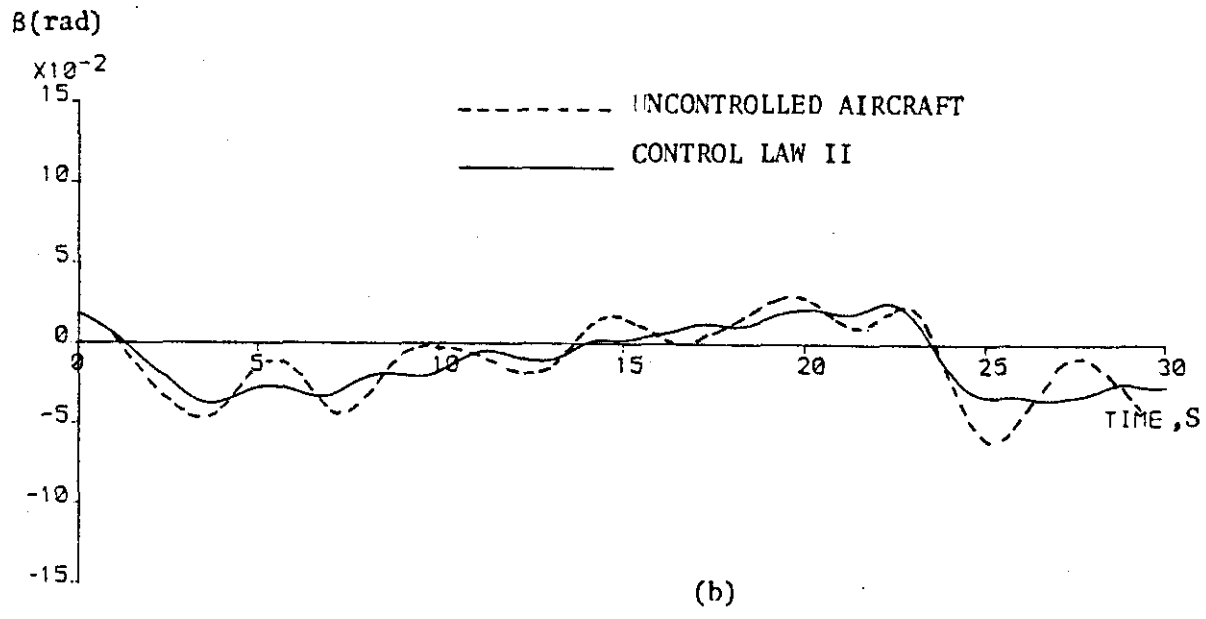
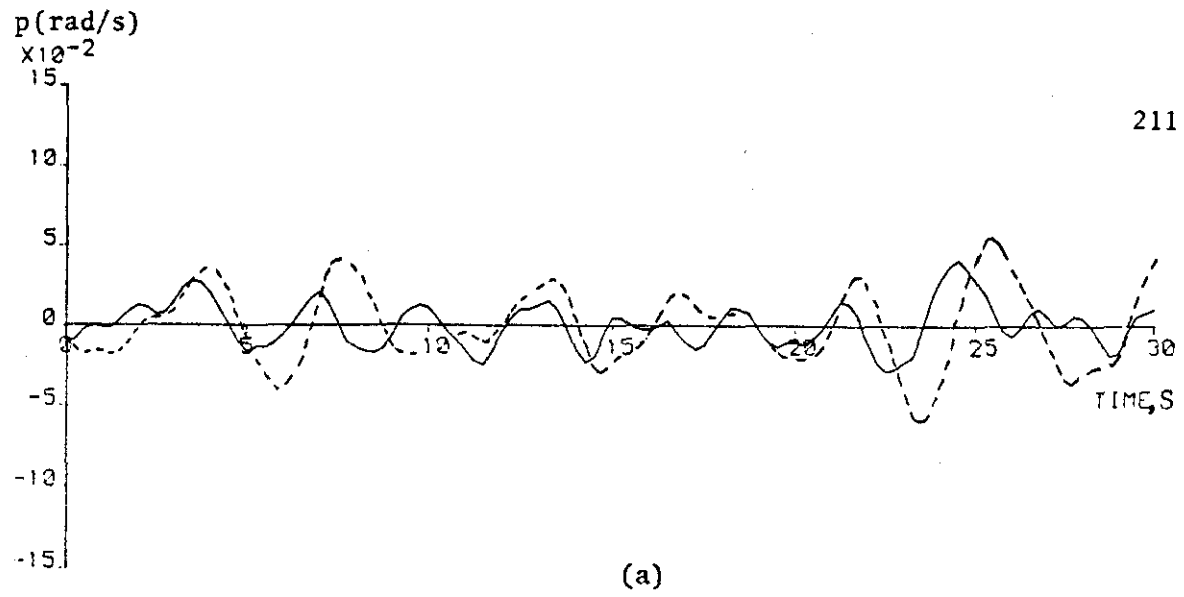
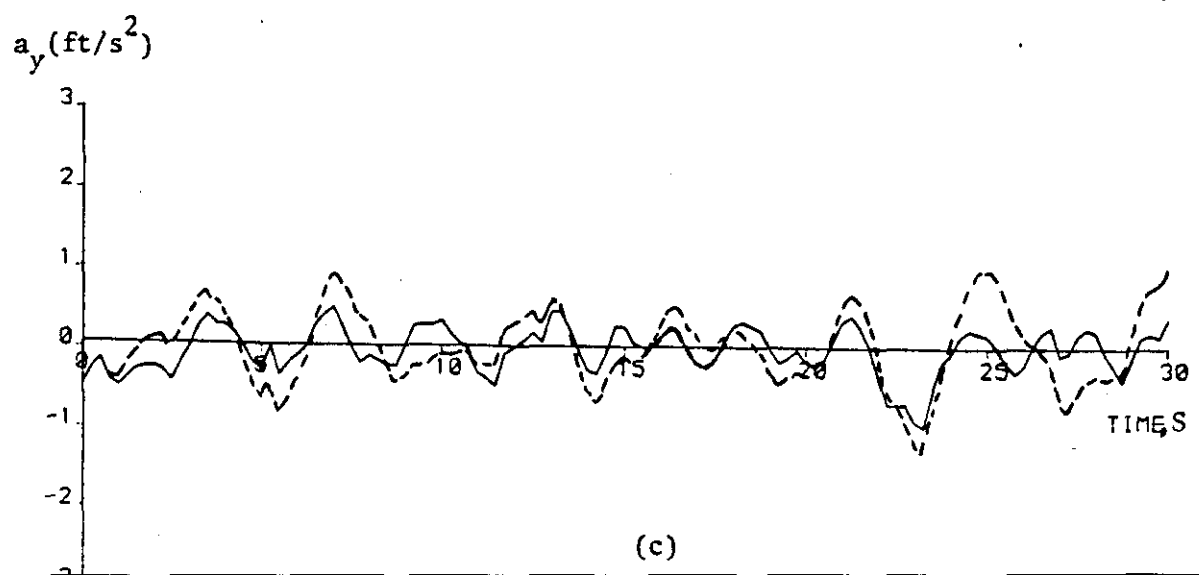


FIGURE 6.41: Effectiveness of CONTROL LAW II for Lateral Motion



aircraft by a 30% increase of the r.m.s. acceleration level. This choice of Q matrix resulted in a relatively heavy weighting of the control surfaces which in effect affected undesirably the dynamic response of the aircraft. On the contrary the final choice of Q as being equal to 0.001 resulted in the dynamic performance shown in Figure 6.42. As for the deterministic input analysis the use of CONTROL LAW II resulted in a slow gradual increase of the heading angle, ϕ . For a 30s simulation the heading angle increase by 6° . This slow increase of the heading angle could be controlled by a control system or the pilot of the aircraft as soon as the deflection angle saturation limits were not exceeded allowing the control surfaces to be used for other tasks.

The control law derived from model matching theory (CONTROL LAW III) for lateral motion achieved significant reductions of r.m.s. accelerations. Figure 6.42 illustrates the lateral dynamic responses of the aircraft obtained with this control law when all the lateral control surfaces were employed. The use of this control law achieves significant reduction in sideslip which in turn reduces the acceleration effectively. For this particular configuration a reduction of 45% of r.m.s. acceleration has been achieved. The instability due to ailerons alone configuration was also detected in the turbulent flight analysis. Figure 6.43 summarizes the results obtained by CONTROL LAW III for all possible configurations. It may be inferred from Figure 6.43(a) that when aileron was used combined with the other control surfaces resulted the best reduction of r.m.s. acceleration (45%). Although CONTROL LAW III achieved for particular configurations the best results, as compared to CONTROL LAWS I and II, in terms of ride quality performance it does not guarantee stability in case of failure of operation of rudder and vertical canard.

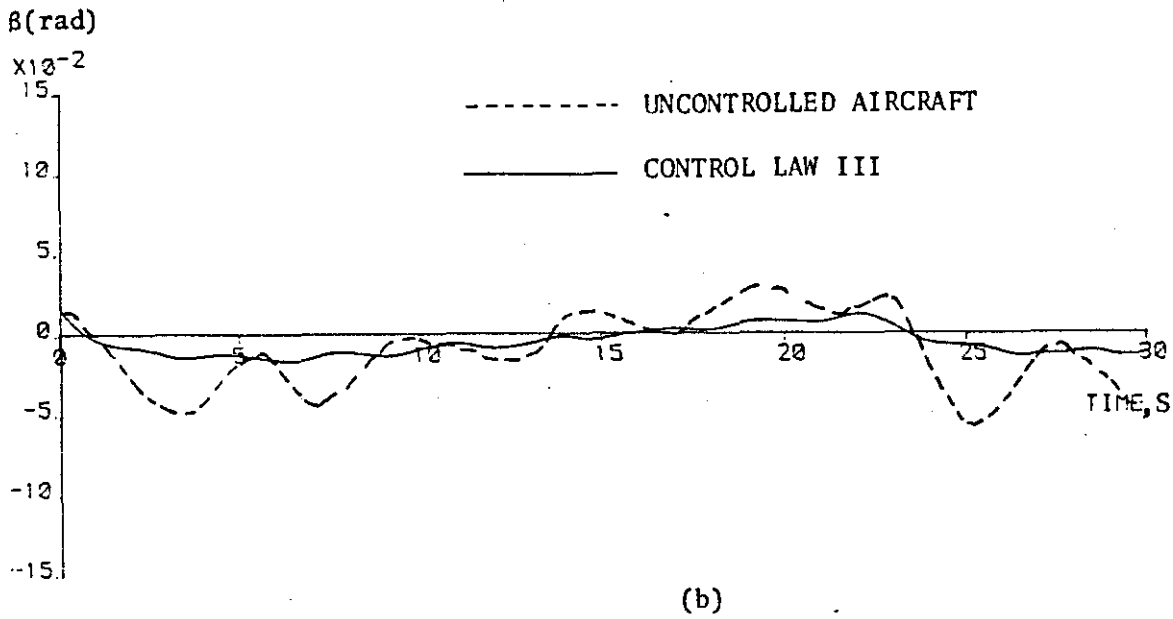
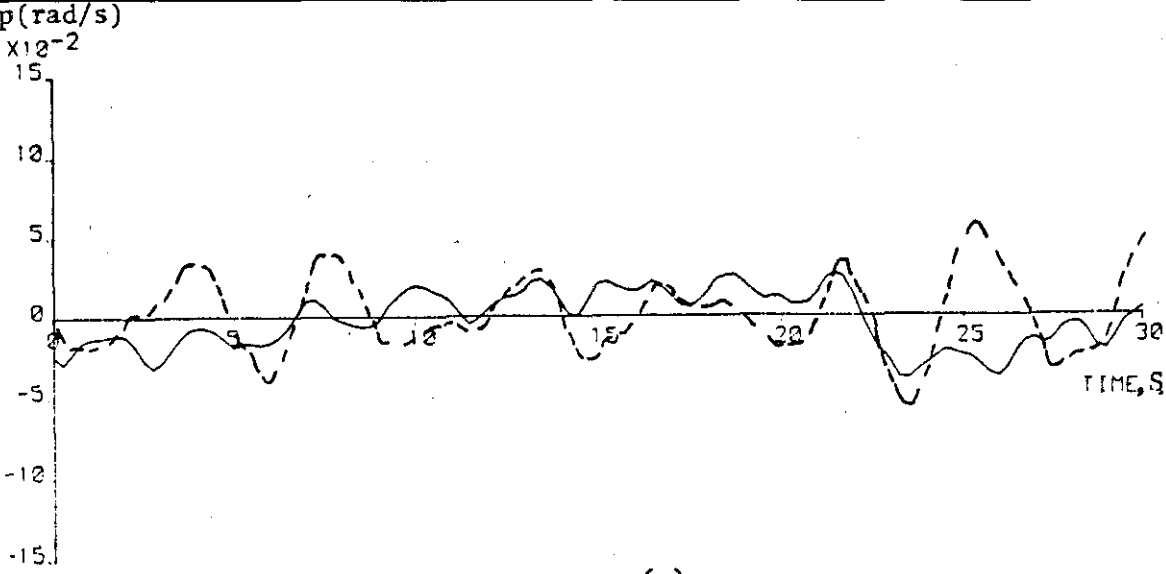
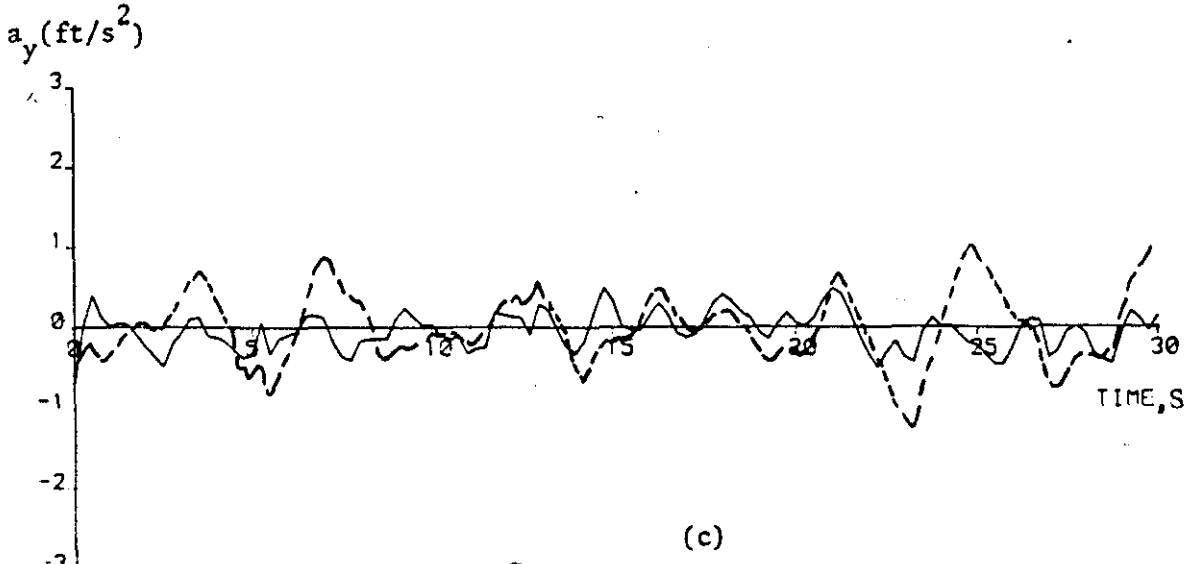
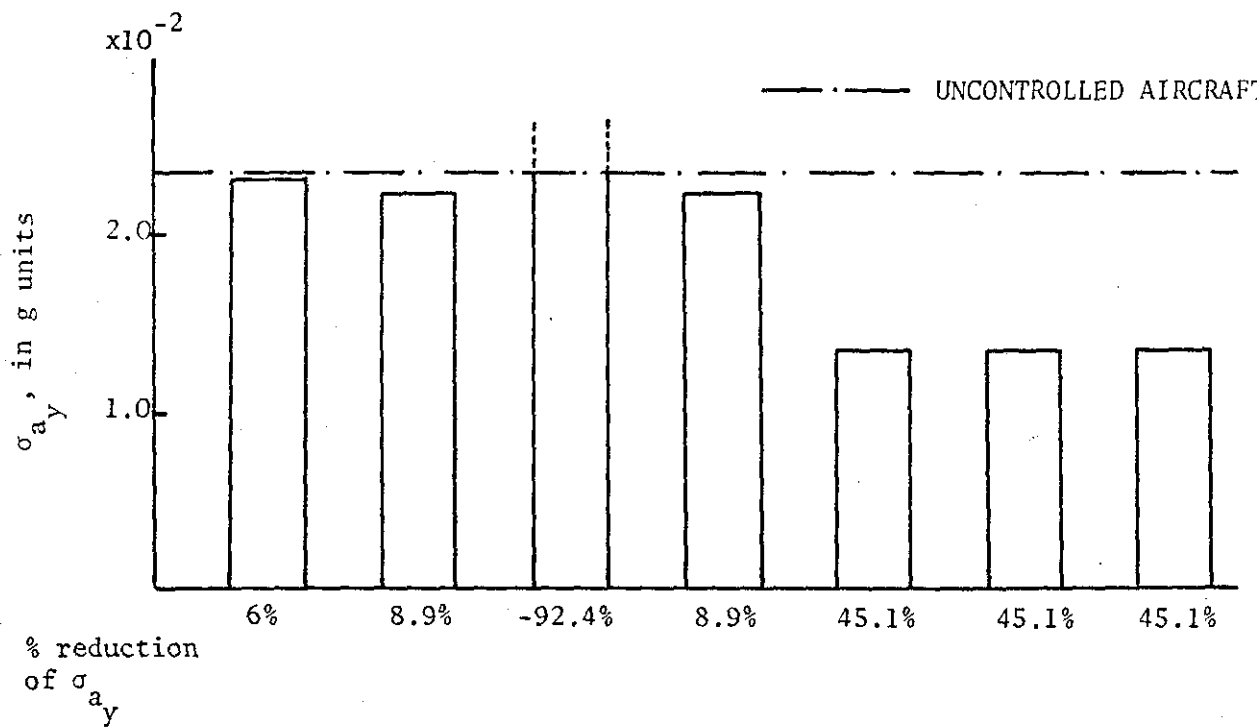


FIGURE 6.42: Effectiveness of CONTROL LAW III for Lateral Motion





OPTION	1	2	3	4	5	6	7
δ_R	0.0816			0.065	0.069		0.068
δ_C		0.632		.0068			0.0071
δ_A			0.073		0.022		0.022

FIGURE 6.43: Effectiveness of CONTROL LAW III for Lateral Motion

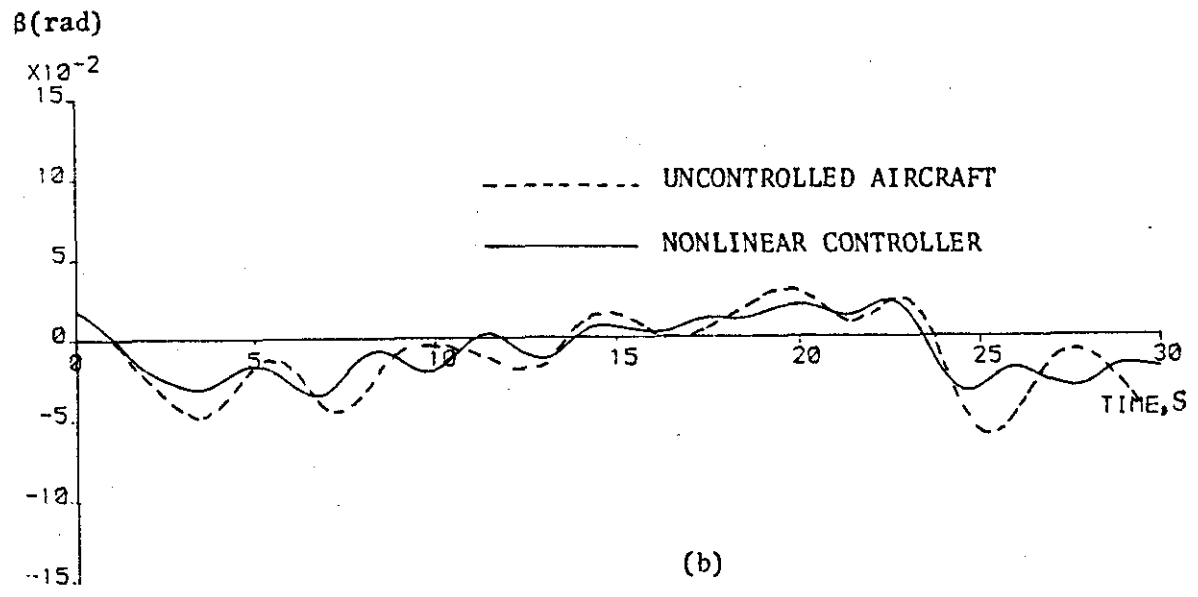
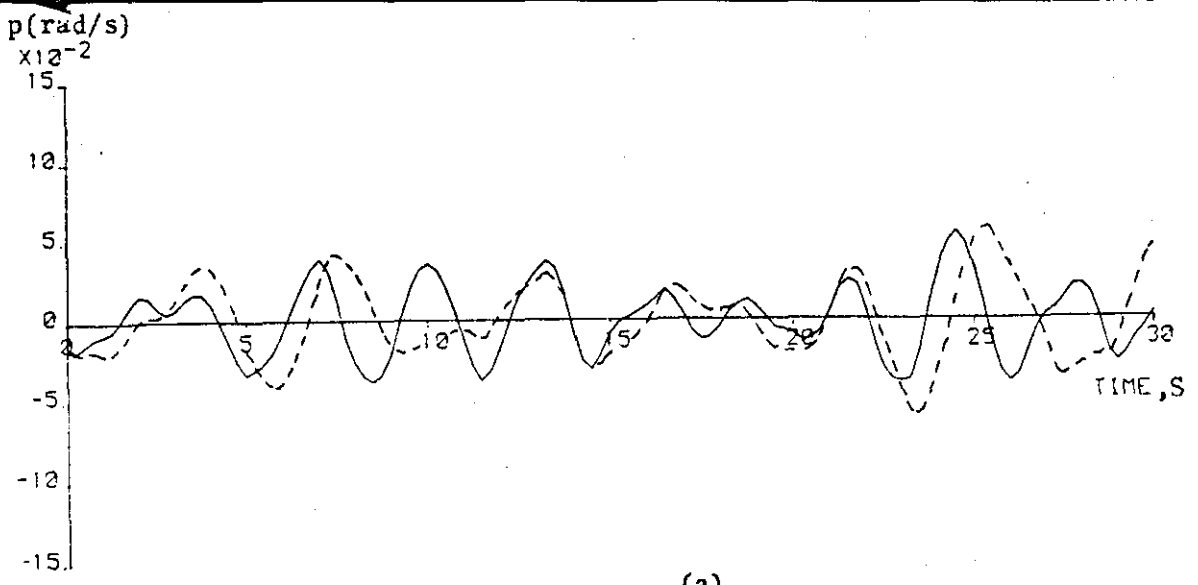
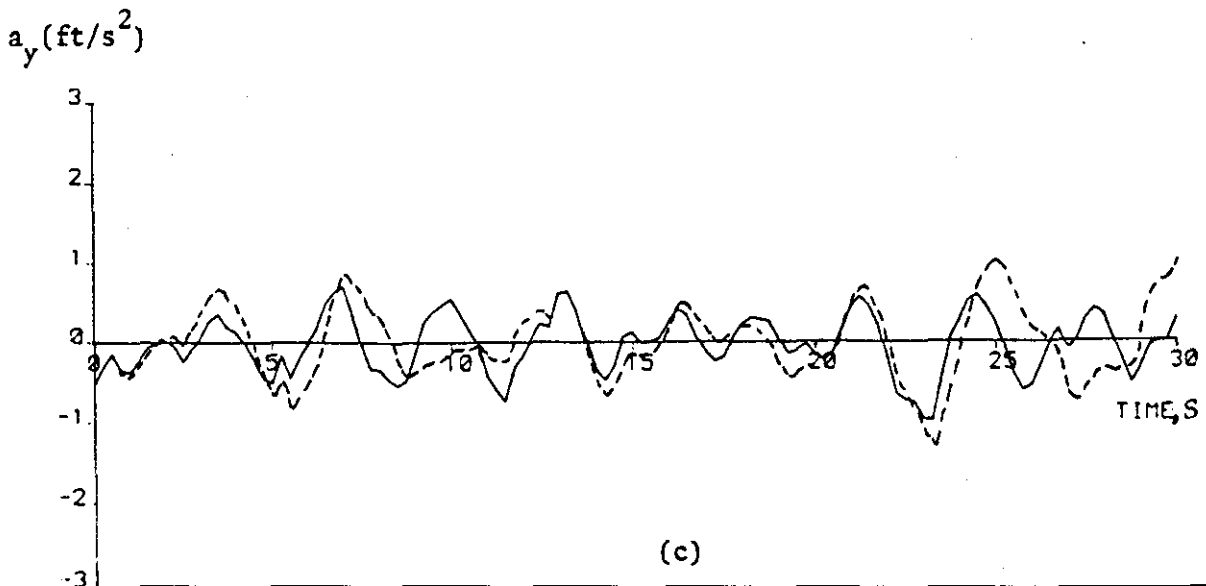


FIGURE 6.44: Effectiveness of the Nonlinear Controller on Lateral Motion TN=400



The nonlinear controller described in the section on longitudinal motion with atmospheric turbulence was tested for the lateral motion. Figure 6.44 illustrates the dynamic responses achieved when τ_f was chosen to be 400. It can be seen from this figure that a slight improvement of the ride performance resulted (30%). The use of the nonlinear controller degraded the performance obtained by the CONTROL LAW I acting on its own. Thus the nonlinear controller did not provide any improvement to the lateral ride quality performance of the aircraft. However, this result would be easily predicted since lateral motion is not characterised by the high frequency components which were evident in the longitudinal motion.

The results achieved by CONTROL LAWS I, II and III are summarized in Figure 6.45. It can be seen that maximum reduction of acceleration has been achieved by CONTROL LAW III (45%). By comparison of the r.m.s. values of the deflection angles it may be inferred that if similar to CONTROL LAW III activity of the control surfaces would be required from CONTROL LAW I or II then even better results could result if appropriate choice of Q matrix could be made.

CHAPTER 7

DESIGN METHOD FOR A RIDE QUALITY CONTROL SYSTEM

(R.C.S.)

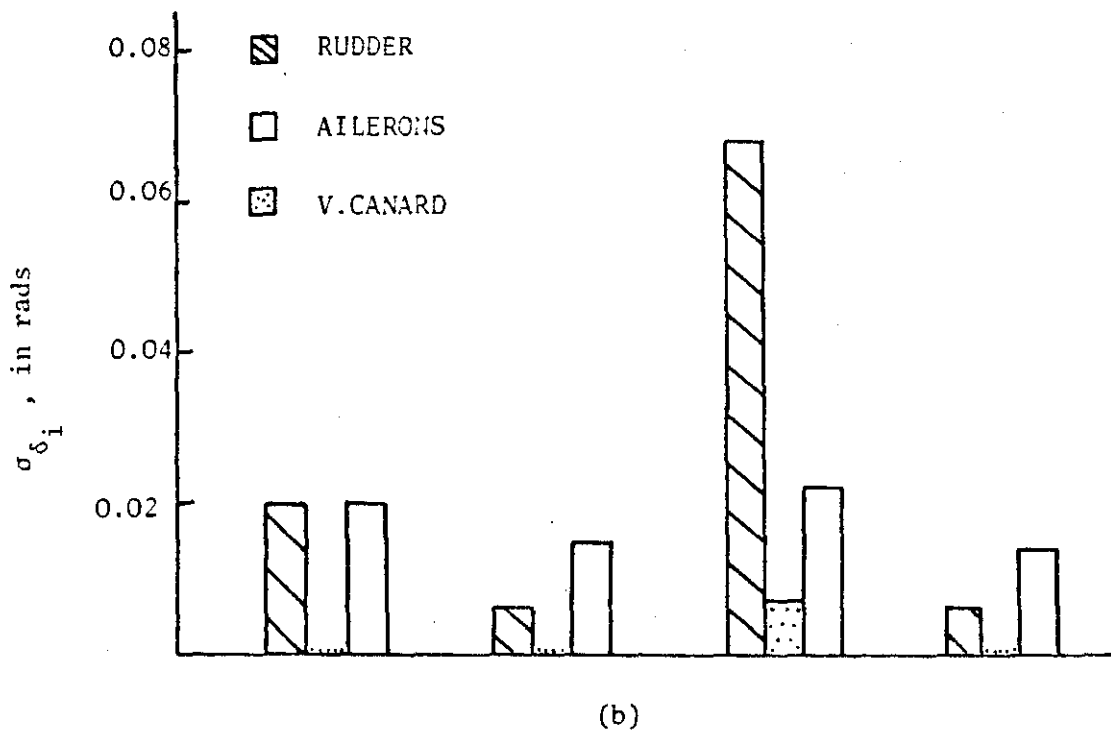
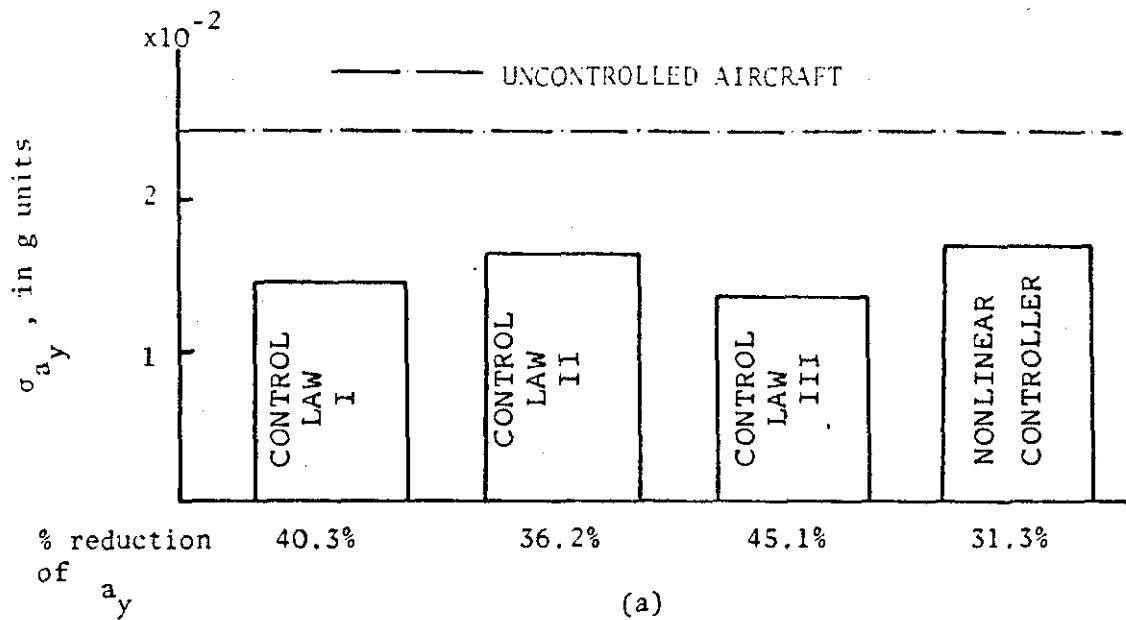


FIGURE 6.45: Effectiveness of CONTROL LAWS I,II, and III and Nonlinear Controller for Lateral Motion when all Lateral Motion Controls are Involved

7.1 INTRODUCTION

It is evident from the work reported in Chapter 6, which concerned a detailed study of the dynamic characteristics of the subject aircraft, that a considerable amount of detailed study is required before the structure and parameters of any R.C.S. is finally chosen.

In this chapter are presented a congruent review of the important points to be found in Chapter 6, for the implementation of modern control theories in conjunction with the use of Direct Lift Control (D.L.C.) and Direct Side Force Control (D.S.F.C.) on an aircraft. The conclusions resulting from the work reported in Chapter 6 could be used as a basis for the design of a R.C.S. for future aircraft which would be capable of using the A.C.T. concept as a means of controlling ride comfort. The end of this chapter is devoted to the design procedures which would be required in order to furnish a design method, similar to that which was considered in this research for a R.C.S.

As a result of the experience gained from this research some useful recommendations for anyone who adopts the same design concepts for a R.C.S. for an aircraft are also given. Finally the role of simulation in the investigation of A.C.T. and C.C.V. concepts is discussed.

7.2 RIDE QUALITY BENEFITS FROM THE USE OF OPTIMAL R.C.S. ON THE MODIFIED JETSTAR (CCV)

As a means of designing a R.C.S. for an aircraft the active control (CCV) approach was found to be beneficial in terms of the reduction of normal and lateral r.m.s. acceleration levels achieved[†]. The use of the A.C.T. concept in this research made it possible to employ modern control theories for a multivariable treatment of the aircraft dynamics. Both linear optimal control and model-matching theories were employed to derive feedback control laws which drove the conventional and auxiliary control surfaces of the rigid body Jetstar CCV.

The consideration of the optimal feedback control laws derived from theory (CONTROL LAWS I and II) for the command input situation resulted in a reduction of the r.m.s. levels of normal and lateral accelerations (σ_{a_z} and σ_{a_y} respectively) of approximately 80%. The same control laws only achieved reductions of the order of 20% and 40% for σ_{a_z} and σ_{a_y} respectively, when atmospheric turbulence was encountered.

The feedback control laws for handling qualities which were derived from model matching theory (CONTROL LAWS III), were considered for the same command input conditions as CONTROL LAWS I and II. The maximum reduction of r.m.s. acceleration achieved by CONTROL LAWS III was of the order of 50% and 60% for σ_{a_z} and σ_{a_y} respectively. The same control laws when tested in turbulent flight resulted in a reduction of σ_{a_y} by 45%. However, CONTROL LAW III failed to achieve any reduction of normal r.m.s. acceleration in turbulent conditions. On the contrary it degraded the ride quality performance of the aircraft when compared to its uncontrolled situation. Table 7.1 summarizes these results.

[†] Reduction of r.m.s. acceleration levels refers to the reduction achieved by comparison to the r.m.s. acceleration levels of the uncontrolled aircraft.

TABLE 7.1

% of $\sigma_{a_z}, \sigma_{a_y}$ reduction	Deterministic Inputs		Stochastic Inputs	
	% of σ_{a_z} reduction	% of σ_{a_y} reduction	% of σ_{a_z} reduction	% of σ_{a_y} reduction
CONTROL LAW I	77%	65%	18.6%	40%
CONTROL LAW II	79%	77%	18.4%	36%
CONTROL LAW III	60%	48%	FAILED	45%

The longitudinal handling qualities of the uncontrolled aircraft were not improved when CONTROL LAWS I and II were employed (see Table 6.2), whereas the implementation of CONTROL LAW III resulted in improved longitudinal handling qualities for the aircraft. However, when CONTROL LAWS I, II and III for lateral motion were investigated in terms of the resulting handling qualities it was found that they each improved the handling qualities of the uncontrolled aircraft (see Table 6.3).

The conventional and auxiliary aerodynamic control surfaces which were used in the ride control schemes for longitudinal and lateral ride quality control were investigated for all possible combinations between them and for all the control laws.

The ability of each control surface configuration to affect the motion variables of the aircraft, and particularly the r.m.s. acceleration levels, was investigated for the uncontrolled and the optimally controlled aircraft.

As a result of this investigation it was determined that for longitudinal ride control the elevator was the most important control surface. However, it was found that consideration of the elevator only as a configuration for ride control would require very high levels of rate activity from the actuating elements associated with it and so the implementation of another control surface would be undoubtedly required. The auxiliary control surface spoilers and horizontal canards were investigated further for this purpose. It was found then, that the consideration of spoilers in conjunction with elevator was beneficial in terms of relieving the excessive rate activity demanded for the elevator. It was pointed out in the analysis of the results that for different selections of Q and G matrices this configuration would be normally expected to provide the best results. This assessment is consistent with the results obtained from Jacobson and Lapins [1977] which concluded an effective R.C.S. for Jetstar longitudinal motion employing the elevator acting in conjunction with flaps. From the investigation on the effectiveness of horizontal canards it was found that they did not necessarily improve the ride performance for this particular aircraft and in the flying conditions considered. The horizontal canards could be probably found to be more effective at higher speeds and altitudes where spoiler use would be considered to be inappropriate.

From the lateral motion analysis it was determined that the conventional control surfaces, rudder and aileron, were the major contributors for minimizing lateral r.m.s. accelerations. However the consideration of the vertical canard acting in conjunction with the two conventional control surfaces resulted in the best lateral ride quality performance. A more careful manipulation of the Q and G matrices could be

expected to improve even further the results achieved with this configuration.

A consideration of the incorporation of actuator dynamics of the aerodynamic control surfaces in the system model degraded slightly the ride performance of the aircraft. The actuators were described by first order differential equations and had an insignificant effect on the dynamic response of the aircraft. Second-order actuators (as for elevator and rudder) had a more noticeable effect upon the dynamic response of the aircraft. A natural consequence of considering actuator dynamics is the consideration of their physical limitations. The nonlinearities which resulted from the physical constraints of the actuators affected only the longitudinal motion when elevator was involved. Effective use of the spoilers removed the consequences of these nonlinear effects due to actuator limitations.

From the investigation which was carried out on the r.m.s. deflection angles required from CONTROL LAWS I and II and all the control surface configurations employed, it was indicated that the operation of the controls remained well within their constraint limits. This feature ensured that for these control laws the ride quality system would not use all the effectiveness of the control surfaces and hence it would enable the pilot or control system to perform other flight tasks. On the contrary CONTROL LAW III allowed unrealistically excessive use of the longitudinal control surfaces which contributed to the degradation of the dynamic performance of the aircraft. However, although the implementation of CONTROL LAW III for lateral motion resulted in higher r.m.s. levels of deflection angles than when CONTROL LAWS I and III were employed, these

still remained well within the design limits.

The low r.m.s. deflection angle levels of the control surfaces apart from allowing the controls to be used for other purposes is desirable for the life of the mechanical components associated with the actuating elements. This characteristic is a significant factor for determining the implementation of the considered control laws.

From the investigation of the longitudinal dynamic response for turbulence it was determined that the minimization of acceleration was accompanied with high frequency components which introduce discomfort. To test whether these high frequency components could be eliminated a control element, with a non-linear function was inserted in the feedback path of the ride control system. A brief investigation of the non-linear function revealed a slight reduction of r.m.s. acceleration level (2%) for and slight elimination of high frequency components for the configuration employing elevator. The favourable effects of this non-linear function should be further explored in order to achieve better improvements on the dynamic performance of the aircraft.

From comparison of the three control laws employed in terms of the resulting dynamic stability of the aircraft it can be said that CONTROL LAWS I and II guaranteed the stability of the aircraft since Q and G matrices were chosen to be positive semidefinite and positive definite respectively. For CONTROL LAW III on the contrary there does not exist any theoretical way of predetermining the stability of the aircraft other than choosing the model matrix appropriately. In order to ensure stability of the closed-loop system the model matrix should be chosen such that the

resulting closed-loop characteristic equation will have all its roots with negative real parts. The stability considerations of the closed-loop system make the choice of the model matrix more difficult. The particular choice of the model matrix made for lateral motion resulted in dynamic instability of the aircraft when only aileron was used. Although for the other six configurations aircraft was stable any configuration employing the aileron is potentially unstable in the event of a failure of the other controls. This has important ramifications for control system redundancy implementation.

However, the implementation of CONTROL LAW II resulted in secondary effects on the dynamic response of the aircraft for both longitudinal and lateral motion. For the longitudinal motion these effects were the slow gradual increase of the vertical velocity, w , which was accompanied by a gradual decrease of perturbed longitudinal velocity, u . These effects were due to the existence of the phugoid mode which was not completely eliminated from the dynamic response of the aircraft by the R.C.S. A similar effect was observed for the motion variable ϕ of the lateral motion. These secondary effects by no means reduce the favourable ride control effectiveness of CONTROL LAW II since they can be easily controlled by the pilot or by some other automatic flight control system. The activity of the control surfaces due to the R.C.S. would allow adequate control surface authority for the effective elimination of such secondary effects.

From the foregoing discussion it is evident that optimal control and model matching theories can be used to improve the ride comfort of an aircraft provided there exists some means of measuring the

state variables of the aircraft. The state variables which had to be measured in this research were all physically measurable by currently available sensing elements. It is therefore possible to implement the feedback CONTROL LAWS I and II for longitudinal and lateral motion provided that it is ensured that the resulting handling qualities of the aircraft remain acceptable. At the same time CONTROL LAW III should be further investigated before it is considered for use as a R.C.S. law.

7.3 DISCUSSION AND FUTURE RECOMMENDATIONS FOR A R.C.S. DESIGN METHOD

A.C.T. and CCV concepts have been employed in this research to derive, on the assumption of rigid-body motion only, a R.C.S. for the NASA Jetstar aircraft. From the experience gained in the investigation carried out on this particular aircraft it may be concluded that the efficiency of a R.C.S. resides in the following factors:

1. Aerodynamic efficiency of the control surfaces selected for the R.C.S.
- and 2. Effectiveness of the feedback control law.

Apart from these two important factors the R.C.S. implementation depends on the efficiency of the actuating elements, the life constraints, and also on the availability of necessary sensing elements which would be required to measure at any time the aircraft motion variables. However, since the dynamic response required from the actuators for the optimal feedback control laws (I and II) is possible using currently available actuators, and also since the sensing elements needed to measure specific motion variables are normally available on any aircraft the attention in the design method of a R.C.S. was centred on the two factors mentioned above.

7.3.1 Aerodynamic Efficiency of the Selected Control Surfaces for the R.C.S.

The aerodynamic efficiency of the control surfaces employed on an aircraft configuration is a factor of primary importance for the aerodynamic and dynamic performance of the aircraft and as such it must be considered at the early stages of the design.

The factors which determine the aerodynamic efficiency of a control surface are first the effective moments and forces which it is capable of generating and then the drag forces which they induce on the aircraft throughout its flight envelope. It is therefore the aerodynamic design, that is, the effective area, the planform, and the location, of the control surface which must be optimized to obtain a required aerodynamic efficiency.

The aerodynamic control surfaces which have been used for the study of the longitudinal R.C.S. were the conventional elevator and the auxiliary control surfaces: spoilers and horizontal canards. From the analysis on the relative effectiveness of the control surfaces being considered it was determined that for the low-speed, low-level flight case being investigated the elevator was the Jetstar's most effective control surface for ride control; however, its implementation required the use of some other auxiliary surface to offset some of the workload required by the ride control mode. Spoilers were the surfaces found to be most suitable for this purpose. For the same flight conditions the horizontal canards selected did not improve the ride performance of the aircraft. However, although for higher speeds and altitudes of the aircraft the elevator force and moment coefficients remain approximately the same, as may be seen from Figure 7.1, the use of spoilers would have an adverse effect on the

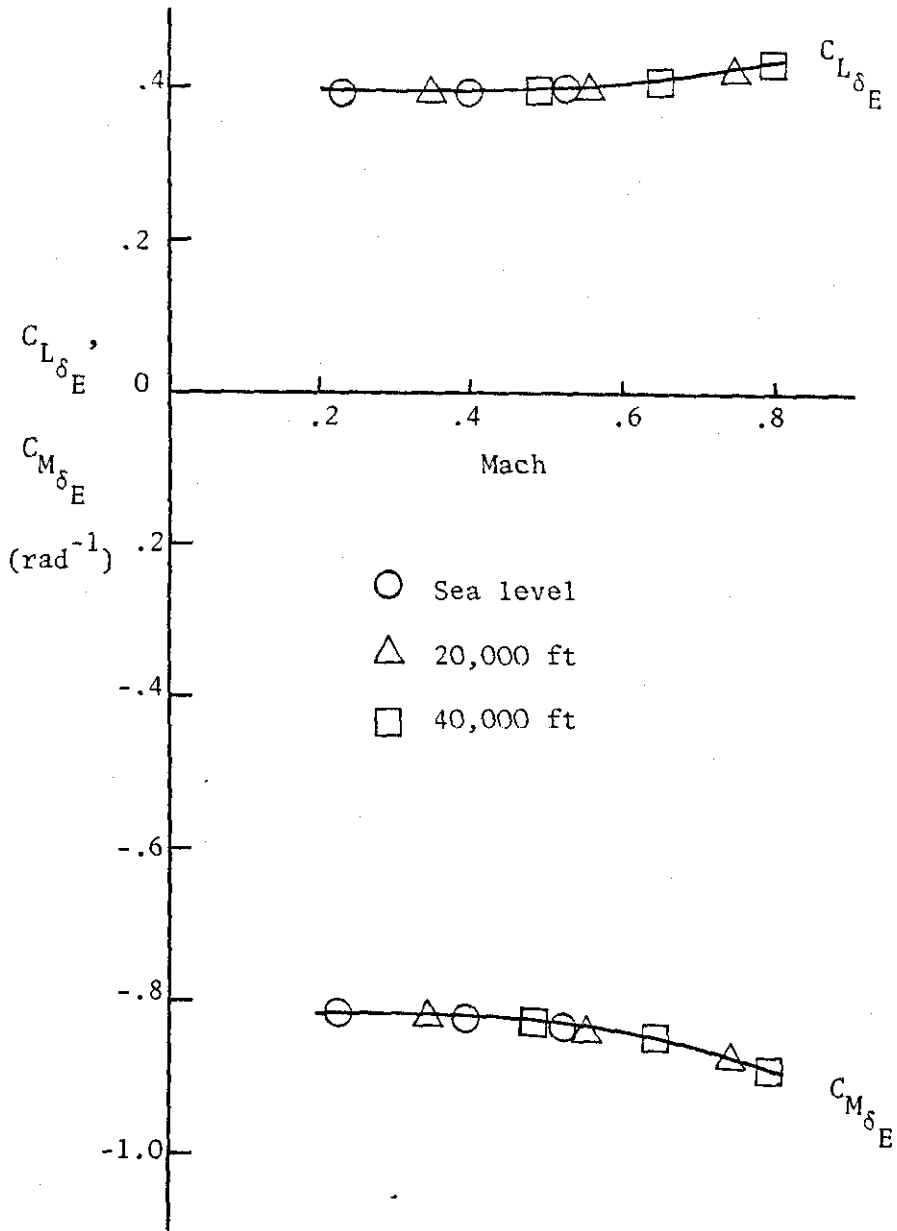


FIGURE 7.1: Variation of $C_{L\delta_E}$ and $C_{M\delta_E}$ with Altitude and Mach Number

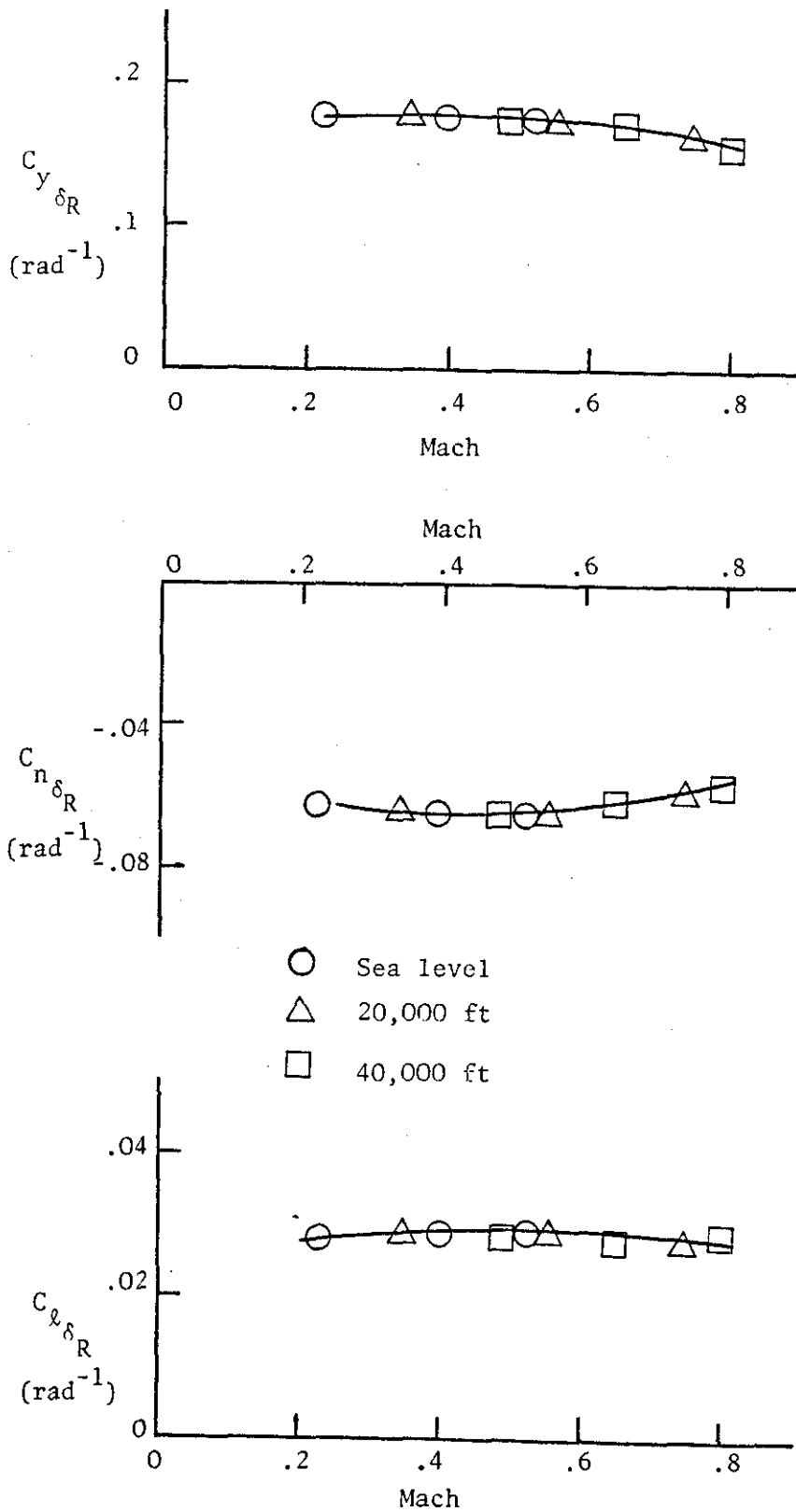


FIGURE 7.2: Variation of $C_{y\delta_R}$, $C_{n\delta_R}$ and $C_{l\delta_R}$ with Altitude and Mach Number

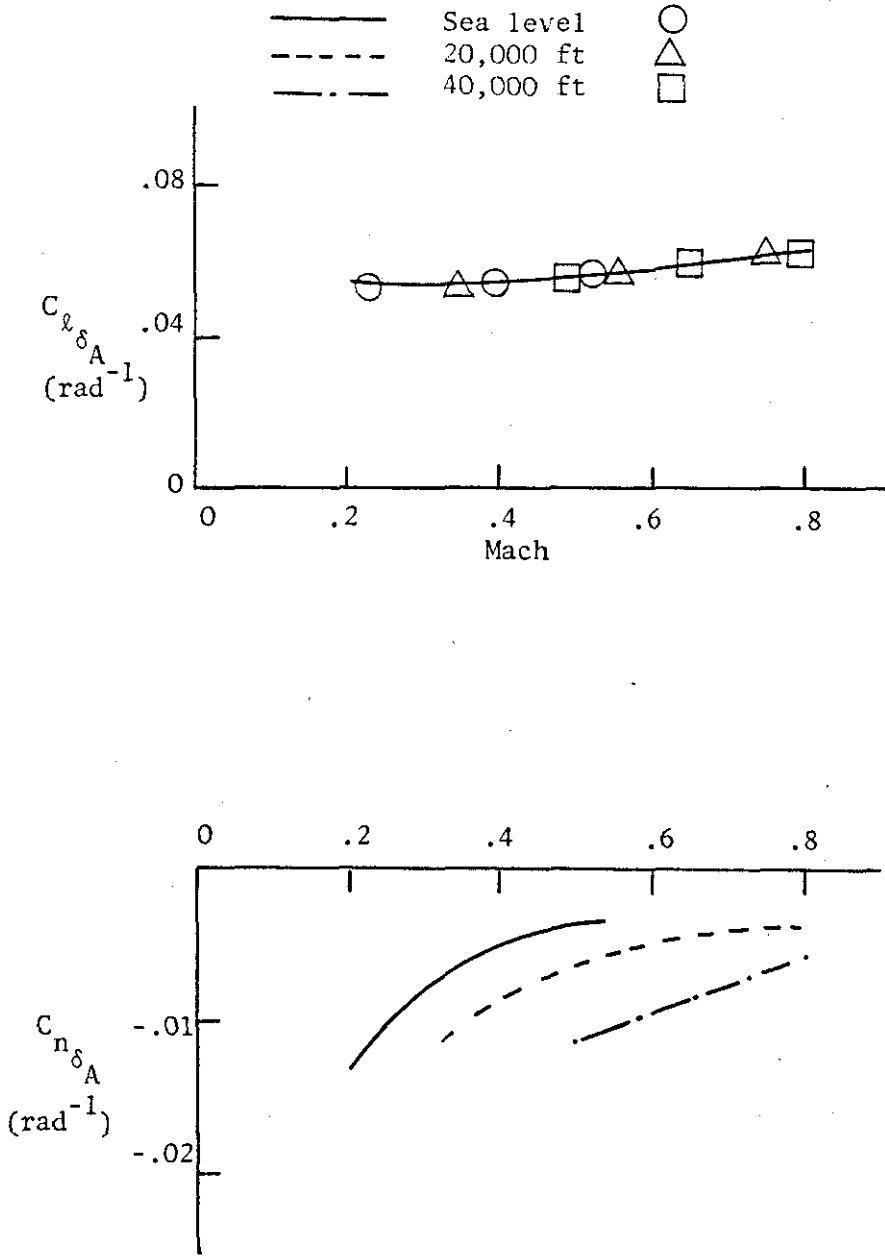


FIGURE 7.3: Variation of $C_{l_{\delta_A}}$ and $C_{n_{\delta_A}}$ with Altitude and Mach Number

aerodynamic performance of the aircraft. Since the spoilers have to operate from a biased position their use at higher speeds would result in an exceedingly high drag penalty on the aircraft. At such flying conditions the horizontal canards could probably be used effectively for ride control, since for these higher speeds they could be expected to become more effective with the advantage of lower drag when compared to spoilers.

From studying appropriate lateral control surfaces for the R.C.S. it was found that when both the conventional control surfaces, the rudder and ailerons, were used they provided good ride quality performance for the aircraft. The use of the vertical canard in conjunction with the rudder and the ailerons resulted in the best lateral ride performance of the aircraft. However, although for higher altitudes (reduction in air density) the effectiveness of rudder and ailerons remain the same for higher speeds, the effect of the ailerons on the yaw motion of the aircraft is reduced (see Figures 7.2 and 7.3), and therefore, at higher speeds, it can be expected that a vertical canard would be found to be even more useful for ride control.

It is important to emphasize that the choice of the dimensions and location of the vertical and horizontal canards was wholly empirical. More detailed selection of these contour surfaces would be expected to provide better results in terms of the ride quality control of the aircraft.

In this research the concept of the CCV was employed through the agency of additional control surfaces on the Jetstar aircraft in order to improve its ride. Use of the other CCV functions could result in significant reductions of the size and weight of the aircraft. In particular, it is expected that a CCV will not require such a great area for vertical

and horizontal tails with resulting savings in weight and drag which will either result in improved performance, or will allow the size of the aircraft to be scaled down to achieve lower operating costs. Active control can be used then to drive conventional and auxiliary control surfaces in order to augment the restoring moments needed for the stability and control of the aircraft.

7.3.2 Effectiveness of the Optimal Feedback Control Laws

Optimal control and model-matching theories can be used quite easily to derive feedback control laws for the purpose of improving the ride quality and the handling qualities of an aircraft. Both optimal control and model-matching can achieve desirable levels of ride quality performance as well as providing acceptable handling qualities. For the optimal output regulator the design objectives are achieved by appropriate choice of the Q and G weighting matrices; for model-matching the method requires a choice of a suitable model matrix. In the following sections of this chapter the required procedures for choosing appropriate matrices for Q and G , and for the model matrix will be presented based upon the experience gained from this research.

7.3.2.1 Choice of the weighting matrices Q and G

It has already been emphasized that the choice of the matrices Q and G is an important step for the determination of an optimal R.C.S. In this research the objective of the R.C.S. was to minimize normal and lateral accelerations induced at the c.g. of the aircraft. The minimization of acceleration with optimal control was attempted by means of minimizing a quadratic performance index. Two different performance indices (P.I.) were considered for this purpose. The first consisted of all the considered

elements of the control and the complete state vector which was assumed to be completely observable. (The aircraft system (A,B) was completely controllable). The second P.I. consisted of the acceleration and the control vector. The feedback control law which resulted from minimizing the first P.I. was called CONTROL LAW I while that which resulted from minimizing the second P.I. was called CONTROL LAW II. The difference between these two P.I.'s in terms of weighting matrices was that for CONTROL LAW I the state and the control vectors were 'directly' weighted by the matrices Q and G; while for the second P.I. the weighting by the Q and G matrices only influenced the output vector via the matrices C and D. (see equations(4.46)). For CONTROL LAW I the original choice of the Q and G matrices was based on the digital program 'WAYMX' (see section 4.5.1). For CONTROL LAW II, G matrix was derived from 'WAYMX' (same as CONTROL LAW I) while Q was chosen empirically. From Table 7.1 it is apparent that the results obtained from CONTROL LAW I for 'WAYMX' weighting were reasonable. Further manipulation of only the matrix, G, did not alter the results significantly. However, the matrix G for CONTROL LAWS I was treated in a way such that it would be possible to derive conclusions about the relative ride control effectiveness of each of the considered control surfaces on the optimally controlled aircraft.

In the investigation of CONTROL LAW II, the matrix Q^\dagger only tested for several different values. A typical example of the importance of particular choices of Q on the lateral acceleration of the aircraft for turbulent flight is given in Table 7.2.

[†]Note: for CONTROL LAW II Q is a scalar, or a matrix of order [1x1]

TABLE 7.2

	G	Q	σ_{a_y}	% reduction
UNCONTROLLED AIRCRAFT	-	-	0.0245	-
CONTROL LAW II	diag(.5,2.0,0.08)	.1	0.035	-43%
		.01	0.0175	28%
		.001	0.0155	36%

From the investigation carried out using different weighting matrices, Q and G and from the analysis of the equations describing a acceleration it is believed that some quantitative relationship between the choice of these two weighting matrices and the resulting control exists. This relationship would be influenced directly by the coefficients of the acceleration (i.e. the output) or the state equations of the aircraft. If such a relationship exists it ought to be possible by simultaneous treatment of Q and G matrices to achieve the maximum possible minimization of acceleration for specified handling qualities.

The optimal feedback CONTROL LAWS I and II although providing acceptable handling qualities for the lateral motion of the aircraft failed to provide acceptable handling qualities for the longitudinal motion. However, it is possible by choosing the matrices Q and G properly to affect the eigenvalues of the closed-loop system in such a way that acceptable handling qualities will result. Although this procedure could possibly result in the degradation of the R.C.S. it is a useful method of approaching the problem with existing theoretical methods.

It has been emphasized repeatedly throughout the analysis of the results that the control surfaces were operating well within their

limits of deflection angle. More specifically, every control surface employed used about 5 to 10% of its maximum capability of deflection angle. On the contrary elevator and rudder rate limits were often very closely approached and sometimes exceeded. To account directly for the rate limits which result from the physical constraints of the actuators a quadratic performance index could be considered as having as its control vector the rate of change of the deflection angles ($\dot{\delta}_i$) instead of the deflection angles themselves.

However, it is not possible to predict any advantages which may result from such control vector since the ride quality of an aircraft expressed by means of acceleration is directly influenced from the deflection angles of the controls rather than the rate of change.

7.3.2.2 Choice of the model matrix

As it has been seen the choice of the Q and G matrices for optimal control determine the effectiveness of the resulting feedback control laws in terms of ride quality and handling qualities improvement of an aircraft. Similarly the choice of the model for model matching theory is the factor which affects the resulting feedback control law in terms of its effectiveness on the two performance parameters referred to above.

However, it is more difficult to choose a model matrix for model matching than to choose Q and G for optimal control because, apart from satisfying the two requirements for handling qualities and ride performance simultaneously, the choice must ensure also closed-loop stability, a property which is automatically guaranteed in optimal control by respecting the definition of the positiveness of the matrices Q and G.

The main problem associated with the choice of the model matrix is that in order to achieve an improvement in handling qualities i.e. to assign the eigenvalues of the closed-loop system, it is possible to affect other characteristics of the aircraft which are closely associated with ride control. A typical example of this type was the effect of CONTROL LAW III on the ride performance of the aircraft. To satisfy the handling qualities requirements the aircraft was made to behave in similar way to a model which was defined with larger values of Z_w or M_w . This in effect resulted in an aircraft with poor ride quality control characteristics which were much in evidence in turbulent flight. This result configured the assessments which could be made from the ride discomfort index (R.D.I.) representation (see equations (2.10) and (2.11)) that the higher are the values of Z_w and M_w the higher is the value of the R.D.I. which indicates poorer ride quality performance. On the contrary CONTROL LAW III for lateral motion resulted in favourable ride performance for the aircraft and also provided acceptable handling qualities. It is evident therefore that the choice of the model for model matching theory is the key to success for the resulting control laws in terms of stability, handling qualities, and ride improvement of an aircraft. However, optimal control is more flexible for this purpose since it only requires manipulation of the Q and G matrices rather than the choice of a model subjected to all the above constraints.

Figure 7.4 summarizes the design procedures required for the design of an optimal R.C.S. when optimal control and model matching theories are employed as the control theories for the A.C.T. approach to the problem.

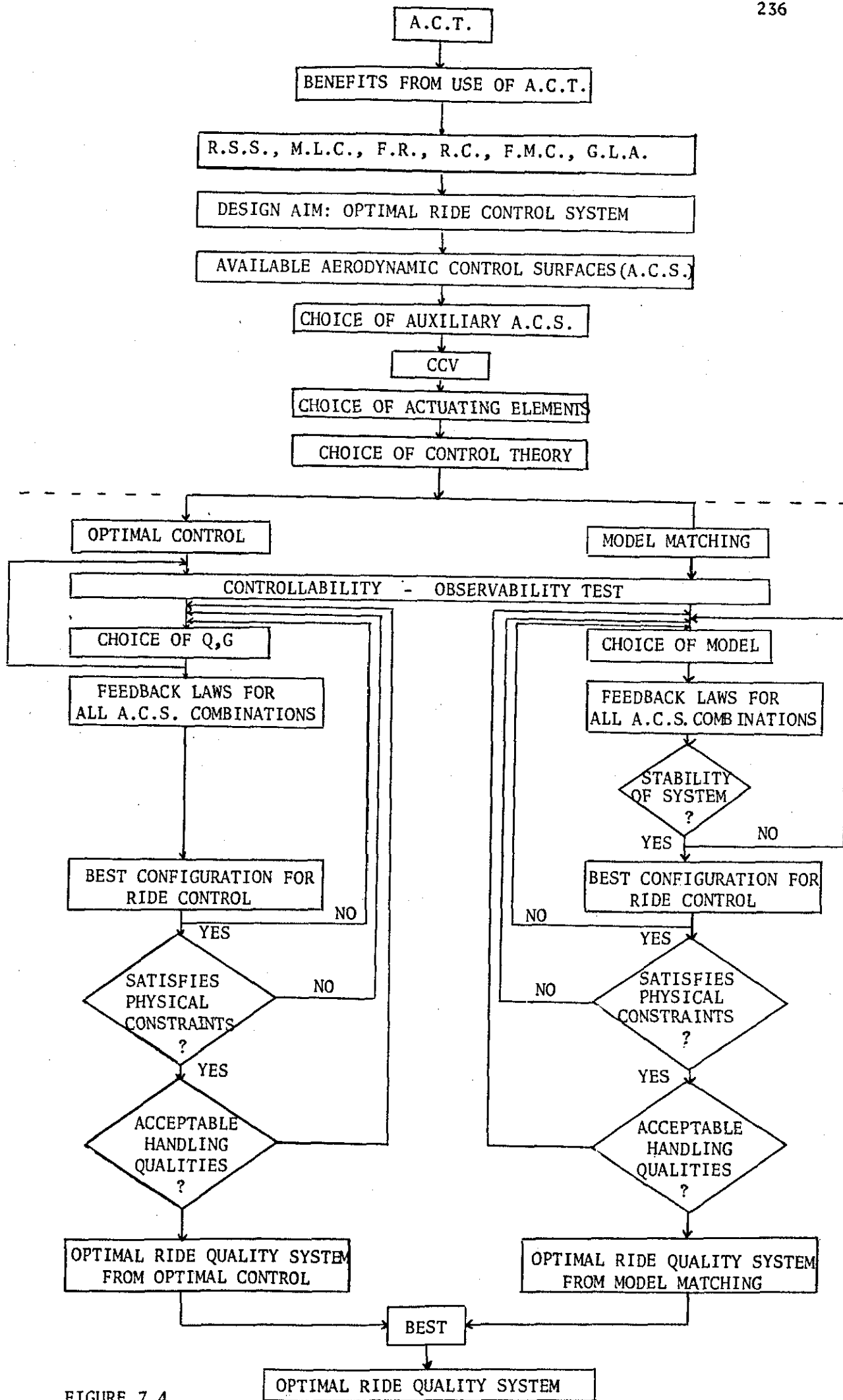


FIGURE 7.4

7.4 THE ROLE OF DIGITAL SIMULATION IN THE DESIGN OF AN OPTIMAL R.C.S.

With the aid of digital simulation multivariable control theories can be analysed and tested for practical or theoretical problems. Digital simulation made it feasible for this research to investigate a R.C.S. for a CCV aircraft. It was found from the use of digital simulation that the flexibility, speed, accuracy and repeatability which it provides makes it superior to analog simulation.

It was shown in Figure 7.4 how the computational stages for the optimization of the final design of an optimal R.C.S. could be very long and cannot be achieved as fast and accurately by any convenient means other than digital simulation.

From the experience gained with SLAM simulation language (Prasad, Saoullis, Tsitsilonis [1979]) it can be said that although it is effective in producing acceptable answers it nevertheless may cause a number of problems in the learning phases of research studies. The main problems which have been encountered with this language were on the simulation of a atmospheric turbulence. Initially the simulation of the Dryden filter proved difficult because 'lead lag' and 'simple lag' functions were used when modelling the transfer function. Because the mathematical operation of differentiation is involved in both functions, numerical instability always resulted when sharp changes, such as is typical of the input noise, were fed in. As a result of this the filter had to be represented as a separate set of differential equations. Another problem which was encountered was that due to a fault in the SLAM compiler at Loughborough University, where precedence was erroneous i.e. the order of evaluation of arithmetic

operations did not necessarily occur as outlined in the language specification. The problem was eventually circumvented by the use of shorter program statements and bracketing where it was believed inconsistencies might occur.

However, with the aid of digital simulation it was shown how modern control theories in conjunction with D.L.C. and D.S.F.C. principles could achieve substantial improvements in the ride quality of an aircraft. The design of optimal R.C.S. for executive jet aircraft of the STOL class is an important step because STOL aircraft technology will undoubtedly be influenced by the A.C.T./CCV approach, particularly at the early stages of airframe design.

CHAPTER 8

CONCLUSIONS

The optimal ride quality control system (R.C.S.) investigated in this research, for a STOL executive jet aircraft flying at low level and in the approach phase, provided substantial ride quality improvement over the aircraft's characteristics in the absence of automatic control by virtue of reductions in the normal and lateral accelerations induced at the centre of mass (c.g.) of the aircraft.

The A.C.T./CCV approach for the design of the R.C.S. of the aircraft emerged with a different aircraft control surface configuration by means of which the ride quality performance of the aircraft would be improved.

The analysis of the dynamic response of the aircraft in turbulence indicated that the longitudinal motion of the aircraft was more sensitive to gusts than was the lateral motion. However, it was demonstrated that the augmentation of the control achieved by conventional control surfaces (such as elevator, rudder and ailerons) by employing auxiliary control surfaces could provide an acceptable improvement in ride quality for both low and high speeds of the aircraft.

The auxiliary control surfaces considered were, in the longitudinal case, direct lift devices such as spoilers and horizontal canards, whereas for lateral motion a direct side force generator employing a vertical canard was used.

The research work showed that the conventional control surfaces of the aircraft can be used effectively for ride quality improvement. Since their effectiveness remains approximately the same within the flight envelope of the aircraft they can be used for ride control purposes without

any need to alter the airframe to introduce auxiliary control surfaces.

Although the use of the conventional control surfaces can provide a more economical solution for ride control, by avoiding the extra costs of airframe modification, it is necessary to ensure before they are so employed that their use for ride control would not impair their effectiveness for the main flying tasks of the aircraft such as trim and flight manoeuvres. A further constraint is that their use must not saturate i.e. exceed the physical limitations of the actuators associated with them.

The consideration of the actuators driving the aerodynamic control surfaces was found to be very important in the design of a R.C.S., for the dynamics of the actuators and their associated non-linearities, which result from their physical limitations, degraded slightly the ride quality performance of the aircraft. In particular, for longitudinal motion, the power limitations of the elevator actuator which was considered in this work imposed the need to use another control surface (spoilers) to share the workload demanded by the optimal feedback control law. It can be concluded therefore that actuator dynamics and their non-linearities must be considered carefully at the very earliest stages of the design of any R.C.S. since it might prove to be necessary to alter the original airframe design of an aircraft to achieve the specific aim.

The modern control theories, optimal control and model matching, used in this research for the design of an optimal R.C.S. were investigated in detail. It was found that both theories could be effectively used for improvement of both the ride quality and the handling qualities of an aircraft. However, from the experience gained from using these control

theories, it can be stated that optimal control is more flexible for optimal R.C.S. work since it only requires appropriate manipulation of the weighting matrices associated with the state and control vectors. On the contrary, the optimization procedure required for the choice of the model, for model-matching theory, is more complex since many design constraints have to be accounted for, before it is possible to implement a R.C.S. design resulting from the use of this theory.

From the investigation carried out on a non-linear control function whose use was considered principally for the potential improvement of the longitudinal motion ride characteristics the results were such as to indicate that some consideration for further use of non-linear controllers for ride control should be given attention since it is possible to achieve improvements in ride which are significant in regard to the frequency content of the resulting acceleration.

Finally, from the experience gained from this research on aircraft ride control some suggestions for future research are given here:

1. There exists a need for a continued investigation to determine any possible explicit relationship between the weighting matrices of the state and control vectors and the achieved reduction in acceleration, subject to the constraints on control surface use.
2. The exploitation of non-linear control for a R.C.S. should be considered particularly in respect of minimising "cobblestone effect".

and

3. An extended investigation into the use of controllers designed on the basis of optimal stochastic controls should be undertaken to determine, if the results obtained are significantly better than those produced by deterministic controllers operating in turbulence conditions. It is known that the feedback control laws obtained from the linear quadratic Gaussian problem are identical to those found in this work. However, this work has depended upon the intrinsic filtering properties of the closed-loop system to reduce the turbulence effects of the feedback signals.

The proposed extended research would indicate whether the undoubtedly more complicated (and expensive) computation to produce an explicit noise filter would produce any worthwhile practical improvement in the aircraft's ride.

It was shown in this research how modern control theories can be applied in conjunction with A.C.T./CCV approach to derive an effective R.C.S. for an executive jet aircraft. With the increasing demand for fuel-efficient short haul transportation and the corresponding advances in STOL technology the implementation of such R.C.S. on future aircraft will aim to attract the fare-paying public by providing the levels of ride comfort demanded and, at the same time, effectively reduce airport congestion problems.

REFERENCES

1. ATHANS, M., CASTANON, D., DUNN, K.P., GREENE, C.S., LEE, W.H., SANDELL, N.R. and WILLSKY, A.S., '*The Stochastic Control of the F-8C Aircraft Using a Multiple Model Adaptive Control (MMAC) Method - Part 1: Equilibrium Flight*', IEEE Transactions on Automatic Control, Vol.AC-22, No.5, 1977, 768-779.
2. ATWOOD, J.L., CANNON, R.H., JOHNSON, J.M., and ANDREW, G.M., '*Gust Alleviation System*', US Patent 2,985,409, 1961.
3. AUSLANDER, D.M., TAKAHASHI, Y., RABINS, M.J., '*Introducing Systems and Control*', McGraw-Hill, 1974, Chapter 10: Noise and Probabilistic Processes.
4. BOOTHE, E.M., and LEDDER, H.J., '*Direct Side Force Control for STOL Crosswind Landings*', J. of Aircraft, Vol.11, No.10, 1974, 631-638.
5. BRAINERD, C.H., and KOHLMAN, D.L., '*A Simulator Evaluation of the Use of Spoilers on a Light Aircraft*', NASA-CR-2121, 1972.
6. BRYSON, A.E., and HO, Y.C., '*Applied Optimal Control*', Ginn and Company, 1969, 148-157, 315-347.
7. BURRIS, P.M., and BENDER, M.A., '*Aircraft Load Alleviation and Mode Stabilization (LAMS)-B52 System Analysis, Synthesis and Design*', AFFDL-TR-68-161, WPAFB Dayton, Ohio, 1969.
8. CHALK, C.R., and WILSON, R.K., '*Airplane Flying Qualities Specification Revision*', J. of Aircraft, Vol.6, No.3, 1969, 232-239.

9. CONNER, D.W., and THOMPSON, G.O., '*Potential Benefits to Short-Haul Transports Through Use of Active Controls*', AGARD-CP-157, 1975.
10. COOPER, G.E., and HARPER, R.P., '*The Use of Pilot Rating in the Evaluation of Aircraft Handling Qualities*', NASA TN D-5153, 1966.
11. CORBIN, M.J., and GODDARD, K.F., '*The Design of Automatic Flight Control Systems to Reduce the Effects of Atmospheric Disturbances*', R.A.E., Technical Memorandum Avionics, 140, 1973.
12. COUPRV, G., '*Some Results on Gust Alleviation*', International Conference on Atmospheric Turbulence, London, May 18-21, 1971.
13. DICKINSON, B., '*Aircraft Stability and Control for Pilots and Engineers*', Sir Isaac Pitman & Sons Ltd., 1968, 32-37, 139-44, 530-541.
14. ERKELENS, L.J.J., and SCHURING, J., '*Investigation on a Passenger Ride-Comfort Improvement System with Limited Control Surface Actuator Performance for a Flexible Aircraft*', N.L.R. TR 75 140U, 1975.
15. ERZBERGER, H., '*On the Use of Algebraic Methods in the Analysis and Design of Model-following Control Systems*', NASA, TN D-4663, 1968.
16. ETKIN, B., '*Dynamics of Atmospheric Flight*', John Wiley & Sons Inc., 1972, 507-528, 529-541.
17. FRY, D.E., and WINTER, J.S., '*The Design of Automatic Ride Systems Using Direct Lift Control*', Symposium: The Institute of Measurement and Control. Dynamic Analysis of Vehicle Ride and Manoeuvring Characteristics, 1978.
18. GORDON, C.K., and DODSON, R.O., '*STOL Ride Control Feasibility Study*', NASA CR-2276, 1973.

19. GREENSITE, A.L., '*Analysis and Design of Space Vehicle Flight Control Systems*', Spartan Books, 1970, 109-112, 162-192.
20. HARVEY, C.A., and STEIN, G., '*Quadratic Weights for Asymptotic Regulator Properties*', IEEE Transactions on Automatic Control, Vol.AC-23, No.3, 1978.
21. HETTLEY, R.K., and JEWELL, W.E., '*Aircraft Handling Qualities Data*', NASA CR-2144, 1972, 166-192.
22. HEATH, R.E., '*State Variable Model of Wind Gusts*', AFFDL/FCC-TM-72-12, 1972.
23. HESS, R.A., '*Optimal Stochastic Control and Aircraft Gust Alleviation*', J. of Aircraft, 1971, Vol.8, No.4, 284-285.
24. HESS, R.A., '*Some Results of Suboptimal Gust Alleviation*', J. of Aircraft, 1972, Vol.9, No.5, 380-381.
25. HIRSCH, R., '*Studes et essais d'un absorbeur des rafales*', DOC Aeropl. 1957, 42, 13-28.
26. HOFMANN, L.G., and CLEMENT, W.F., '*Vehicle Design Considerations for Active Control Application to Subsonic Transport Aircraft*', NASA CR-2408, 1974.
27. HOLLOWAY, R.B., BURRIS, P.M., and JOHANNES, R.P., '*Aircraft Performance Benefits from Modern Control Systems Technology*', J. of Aircraft, 1970, Vol.7, No.6, 550-553.
28. HOLLOWAY, R.B., THOMPSON, G.O., and ROHLING, W.J., '*Prospects of Low Wing-Loading STOL Transports with Ride Smoothing*', J. of Aircraft, 1972 Vol.9, No.8, 525-530.

29. HOUBOLT, J., *'On the Response of Airplanes in a Three Dimensional Gust Field'*, AD-762-511, ARAP-161, 1972.
30. HUNSAKER, J.C., and WILSON, E.B., *'Report on Behaviour of Aeroplanes in Gust Turbulence'*, NACA TM-1(MIT), 1915.
31. JACOBS, O.L.R., *'Introduction to Control Theory'*, Clarendon Press, Oxford, 1974, 103-115, 235-259.
32. JACOBSON, I.D., and JOSHI, D.S., *'Investigation of the Influence of Simulated Turbulence on Handling Qualities'*, J. of Aircraft, Vol.14, No.3, 1977, 272-275.
33. JACOBSON, I.D., and KUHLTHAU, A.R., *'Determining STOL Ride Quality Criteria-Passenger Acceptance'*, J. of Aircraft, Vol.10, No.3, 1973, 163-166.
34. JACOBSON, I.D., KUHLTHAU, A.R. and RICHARDS, L.G., *'Passenger Airline Flights'*, NASA, TN-X-3295, 1975, 409-436.
35. JACOBSON, I.D., KUHLTHAU, A.R., RICHARDS, L.G., and CONNER, D.W., *'Passenger Ride Quality in Transport Aircraft'*, J. of Aircraft, Vol.15, No.11, 1978, 724-729.
36. JACOBSON, I.D., and LAPINS, M., *'Application of Active Control Technology to Aircraft Ride Smoothing'*, J. of Aircraft, Vol.14, No.8, 1977, 775-781.
37. JONES, J.G., *'A Unified Discrete Gust and Power Spectrum Treatment of Atmospheric Turbulence'*, International Conference on Atmospheric Turbulence, London, May 18-21, 1971.
38. JONES, J.G., *'Design of Control Laws to Implement A.C.T. Benefits'*, R.A.E., Technical Memorandum FS 267, 1979.

39. KRIECHBAUM, G.K.L., and STINEMAN, R.W., '*Design of Desirable Airplane Handling Qualities via Optimal Control*', J. of Aircraft, Vol.9, No.5, 1972, 365-369.
40. KUHLTHAU, A.R., and WICHANSKY, A.M., '*Summary Report: Workshop on Vehicle Ride Quality*', Williamsburg, Virginia, August 13-15, 1975, 73-90, NASA-CP-2013.
41. KUO, B.C., '*Automatic Control Systems*', Prentice-Hall Inc., 1975, (3rd Edition), Chapter 11: Introduction to Optimal Control.
42. LALLMAN, F.J., '*Gust Alleviation for a STOL Transport by Using Elevator, Spoilers and Flaps*', NASA TN D-7559, 1974.
43. LANGE, R.H., CAHILL, J.F., CAMPION, M.C., BRADLEY, E.S., MACWILKINSON, D.G. and PHILLIPS, J.W., '*Application of Active Controls Technology to the NASA Jetstar Airplane*', NASA CR-2561.
44. LAPINS, M. and JACOBSON, I.D., '*Application of Active Controls Technology to Aircraft Ride Smoothing Systems*', NASA-CR-145980, 1975.
45. LORENZETTI, R.C., NELSEN, G.L. and JOHNSON, R.W., '*Computetized Design of Optimal Direct Lift Controller*', J. of Aircraft, Vol.6, No.2, 1969, 137-143.
46. LORENZETTI, R.C., NELSEN, G.L., and JOHNSON, R.W., '*Direct Lift Control for Approach and Landing*', J. of Aircraft, Vol.6., No.3, 1969, 240-244.
47. LUTZE, F.H., and CLIFF, E.M., '*Control-Configured General Aviation Aircraft*', S.A.E. Paper 730303, 1973.

48. LYKKEN, L.O., and SHAH, N.H., '*Direct Lift Control for Improved Automatic Landing and Performance of Transport Aircraft*', *J. of Aircraft* Vol.9, No.5, 1972, 325-332.
49. MARSHAL, S.A., and NICHOLSON, H., '*Optimal Control of Linear Multivariable Systems with Quadratic Performance Criteria*', *Proceedings Control and Science, the Institute of Electrical Engineers*, Vol.117, No.8, 1970.
50. MCLEAN, D., '*Gust-Alleviation Control Systems for Aircraft*', *Proceedings of the Institution of Electrical Engineers, Control & Science*, Vol. 125, No.7, 1978.
51. MCLEAN, D., '*A Ride Quality Control System for a Fighter Aircraft*', *Dynamic Analysis of Vehicle Ride and Manouvering Characteristics Symposium, The Institute of Measurement and Control*, 1978.
52. MCRUER, D., ASKENAS, I., and GRAHAM, D., '*Aircraft Dynamics and Automatic Control*', *Princeton University Press*, 1973.
53. MODIJ, H.A., '*Handling Quality Criteria Development for Transport Aircraft with Fly-by-Wire Primary Flight Control Systems*', *AGARD-CP-157*, 1975.
54. NEUHART, D.H., and OETTING, R.B., '*Performance of Plain-Type Spoilers Applied to the GA(W)-1 Wing*', *J. of Aircraft*, Vol.14, No.10, 1977, 1019-1020.
55. NEWTON, G.C., GOULD, L.A., and KAISER, J.F., '*Analytical Design of Linear Feedback Controls*', *John Wiley & Sons, Inc.*, 1957, 109-118.

56. OEHMAN, W.I., '*Analytical Study of the Performance of a Gust Alleviation System for a STOL Airplane*', NASA TN D-7201, 1973.
57. OLCOTT, J.W., ELLIS, D.R., and FAYE, A.E.; '*The Application of Spoilers to a Small, Fixed-wing General Aviation Aircraft*', S.A.E. Paper 710387, 1971.
58. OSTGAARD, M.A., '*Active Control Technology*', AFFDL.FGT WPAFB, OHIO 45433, 1976.
59. OSTGAARD, M.A. and SWORTZEL, F.R., '*CCVs: Active Control Technology Creating New Military Aircraft Design Potential*', *Astronautics & Aeronautics*, 1977, 42-59.
60. PERRY, B., '*An Analytical Study of Turbulence Responses including Horizontal Tail Loads*', NASA TN D-8142.
61. PHILLIPS, W.H., and KRAFT, C.C., '*Theoretical Study of Some Methods for Increasing the Smoothness of Flight Through Rough Air*', NASA TN 2416, 1951.
62. PINSKER, W.J.G., '*The Control Characteristics of Aircraft Employing Direct Lift Control*', Reports and Memoranda No.3629, 1968.
63. PINSKER, W.J.G., '*Active Control as an Integral Tool in Advanced Aircraft Design*', AGARD-CP-157, 1975.
64. POWERS, B.G., '*Analytical Study of Ride Smoothing Benefits of Control System Configurations Optimized for Pilot Handling Qualities*', NTIS 1831963, 1978.
65. PRASAD, R.A., SAOULLIS, S.L.A., and TSITSILONIS, L., '*The Role of Simulation in Automatic Flight Control Systems Research*', presented in Royal Aeronautical Soc., Symposium 'Is flight simulation of academic interest?', 1979, London.

66. PRESS,H., and MEADOWS,M.T., '*A Re-evaluation of Gust-Load Statistics for Applications in Spectral Calculations*', NACA TN 3540, 1955.
67. PRESS,H., and STEINER,R., '*An Approach to the Problem of Estimating Severe and Repeated Gust Loads for Missile Operations*', NASA TN 4332, 1975.
68. ROBERTS,P.A., SWAIM,R.L., SCHMIDT,D.K., HINSDALE,A.T., '*Effects of Control Laws and Relaxed Static Stability on Vertical Ride Quality of Flexible Aircraft*', NASA CR 143843, 1977.
69. ROESCH,P., and HARLAN,R.B., '*A Passive Gust Load Alleviation System for Light Aircraft*', AIAA Paper No.74-773, 1974.
70. ROHLING,W.J., '*Flying Qualities: an Integral Part of a Stability Augmentation System*', J. of Aircraft, Vol.6, No.6, 1969, 510-515.
71. ROSKAM,J., BARBER,M.R., and LOSCHKE,P.C., '*Separate Surfaces for Automatic Flight Control Systems*', S.A.E. 730304.
72. RUSTENBURG,J.W., '*Ride Quality Design Criteria for Aircraft with Active Mode Control Systems*', AD/D-004456, ASD/WPAFB OHIO, 1972
73. SCHULTZ,D.G., MELSA,J.L.,'*State Functions and Linear Control Systems*', McGraw-Hill Series in Electronic Systems., 1967.
74. SCHWARZENBACH,J., and GILL,K.F., '*System Modelling and Control*', Edward Arnold, 1978, 21-26, 102-129, 191-197.
75. SCHOONOVER,W.E., '*Ride Quality of Terminal Area Manoeuvres*', NASA TM-X-3295, 1975, 387-408.
76. SPRATER.A., '*Stabilizing Device for Flying Machines*', US Patent 1 119234, 1914.

77. STEPHENS, D.G., '*Development and Application of Ride-Quality Criteria*', S.A.E. Paper No. 740813, 1974.
78. STEWART, E.C., '*Discussion of an Aeromechanical Gust Alleviation System to Improve Ride Comfort of Light Airplanes*', S.A.E. Paper No. 750544, 1975.
79. STINTON, D., '*The Anatomy of the Aeroplane*', G.T. Foulis & Co. Ltd., 1966, 41-44, 152-154.
80. STOCKDALE, C.R., and POYNEER, R.D., '*Control Configured Vehicles Ride Control System Design*', AFFDL-TR-73-83, 1973.
81. STUMPFL, S.C., and WHITMOYER, R.A., '*Horizontal Canards for Two-Axis CCV Fighter Control*', AFFDL-WPAFB, OHIO 45433, AGARD CP-157, 1975.
82. SWAIM, R.L., SCHMIDT, D.K., ROBERTS, P.A., and HISDALE, A.J., '*An Analytical Method for Ride Quality of Flexible Airplanes*', AIAA Journal, Vol. 15, No. , 1977.
83. TAYLOR, G.I., '*The Statistical Theory of Istropic Turbulence*', J. of the Aeronautical Sciences, Vol. 4, No. 8, 1937, 311-315.
84. TAYLOR, J., '*Manual on Aircraft Loads*', Pergamon Press, 1965, 191-202, 205-218.
85. TOBAK, M., '*On the Minimization of Airplane Responses to Random Gusts*', NASA TN 3290, 1957.
86. TRUXAL, J.G., '*Control Systems Synthesis*', McGraw-Hill, 1955, Chapter 7: Principles of Statistical Design.

87. TURNER, E.W., '*Aircraft Response to Atmospheric Turbulence Using P.S.D. Analysis Techniques*', AFFDL-TR-76-162, 1977.
88. TYLER, J.S., '*The Characteristics of Model-Following Systems as Synthesized by Optimal Control*', IEEE Transactions on Automatic Control, Vol. AC-9, No.4, 1964, 485-498.
89. VON KARMAN, TH., '*The Fundamentals of the Statistical Theory of Turbulence*', J. of Aeronautical Sciences, Vol.4, No.4, 1937, 131-138.
90. VON KARMAN, TH., '*Progress in the Statistical Theory of Turbulence*', J. of Marine Research, 1948, 252-264.
91. VON KARMAN, TH., and HOWARTH, L., '*On the Statistical Theory of Isotropic Turbulence*', From Proceedings of the Royal Society A164, 1938, 192-215.
92. WHITMOYER, R.A., '*Aerodynamic Interactions on the Fighter CCV Test Aircraft*', Symposium on Dynamic Stability Parameters, Athens, 1978.
93. WOLF, T.D., REZEK, J.W., and GEE, S.W., '*Passenger Ride Quality Response to an Airborne Simulator Environment*', NASA TM-X-3295, 1975, 373-385.
94. '*STOL Technology*', NASA SP-320, 1972, 1-35, 215-226.
95. JANES ALL THE WORLD'S AIRCRAFT, 1966-67, 276-277.

APPENDIX A

DERIVATION OF THE \hat{Q} AND \hat{G} MATRICES FOR THE OUTPUT REGULATOR

The performance index which is required to be minimized for the output regulator is given from (4.44):

$$J_0 = \frac{1}{2} \int_0^{\infty} \{ (\underline{Cx} + \underline{Du})^T Q (\underline{Cx} + \underline{Du}) + \underline{u}^T \underline{Gu} \} dt \quad (A1)$$

where C, D, Q and G are (p×n), (p×m), (p×p) and (p×m) matrices and \underline{x} and \underline{u} are n- and m-dimension vectors respectively.

The term $(\underline{Cx} + \underline{Du})^T Q (\underline{Cx} + \underline{Du})$ yields:

$$(\underline{Cx} + \underline{Du})^T Q (\underline{Cx} + \underline{Du}) = \underline{x}^T C^T Q C \underline{x} + \underline{u}^T D^T Q D \underline{u} + \underline{x}^T C^T Q D \underline{u} + \underline{u}^T D^T Q C \underline{x} \quad (A2)$$

The terms $\underline{x}^T C^T Q D \underline{u}$ and $\underline{u}^T D^T Q C \underline{x}$ are scalars or [1×1] matrices and hence

$$\underline{x}^T C^T Q D \underline{u} = (\underline{x}^T C^T Q D \underline{u})^T = \underline{u}^T D^T Q C \underline{x} \quad (A3)$$

Thus (A2) can be rewritten according to (A3) as follows:

$$(\underline{Cx} + \underline{Du})^T Q (\underline{Cx} + \underline{Du}) = \underline{x}^T C^T Q C \underline{x} + \underline{u}^T D^T Q D \underline{u} + 2 \underline{x}^T C^T Q D \underline{u} \quad (A4)$$

Therefore

$$\underline{y}^T Q \underline{y} + \underline{u}^T \underline{Gu} = \underline{x}^T \tilde{Q} \underline{x} + \underline{u}^T \hat{G} \underline{u} + 2 \underline{x}^T \underline{W} \underline{u} \quad (A5)$$

where

$$\left. \begin{aligned} \tilde{Q} &= C^T Q C \\ \hat{G} &= D^T Q D + G \\ \text{and } W &= C^T Q D \end{aligned} \right\} \quad (A6)$$

It can be shown that, by completing the square,

$$\underline{y}^T Q \underline{y} + \underline{u}^T \underline{Gu} = \underline{x}^T [\tilde{Q} - \underline{W} \hat{G}^{-1} \underline{W}^T] \underline{x} + [\underline{u} + \hat{G}^{-1} \underline{W}^T \underline{x}] G [\underline{u} + \hat{G}^{-1} \underline{W}^T \underline{x}] = \underline{x}^T \hat{Q} \underline{x} + \underline{u}^T \hat{G} \underline{u} \quad (A7)$$

where

$$\begin{aligned}
 \hat{Q} &= \tilde{Q} - W G^{-1} W^T \\
 &= C^T Q C - C^T Q D [D^T Q D + G]^{-1} [C^T Q D]^T \\
 &= C^T Q C - C^T Q D [D^T Q D + G]^{-1} D^T Q C \\
 &= C^T \{ [I] - Q D [D^T Q D + G]^{-1} D^T \} Q C
 \end{aligned} \tag{A8}$$

and therefore

$$\hat{u} = u + G^{-1} W^T \underline{x} \tag{A9}$$

APPENDIX B

AIRPLANE CLASSIFICATION

In the revision of the airplane flying qualities specification (Chalk and Wilson [1969]) the classes of aircraft were described as illustrated in Table B1.

TABLE B1.

CLASS	CHARACTERISTICS
I	Small, light-weight medium maneuverability airplanes
II	Medium-weight, low to medium maneuverability airplanes
III	Large, heavy-weight, low-maneuverability airplanes
IV	High-maneuverability airplanes

The approach taken to distinguish different control tasks or flight phases in the -8785 revision, was to divide the mission flight phases into three categories. First, the flight phases were divided into terminal or non-terminal groups. The non-terminal flight phases were further divided into two categories as defined in Table B2.

TABLE B2NON-TERMINAL FLIGHT PHASES

Category A: Those non-terminal flight phases that require rapid maneuvering, precision tracking, or precise flight-path control

- | | |
|------------------------------|-----------------------------------|
| 1. Air-to-air combat | 6. Reconnaissance platform |
| 2. Ground attack | 7. In-flight refueling (receiver) |
| 3. Weapon delivery or launch | 8. Terrain following |
| 4. Aerial delivery | 9. Antisubmarine search |
| 5. Aerial recovery | 10. Close formation flying |

Category B: Those non-terminal flight phases that are normally accomplished using gradual maneuvers; although accurate flight-path control may be required, precision tracking is not necessary

- | | |
|-----------|---------------------------------|
| 1. Climb | 5. In-flight refueling (tanker) |
| 2. Cruise | 6. Descent |
| 3. Loiter | 7. Emergency descent |
| 4. Glide | 8. Emergency deceleration |

TERMINAL FLIGHT PHASES

Category C: Terminal flight phases consisting of the following

- | | |
|-------------|------------------------|
| 1. Takeoff | 3. Waveoff (go-around) |
| 2. Approach | 4. Landing |

APPENDIX C

FREQUENCY RESPONSES OF THE ACTUATOR DYNAMICS EMPLOYED

To investigate the frequency responses of the actuating elements employed in the R.C.S. their Bode diagrams were considered.

Figure C1 illustrates the frequency response of a first-order actuator associated with spoilers. It is evident from this figure that the bandwidth of this control element is sufficiently above the highest natural frequencies of the dynamic modes of the aircraft and hence mutual interference will not occur. Similar responses were obtained from all the other 1st-order actuators associated with ailerons and horizontal and vertical canards.

Figure C2 illustrates the frequency response of a 2nd order actuator associated with elevator. (Similar response must be obtained for the 2nd-order actuator of rudder for the dynamics were assumed to be identical). From this figure it may be seen that although there was not a major interference with the dynamic modes of the aircraft it was expected that second order actuators would affect the performance of the aircraft more than dynamics of the first order actuators.

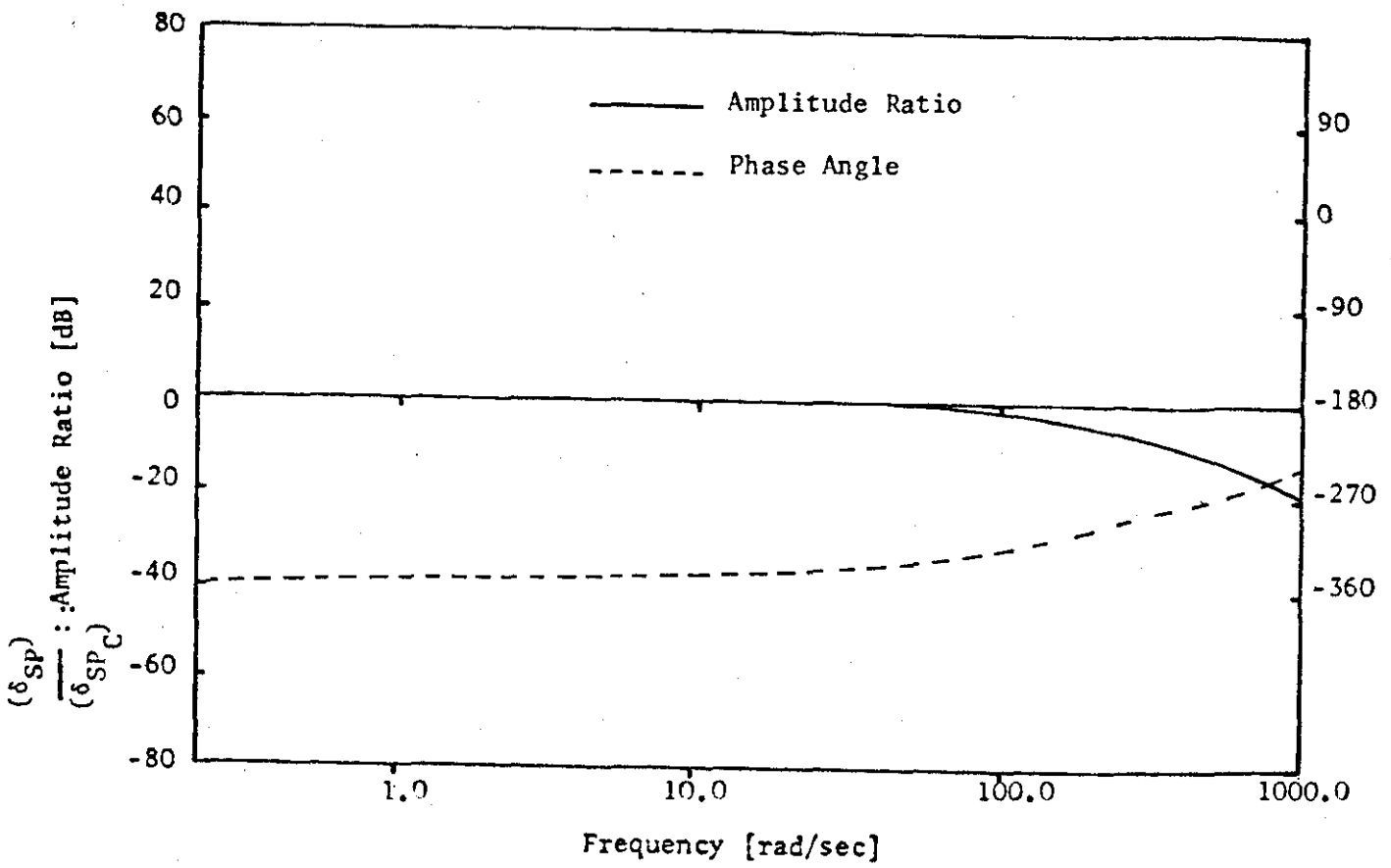


FIGURE C.1

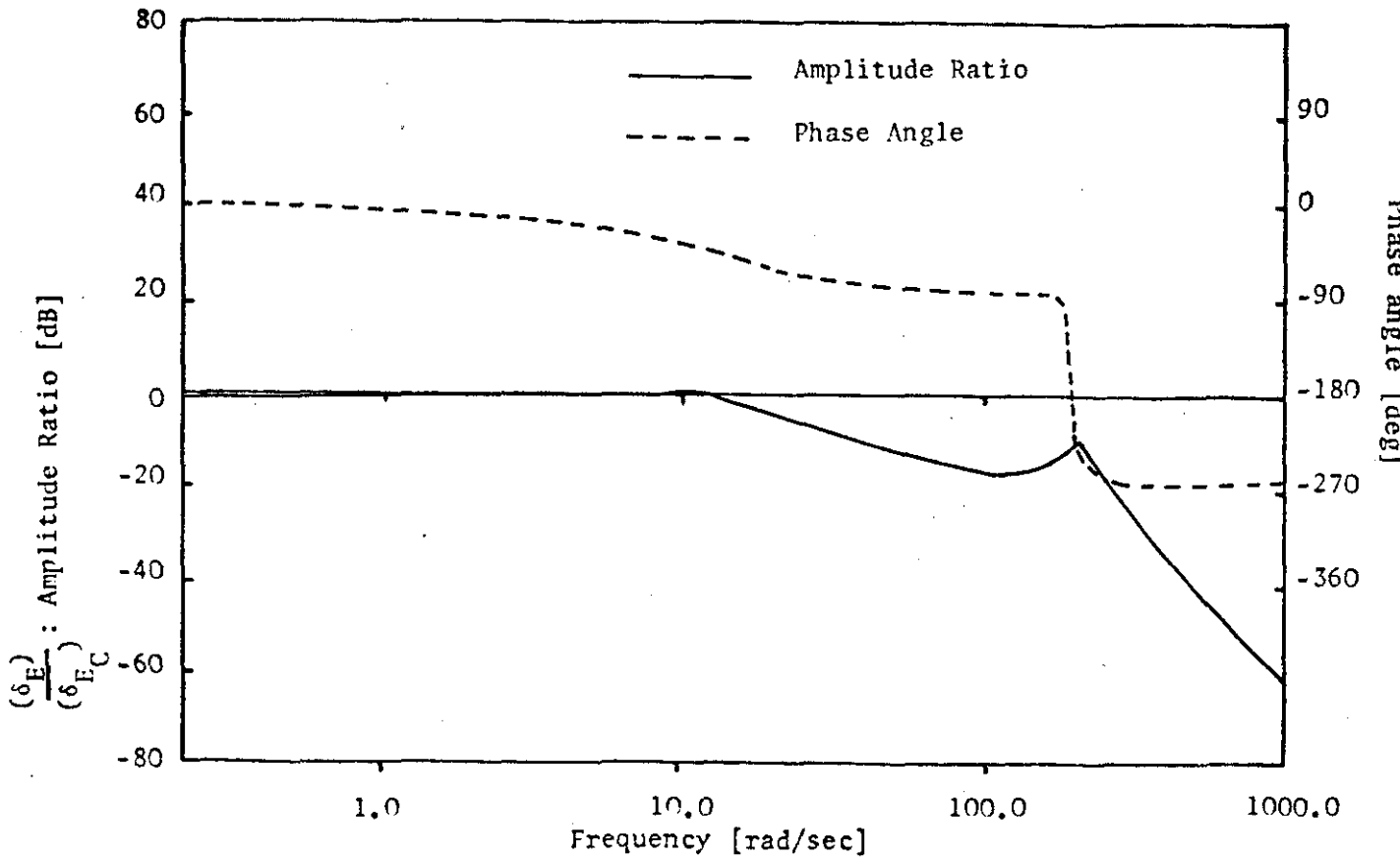


FIGURE C.2

APPENDIX D

GENERAL CHARACTERISTICS OF THE

BASIC JETSTAR AIRCRAFT

D.1 FLIGHT CONDITION PARAMETERS AND STABILITY DERIVATIVES

The Jetstar aircraft was investigated for a power approach phase described by the following flight condition parameters:

- . H = sea level
- . Slipper Tanks Installed
- . Light Gross Weight
- . Gear down
- . 40% flaps
- . $\alpha_0 = 0.0$
- . $1.4 V_s = 224 \text{ ft/s}$
- . W = 23904 lb
- . c.g. at $0.25\bar{C}$, W.L. 94.2
- . $I_x = 42273 \text{ slug -ft}^2$
- . $I_y = 126099 \text{ slug -ft}^2$
- . $I_z = 160104 \text{ slug -ft}^2$
- . $I_{xz} = 5470 \text{ slug -ft}^2$

Table D1 summarizes the power approach non-dimensional stability derivatives for the above flight conditions.

TABLE D1

POWER APPROACH NON-DIMENSIONAL STABILITY DERIVATIVES

Longitudinal	Lateral-Directional (Body Axis)
$C_L = .737$	$C_{y\beta} = -.72/\text{rad}$
$C_D = .095$	$C_{n\beta} = .137/\text{rad}$
$C_{L\alpha} = 5.0/\text{rad}$	$C_{\ell\beta} = -.103/\text{rad}$
$C_{D\alpha} = .75/\text{rad}$	$C_{\ell p} = -.37/\text{rad}$
$C_{m\alpha} = -.80/\text{rad}$	$C_{n p} = -.14/\text{rad}$
$C_{m\dot{\alpha}} = -3.0/\text{rad}$	$C_{\ell r} = .11/\text{rad}$
$C_{m q} = -8.0/\text{rad}$	$C_{n r} = -.16/\text{rad}$
$C_{L\delta e} = .4/\text{rad}$	$C_{n\delta a} = -.0075/\text{rad}$
$C_{m\delta e} = -.81/\text{rad}$	$C_{\ell\delta a} = .054/\text{rad}$
	$C_{y\delta r} = .175/\text{rad}$
	$C_{n\delta r} = -.063/\text{rad}$
	$C_{\ell\delta r} = .029/\text{rad}$

Table D2 summarizes the longitudinal and lateral directional dimensional derivatives for body axis system for the above flight conditions.

TABLE D2

LONGITUDINAL AND LATERAL DIRECTIONAL DIMENSIONAL
STABILITY DERIVATIVES

Longitudinal		Lateral	
X_u	-.0166	Y_v	-.140
Z_u	-.175	Y_β	-31.2
M_u	.00131	L'_β	-4.05
X_w	.108	N'_β	1.34
Z_w	-1.01	L'_p	-1.85
M_w	-.00991	N'_p	-.245
Z^*_w	0.	L'_r	.517
Z_q	0.	N'_r	-.190
M^*_w	-.00091	$Y^*_{\delta A}$	0.
M_q	-.546	$L'_{\delta A}$	2.21
$X_{\delta E}$	1.97	$N'_{\delta A}$	-.00557
$Z_{\delta E}$	-17.2	$Y^*_{\delta R}$.034
$M_{\delta E}$	-2.26	$L'_{\delta R}$	1.11
		$N'_{\delta R}$	-.644
		L'_{r_g}	-.027
		N'_{r_g}	-.208

D.2 LONGITUDINAL AND LATERAL-DIRECTIONAL HANDLING QUALITY PARAMETERS

The longitudinal handling quality parameters considered but not presented in this work are defined in Table D3.

TABLE D3

LONGITUDINAL HANDLING QUALITY PARAMETERS

Standard Notation Definition	Equation	Value
N_{z_α} , g/rad	$-\frac{U_0}{g} \frac{N_\delta^a z(s)}{N_\delta^w(s)}$ for $s=0$	6.32
Control anticipation parameter, rad/sec ² /g	$-(s^2 \frac{N_\delta^\theta(s)}{\Delta(s)} \Big _{s=\infty}) / (\frac{1}{g} \frac{N_\delta^a z(s)}{\Delta(s)} \Big _{s=0})$.425

$\Delta(s)$ represents the characteristic equation for longitudinal motion and it is defined as follows

$$\Delta(s) = \{s^2 + 2\zeta_p \omega_p s + \omega_p^2\} \{s^2 + 2\zeta_{sp} \omega_{sp} s + \omega_{sp}^2\} \quad (D1)$$

where ζ_p , ω_p and ζ_{sp} and ω_{sp} are the damping ratios and natural frequencies of the phugoid and short period modes of the aircraft.

For the flight conditions considered $\Delta(s)$ was defined as follows

$$\Delta(s) = \{s^2 + 2(0.188)(0.0087)s + (0.188)^2\} \times \{s^2 + 2(1.667)(0.532)s + (1.667)^2\} \quad (D2)$$

Thus by comparison to D1, D2 yields

$$\zeta_p = 0.188, \quad \omega_p = 0.0087, \quad \zeta_{sp} = 0.532 \text{ and } \omega_{sp} = 1.667 \quad (D3)$$

[†] $N_y^x(s)$ represents the numerator of a transfer function $X(s)/Y(s)$

D3 gives the flying characteristics of the uncontrolled aircraft in the flying conditions considered.

The lateral-directional handling quality parameters considered in this work are given in Table D4.

TABLE D4

Standard Notation Definition	Value
$\Delta\beta_m$: maximum sideslip excursion at the c.g., occurring within two seconds or one half period of the dutch roll, whichever is greater for a step aileron command	.381
$ \phi/\beta $ at $s=(\zeta;\omega_n)_d$ rad/rad	1.22

The characteristic equation for lateral motion is defined as

$$\Delta(s) = (s+1/T_S)(s+1/T_R)(s^2+2\zeta_d\omega_d s+\omega_d^2) \quad (D4)$$

where T_S and T_R are the time constants of the spiral and roll subsidence modes and ζ_d and ω_d are the damping ratio and natural frequency of the dutch roll mode. For the flight conditions considered $\Delta(s)$ was given by:

$$\Delta(s) = (s+0.00268)(s+2.108)\{s^2+2(1.397)(0.0248)s+(1.397)^2\} \quad (D5)$$

Hence from comparison of (D4) and (D5) the flying characteristics of the lateral-directional motion of the uncontrolled aircraft were the following:

$$T_S = 373s, \quad T_R = 0.474, \quad \zeta_d = 0.0248 \quad \text{and} \quad \omega_d = 1.397$$

